20513-6006-R0-00

STUDY OF A
COMET RENDEZVOUS MISSION

FINAL TECHNICAL REPORT
VOLUME I

MAY 12, 1972

"This work was performed for the Jet Propulsion Laboratory, California Institute of Technology sponsored by the National Aeronautics and Space Administration under Contract NAS7-100."

(JPL Study Contract No. 953247)

TRW
One Space Park
Redondo Beach, California

COMET ENCKE 6 JANUARY 1961

There was an old comet in space,
Whose end was a notable case.
    It puffed and it fumed
    Till its coma was doomed,
And a dead asteroid took its place.

E.W.G.

ABSTRACT

This repor is concerned with feasibility, scientific objectives, modes of exploration and implementation alternatives of a rendezvous mission to Encke's comet in 1984. The principal emphasis of this study was placed on developing the scientific rationale for such a mission, based on available knowledge and best estimates of this comet's physical characteristics, including current theories of its origin, evolution and composition. A main section of the report is devoted to a compilation of these data and theoretical results, giving an up to date model of Encke's phenomena.

Our aim was to formulate a basic mission concept devoid of overly costly and complex elements not absolutely necessary in achieving the principal scientific objectives of the rendezvous mission. With this restriction in mind we studied mission profile alternatives, performance tradeoffs, developed a preferred exploration strategy, and defined a spacecraft design concept capable of performing this mission.

The study showed that the major scientific objectives can be met by a Titan IIID/Centaur-launched 17.5 kw solar electric propulsion spacecraft (13 kw of this power being used for propulsion) which carries 60 kg of scientific instruments and is capable of extensive maneuvering within the comet envelope to explore the coma, tail and nucleus. Launched in December 1981, and arriving at the comet after nominally 800 days in February 1984, 40 days before perihelion passage, the spacecraft will stay in the comet envelope for at least 80 days. The residence time can be extended by several 100 days as the comet recedes from the sun, for additional scientific observations during the comet's dormancy.

Results of this study are presented in two volumes:

I Technical Report

II Appendix

ACKNOWLEDGEMENTS

This study has been performed by the technical staff of TRW Systems Group with the consulting support of Dr. G. W. Wetherill (University of California, Los Angeles) and Dr. W. I. Axford (University of California, San Diego) in the fields of space science and cometary physics.

Messrs. K. L. Atkins and R. Newburn of JPL have monitored the study from its beginning and have contributed valuable suggestions and corrections. Mr. Carl Sauer of JPL has provided trajectory data for a 1984 Encke rendezvous and Dr. A. Friedlander of the Illinois Institute of Technology Research Institute (IITRI) has supplied mission analysis data stemming from concurrent and earlier comet mission studies for NASA and JPL.

These contributions have been most helpful in the performance of this study and are reflected in the data presented herein.

Members of TRW's study team are listed below:

H. F. Meissinger	Study Manager System Engineering and Mission Analysis
E. W. Greenstadt	Physical Model of Comet Encke, Scientific Mission Objectives, and Payload Selection
W. McMinimy	Payload Instruments
R. C. Africano	Trajectory Studies
A. H. Carlin	Configuration
D. S. Goldin	Electric Propulsion and Power
J. V. Flannery	TV Image System Conceptual Design
J. C. Slattery	Meteoroid Environment
L. E. Laaksonen	Thermal Design Concept
J. M. Sellen	Electric Propulsion Interactions
S. Cushner	Radar Altimetry

CONTENTS

CONTENTS (CONTINUED)

CONTENTS (CONTINUED)

CONTENTS (CONTINUED)

CONTENTS (CONTINUED)

ILLUSTRATIONS

ILLUSTRATIONS (CONTINUED)

ILLUSTRATIONS (CONTINUED)

ILLUSTRATIONS (CONTINUED)

TABLES

1. INTRODUCTION AND SUMMARY

1.1 STUDY OBJECTIVES

In this study we have investigated the feasibility, scientific objectives, modes of operation, and implementation alternatives of a rendezvous mission to the comet Encke in 1984. It is assumed that by the time this mission will be launched, i.e., in 1981/82, the new technology of solar-electric propulsion will be sufficiently well established and flight-proven to make a rendezvous mission, rather than a mere flythrough, practical and economically attractive.

The study differs in scope from previous spacecraft feasibility and design studies by aiming to establish principal goals and priorities of the mission rather than assuming them for granted and proceeding to the technical implementation problems. In fact the main effort was devoted to defining the physical environment at the comet and developing a strategy for conducting the exploration. As a result we formulated a mission concept that we believe to be most effective in achieving the desired scientific objectives. Spacecraft design tasks were given much less emphasis by comparison. This allocation of task priority was made in concurrence with the technical direction given us by JPL.

The overriding ground rule that we applied in formulating this mission concept was simplicity and cost economy. Thus, of the many alternate options that appeared attractive and feasible, only the one that could be defended as essential to the basic scientific objective of a rendezvous mission was adopted as the preferred option. The ultimate criterion of acceptibility of any payload instrument, observation mode, or spacecraft feature was relevance to the basic rendezvous objective. Features that would enhance the mission but did not contribute an essential ingredient were considered as luxury and had to be given up. This applied particularly in the payload instrument selection.

In performing the study we took into consideration the cometary exploration goals published in recent years, particularly the preliminary report material available from the two recent NASA-sponsored comet conferences at the University of Arizona (Tucson, March 1970, Reference 1-1), and at Yerkes Observatory (June 1971, Reference 1-2). Recent

studies of comet rendezvous mission concepts performed by the Illinois Institute of Technology Research Institute (References 1-3 and 1-4) also provide useful and up-to-date source material. In addition, the recently completed design studies of electric propulsion rendezvous spacecraft by JPL, TRW, and North American Rockwell (References 1-5, 1-6, and 1-7) provided practical design concepts and a thorough documentation of the technology base available today for implementing a solar electric propulsion (SEP) mission such as an Encke rendezvous.

Comet Encke was specified as the rendezvous target prior to initiation of this study. It is well suited as a target for a deep space probe because its short orbital period has allowed it to be observed on many perihelion passes since its discovery, and its orbital parameters as well as perturbative influences are better established than most other comets'. For purposes of our study we assume that an Encke flyby mission in 1980 will precede the 1984 rendezvous mission, and that this flyby mission will have established the existence of a nucleus. More detailed observation of this nucleus is assumed as one of the principal objectives of the rendezvous mission.

The rendezvous spacecraft being considered has the capability of performing in-situ experiments at the nucleus, as well as in the coma and tail of the comet for a prolonged time period. This permits observation of time varying phenomena during the closest approach to the sun and correlation with concurrent observations from earth to enhance understanding of cometary physics. The mission plan foresees a rendezvous 40 days prior to perihelion passage with residence at the comet for at least 80 days thereafter.

The principal advantage of electric over chemical propulsion in this application is reduction by an order of magnitude of the propellant mass for the large maneuvers in deep space that a comet rendezvous mission entails, and hence a significant increase in payload capacity. Another useful attribute of an electric propulsion system is the power capacity of several kilowatts that becomes available for operation of sophisticated payload instruments and high-data-rate telemetry after arrival at the comet.

1.2 TENTATIVE COMET MISSION SCHEDULE

A tentative sequence of major events leading to the launch in 1981/1982 of an Encke rendezvous spacecraft is illustrated in Figure 1-1. We postulate that the rendezvous mission is preceded by a flythrough mission to Encke in 1980 which will provide basic data on the unknown physical phenomena and hazards to be encountered at the comet. An alternate target for an earlier flythrough mission would be Comet d'Arrest (1976) but this mission is unlikely to be approved, considering its time constraints. The time interval between the flythrough event (October 1980) and the launch date (early or late in 1981) of the rendezvous mission allows some design changes or adjustments of critical parameters in accordance with the data obtained from the precursor mission. Short transfers of 700 to 800 days (Option B) would defer the launch date by about ten months compared to long transfers (Option A), thus increasing the time margin for any necessary spacecraft (or payload) modifications from about 5 to 15 months, as shown in the lower right of Figure 1-1.

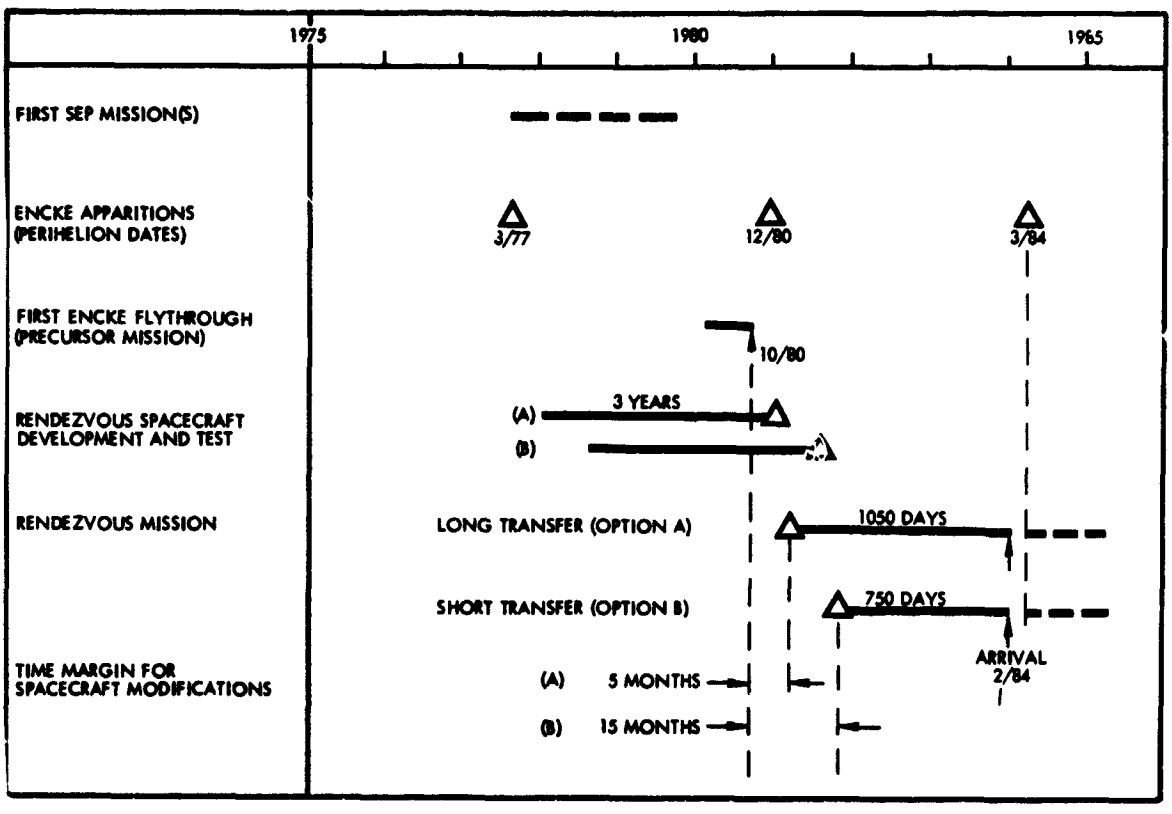

Figure 1-1. Key Events Leading to 1984 Encke Rendezvous

1.3 SOME CHARACTERISTICS OF COMET ENCKE

The general characteristics of comets, their significance in models of solar system formation, and the broad aims of cometary observation, whether pursued with earthbound or spaceborne instruments nave been well documented in the literature. Certain less familiar physical features of comet Encke which can affect the planning of a rendezvous mission are summarized in the following paragraphs.

Encke has passed fifty-six times through perihelion, at 0.34 AU, since its discovery in 1786. Its orbital parameters have long been well established, even to the extent that a mass loss of some 0.03 percent per orbit has been inferred with confidence from its secular perturbation. Despite its accurately calculable earth-crossing trajectory, however, recovery and observability of Encke have not been consistently easy or predictable. Recovery has commonly occurred several months before perihelion at distances of 1 to 3 AU, but has occasionally been delayed until perihelion, or even later. Variable Earth-Encke distances and angles, inconsistent seeing conditions, diversity of viewing technique, intrinsic variability of the comet, and relatively faint apparitions have combined to give Encke a widely changing image. The comet has appeared on a few occasions as a naked-eye object; it has been described as having no nuclear condensation at all, having a clear condensation asymmetrically located in the antisolar section or at the edge of the coma, and having even two separate bright condensations.

The oval or fan shaped coma varies in apparent diameter, appears to shrink as Encke approaches perihelion, and is commonly diffuse and difficult to see after perihelion. Tails have been observed to extend to several times the coma diameter in length or have not been observed at all. Presence or absence of a tail has been reported with roughly equal frequency. Fan shaped and long narrow tails have both been observed.

Physically, Encke appears to be an old comet which is depleted in solid particles, since it has shown little or no continuum spectrum of reflected sunlight. Its coma and tail are primarily gaseous, with emission

spectra displaying strongly the presence of CN, C_2, and C_3, and weakly the presence of CH, NH, NH_2, OH, CO^+, and N_2^+. A comprehensive model of Encke giving estimates of gas and particle densities and distributions apparently does not exist. Recently, Encke became the third comet, and the first short-period comet, around which an extensive envelope of neutral hydrogen Lyman-α was discovered by measurements from earth satellites.

The following are some elementary parameters describing Encke which are relevant to the formulation of the mission concept:

Orbital period	3.3 years
Aphelion distance	4.1 AU
Perihelion distance	0.34 AU
Orbital inclination	12.0 degrees
Velocity at 1 AU	37.1 km/sec
Velocity at perihelion	69.9 km/sec
Estimated diameter of coma	20×10^3 to 360×10^3 km
Estimated diameter of nucleus	1 to 4 km
Estimated minimal length of tail, when present	2×10^5 to 2×10^6 km

1.4 SCIENTIFIC OBJECTIVES AND EXPLORATION STRATEGY

In formulating the mission concept described herein, it is assumed that a precursor mission has established the existence of a compact nucleus. The projected mission profile, exploration strategy, and payload composition are governed by two principal overall objectives which are, in order of priority:

1. To determine the mass, dimension, physical structure, and composition of the nucleus.

2. To examine the configuration and composition of coma and tail, together with solar wind interaction processes affecting them.

The priority which is given to investigation of the nucleus does not downgrade the importance of other goals. The large net payload and extensive maneuver capacity provided by a solar-electric spacecraft strongly

suggests that comprehensive measurements throughout the comet's environment be included in the mission plan. The assignment proposed here of spacecraft resources and capabilities reflects the view that most cometary investigation will continue to be by remote (telescopic) observation, either with surface or earth-orbiting equipment, and that on-site observations should be pursued in such a way as to improve the yield from analysis of such earth-based optical measurements. A high-resolution imaging system carried by the spacecraft will permit correlation of phenomena observed optically from outside the comet with observations made locally inside the comet. An important further objective is to correlate changing solar wind parameters outside the comet with processes observed within the comet. The exploration strategy and payload composition arrived at in this study are addressed to these requirements.

The primary objectives of the mission will be met by the spacecraft penetrating the coma and the nearby tail region and performing excursions that permit systematic mapping of physical characteristics provided that adequate thermal protection of the spacecraft is feasible. Excursions to distances 50×10^3 km downstream of the comet center can be readily carried out using the electric propulsion system for maneuvering. During this phase the spacecraft will also search for and detect the nucleus (unless this has been achieved prior to rendezvous) and approach the nucleus for close-up observation.

1.5 TYPICAL MISSION PROFILE

A typical transfer trajectory that arrives at the comet 50 days before perihelion is shown in Figure 1-2. 1984 trajectories require typically 750 or 1100 days with low-thrust propulsion continuing during most of the transfer phase. Propulsion during the last several hundred days prior to arrival is critical to matching the comet's orbital velocity and to achieving rendezvous. Terminal guidance corrections can be executed conveniently during this phase, facilitated by the low approach velocity. After zero velocity rendezvous the spacecraft will maneuver in a flexible manner on command from earth to search for and explore the nucleus, coma and tail. Residence time near the comet will be about

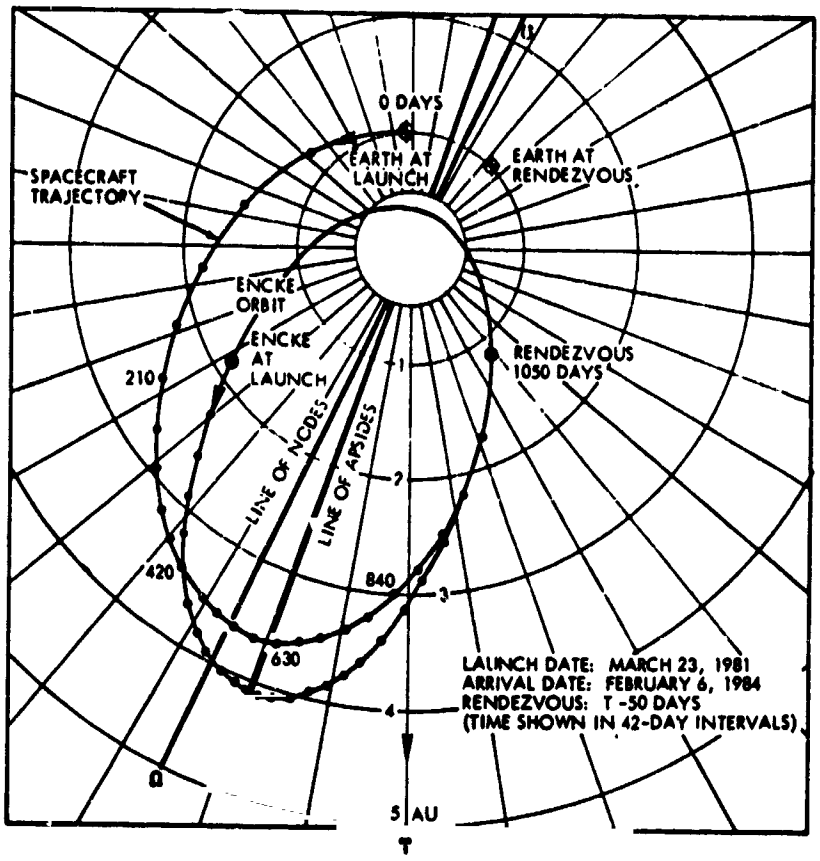

Figure 1-2. Typical 1984 Encke Rendezvous Trajectory Profile

100 days but can be extended if desired. This permits in-situ observation of the comet through perihelion and perhaps all the way to aphelion.

In summary, compared with ballistic flythrough the rendezvous mission profile offers the following principal advantages:

- Flexibility of the mission profile, in terms of the departure and arrival dates and the shape of the transfer trajectory.
- Extended residence time at the comet for hundreds of days, if desired.
- Large excursions for systematic mapping and exploration of the comet's head and tail.
- Ability to search for, rendezvous with, and hover in close vicinity of the nucleus, for detailed observation of surface features and measurement of gravity.
- Flexibility of exploration strategy with adaptation to unforeseeable phenomena.

1.6 MISSION CONCEPT OPTIONS

Figure 1-3 summarizes alternative mission options and spacecraft types considered in this study and indicates the preferred concepts selected by us. The selection made at each level is shown in heavy outline with principal criteria for making each choice stated on the right. The following paragraphs briefly describe the selected spacecraft and mission concept. These will be discussed in greater detail in Sections 5 through 7.

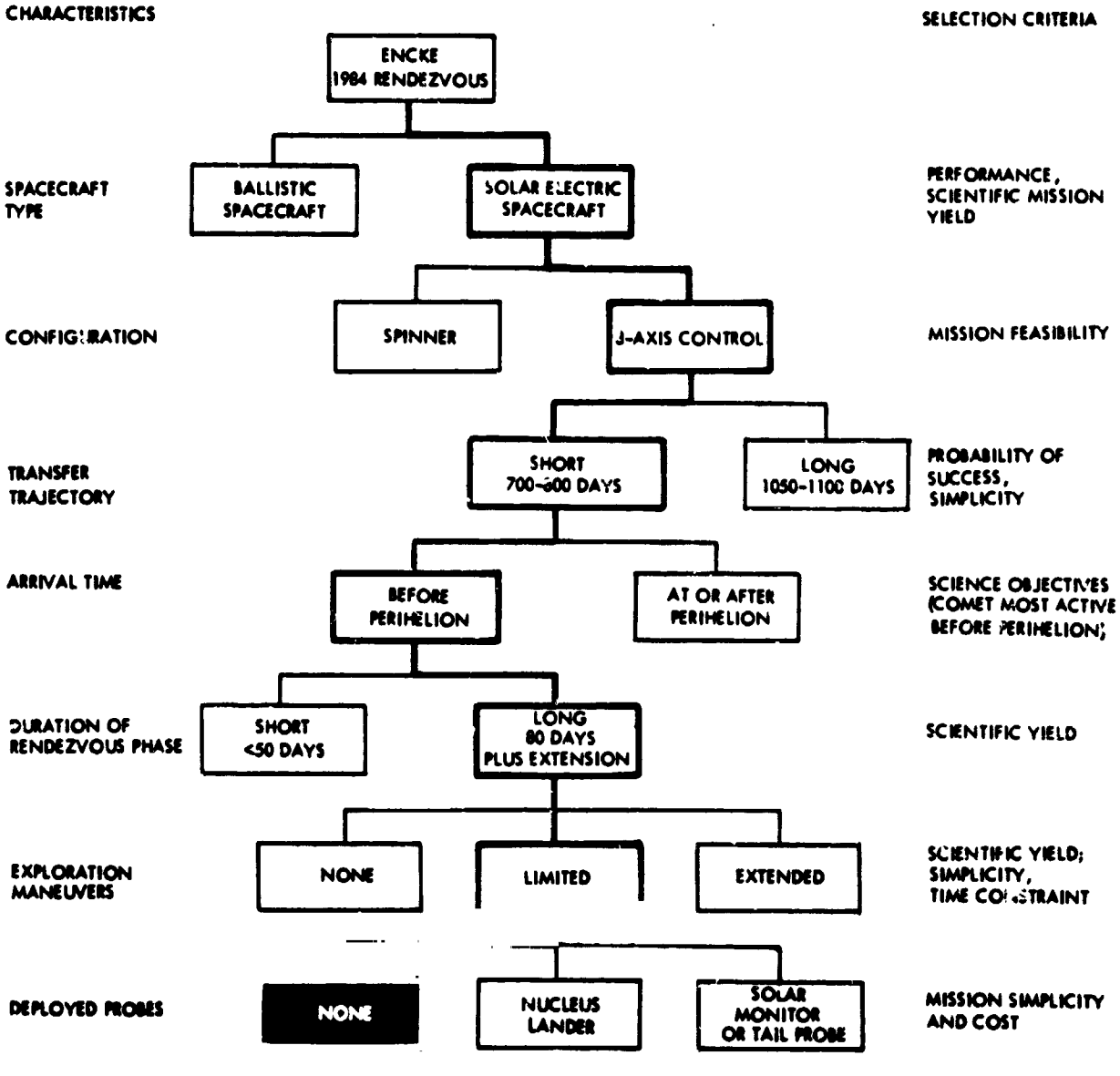

Figure 1-3. Mission Concept Options

1.7 SPACECRAFT CONFIGURATION

Figure 1-4 shows a typical three-axis stabilized spacecraft configuration which may be used for this mission. The same configuration has been proposed by JPL for several other interplanetary missions in the 70's and 80's (Reference 1-5). The solar-electric panels, measuring 40 meters tip-to-tip, can be rotated around their common axis for protection against excessive heating when close to the sun, for unconstrained thrust pointing, and convenient comet observation. The large gimballed parabolic antenna provides unconstrained earth pointing at all times for high-data-rate telemetry at tens of kilobits per second.

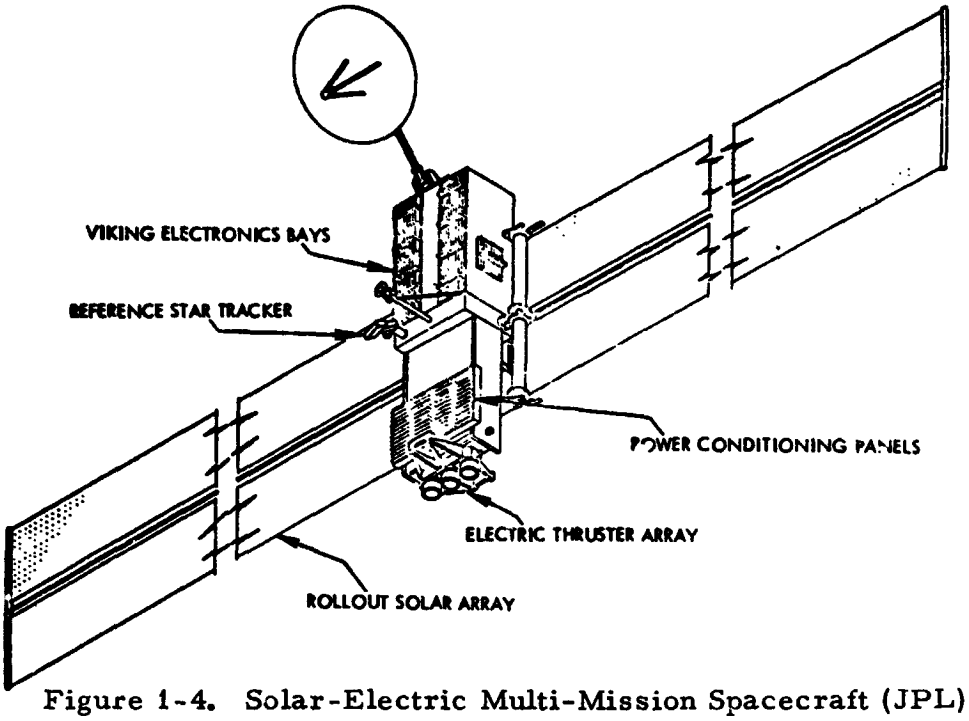

Figure 1-4. Solar-Electric Multi-Mission Spacecraft (JPL)

1.8 SUMMARY OF SYSTEM CAPACITY

The system capacity and the proposed operating modes, deployment and maneuver options, and payload assignments are summarized as follows.

A large payload capacity (fifty to several hundred kilograms, depending on selected solar electric power level) is available for scientific instruments. A portion of the available payload capacity can be

allocated, if desired, to extend stationkeeping and maneuver capabilities rather than to scientific instruments. Payload capacity can also be reduced and propellant loading increased to provide greater flexibility in the choice of departure and arrival dates. Thus a reduction of the transfer time by nearly one year (to gain time for evaluation and use of the results of the earlier Encke flythrough mission) is possible but would reduce the payload capacity by more than 50 percent. Arrival prior to perihelion permits observation of important sun-comet interaction phenomena and correlation with simultaneous observations from earth. Earlier arrival implies reduced performance, for example, an arrival 100 days rather than 50 days prior to perihelion would reduce the payload capacity by 40 to 60 percent.

The large solar-electric power of 10 to 15 kw which becomes available after arrival at Encke can be used for operation of sophisticated payloads, and for high-data rate telemetry. The spacecraft is three-axis stabilized to permit most effective use of solar-electric propulsion. Body-mounted scientific instruments can be pointed over a wide range of view angles unconstrained by solar paddle orientation. A two-axis gimballed scan platform is also provided for convenient pointing of selected instruments.

REFERENCES, SECTION 1

1-1 "Proceedings of the NASA Comet Conference," Univ. of Arizona, Tucson, Ariz., April 8-9, 1970 (in preparation).

1-2 "Proceedings of the Cometary Science Working Group," Yerkes Observatory, Williams Bay, Wisc., June 1971.

1-3 A. L. Friedlander, J. C. Niehoff, J. I. Waters, "Trajectory and Propulsion Characteristics of Comet Rendezvous Opportunities," Report No. T-25, Astro Sciences, IIT Research Institute, Chicago, Ill., for Planetary Programs, NASA, Washington, D. C., Contract No. NASW-2023, August 1970.

1-4 "Comet Rendezvous Mission Study," presented to Planetary Programs, OSSA, NASA Headquarters by Astro Sciences, IIT Research Institute, June 1971

1-5 F. E. Goddard, R. J. Parks, Anthony Briglio, Jr., and John C. Porter, Jr., "Solar Electric Multimission Spacecraft (SEMMS) Phase A Final Report, Technical Summary," Report 617-2, Jet Propulsion Laboratory, Pasadenia, Calif., Sept. 10, 1971.

1-6 "Study of a Common Solar-Electric-Propulsion Upper Stage for High-Energy Unmanned Missions," Volume II, Technical, prepared for NASA/OART, Advanced Concepts and Missions Division, Moffett Field, Calif., under Contract NAS2-6040, TRW Document No. 16552-6007-R0-00, July 14, 1971.

1-7 "Feasibility Study for a SEP Stage and Spacecraft and Integrated SEP Spacecraft, PD72-2, Final Briefing, North American Rockwell Space Division, prepared for Marshall Space Flight Center (MSFC), Huntsville, Ala., Contract NAS8-27360, Jan. 18, 1972.

1-8 "A Feasibility Study of Unmanned Comet and Asteroid Rendezvous and Docking Concepts Using Solar Electric Propulsion (CARD), SP-250-1003, Final Briefing, Northrop Services, Inc., Huntsville, Ala., Sept. 1971.

2. MODEL OF PHYSICAL CHARACTERISTICS OF COMET ENCKE

2.1 PRINCIPAL FEATURES OF ENCKE

Encke has exhibited at one time or another most of the familiar features of comets, the principal exception being a Type II (dust) tail. The comet has appeared as a diffuse object without an obvious nucleus, but a well-developed, bright condensation has also been noted, and a star-like appearance has even been ascribed to the comet's brightest feature. On one occasion (1918) two condensations in the coma were reported.

The tail, when present, has been described as wide (1905), narrow and straight (1914), slightly curved (1914), serpentine (1924), short (1937), and long (1895). Rapid increases or decreases in brightness have been observed, indicating transient variations of the comet's activity, but spectacular dynamic effects common to the comas and tails of larger comets have not been seen at Encke.

One feature which seems to be typical of Encke is an elongated coma, sometimes fan-shaped, but repeatedly having the nucleus located toward the antisolar apex of the eccentric coma. This characteristic of Encke was apparent in January 1961, as shown in Figure 2-1. The nucleus has even appeared detached and separate from the coma (1937). A description of Encke's 1961 apparition given by Roemer (Reference 2-1) includes most of the features seen separately or in partial combinations at other times. She wrote: "Comet Encke was a rather strange looking object during January, as it moved into the evening twilight just before perihelion passage. The nucleus was a quite sharp, though no longer stellar, point at the apex of a fan-shaped coma extending westward several minutes of arc. Early in January a narrow tail developed, and this tail increased both in brightness and in length as time went on."

The approximate positions of Encke and earth at the time of the above observation are shown in Figure 2-2. Westward was sunward of Encke when looking at the comet from earth.

Another consistent characteristic for which Encke is noted is its faintness and featurelessness after perihelion. Generally, after

perihelion it is difficult to recover, even though its distance from earth may not be excessive (see Appendix B). On two occasions, however, in 1921 and 1951, condensations were reported by post-perihelion observers. On individual passes in which a comparison is possible, Encke's brightness has been about one magnitude less after perihelion than before perihelion, for the same heliocentric distance (Reference 2-2).

Since the principal features of Encke are by no means universally observed, it is important in planning or evaluating a mission to this comet to assess the prospects for on-site observation of those main features which give comets their scientific interest. Figure 2-3 displays the orbit of Encke and the positions along the orbit where the appearance of a nucleus or central condensation (N), tail (T), or coma (C) was first reported before perihelion or last reported after perihelion. The observations cover the interval between 1885 and 1951 (Reference 2-3). The symbol 2N indicates the report, in 1918, of two distinct condensations. The target point for the rendezvous of this study, 40 days before perihelion, is denoted by the small black circle just inside the 1 AU distance.

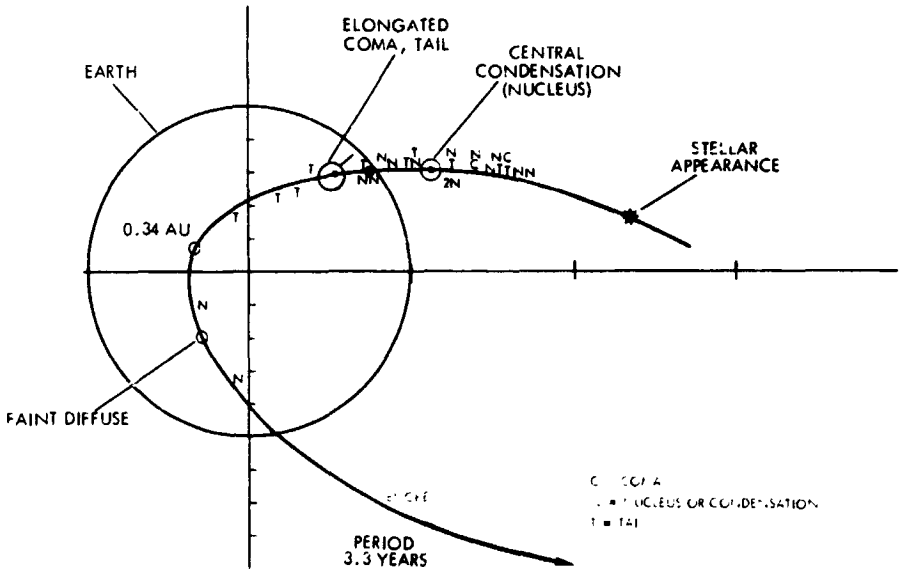

Figure 2-3. Location of First Observation of Encke Features.

On some passes, of course, certain features were not recorded at all. The data show, however, that a "nucleus" was first sighted when the comet was between 0.9 and 1.8 AU from the sun in every case where it was reported. Thus, the chances are excellent that this feature will have been under observation from earth by the time rendezvous is achieved in 1984. Since recovery in the sequence of favorable passes, and generally in recent years, has taken place when the comet was between 1.6 and 3 AU, it seems almost certain that an ionized, gaseous coma is well developed outside of 1.5 AU and that both the coma and its central condensation will be accessible to both earth and spacecraft measurements 40 days before perihelion.

Initial appearance of Encke's tail has often been reported when the comet was between 0.4 and 1 AU. However, the initial appearance has occurred just as often between 1 and 1.7 AU. Overall, the appearance of the tail has been reported less often than appearance of the nucleus. Thus the probability of having the tail in view from earth at the beginning of rendezvous is not high. Observation of the tail, or of tail formation, by the spacecraft while this feature is still invisible from earth may be a valuable contribution of the mission, but any phase of the mission directed at recording tail phenomena will have the best prospect of success if delayed until the comet approaches within, say 0.6 AU of the sun.

This conclusion is reinforced by examination of the possible effect of solar activity on visibility of the tail. In Figure 2-4, all observations of Encke are divided into two classes: those in which a tail was recorded and those in which no tail was recorded. For each class, the number of cases in each 20-unit interval of Wolf annual sunspot numbers, R, has been plotted to form a solid-line histogram (the shading is discussed in a later paragraph). The almost raw information represented in Figure 2-4 does not take into account variations in viewing conditions from pass to pass, but each observational result is associated with the sunspot number for the year of observation rather than the year of perihelion. The graph suggests that high levels of solar activity are more favorable for tail visibility than low levels.

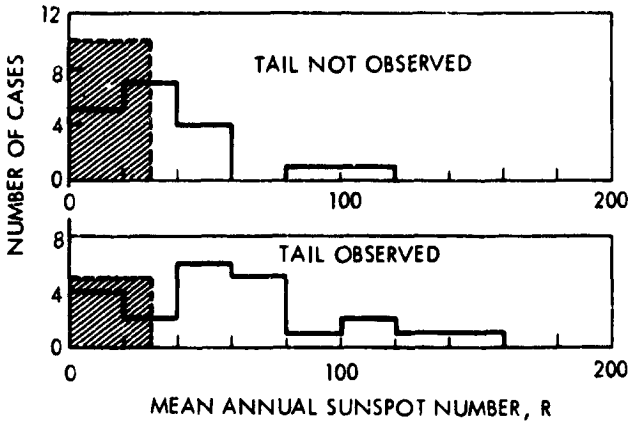

Figure 2-4. Histograms of the Number of Times the Tail of Encke Was Observed or Not Observed, Versus Sunspot Number

According to Biermann and Lüst (Reference 2-4), statistical studies have determined that the existence of cometary tails is independent of solar activity. This is not surprising, since the magnetized solar wind blows continuously. The implication of Figure 2-4, then, is that enhancements in solar activity contribute to raising some property of Encke's tail above a threshold separating conditions of visibility from conditions of invisibility.

This leads to an important conclusion for a 1984 rendezvous, which would take place about two years before the expected 1986 minimum in the sunspot cycle. Figure 2-5 shows the mean sunspot curve shifted on the time axis to represent the next sunspot cycle, with the intervals of hypothetical 1980 and 1984 rendezvous with Encke indicated on the graph. From the figure, the average annual sunspot number of 1984 can reasonably be set at less than 30. The shaded boxes (dashed outlines) in Figure 2-4 represent the respective numbers of observations for $R < 30$. The number of apparitions of Encke with no tail outweighs the number of apparitions with a tail 2 to 1 in this range of R. It follows that tail activity should be at minimal levels during the proposed mission. Visibility of the tail from earth will therefore be unlikely for any comet position, based on these data.

The correlation of Encke's features with sunspot numbers was statistically evaluated by Whipple and Douglas-Hamilton (Reference 2-5). The results showed that the tail of Encke is observed predominantly when

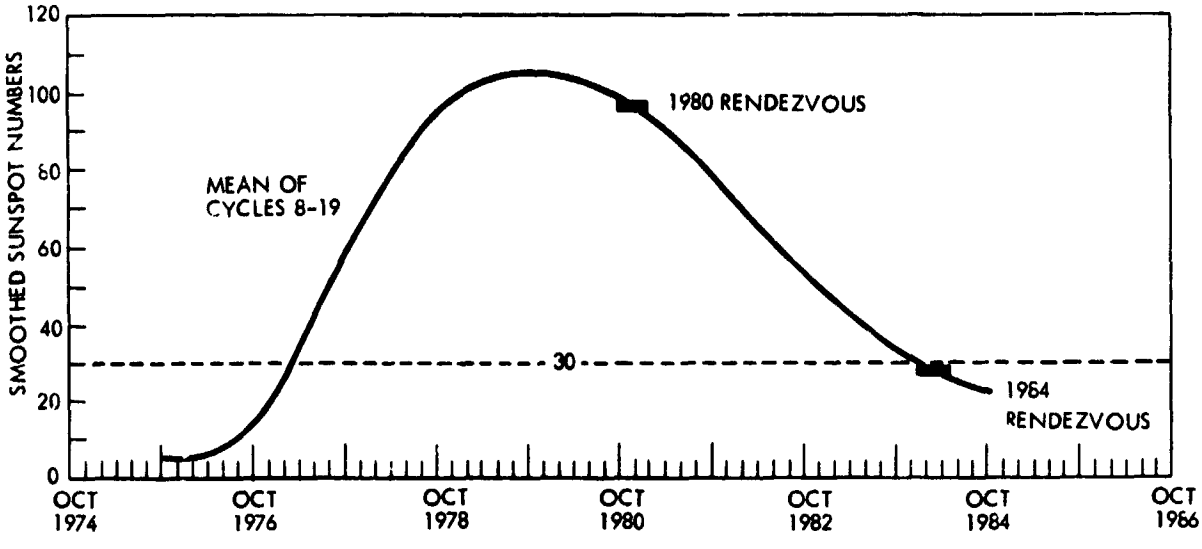

Figure 2-5. Occurrence of Prospective 1980 and 1984 Rendezvous Missions with Respect to the Sunspot Cycle

sunspot numbers are higher than the median and that the "nucleus" tends strongly to be recorded when the tail is also recorded. A third correlation showed independently the tendency for the "nucleus" to be noted at times of enhanced solar activity. However, the possible effect of Encke's highly variable visibility (Section 2.7.1) on the sunspot correlations was not evaluated by Whipple and Douglas-Hamilton either. The effect could be significant, and Whipple (conversation 1972) has stated his belief that the correlation with solar activity is in reality a correlation with Encke's optical accessibility from earth and that the evidence does not establish a clear physical connection with sunspot numbers. One implication is clear if these solar activity correlation studies are valid: Most recorded apparitions of the nucleus have, in fact, been enhancements of a central, bright cometary feature made visible by heliogenic processes affecting the material of Encke's atmosphere and were not images of the nucleus at all.

An isolated solar event, or series of events, which can occur during solar minimum, might activate the tail and "nucleus" during an extended rendezvous. The earth will have at least the western side of the disc (from Encke's view) in sight as the comet approaches perihelion. If the tail, or condensation, does become visible, there is a fair chance that a preceding solar event will be noted and coordinated measurements

obtained. The chances of this occurring will improve steadily as Encke moves in closer than 0.6 AU from the sun. When Encke is at 0.6 AU, the central meridian from the comet's view will be roughly the east limb from the earth's view. Of course, locally the comet may be expected to respond primarily to long term, relatively stable solar wind features, such as sector boundaries. These features can be monitored with some confidence at or near earth assuming they have previously corotated past the comet.

2.2 DIMENSIONS OF ENCKE'S FEATURES

Like those of most comets, the dimensions of Encke are conjectural at best. The only values that can be attached to individual features are limits or ranges based on apparent sizes obtained with varying observational difficulty. Part of the uncertainty stems, of course, from the intrinsic mutability of the coma and tail. Only the nucleus may be thought of as having a definite size at all.

2.2.1 Nucleus

The nucleus cannot be resolved as an object of distinct outline by telescope from earth, but reasonable limits to its dimensions can be derived from analysis of the way the brightness of its reflected light varies with solar distance. That portion of the comet's light which is reflected from the nucleus should be identifiable by its inverse square rather than inverse fourth power dependence on heliocentric distance r. Unfortunately, it is difficult to resolve the contribution of the nucleus to the comet's image, as the preceding discussion indicates. In measuring the brightness of the nucleus, one must distinguish the faint, stellar-appearing nucleus from the much brighter coma. The distinction has been attempted in recent years with telescopes of large aperture and of long focal length. With such instruments, it is possible in some cases to show that the central star-like condensation follows an asteroidal law: brightness $\propto 1/(r^2 \Delta^2)$, where r and Δ are the heliocentric and geocentric distances of the comet, respectively. In these cases, it is plausible to interpret the measurements as referring to a small body of constant radius (the nucleus). Following this interpretation the radius of the nucleus can be calculated, assuming a value for the albedo, and a plausible phase function. This was done by Mianes, Grudzinska, and

Stanikowski (Reference 2-6) for P/Encke and P/Giacobini-Zinner, and later by Roemer (Reference 2-7) for Encke as part of a more general comet survey.

The actual dependence of magnitude on heliocentric distance for Encke's "nucleus" is not, even in the best data, strictly asteroidal. Indeed, some asteroids follow the r^{-4} brightness law. (Reference 2-8.) It remains difficult to separate phase and distance effects, and efforts are still being made to isolate these factors (Roemer, Marsden, private communications). The magnitude estimates used by Roemer are reasonably close to a variation with r^{-2}, certainly far better than the $r^{-3.3}$, r^{-4} dependence typically ascribed to Encke's magnitudes, and probably represent an approximation to true data on the nucleus itself, subject to qualifications treated in Section 2.7.

In computing radii from the magnitude estimates, Roemer followed the analysis:

$$H_N = H_\odot - 5 (\log R_N - \log r - \log \Delta) - 2.5 [\log A + \log \phi(\theta)].$$

where the magnitude of the sun, $H_\odot = -26.72$, and

r = heliocentric distance of the comet (in AU),

Δ = geocentric distance of the comet (in AU),

R_N = radius of the cometary nucleus (in AU),

A = the (geometric) albedo

$\phi(\theta)$ is the phase function, according to Lambert's law.

The result of the calculation is $AR_N^2 = 0.24$, giving the radius versus albedo dependence of Figure 2-6. The albedo was assumed to lie between limits of 0.02 and 0.7. The former value corresponds to material having the reflectivity of the blackest asteroids (Reference 2-9), and may be compared with the value of ~0.03 for some carbonaceous chondrites, the blackest extraterrestrial material known. The 0.7 value corresponds to that of H_2O solids and to Venus. Corresponding to these limits of A, the radius of Encke was found to lie between 0.6 and 3.5 km.

An intermediate value of A = 0.1, roughly the albedo of the moon, gives a radius of 1.6 km. (Reference 2-7.) The probable range of R_N, indicated by shading in Figure 2-6 is based on the concept of Encke's nucleus as a dying, asteroid-like object of low albedo (see Section 2.3).

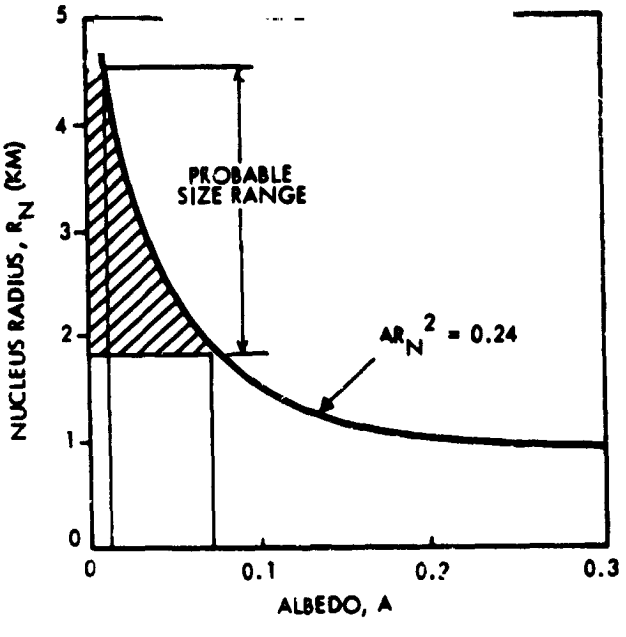

Figure 2-6. Inferred Size of Nucleus Dependent on Assumed Albedo

Additional photometric work by Roemer for the same range of albedos on 19 periodic comets and 10 nearly parabolic comets showed that these values of the radius are typical of periodic comets, although a few (e.g., Otema) are significantly larger. Nearly parabolic comets are typically about twice as great in radius; some (e g., Humason and Wirtanen) appear to be very large. However, it is possible that these comets are only apparently very large, their great brightness being at least in part a result of their possessing an unusually high albedo or an optically thick atmosphere or halo.

2.2.2 Coma

The diameter of the coma is decidedly variable In Vsekhsvyatskii's compilations (Reference 2-3)*, there are thirty-seven instances, from 1848 to 1964, in which the observational data on apparent diameter of Encke have been evaluated and normalized to produce an estimated

*See also Appendix J.

" reduced head diameter D_1 (corresponding to Δ = 1 AU) ... averaged over a certain time inverval". Δ is the symbol used for earth-comet distance; D_1 is given in minutes of arc. The interval and the number of measurements contributing to each determination of D_1 are unspecified.

Figure 2-7 is a histogram of all the values of D_1 given by Vsekhsvyatskii, converted to kilometers. In some cases, ranges of D_1 were given, and the two extremes of each range were counted as separate items, so there are more than 37 entries (actually 51) contributing to the histogram. It is obvious that the bulk of observations (65 percent) has given an observable coma diameter of 25,000 to 125,000 km. The most probable range of diameters is 75,000 to 100,000 km. This range is most probable in a special sense for the rendezvous mission because the apparent size of Encke is dependent on its solar distance, and it is at rendezvous distance ($\lesssim$ 1 AU) that the comet is commonly measured in this range. All but one of the values above 1.4×10^5 km were observed when the comet was beyond 1 AU.

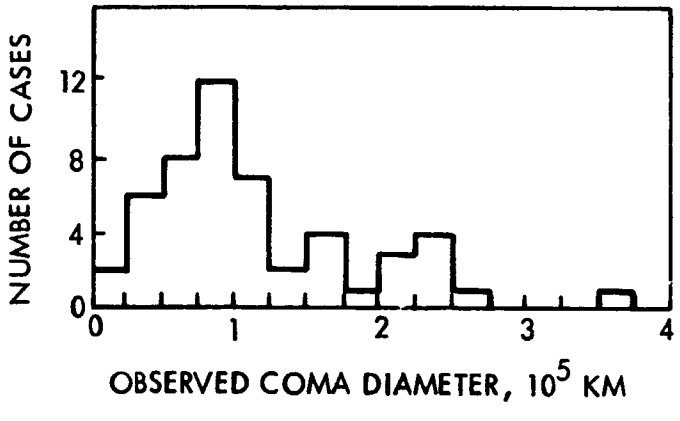

Figure 2-7. Histogram of Coma Measurements Give a Probable Diameter less than 10^5 km for Encke's Coma.

Encke's well-known dependence of D_1 on solar distance r is shown in Figure 2-8(a), where all preperihelian measurements have been plotted from which Vsekhsvyatskii's compilation gives a date or distance associated with the reduced diameter. In some cases, distances or diameters, or both, are seen to have broad ranges. The direct trend with distance is

apparent, but considerable scatter is present. Much of the scatter is undoubtedly introduced by the variability of Encke's absolute size. The strength of the diameter's dependence on distance is more clearly demonstrated in Figure 2-8 (b), where pairs of distance-diameter combinations obtained on three individual passes spanning a century are distinguished from each other.

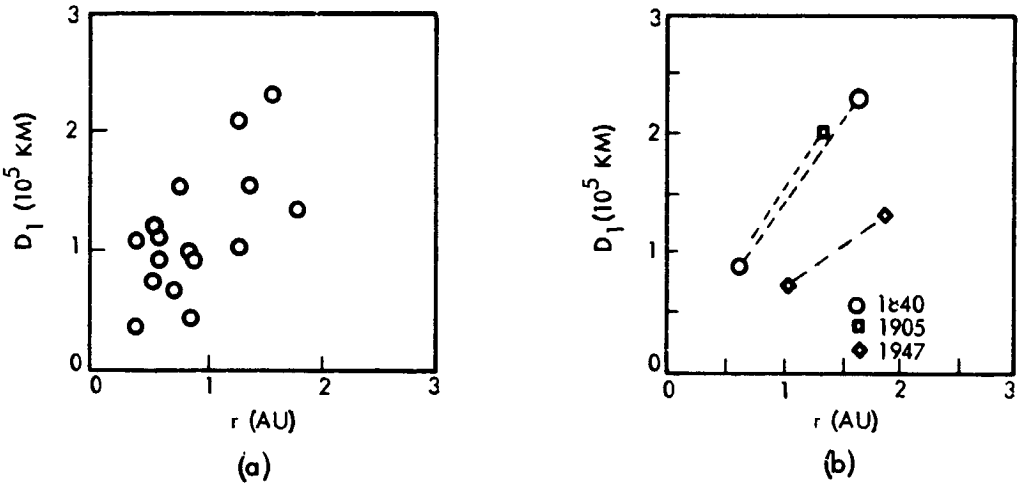

Figure 2-8. Dependence of Coma Size on Heliocentric Distance

The shrinking of the coma with solar approach is consistent with behavior expected from theoretical considerations. According to one point of view, the visible diameter of the whole coma is proportional to the initial (thermal) expansion velocity of the gases, w, and the photodissociation time τ_d. If w depends on temperature as $T^{1/2}$ and $T \propto r^{-1/2}$, then $w \propto r^{-1/4}$. The dissociation time τ_d depends inversely on solar radiation, which increases with diminishing r, so $\tau_d \propto r^2$. It follows that D_1 should increase or decrease as r increases or decreases:

$$D_1 \propto (w)(\tau_d) \propto r^{-1/4}\, r^2 = r^{7/4}.$$

In Delsemme's picture of coma formation, the inner coma contains an icy halo from which gases are emitted. (Reference 2-10.) The halo itself contracts with solar approach because increasing solar radiation reduces the vaporization time of the icy grains (Reference 2-11). The observed coma size behavior probably results from a combination of both effects.

2.2.3 Tail

The tail of Encke has been highly erratic in observability. Moreover, the apparent relationship between its visibility from earth and solar activity implies that dimensions of the visible part of the tail may have little to do with size of the tail itself. Figure 2-9 is a histogram of tail lengths. Clearly, the range of measured lengths is extreme, but most estimates have been below 10^6 km. The two high values were obtained when annual sunspot numbers were over 60. If actual tail length is proportional to visible tail length, the relatively low solar activity expected in 1984, which may leave the tail unobserved from earth, suggests that values well under 10^6, say (1-2) x 10^5 km, may be appropriate for that epoch. Maneuvers to carry a spacecraft into the tail need not provide extreme excursions in the antisolar direction from the comet.

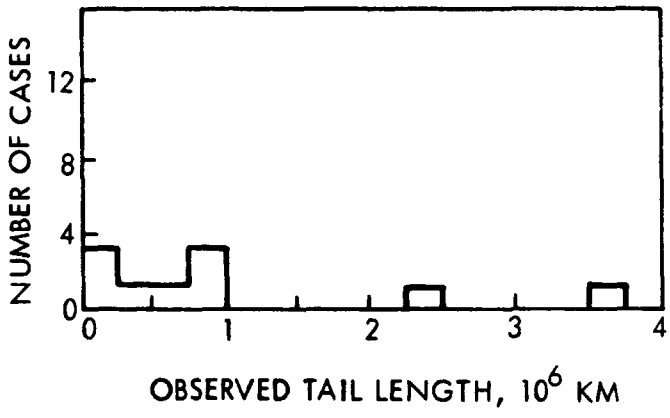

Figure 2-9. Histogram of Tail Measurements Giving a Probable Length Less than 10^6 km for Encke's Tail.

No comparable measurements of tail diameter have been made. Theoretical considerations of tail formation, discussed in a later section, suggest that the diameter should be between 10^3 and 10^4 km, at least near the coma.

2.3 THE NUCLEUS OF ENCKE'S COMET

Direct, observational data on cometary nuclei consist only of photometric measurements as a function of distance from the sun (preceding paragraphs; Reference 2-7). Further information concerning the nucleus of the comet depends upon inferences based on observations of the coma and tail, which are composed of material emitted from the nucleus, and from studies of meteoroids derived from cometary nuclei (References 2-12, 2-13, and 2-14). It is possible that some meteoritic material, certain carbonaceous chondrites (C1 in the classification of Van Schmus and Wood, Reference 2-15), for example, are derived from the nuclei of comets (Reference 2-16). It is also possible that some asteroids, notably Icarus, are dead comets so that further study of them might be directly applicable to cometary research.

Studies of the comas and tails of comets indicate that not all cometary nuclei are identical. It is possible that cometary nuclei represent a uniform type of object initially, but exhibit different stages of a rapid evolution (time scale ~100-1000 periods) having been subject to relatively recent exposure to solar radiations. It is also possible, of course, that there really are fundamentally different types of comets reflecting differences in their formational processes, which probably took place $4.5 - 4.6 \times 10^9$ years ago. A long-range priority goal of cometary investigations, both earthbased and from spacecraft, is to obtain data bearing on these possibilities and thereby increase our understanding of processes during the formation interval of the solar system.

Inferences based on studies of the coma and tail, and of meteoroids, place considerable constraints on possible nuclear models of Encke. The model presented here is eclectic, based on the observations and ideas of numerous workers, and the references provided are meant to be helpful rather than complete. The obvious uncertainties in the model may provide some additional incentive to further earthbased study of Comet Encke prior to the actual planning and payload selection of an Encke mission, thereby increasing the scientific information obtainable.

2.3.1 Evolution of a Typical, Periodic Cometary Nucleus

The peculiar changes in periodic comets led to a general model of their evolution. The following is quoted from Sekanina, Reference 2-17, but with the appropriate figure number changed to refer to Figure 2-10.

> "The evolution of the nucleus of the suggested "core-mantle" model is schematically represented in Figure 2-10. Owing to intense heating of the surface of the nucleus during possibly thousands of approaches to the sun, the icy envelope, originally of considerable thickness (Figure 2-10(a)), gradually sublimates, the radius of the nucleus shrinks (Figure 2-10(b)), and after some time the underlying nonvolatile core becomes exposed to the direct effects of solar rays (Figure 2-10(c)). In the subsequent development, molecular desorption from the unprotected core's surface replaces free sublimation in producing the comet's atmosphere, the transfer of volatiles from the core's interior to its surface being provided by activated diffusion. The ability of the nucleus to regenerate sufficient icy materials at the surface is gradually weakened with time (Figure 2-10(d)), and finally the whole reservoir of volatiles is completely exhausted (Figure 2-10(e)). The model comet becomes a "dead" body.
>
> We believe that Figure 2-10 gives a general idea of the possible development of the nucleus of a typical short-period comet, though the above description is extremely simplified. To create a more realistic model, we should, for instance, assume a nonvolatile constituent with mass density and tensile strength increasing and porosity decreasing toward the center of the nucleus, and understand the surviving deactivated core as only a portion of the original solid matrix having sufficient tensile strength to withstand the pressure of the ejected gases. This and similar refinements, however, do not change the principal character of the model."

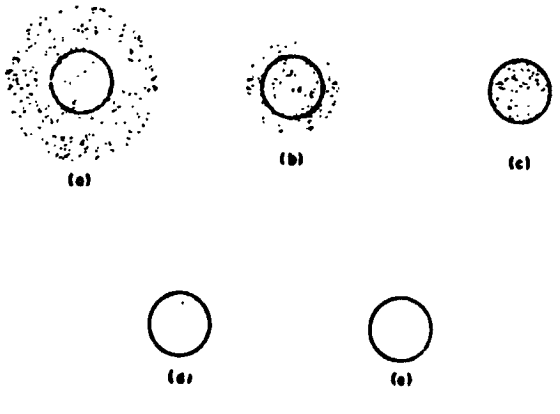

Figure 2-10. Typical Evolution of Icy Conglomerate Nucleus. Suggested evolution of the core-mantle model: dotted areas show the distribution of ices; empty area within the circle marks the presence of nonvolatile material only.

The model sketched above is complex in application. For example, the secular acceleration is affected by the phase lag of maximum outgassing as well as by the amount of outgassing. (Marsden, Reference 2-18, has deduced that for several comets the phase lag is of the order of 6 degrees.) The phase lag must in turn be controlled by the rate of rotation, lack of spherical symmetry, and the structure of the outer layers of the nucleus, but it is difficult to include the variations of these quantities with time in any reasonably simple model. Despite such shortcomings, the interpretation of nongravitational forces in terms of the icy conglomerate model seems to have been successful. In particular, it provides an explanation for the characteristics of the orbit of Encke without invoking an encounter with one of the inner planets. Sekanina, Reference 2-19, showed that the aphelion distance of Encke must have decreased at the rate of 1 AU/10^4 years as a result of nongravitational forces; hence it is reasonable that it was originally brought into the inner solar system as a result of encounters with Jupiter.

2.3.2 Evidence for the Evolution of Encke's Nucleus

2.3.2.1 Decline in Magnitude

The mean absolute magnitude of Encke has declined noticeably since 1786, when it was first observed. Figure 2-11 shows the secular change in the absolute luminosity of Encke for forty apparitions, in terms of the residuals during each apparition, for two models of distance dependence: a) $H_{10}(1/r^4\Delta^2)$ and b) $H_{10'}(1/r^4\Delta)$, where r and Δ are the solar and geocentric distances in AU. The solid curves through the observed points are obtained from a simple theory of the secular brightness changes (Reference 2-5). Figure 2-12, abstracted from a figure of Vsekhsvyatskii and Il'ichishina (Reference 2-20), shows a second version of the change in magnitude (decrease in brightness) from $m \approx 6$ to $10 \lesssim m \lesssim 14$ for the entire 185 years. Figure 2-11 suggests that the comet will die (i.e., lose its cometary characteristics) during 1990-2000, but as is evident from the figures the agreement between model and observations is fairly rough. Indeed, Sekanina, Reference 2-17, in a more careful analysis, deduces that the "death date" will be 2030. However "death" is misleading; it might be argued that we are witnessing the "birth" of a minor planet, or Apollo-like asteroid, and it is perhaps in this respect that Encke is most interesting.

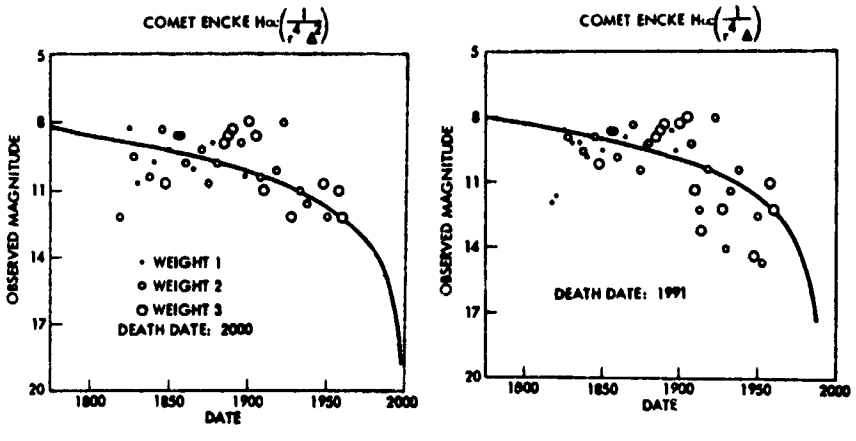

Figure 2-11. Decay of Encke's Magnitude with Time for Two Brightness Versus Distance Dependences

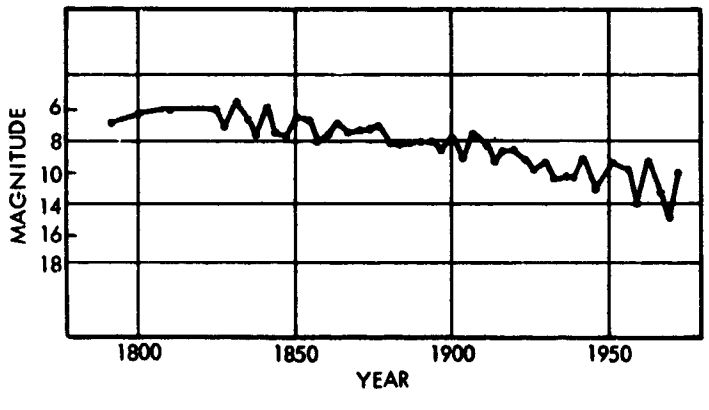

Figure 2-12. Decline of Encke's Absolute Magnitude with Time

2.3.2.2 Nongravitational Forces

Encke's was the first comet to show evidence for secular acceleration, and it was suggested by Encke himself that a nongravitational process might be involved (Reference 2-21). These observations have been subsequently confirmed by numerous workers, and in fact Encke's behavior was the inspiration for the general (icy conglomerate) model.

The nongravitational effect was at first attributed to motion in a resisting medium, but later work (References 2-22 and 2-23) favored an interpretation in terms of reactive forces, associated with the ejection of cometary matter (covered in next heading). Similar effects have been reported for many other comets. The most complete and recent study is described in a series of three papers by Marsden, References 2-8, 2-18, and 2-24, and a fourth by Marsden and Sekanina, Reference 2-25. In the first of these papers it is definitely established that the nongravitational acceleration of Encke was 0.04 day/period for the interval 1947-67. The second paper contains the results of computations in which nongravitational forces of assumed form were explicitly included in the equations of motion of many comets besides Encke, and solutions to the equations were found whose orbital elements yielded the smallest residuals when fitted to observational data. A continuous, rather than impulsive, force was assumed, that increased exponentially with decreasing heliocentric distance and decreased exponentially with time. The nongravitational force was introduced with its full three components, F_1, F_2, F_3 in a rotating frame, the first radially outward, the second in the orbital plane normal to the first and positive in the direction of the comet's velocity vector, and the third normal to the orbital plane and positive in the right-handed sense with respect to the other two (northward). For most comets, F_1 and F_2 are positive, with $F_1/F_2 \approx 10$, i.e., with a net force outward and about six degrees from the radial and in the forward direction of motion. For Encke, the best solution for the in-plane forces (smallest residuals) give negative values for both F_1 and F_2, with $F_1/F_2 \approx 5/3$. This implies a net nongravitational force pointing toward the sun and opposing the orbital velocity, 194 degrees to 210 degrees from the outward radial (counterclockwise, looking down from north of the orbital plane). The out-of-plane component was found to have no significant effect on the residuals, but inclusion of the long-term time dependence of the forces was necessary to maximize the agreement with observation.

Although the solutions just described gave a good formal fit of the orbital elements to observed parameters of Encke's trajectory, projection of the trajectory backward in time gave cumulative, systematic disagreements with measurement. The third paper of the series (Reference 2-24) describes a still more elaborate force function having a double-exponential

time dependence. Application of this form removed some of the systematic error. Examination of various sets of solutions for the nongravitational forces (in both References 2-18 and 2-24) showed that while the "transverse" force F_2, remained fairly steady from set to set, the radial component F_1 was not so reproducible, even becoming positive in one case. Recent unpublished work (Marsden, private communication) has shown considerable historic variation in the apparent radial component, although the two solutions of the most recent years, based on the most reliable data available, have been consistent and have yielded a positive F_1. In sum, the radial component is not well determined, but, very importantly, it is definitely not outward and ten times the transverse component, as for other comets, so that the angle of the net force to the radial direction is probably not as small for Encke as for most comets studied by Marsden.

In the fourth paper of the series (Reference 2-25) some additional inferences about the composition and nature of the nongravitational forces are drawn, based on a physical model of forces developed by Sekanina, Reference 2-17. One important quantity is an isotropy factor λ, which is a measure of the net unidirectional force on the nucleus caused by the center of most of the escaping gas. Essentially, λ is the fraction of escaping mass emitted in the direction of escape of the center of mass of emitted gas. Perfectly isotropic emission would yield no net force and would correspond by definition to $\lambda = 0$; perfect anisotropy, i.e., emission from a restricted region of the nucleus all in one direction, would correspond to $\lambda = 1$. An anisotropy caused by vaporization proportional to solar insolation* would have $\lambda = 0.44$. The paper of Marsden and Sekanina (Reference 2-25) quotes a recent estimate of Sekanina's that, for Encke, $\lambda \approx 0.3$, as if 30 percent of the mass emitted from Encke's nucleus were lost in a single direction, thus providing the thrust responsible for its nongravitational force. The value $\lambda = 0.3$ was derived on the assumptions of constant emission at 600 m/sec and of a large ratio of transverse to radial force components. The authors concede that the actual value of λ is "very uncertain."

*Insolation synonymous with incoming solar radiation flux.

2.3.2.3 Nonvolatile Component of Encke's Nucleus

Evidence for the presence of nonvolatile compounds in cometary nuclei is provided by the dust tails often associated with new and long-period comets (Reference 2-13) and by the presence of reflected solar continuum in the spectrum of the comas and tails. A spectrum of Encke showing continuum at 0.76 AU, before perihelion in 1947, appears in the Atlas of Representative Cometary Spectra, Plate 16, University of Liège and Astrophysics Institute (1955), compiled by Swings and Haser. For this comet, the ratio of the intensity of the 5165Å C_2 band to the continuum is >5 at a solar distance of 0.68 AU, whereas at the same distance the nearly parabolic comets Arend-Roland and Mrkos had a corresponding ratio of 2.0 (Reference 2-26). The dust component of Encke's coma is thus very weak. However, the Taurid meteors, which are derived from Encke at some rather uncertain time in the past, are relatively rigid structures, show practically no fragmentation, but have average mass-luminosity properties (References 2-27 and 2-28). This represents evidence for the former presence of relatively nonvolatile substances in the nucleus of this comet, and it is assumed that a residual nonvolatile component is still present.

2.3.3 Model of the Nucleus

The evidence discussed above leads to the following tentative model of the nucleus of this comet, based fundamentally on the icy conglomerate model of Whipple, Reference 2-23 (1951) and its more recent extension by Marsden and Sekanina, Reference 2-25, and by Sekanina, References 2-17, 2-29 and 2-30, as quoted earlier. Models of this general kind appear most suited to explain the diversity of phenomena observed in Encke's comet as well as others i.e., models of gas loss from icy nuclear component. The nucleus is viewed as an icy conglomerate of meteoric, or lithic, matter mixed with, or containing a mantle of, frozen gases, mostly water-ice or clathrite components. Whipple, Reference 2-23, showed that the secular acceleration can be accounted for on the basis of mass loss from a rotating, icy-conglomerate nucleus. An attempt to describe the secular change of the magnitude in terms of the icy conglomerate model of comets was made subsequently by Whipple and Douglas-Hamilton (Reference 2-5).

2.3.3.1 The Residual Core

The weakness of the continuum radiation from Encke suggests that relatively little solid material is being ejected by the comet, in contrast to younger comets, as described by Sekanina. The peculiar asymmetric behavior of the gaseous coma of Encke with respect to its brightness before and after perihelion passage also appears to be consistent with the idea that most of the small-sized, loose solid material has long been lost and that the nucleus now consists of a relatively stable, but porous, non-volatile core surrounding or containing an icy-conglomerate component. There is a fair probability that, in fact, Encke is evolving into an asteroid very much like Icarus.

Thus, comet Encke is a highly evolved comet of the core-mantle type which may originally have consisted of a mantle of volatiles and dust particles overlying a porous core consisting primarily of nonvolatile meteoric material, possibly similar to type 1 carbonaceous chondrites, but also containing ices of volatile materials within pores and crevices of the core. These ices primarily consist of H_2O, probably containing other more volatile materials as clathrates. In the case of Encke, the mantle has been lost by sublimation due to solar radiation, and the residual activity of this comet requires the migration of volatile material to the surface before it can be emitted into the coma. In such a model the surface is presumed to be steadily supplied with volatiles which condense following sublimation from the core; the temperature of the surface and its condensations varies greatly along the orbit, and on approaching the Sun it becomes sufficiently high for the evaporation rate to be so enhanced as to exhaust the immediate supply of condensed volatiles. We must be prepared to take this feature of Encke into account in interpreting observations obtained from a rendezvous mission in terms of general cometary characteristics.

The model assumes the nucleus to be rotating about an axis normal to the plane of its orbit. In this orientation, the nucleus is exposed to the sun's rays equally before and after perihelion, so the only explanation possible for its unequal magnitude before and after perihelion is depletion of volatile materials on the surface during the inbound journey. If the

spin axis were in an arbitrary direction, not necessarily normal to the orbit plane, the comet's asymmetric behavior with respect to perihelion might imply an irregular, nonuniform surface which exposes an accumulation of volatiles to the sun inbound, but shadows the pocket outbound. Attempts to separate inbound and outbound nongravitational forces have not yielded a positive result, largely because post-perihelion data on Encke are of poor quality (Marsden, private communication). This "orientation' explanation of Encke's visual behavior would modify, but not necessarily exclude, the hypothe s of migrating volatiles.

2.3.3.2 Mass Loss

Sekanina, References 2-17 and 2-19, developed a formula relating the mass loss $\Delta M/M$ to the nongravitational forces. His careful analysis indicated that the mass-loss rate for a typical comet must be of the order of 0.01-1 percent of the total mass per revolution. For Encke, the average mass-loss rate during the last 40 years is estimated to be 0.03 - 0.7 percent per revolution, assuming the gas leaves the surface of the nucleus with a mean speed in the range 220-500 m/sec^{-1}. Indeed, $\Delta M/M$ for Encke has been calculated as a function of time (Sekanina, Reference 2-19), with the result that $\Delta M/M$ has decreased from 0.24 to 0.03 percent per revolution between 1800 and 1967. Marsden and Sekanina, Reference 2-25, give $\Delta M/M \approx 0.03$ percent for the 1967 pass.

The variation of Encke's "nongravitational parameter" (κ) versus time is shown in Figure 2-13 (from Reference 2-17) and mean values of both κ and the mean absolute magnitude (H_{10}) for short periods are given in Table 2-1 (Reference 2-19). The curves of Figure 2-13 represent theoretical formulas for the acceleration (due to mass loss) κ appearing in Sekanina's paper. At the present time the nongravitational effects on Encke appear to be regular hence predictable, rather than erratic as is the case for other comets, e.g., Schaumasse.

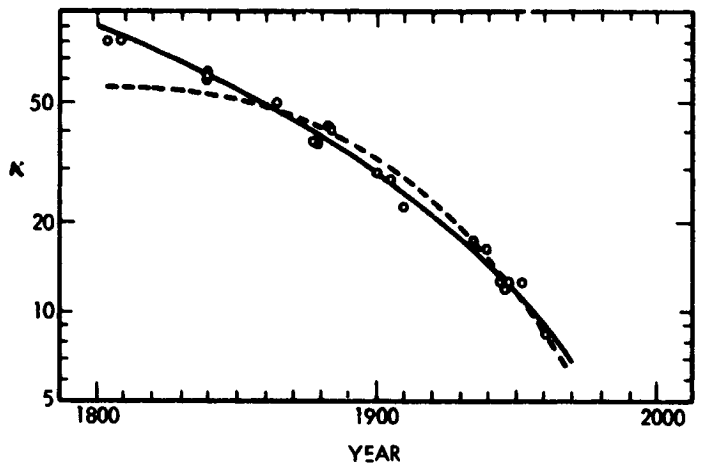

Figure 2-13. Nongravitational Acceleration κ (Seconds per Orbit) Versus Time

Table 2-1. "Dynamical" and "Photometric" Mass Loss Rates and Their Effective Ratio (R) for Encke During 1786-1967

Comet	q (AU)	e	Apparitions	κ	H_{10} (mag)	ΔM_{dyn} (grams)	ΔM_{phm} (grams)	log R
Encke	0.34	0.847	1786-1819	+79.8	8.3	$9.3.10^{13}$	$1.1.10^{11}$	2.91
			1819-1838	+58.0	8.5	$6.7.10^{13}$	$9.9.10^{10}$	2.83
			1819-1848	+58.7	8.6	$6.8.10^{13}$	$9.2.10^{10}$	2.87
			1829-1848	+63.3	8.8	$7.4.10^{13}$	$7.8.10^{10}$	2.97
			1819-1858	+60.0	8.7	$7.0.10^{13}$	$7.9.10^{10}$	2.94
			1858-1868	+50.0	8.9	$5.8.10^{13}$	$6.6.10^{10}$	2.94
			1868-1885	+37.3	9.5	$4.3.10^{13}$	$3.8.10^{10}$	3.06
			1871-1881	+32.4	9.6	$3.8.10^{13}$	$3.5.10^{10}$	3.04
			1871-1885	+36.5	9.7	$4.2.10^{13}$	$3.4.10^{10}$	3.09
			1868-1895	+42.0	9.5	$4.9.10^{13}$	$4.0.10^{10}$	3.08
			1871-1895	+40.6	9.5	$4.7.10^{13}$	$3.8.10^{10}$	3.09
			1895-1905	+29.5	9.7	$3.4.10^{13}$	$3.2.10^{10}$	3.03
			1898-1911	+27.2	10.1	$3.2.10^{13}$	$2.3.10^{10}$	3.15
			1905-1914	+22.5	10.2	$2.6.10^{13}$	$2.0.10^{10}$	3.11

Table 2-1. "Dynamical" and "Photometric" Mass Loss Rates and Their Effective Ratio (R) for Encke During 1786-1967 (Continued)

Comet	q (AU)	e	Apparitions	κ	H_{10} (mag)	ΔM_{dyn} (grams)	ΔM_{phm} (grams)	log R
			1924-1934	(+22.8)	11.3	$(2.6.10^{13})$	$7.2.10^{9}$	(3.56)
			1931-1937	+15.4	11.1	$1.8.10^{13}$	$9.1.10^{9}$	3.29
			1931-1947	+16.3	11.3	$1.9.10^{13}$	$7.9.10^{9}$	3.38
			1937-1951	+12.4	11.1	$1.4.10^{13}$	$9.1.10^{9}$	3.20
			1937-1954	+11.9	11.3	$1.4.10^{13}$	$7.3.10^{9}$	3.28
			1947-1957	+12.6	11.1	$1.5.10^{13}$	$8.9.10^{9}$	3.22
			1947-1967	+10.9	11.8	$1.3.10^{13}$	$4.3.10^{9}$	3.42

2.3.3.3 Radius, Mass, and Gravity

Marsden and Sekanina have re-evaluated Roemer's (Reference 2-7) calculation of the radius of Encke by using a phase function more appropriate to the unmantled core of meteoric material than Lambert's law, as assumed by Roemer. Their assumption of a geometric albedo of 0.1 leads to a radius of 1.8 km. Uncertainty in the porosity of the residual volatile material causes some uncertainty in the density. An assumed density of 1.0 leads to a mass of 2×10^{16}g. Matsen (Reference 2-9), has reported much lower albedos, in the range of 0.01 to 0.02 for some asteroids. The surface of these bodies probably consists of carbonaceous material. If the surface of Encke is similar, and is free of highly reflective icy material, a similarly low albedo may be appropriate. An albedo of 0.02 leads to a radius about 2.2 times larger, and a mass of about 2×10^{17}g.

When the uncertainty in radius is combined with the uncertainty in the density of comets, the uncertainty range of mass becomes large. In the case of Encke, the combination of a low density (e.g., 0.1 g/cm^3, corresponding to a porous structure) and a high albedo leads to a mass

of about 10^{14}g. On the other hand, the combination of a high density (e.g., 3 g/cm^3, corresponding to silicate rock) with a low albedo leads to a mass of 5×10^{17}g. If we take the mass to be on the order of 10^{16} -10^{17} gm. the acceleration of gravity at the surface is 0.025 - 0.25 cm sec^{-2}. Note that the derived radius scales as $A^{-1/2}$, the mass as $A^{-3/2}$, and the acceleration of gravity as $A^{-3/2}$.

2.3.3.4 Chemical Composition

Indirect information concerning the chemical composition of the nucleus may be obtained from emission spectra of the coma and tail. For Encke, strong lines of CN, C_2, and C_3, with weak lines of CH. NH, OH, CO^+, and N_2+ (References 2-31 and 2-32) are observed. These compounds are almost certainly not constituents of the nucleus but derived by dissociation of compounds such as H_2O, NH_3, CH_4, CO_2, and possibly more complex molecules. While it is not possible to infer the abundance, or even the exact nature of these parent molecules from the spectral data, the spectra indicate that the abundant elements of the C, N, O group played a major role in the condensation and accretionary processes leading to the formation of the cometary nucleus. Hydrogen is present at least insofar as it combined to form compounds such as H_2O, NH_3, and CH_4, and as indicated by hydrogen Lyman-α emission observed surrounding Encke (around one tenth the amount surrounding comet Bennett). It is likely that highly volatile compounds such as CH_4 are trapped as clathrate compounds (Reference 2-10). Helium, and the other inert gases were probably depleted, whereas the lithophilic elements Mg, Fe, Si, Ca. etc. were probably present in something like their solar abundance relative to the CNO group. This assumption leads to the conclusion that about 20 percent (by weight) of the cometary nucleus consists of oxidized compounds of these elements.

2.3.4 Relationship of Encke to the Taurid Meteors

It is established that the Taurid meteor shower is associated with ejecta from Encke. Since volatile materials would be quickly lost from such small bodies well beyond their perihelion distance, the existence of these bodies is clear evidence that the nucleus of Encke contains a non-volatile component. The absence of fragmentation in these meteors

indicates that this nonvolatile material is well bonded. Taurids are observed not only as relatively small (~1 g) photographic meteors, but also as bright fireballs photographed by the Smithsonian Astrophysical Observatory, indicating the presence of bodies up to tens of kilograms in this meteor stream (Reference 2-33).

Estimates of the age of this stream (Reference 2-34) are in the range of thousands of years. If correct, these calculations show that Encke's comet has been a member of the inner solar system for a long time, and lost a large amount of mass, both in volatile and nonvolatile form.

It is difficult to estimate the mass of material in the Taurid stream, as its dimensions are not known. If it is assumed that the present mass of Encke is 2×10^{16} g (corresponding to a radius of 1.8 km and a density of 1 g/cm^3), and that the average mass loss $\Delta M/M$ per orbital period over the last century is 0.2 percent, then the recent rate of loss of material from Encke is about 10^{13} g/yr. Although the relatively great age of Encke (in terms of time spent in the inner solar system) argues in favor of its nucleus being enriched in nonvolatile material over its original value of ~20 percent, it is likely that gas loss still predominates over loss of nonvolatile matter, so a rate of loss of particulate matter of the order of 10^{12} g/yr or less is plausible. This must be primarily in the form of large particles (e.g., ~1 cm and larger) to account for the absence of solar continuum radiation from its coma at the present time. Monte Carlo calculations (Wetherill, unpublished) indicate that approximately 10 percent of the solid matter in this size range ejected from Encke will ultimately strike the earth, provided that the particles are sufficiently strong to resist prior disruption by collision with interplanetary matter in the ~10^7 years for the earth to sweep up this material. If Encke has been more or less in its present orbit for 1000 years, the total ejected solid matter is ~10^{15} g at the rate assumed above. These calculations indicate that the fraction swept up per year will be $10\%/10^7 = 10^{-8}$, giving a total yield of ~10^7 g/yr. The actual impact rate of Taurids is greater, perhaps ~10^9 g/yr, probably in part as a consequence of the argument of Encke's perihelion having been such that over this period of time close approaches to the earth have had a greater probability than

that associated with a random orientation of the argument of perihelion. In addition, the rate of mass loss was probably greater in the past. Liller (Reference 2-26) estimates the mass of a "new" periodic comet to be $\sim 10^{18}$g, therefore containing $\sim 2 \times 10^{17}$g of nonvolatile matter. During the initial phase of the comet's life, much of the emitted matter would have been in the form of micron-size particles, subject to nongravitational forces such as radiation pressure, Poynting-Robertson effect, and solar wind impact. The survival of five percent of this mass in the form of large particles would lead to a mass in the Taurid stream of $\sim 10^{16}$g. Although all these calculations contain large uncertainties, estimates of the rate at which meteors from the Taurid stream strike the earth are consistent with estimates of the rate of loss from the nucleus of Encke.

It seems most plausible to suppose that the nonvolatile material from which the meteoroids are derived was detached from the nucleus near perihelion, being swept along with the escaping gas. However, Hamid and Whipple (Reference 2-35) have concluded that the dispersion among the Taurid orbits indicates that ejection took place in the asteroid belt, presumably because of collisons with asteroidal material. The mass of material in the Taurid streams is inconsistent with the yield expected from a well-bonded body of this size moving through the asteroid belt (Reference 2-36). It is possible that the sublimation of icy material near perihelion leaves loosely bonded nonvolatile material on the surface, which is more readily removed by collision in the asteroid belt, or that cometary flares in the asteroid belt ejected this material at an earlier, more active, stage in the history of the comet.

2.4 THE COMA OF ENCKE'S COMET

2.4.1 General Properties of Cometary Comas Applicable to Encke

2.4.1.1 Gas Emission

The simplest model for the coma of a comet assumes spherical symmetry of the nucleus both in terms of its physical properties and its temperature, and the rotation of the nucleus and all temporal effects (both transitory and evolutionary) are ignored (Reference 2-37). Since the cosmic abundance of oxygen is large relative to that of carbon and nitrogen, it is assumed tnat the bulk of the gas which escapes from the nucleus is H_2O (References 2-38, 2-39, 2-40, 2-41). It is not obvious on theoretical grounds that this must be the case, since H_2O is less easily vaporized than other volatiles (see Figure 2-14). However, since OH and large quantities of H are observed to be associated with P/Encke, it seems reasonable to assume that H_2O is the dominant molecule. Moreover, the laboratory work of Delsemme and Wenger (Reference 2-10) suggests the gases more volatile than H_2O are incorporated with water in the structure of clathrate snows, so that independent vaporization rates may have limited meaning in the actual cometary environment. The predominance of H_2O among the volatile components of another comet (1969g) has been argued by Delsemme (1971) (Reference 2-42) on the basis that an observed, identical heliocentric dependence of both H^+ and OH^- light flux probably arises from a three-step process in which vaporization of water is the most plausible first step. Other molecules can be assumed to be carried along with the H_2O gas, but to behave independently as far as photochemical and plasma interaction processes are concerned.

It is expected that gas leaves the surface of the nucleus at approximately the speed of sound corresponding to the temperature of the surface, and that the Mach number is unity at the surface, corresponding to 400-700 m sec^{-1} for surface temperatures of 250-750°K. As a consequence of the spherical divergence of the flow, the Mach number increases rapidly, as shown in Figure 2-15a for r = 1 AU, and beyond a distance equal to a few times the radius of the nucleus the bulk speed is essentially constant and the temperature very small. The number

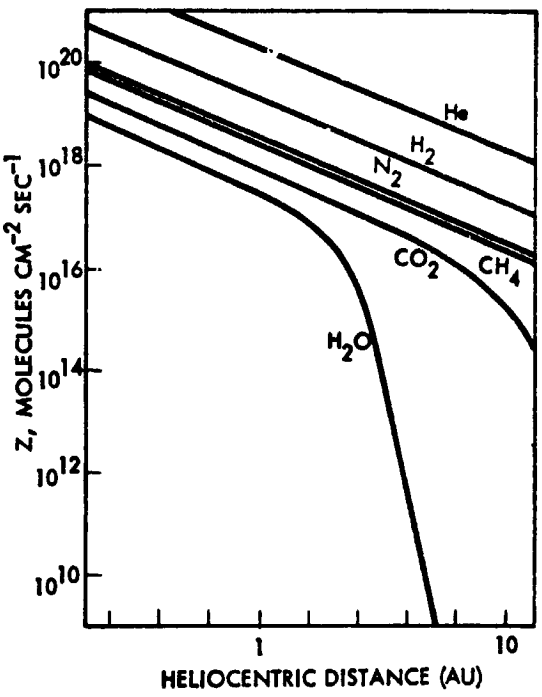

Figure 2-14. Vaporization rate z, mol cm^{-2} sec^{-1}, for various snows as a function of heliocentric distance, in AU, computed for the steady state temperature of a rotating cometary nucleus with an albedo a = 0.1

densities of H_2O and other molecules decreases approximately as the inverse square of the distance from the nucleus out to a distance of the order of 10^4 km, where the effects of photodissociation become important. Figure 2-15b illustrates the exchange of dissociation products for water with increasing distance from the nucleus.

The radius of the region within which the gas is mostly in the form of parent molecules must be of the order of τ /V, where τ is the characteristic time for photodissociation by sunlight, and V is the expansion speed of the undissociated gas. Since for most molecules, τ 10^4 -10^5 sec at 1 AU, the characteristic size of the "molecular"

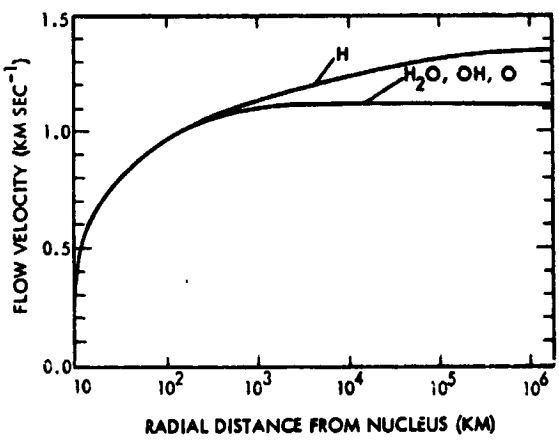

Figure 2-15(a). Velocity Profiles for the Cometary Atmosphere at 1 AU

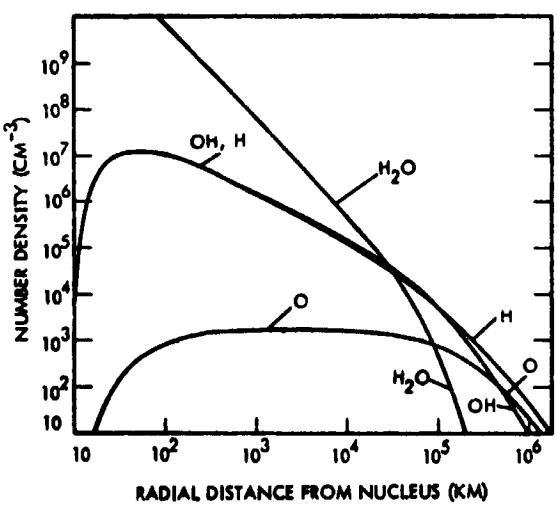

Figure 2-15(b). Density Profiles for a H_2O, OH, H, O Cometary Atmosphere at 1 AU (According to a Calculation by Mendis et al,) (Reference 2-37)

region must be of the order of 4×10^4 - 4×10^5 km at 1 AU. The region must shrink as the comet approaches the sun, since V is a very weak function of r, whereas $\tau \propto 1/r^2$. On the other hand the total brightness of the coma must increase as the comet approaches the sun since this depends only on the solar photon flux and on the total number of molecules present, unless the coma is optically thick.

The overall distribution of a given species of parent molecule should be such that the density varies as $r^{-2} \exp(-V/r\tau)$, with the appropriate value of τ being used for any given species. As indicated in Figure 2-15b, neutral daughter products should be absent from a small region around the nucleus, and beyond that their density must decrease less rapidly than that of the parent molecules, since the dilution associated with the spherical expansion of the flow is to some extent counteracted by continued production. Eventually, however, when the parent molecules are removed, the density of the daughter products in turn decreases rapidly as they too are removed by photodissociation, photoionization, or collisions with solar wind particles. In the case of H atoms, the main loss process is charge exchange with solar wind protons, but for other species the main loss processes are probably photodissociation in the case of molecules and radicals, and photoionization in the case of atoms. In order to conserve momentum, any excess energy (i. e., above that required for dissociation) should be given mainly to the lightest of the daughter products if it is not absorbed in electronic, vibrational, or rotational excitation. Thus we must expect that the atomic hydrogen component of the coma gas may be strongly heated, and can therefore expand at a considerably higher speed (i. e., perhaps several kilometers per second), than the 400-700 meters sec^{-1} to be expected for the parent molecules and heavier radicals. This higher speed, together with a smaller loss rate, enables the atomic hydrogen component of the coma to extend to far greater distances than any other component (i. e., 10^5-10^6 km).

These estimates of the expansion velocities and radial scales for the density variation of the neutral gaseous coma are essentially independent of the comet concerned, since the state of the nucleus does not affect any of the arguments substantially. The nucleus must, of

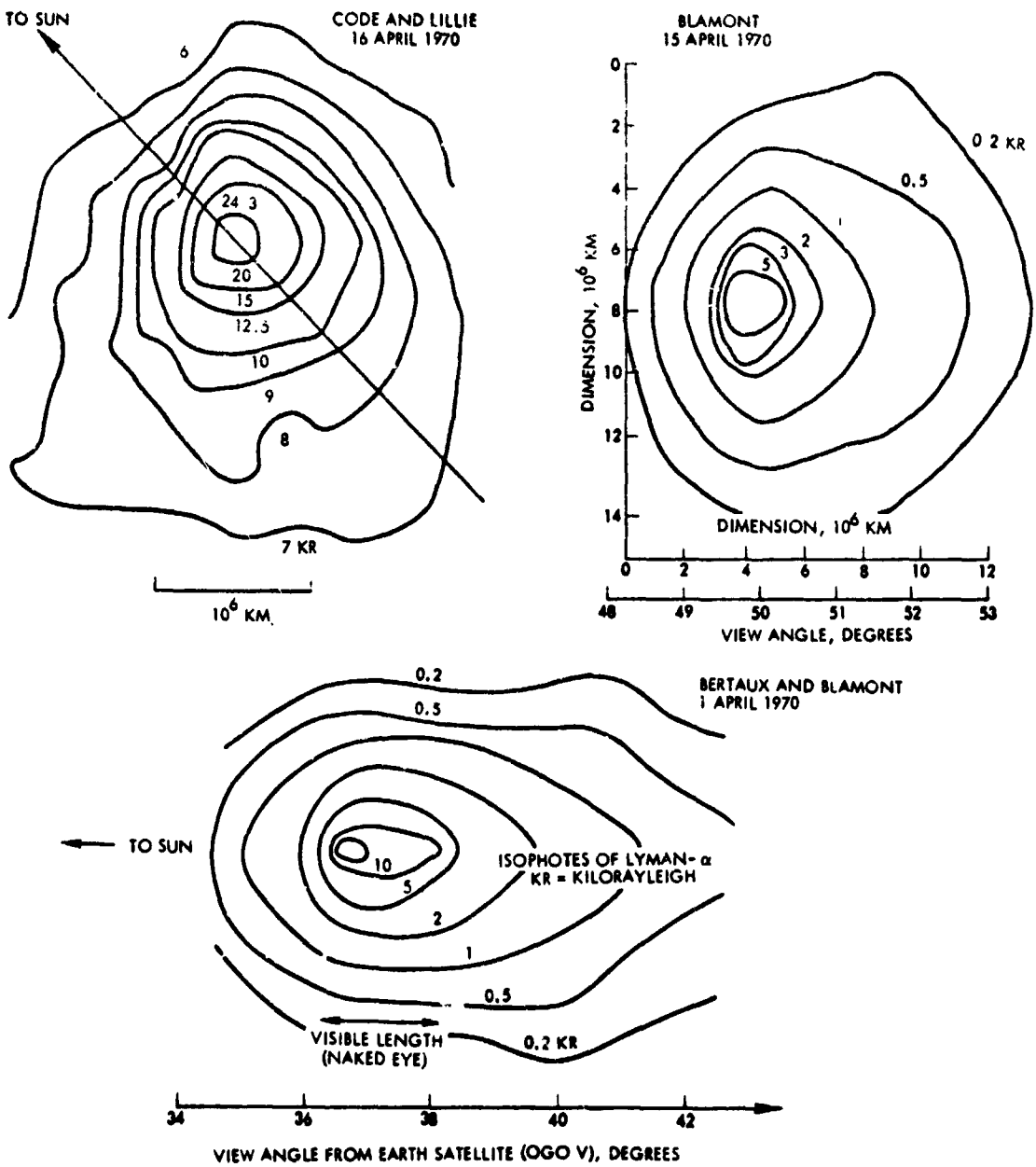

Figure 2-16. Isophotes of Constant Lyman-α Emission from Comet Bennett on 1, 15 and 16 April 1970 (Reference 2-43)

course, control the net flux of parent molecules so that the number density at any given distance from the nucleus can be expected to vary from one comet to another, even if the scales of the spatial variations must be more or less the same. Some distortion of the atomic hydrogen coma from a meteorless spherical distribution can be expected since the radiation pressure of solar Lyman-α is comparable with solar gravity, and this presumably is the explanation for the slightly elongated emission contours that are observed for the scattered Lyman-α (Figure 2-16). This observation of Comet Bennett was made by OGO V.

An important consequence of an expanding cometary coma is that it will cause solid material (perhaps coated with ice) eroded away from the surface of the nucleus as the volatiles evaporate to be blown away from the nucleus. For a particularly active comet, the nucleus may be completely enshrouded by radially moving grains so that the apparent magnitude of the nucleus can change significantly. The dynamics of grain motion has been discussed by Finson and Probstein (Reference 2-44), and Delsemme et al., (References 2-10, 11, 42, 45). As far as the grains are concerned the flow is free-molecular, although the expansion of the coma gas as a whole is essentially hydrodynamic. The very smallest grains could, in principle, achieve speeds as large as the expansion speed of the gas (i. e., several hundred meters sec^{-1}); however, speeds of the order of 1-10 meters sec^{-1} appear more likely for snowflake-sized particles. The thin, sheet-like structure of Type II tails is clear evidence that most of the grains involved have not been accelerated to very high speeds. The smallest grains are strongly affected by solar radiation pressure, and all grains which undergo a substantial mass loss by evaporation may have their trajectories affected if the mass loss is not symmetrical.

2.4.1.2 The Icy Grain Model

Delsemme and Miller (Reference 2-45) have pointed out that the processes of photodissociation and ionization associated with emission of neutral gas from the nucleus cannot account for all the properties of the coma and tail because the solar flux is insufficient over a 10^{3}-10^{4} km cross section of neutral gas at several AU to account for the amount of excited material needed to supply these features. They

have suggested that gases emitted from the nucleus are already in the form of radicals or molecules in elevated energy states. Also, the desorption times of gases trapped on an icy nucleus are too long to provide the observed mass of the coma.

Combining these objections with the results of laboratory experiments simulating cometary conditions (Reference 2-10), Delsemme and Miller proposed a model of cometary emissions along the following lines: The type of environment in which comets find themselves when far from the sun favors the condensation of water in a snowy, lattice-like, rather than smooth, icy form (e.g., $CH_4 \cdot 6H_2O$). The snowy substance is a clathrate if it is or partially formed of radical gases. As a cometary nucleus including an exposed clathrate component approaches the sun, some of the most volatile absorbed gas or gases of the core or icy mantle (CH_4 is a good candidate) is desorbed by energy from the increasing solar flux and expelled from the surface of the nucleus. On being expelled, the gas detaches small icy grains of the snow, an effect consistent with that observed in the laboratory, and presumably releases frozen nonvolatile particles as well. The gas molecules are then accelerated and dissociated and ionized. In leaving the nucleus, the escaping gas blows the smaller detached icy grains and released dust along with it. The grains in turn contain more trapped, volatile gas which they release by absorbing solar radiation as they move outward. They also evaporate to water vapor as they go, and the trapped gas molecules break them up further as they escape from the grains themselves, perhaps releasing additional dust as well. Water vapor is, of course, evaporated directly from ice in the nucleus as well.

The result of the process should be to surround the nucleus with a halo of icy particles which are accelerated from the nucleus along with the primary neutral gas. The grains become progressively smaller with increasing cometocentric distance because of sublimation by solar energy and pulverization by secondary desorption of additional trapped gas. The grains presumably deliver radicals to larger cometocentric distances in this way, acting as a surrogate nucleus of enlarged diameter in place of an inner coma of pure neutral gas.

The icy halo model has implications with respect to every cometary feature, but the model is still too new to have been evaluated thoroughly in all its ramifications. No attempt at such an evaluation is made here, but selected attributes of the halo are quoted or deduced where appropriate.

Delsemme and Miller (Reference 2-11), in the third of a series of four papers on the halo, give considerable attention to vaporization rates of various possible volatile constituents of cometary ices. Their estimate of the number and mass of grains in the halo follows (reproduced from their paper):

> "Two ways are open to assess the possible number of grains in the halo: the laboratory experiments (paper I) and the cometary observations.
>
> In the laboratory, the production rate observed was only assessed visually. This gives an order of magnitude of one grain cm^{-2} sec^{-1}. The average grain's diameter is 0.6 mm (Fig. 2A, paper I). With an apparent density of 0.44 cm^{-3}, its average mass is about 5×10^{-5} g, giving a mass production rate of grains of 5×10^{-5} g cm^{-2} sec^{-1}, as compared with a mass production rate of water vapor + methane of 2.65×10^{18} mol cm^{-2} sec^{-1} = 8×10^{-5} g cm^{-2} sec^{-1}. The ratio of the grain and gas production rates is therefore m = 0.63, whose order of magnitude only should be meaningful.
>
> The assessment from cometary observations relies on the comparative brightness of the central condensation to the global brightness of the continuum. In many comets showing a continuum, and in particular in new quasi-parabolic comets which usually show a strong continuum the light distribution is often stronger in the continuum than in the molecular emissions. (On the other hand, E. Roemer's determinations (1969) show that in most cases, the brightness of the head is, on the average, at least five magnitudes, that is 100 times brighter, than the central condensation.) Assuming that the albedo of the grains is the same as the albedo of the nucleus, the total cross sectional area of the visible grains is at least 100 times larger than the cross sectional area of the central condensation, which might still be slightly brighter than the 'true nucleus'. This conclusion is independent of any phase function, as it would be the same for the nucleus and the grains. If we assume a spherical nucleus of 2 km radius, its cross sectional area is $10^{11.1}$ cm^2. This means a cross sectional area of at least $10^{13.1}$ cm^2 for the visible grains. The initial mean diameter of the grain being 0.6 mm, as the evaporation proceeds linearly, the average cross-section per grain is $10^{-2.7}$ cm^2 and there are 10^{16} gr visible in the coma.

This result implies that the number density of the grains is small enough to see almost all of them. Their lifetime being $10^{4.5}$ sec (Section 9, formula (25), with $Z = 10^{17.2}$), there is a grain production of $10^{11.5}$ gr/sec^{-1}, or a production rate of 0.67 g/cm^{-2} sec^{-1}. Their initial mass being $10^{-4.3}$ g, the mass flow rate of the grains is about $10^{7.2}$ g sec^{-1}, or a mass flux of $m_G = 10^{-4.5}$ g cm^{-2} sec^{-1}. Therefore $m = 0.43$.

This could be a lower limit, as it is based on the assumption that the central condensation brightness is the brightness of the true nucleus. It could also be an upper limit as the fine dust component might also contribute a sizable fraction of the continuum light even if its mass component remains negligible, because of the small size of a large number of grains, therefore diminishing the contribution of the large icy grains. The fact that our two assessments point to the same order of magnitude shows that there is at least no inconsistency."

One of the principal effects of the halo phenomenon would be to alter the relative amounts of constituents of the coma at various distances from the nucleus. Since some of the water vapor would be produced by sublimation of the expelled grains rather than the snow or ice of the nucleus itself, and some radicals would be preformed in the ice, having been deposited with, and trapped in, the snow, the curves of Figure 2-15b should be modified to account for the necessary redistribution of densities. No quantitative assessment of the redistributed densities is available, but radical modification is not anticipated. The relative grain and gas production rates quoted above suggest that perhaps half the water in the coma arises from the grains rather than the nucleus, thus flattening the initial slope of the H_2O curve in Figure 2-15b and moving the remainder of it outward. Adjustment of the other curves would have to be made accordingly.

The dynamic behavior of icy grains is treated extensively in the third paper of Delsemme and Miller. Most grains reach their terminal velocities of 0.1 to 1 km/sec within 1000 seconds of their departure from the nucleus. The size of the halo is also estimated in this paper. The radius of the halo is not unique but is a function of grain size. Figure 2-17 and its caption, adapted from Delsemme and Miller (Reference 2-11), show the dependence of halo radius on certain selected particle sizes. The unshaded section of the graph defines the range of heliocentric distance, 0.34 to 1 AU, applicable to the 1984 Encke rendezvous.

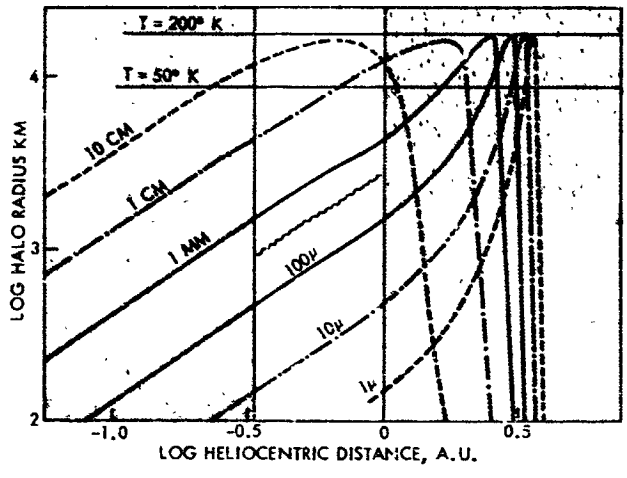

Figure 2-17. Extent in Kilometers of a few Icy Halos Built Up with Grains of a Single Size, as a Function of the Heliocentric Distance, AU.

The parameters correspond to grains of clathrate hydrates plus some free methane ($k = 5$, $A_o = 0.9$) stripped from a nucleus whose radius is 2 km. Eighty-seven percent of the distribution observed in the laboratory lies between the two solid lines ($a_o = 0.1$ and 1 mm); the radius of grains is given for other hypothetical halos in dotted and dashed lines. The envelope of all halos for different particle sizes is also shown by a thin solid line near $\log R_\pi = 4.2$ for a nuclear temperature of 200°K, and $\log R_\pi = 3.9$ for a nuclear temperature of 50°K. Observe the sharp gravitational cutoff near 3.5 AU.

Nearly 90 percent of the particles, as anticipated from laboratory results, would go no farther than 4000 km from the nucleus at 1 AU, and the largest would not survive beyond 16,000 km. The radius for all but the largest grains decreases monotonically with decreasing r. The dependence of the average halo radius R_H on heliocentric distance r for the average 0.3 mm grains, represented in the figure by the wavy line segment, can be written $R_H = 3200r^{1.22}$, with r in AU, R_H in kilometers. Clearly, the halo is expected to occupy much the same region as is generally conceded to the neutral inner coma in prehalo models of coma formation (Figure 2-15b).

An important aspect of the halo is its visibility. Figure 2-18, from Delsemme and Miller (Reference 2-11) illustrates the calculated brightness profile based on their model. The halo is clearly expected to be substantially brighter in the center than at the circumference.

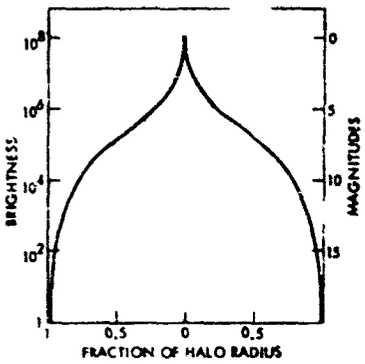

Figure 2-18. Brightness Profile of the Continuum, Reflected by the Icy Halo, as a Function of its Distance from the Nucleus. To limit the central peak, a simulated seeing of x = 0.01 has been adopted. This corresponds, for a halo radius of 10 km, to a 0.3 seeing when the comet is at a geocemtric distance of 0.4 AU.

2.4.2 Specific Properties of Encke's Coma

2.4.2.1 Emitted Mass

The nucleus of Encke begins to emit sufficient quantities of volatile material to produce a visible coma at a distance of about 1.5 AU. The total emission of gas per perihelion passage is at present 0.03 percent of the mass, according to Marsden and Sekanina (Reference 2-25). Using the value of the albedo adopted by these authors, this corresponds to a mass loss of 6×10^{12} g per perihelion passage, or an average loss of $\sim 6 \times 10^{5}$ g/sec during the approximately 100-day active phase of the perihelion passage, primarily prior to perihelion.

2.4.2.2 Volatile Component

If we adopt Sekanina's value of 10^{13} g per revolution as a first estimate of the present outgassing rate, the density of H_2O molecules in the coma is approximately a factor 10 less than indicated in Figure 2-15b and a factor of 40 to 800 less than the estimate of Delsemme and Miller quoted earlier, which was not for Encke, but for another comet. The mass loss which takes place during the few months around perihelion (where the planned rendezvous will occur) corresponds to an evaporation rate of the order of 10^{29} H_2O molecules sec^{-1}. A better estimate will be possible when details of recent observations of the Lyman-α emission from the coma of Encke become available. According to the icy halo model, roughly half the emission would be in the form of icy grains.

2.4.2.3 Nonvolatile Component

Although the "dismantled core" consists primarily of nonvolatile material, according to the proposed model of the nucleus this material is now in the form of large aggregates, possibly a single piece, and is not

readily swept along with the escaping gas. If Encke has a radius of 1.6 km, a mean density of 1.0 gram cm^{-3}, and emits 10^{29} H_2O molecules sec^{-1} at a velocity of 500 meters sec^{-1}, then the maximum radius of grains with density 1.0 gram cm^{-3} which can be blown away from the comet is ~2.5 cm, assuming a drag coefficient of unity. The absence of continuum radiation in the coma of Encke (References 2-26, 2-32) suggests that the coma wind is too weak to blow any significant quantity of solid material away from the nucleus, or the supply of sufficiently small grains in the surface layers has been exhausted. Although the low continuum radiation still permits as much as 10 percent of the emitted matter to be in the form of grains a few millimeters in radius and an even greater amount in the form of larger particles with a lower ratio of surface to mass, there is no evidence that such particles are now in the coma, and it seems plausible that the fraction of volatile material lost is considerably greater than the fraction of nonvolatile material. A figure of 6×10^4 g/sec during the active phase can be used for the rate of emission of meteoric matter; an uncertainty of at least an order of magnitude should be associated with this figure.

2.4.2.4 Asymmetry

The earlier discussion of the nucleus of Encke pointed out the probable asymmetry of emissions that are implied by the existence of a nongravitational acceleration. It may be inferred that the coma densities share the asymmetry of the emitting surface, thus explaining, at least in part, the asymmetric coma described in an earlier section. To a first approximation, then, it should be anticipated that gases in some parts of the coma are two or three times as dense as they are elsewhere. The same statement would apply to icy grains and lithic dust particles in the absence of any theory or data to the contrary.

2.4.2.5 Visible Constituents

Sekanina (Reference 2-19) has compared the total gas abundance deduced from dynamical considerations with the observed abundance of C_2 for 23 short-period comets (see Figure 2-19). There is some evidence that the ratio between the total and C_2 densities might tend to

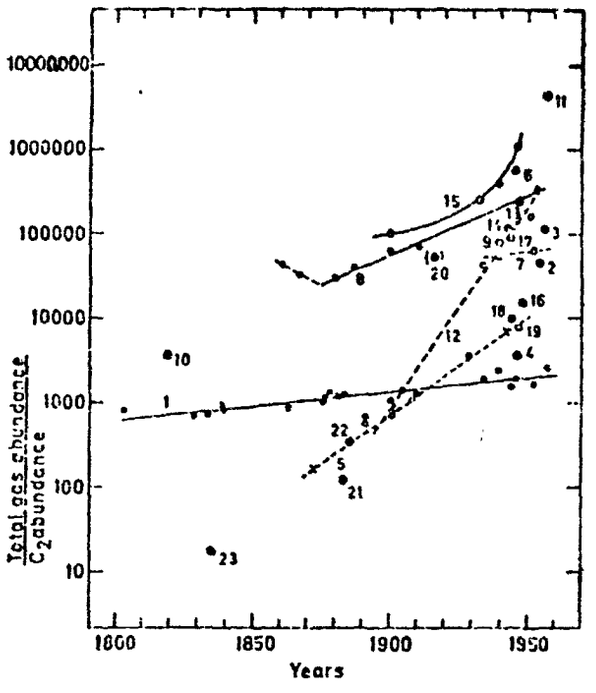

Figure 2-19. The ratio of the total gas abundance in comets in units of C_2 abundance for 23 short period comets vs time. The curve labelled one is drawn through the points obtained for Encke. The comets are identified by number in Reference 2-19.

increase secularly. This is not surprising, since one would expect different volatiles to escape with differing rates from the nucleus. Despite the fact that the nongravitational parameter has decreased markedly and the comet appears to be approaching its death date, Encke still shows evidence for a surprisingly large amount of gas. Its spectrum is well-documented, and all the molecular species typical of comets have been observed. The spectrum is especially strong in C_2 and C_3 and especially weak in continuum. Furthermore, Encke has recently been observed to have a large hydrogen cloud associated with it. Accordingly, we might expect that the physical processes associated with the coma are similar to those in younger and more spectacular comets, but on a somewhat reduced scale. Table 2-2 lists the identified molecular constituents of Encke's coma and tail. Presumably these species are in the coma in varying proportions beyond 10^4 km from the nucleus, and they or their (invisible) parent species (H_2O, NH_3, CH_4, etc.) are in the inner coma as well.

Table 2-2. Gas Species Present in Coma of Encke

Molecular Species	Emission Wavelengths	P/Encke
CN	388 nm	S
C_2	474	S
	516	
	564	
C_3	405	S
CH	428	W
NH	336	W
NH_2	630	W
OH	309	W
CO^+	400	W
	426	
	455	
N_2^+	391	W
Continuum	-	W

S = Strong M = Moderate W = Weak

2.5 INTERACTION WITH THE SOLAR WIND: THE CONTACT SURFACE AND THE TAIL

One major area of interest in cometary research is the nature of the interaction between the plasma of the solar wind and the gases of the coma. The interaction may involve as many as three related processes. First, the solar wind flux may contribute to the mechanism by which the neutral parent molecules of gases emitted from the nucleus are dissociated and ionized. Second, the solar wind, and the interplanetary magnetic field embedded in it, must play a dominant role in sweeping the ionized constituents of the coma into the Type I (ion) tail and in shaping and maintaining the tail as it streams away from the coma in the antisolar direction. Third, the solar wind, being supermagnetosonic and superalfvenic, must prepare well upstream for its encounter with the ionized coma by a plasma physical process of deceleration, either through a collisionless shock or a transonic ion exchange sheat.

Encke has shown a Type I (ion) tail, especially during years of enhanced solar activity. Whether visible from Earth or not, a tail should be present as long as gases are emitted. Type I comet tails are the direct result of the interaction of the solar wind with the coma. The solar wind does not impact directly upon the nucleus of the comet itself, except perhaps at very great distances from the Sun where the surface temperature is so low that the coma effectively disappears. The cross sections for the various interactions between neutral atoms, radicals and molecules in the coma, and ions and electron in the solar wind, yield such small collision rates that the neutral gas comprising the coma can expand freely through the interplanetary plasma and magnetic field. On the other hand the interplanetary magnetic field introduces an effective coupling between the solar wind and any ions produced from the neutral coma gas by charge exchange or photoionization. This can have a pronounced effect on the dynamics of the solar wind, since a transition to subsonic flow should occur approximately at a point where the solar wind has doubled its mass flux by picking up new ions of cometary origin.

Two concepts of a comet's plasma interaction are current. The first postulates a process analagous to that sunward of the earth's magnetosphere, where a collisionless shock would form upstream from the

comet. This model is still being developed by Bierman, Lüst, Schmidt, and their collaborators. The second concept, developed by Wallis, proposes a "transonic" process in which no shock forms.

A detailed description of the shock interaction model of the solar wind and the neutral coma gas is provided by Bierman et al., Reference 2-46 (see Figure 2-20). The calculations were carried out only along the line joining the Sun and the nucleus of the comet. Apart from the effects of the inerplanetary magnetic field, this should be an approximate axis of symmetry for the flow, and there should be a stagnation point somewhere ahead of the nucleus. The hydromagnetic detached shock stands somewhere from 10^6 to 10^7 km upstream, reducing the bulk flow velocity from an average of about 400 to 100 km/sec, and heating the plasma. Behind the shock, the solar wind gradually flows to a few Km/sec before arriving at the contact surface, where an accumulated flux of interplanetary field stops or deflects the flow completely.

Unfortunately the calculations of Biermann et al. are not completely consistent in that the treatment is quasi one-dimensional, and the divergence of the flow around the comet is accounted for in an ad hoc manner. It is found that the stagnation point occurs some 10^4 -10^5 km ahead of the nucleus, under the conditions assumed. This stagnation point is interpreted to lie on a contact surface which separates plasma of cometary origin (on the inside, in the region containing the nucleus), from plasma which is partly of solar origin and partly of cometary origin on the upstream (solar) side. The calculation is consistent only if the cometary plasma within the contact surface can exert a sufficient pressure to balance the solar wind pressure, which is unlikely at such a large distance from the nucleus. It is more probable that the contact surface lies at a distance of 10^3 -10^4 km in front of the nucleus, with the smaller figure probably more appropriate in the case of Encke. It seems therefore that Biermann and his colleagues overestimated the effects of flow divergence in their first calculations, especially since this is the only parameter controlling the position of the contact surface if the solar wind parameters, and the parameters determining the flow of gas from the nucleus to the coma, are fixed.

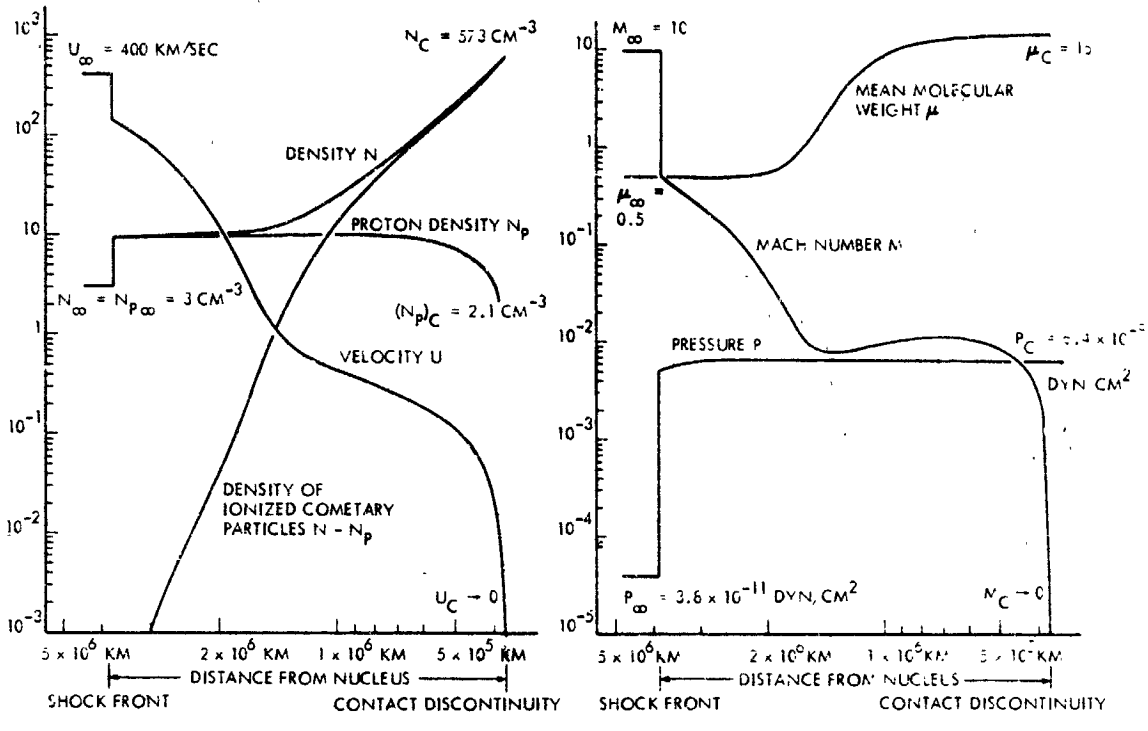

Figure 2-20. Dependence of Various Plasma Properties on Cometocentric Distance

An important process in the deceleration of the solar wind behind the shock is exchange of charge between the solar wind and the cometary gases. Some of the solar wind protons are neutralized while some of the cometary gases are ionized and forced to flow downstream with the interplanetary field. The relatively massive local ions added to the flow result in a net deceleration of the plasma. This process has led Wallis, in a calculation ignoring divergence of flow altogether, to the conclusion that charge exchange and photoionization can occur in such a way that the solar wind is gradually and smoothly decelerated from supersonic to subsonic speed without the generation of any shock at all. This result, which contradicts earlier suggestions that a strong shock should be present, is probably close to the truth. However, since it does not allow for any divergence from the flow, it does not help us estimate the position of the contact surface, which should certainly be present.

The general character of the solar wind or interaction with the coma of Encke at 1 AU is indicated in Figure 2-21. A shock transition occurs on the fringes of the interaction region, but immediately ahead of

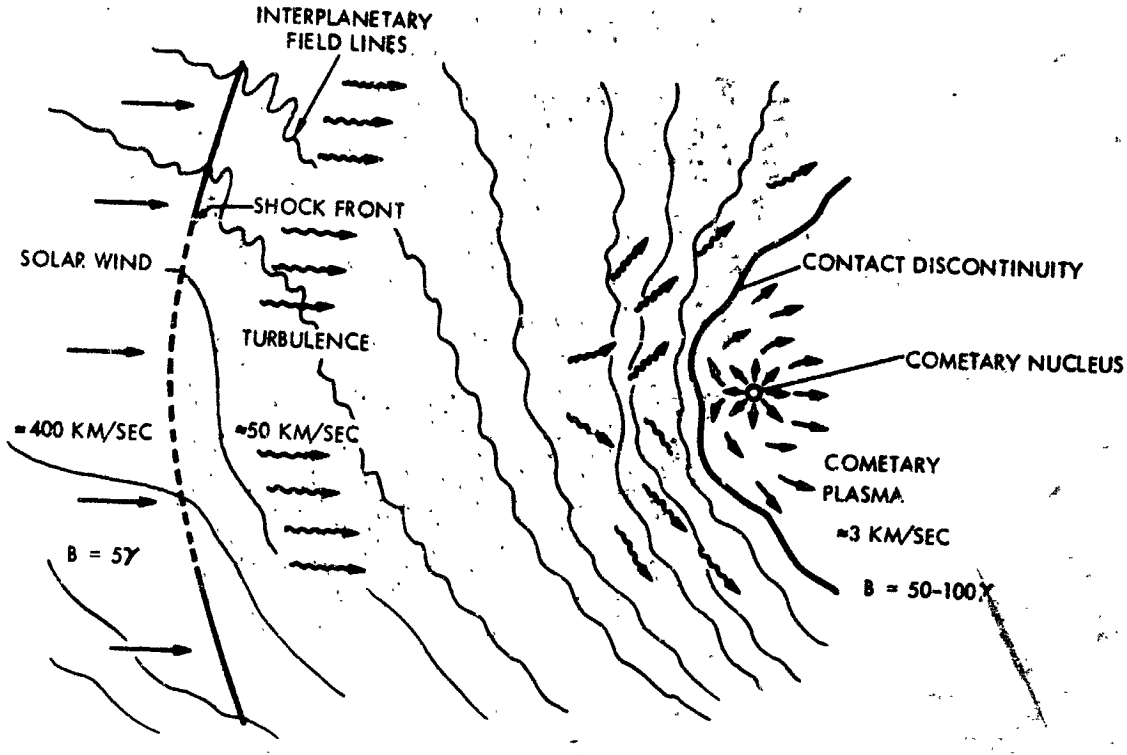

Figure 2-21. Principal Regions of Coma and Solar Wind

the comet the transition from supersonic to subsonic flow may be smooth as described by Wallis. This is indicated by the dashed section of the nominal shock curve in the figure. Within the subsonic region behind the shock wave, the plasma is heavily loaded with ions of cometary origin, and the magnetic field is stronger than it would be in the undisturbed solar wind. The mixed cometary and solar plasma flows around the contact surface and the interplanetary magnetic field is compressed against it with the field strength reaching something like the stagnation value of 50-100 γ. Within the contact surface there can be no solar wind plasma, and the plasma that exists must be entirely produced by photoionization of neutral coma gas. Collisions between the outflowing neutral coma gas and the coma plasma force the latter against the inside of the contact surface in such a manner that there is pressure balance across the surface. Ultimately of course the momentum flux of the solar wind can be considered as held off by the friction between the coma plasma and the flowing neutral coma gas. Unfortunately the detailed behavior of the coma plasma has not yet been analyzed quantitatively. Consequently we do not

yet know whether the coma plasma is lost mostly by recombination in the vicinity of the contact surface or by the flow into the wake of the comet, thus leading to the formation of a Type I tail.

The temperature of the coma plasma should be maintained almost entirely by photoelectron heating, since there is almost no other source. In any case, the mean thermal energy per electron ion pair cannot be more than about 1 eV. Consequently to achieve a pressure balance at the contact surface, it is necessary that the number density of the coma plasma be of the order of 10^4-10^5 cm^{-3}. At such densities the recombination rate can be expected to be rather high, since most of the ions concerned will be molecular (e.g., CO^+, CO_2^+) and therefore liable to dissociative recombination with a recombination lifetime of the order of 10^2-10^3 seconds. These lifetimes are less than or of the same order of the time required for plasma to flow out of the coma if the characteristic speed of the flow is 1 km sec^{-1}, and hence recombination must be an important process as far as the coma plasma is concerned.

The contact surface is liable to flute instabilities on its forward side since the interplanetary magnetic field around the outside is curved in such a way that it would be likely to contract and enter the region of coma plasma. Friction between the outflowing neutral coma gas and the coma plasma may exert a stabilizing influence, but it is far from clear that complete stabilization can be achieved. Indeed just such an instability is required to mix the coma plasma with the interplanetary field and so produce the rays and other features associated with Type I tails; hence the above description which implies the existence of a sharp contact surface should be modified accordingly. The contact surface is also liable to Helmholtz instabilities wherever there is a substantial shear between the coma plasma and the external flowing plasma. However, it is not easy to see the effects of such an instability in the presence of the flute instability, which in a sense allows magnetic fields to diffuse into and be captured by the coma plasma; thus producing a protective envelope which could tend to stabilize the contact surface.

Many attempts have been made to correlate tail activity with activity on the sun. Some such correlation might be expected since solar activity is associated with increased solar wind flux, and an enhancement of the

solar UV flux. The empirical results of Whipple and Douglas-Hamilton (Reference 2-5) and Whipple's recent amendment of them are described in an earlier section.

2.6 ENCKE CHARACTERISTICS COMPARED WITH OTHER COMETS

The value of a selected comet mission sould depend heavily on whether the targeted comet is likely to provide information on comets as a class. For the forseable future, no mission to a nonperiodic comet can be anticipated, so a target for a comet mission will necessarily be drawn from the subclass of periodic comets, and it is all the more important to know that a given comet is a suitable object of study.

Although all comets are individuals, Encke is reasonably representative of others in dimension and composition. Figure 2-22 shows how certain characteristics of Encke compare with the range of these characteristics shared with comets in general. A separate compilation of the comparison follows in Table 2-3.

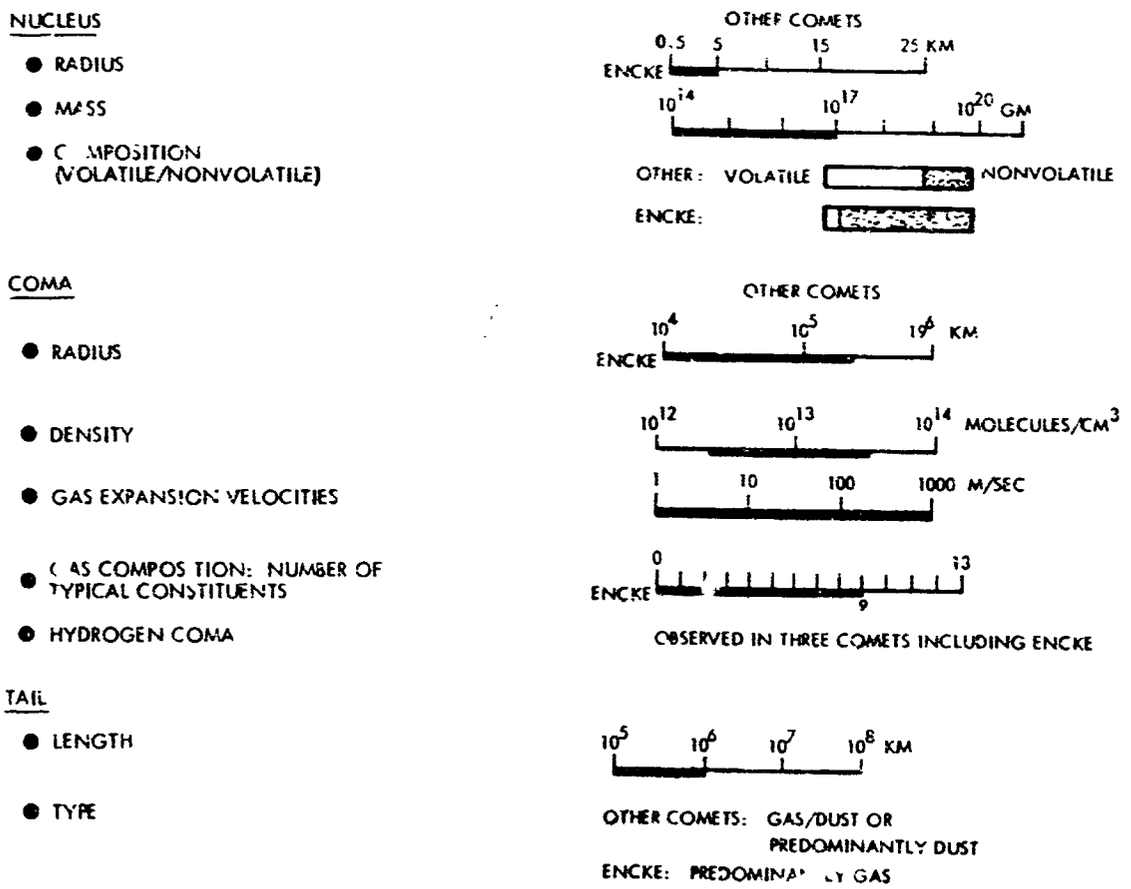

Figure 2-22. Encke Characteristics Compared with Other Comets

Table 2-3. Characteristics of Encke Compared with Other Comets

	Other Comets (From "Atlas of Cometary Forms")	Encke
General:	The composition, especially the gas/dust ratio, varies widely among comets	High gas/dust ratio, ~90 percent
Nucleus:	Diameter, 1 to 50 km	Diameter, 0.5 to 5 km
	Mass, 10^{15} to 10^{21} g	Mass, 10^{14} to 10^{17} gm
	Composition, volatile molecules (parents of observed species), Meteoric particles, micron grains	Composition, nonvolatile core with exposed volatile constituents
Coma:	Observed constituents, O, CN, C_2, C_3, CH, NH, NH_2, OH, CO^+, CO_2^+, N_2^+, CH^+, OH^+, dust	Observed constituents, CN, C_2, C_3, CH, NH, NH_2, OH, CO^+, N_2^+
	Diameter, 10^4 to 10^6 km	Diameter, 10^4 to 4×10^5 km
	Gas density, 10^{14} molecules/cm^3 at nucleus for very bright comets	Gas density, 4×10^{12} - 5×10^{13} cm^{-3}
	Velocities, neutral species and dust-up to 1 km/sec expansion	Velocities, V $\leq$1 km/sec
	Hydroge.. coma, postulated, observed in three cases	Hydrogen coma, observed
Tail:	Length, up to 10^8 km	Length, 10^5 to 4×10^6 km
	Width, up to 10^6 km	Width, $\ll 10^6$ km
	Ion tails are present in about 30 percent of comets	Ion tail only

2.7 MISSION RELATED PROPERTIES OF ENCKE

2.7.1 Viewing Conditions

Coordination between local measurements by spacecraft instruments and remote measurements by earth-based observations will undoubtedly play an important role in a rendezvous mission. The duration and quality of earth-based observations for a given mission will depend on the changing relationships of earth, sun, and comet. Since the orbits of earth and Encke are asynchronous, these relationships vary from pass to pass, and are not all equally advantageous from the standpoint of acquiring correlated observations.

Apparitions of Encke can be divided into three categories: those in which the comet is observed only before perihelion, only after perihelion, or both before and after perihelion. A history of Encke acquisitions from 1885 to 1951 is the subject of Appendix B. The implied viewing conditions for possible Encke missions are summarized here.

The categories of Encke acquisition are defined by the position of the earth in its orbit at the time of the comet's perihelion. Figure 2-23 displays three views of the earth's orbit corresponding to the three categories designated above. At the left, the heavy arc corresponds to the

range of positions of the earth, at times of Encke's perihelion (small circles), for which the comet was observed only inbound. In the center, the heavy arc has the same meaning for acquisitions only outbound. At the right, the heavy arc represents the range of earth's positions corresponding to acquisition before and after perihelion. The asterisk on the arc at left indicates the location of earth at the time of Encke's 1980 perihelion; telescopic observations of the outbound comet in 1980-81 are extremely unlikely in this case. The asterisk at right shows the earth's location at the time of the comet's perihelion in 1984: Conditions governing telescopic observation of Encke both before and after perihelion are favorable in this case.

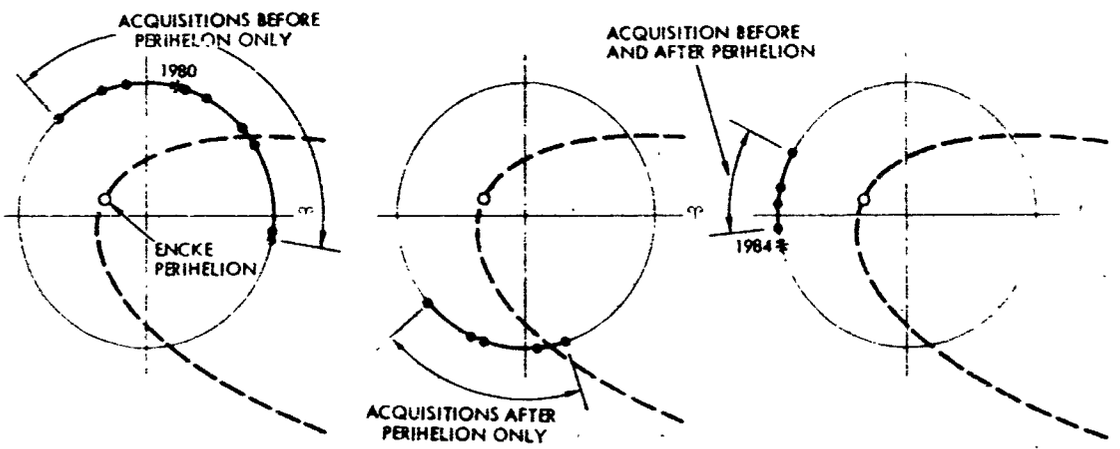

Figure 2-23. Positions of Earth at Encke's Perihelion Times for Various Viewing Conditions

Figure 2-24 shows an ecliptic plane projection of earth and Encke orbits in an inertial system. Simultaneous positions of earth and Encke are shown in the upper half of the figure for the comet's 1984 approach to the sun. Actual positions of observation during the 1951 approach, one of the most completely monitored of all, are shown in the lower half of the figure. The 1951 experience and the summary of historical conditions in Figure 2-23 suggest that the viewing angles of 1984 should be advantageous to comprehensive telescopic observations of Encke from earth and correlation with measurements made at the comet.

The next duplication of the favorable geometry of the 1984 opportunity will occur in 1994. The 1987 pass, with perihelion in July, belongs to a sequence of relatively unfavorable passes. It would be represented

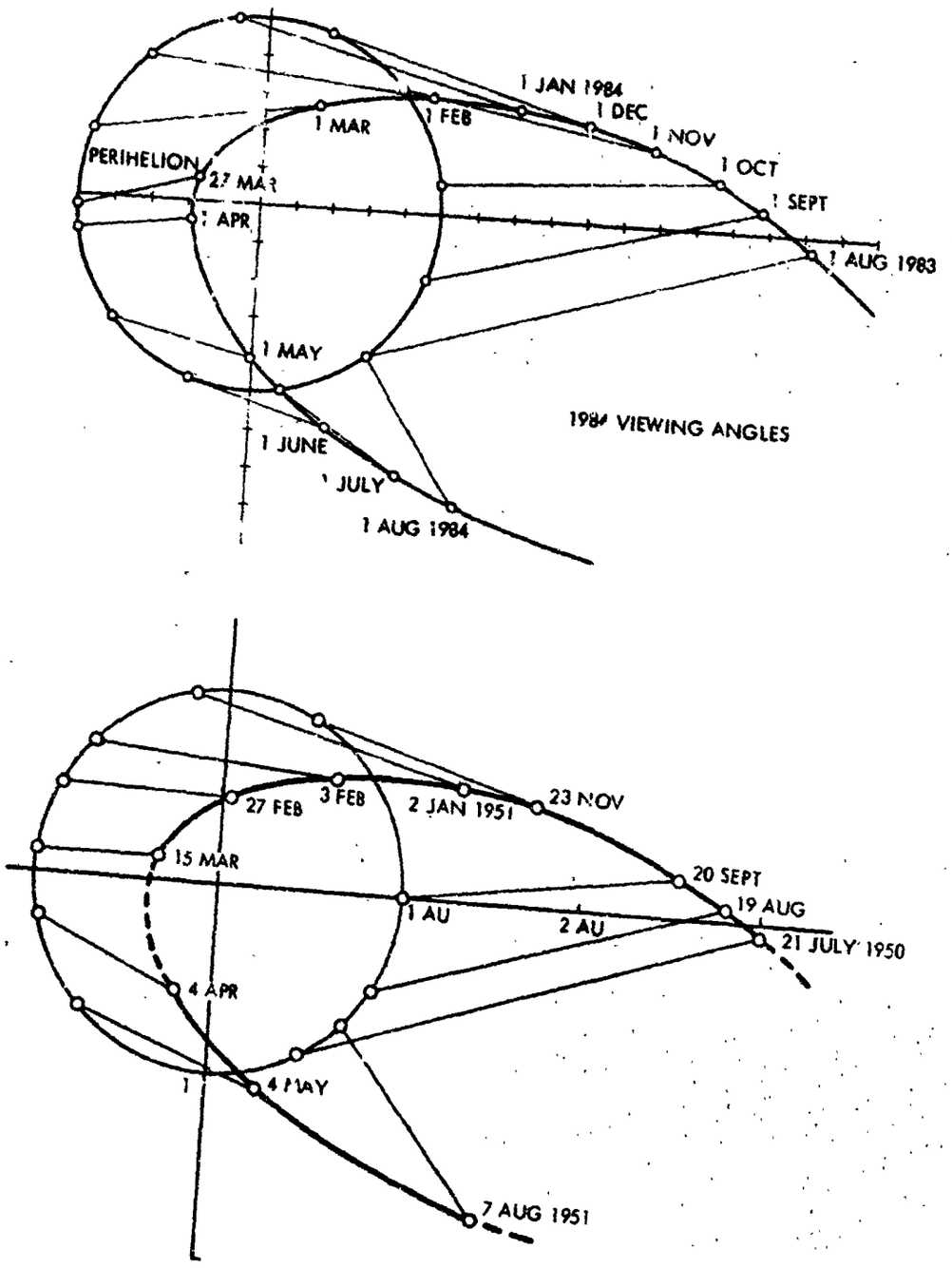

Figure 2-24. Comparison of Viewing Geometry from Earth to Encke for 1964 and 1950 Apparitions

by a point in the lower right quadrant a little beyond the end of the heavy arc in the center of Figure 2-23. During the most recent of these unfavorable passes, in 1954, the brightness of Encke was never reported as better than 19th apparent magnitude, according to Vsekhsvyatskii's notes. The 1980 pass, with perihelion in December, is part of a relatively favorable sequence in which good observations have been made before perihelion, but there were no post-perihelion recoveries in 1937 and 1947, according to Vsekhvsyatskii. The 1980 opportunity should on balance, be almost as good as the 1984 one, as far as pre-perihelion coordination with earth-based observations is concerned.

2.7.2 Nonuniformity of the Nucleus

It is not possible to say anything with much certainty concerning the details of the structure of either the surface or the interior of the nucleus. It is possible, however, to draw some inferences for mission planning. It seems quite reasonable, for example, that escaping gases have caused the surface of the nucleus to become vesicular, but the size of the pores is a completely open question. The internal structure of the nucleus could consist of a single core or of a number of smaller bodies which will become separated following the final loss of all the volatile material. Migration of material from the interior reservoir of volatiles could be either through a single porous structure or through the interstices of a conglomerate of individual accumulations of nonvolatile material. The former seems the more likely prospect for this apparently late stage of Encke's active era.

Regardless of how the material to be emitted finds its way to the surface, where pre-perihelion heating removes the bulk of it, it is clear that emission itself is not uniform over the surface of the body. An asymmetric emission is necessary to account for the imbalance of forces causing the nongravitational acceleration. Moreover, the well-known asymmetry of Encke's egg-shaped coma suggests a higher density of expelled gases on one side of the comet than on the other. The preferred direction of efflux seemed to be toward the sun and in the direction of motion of the body along its orbit, with an angle to the sun-comet line greater than the six degrees that applies to a number of other comets. Since the maximum insolation occurs at the subsolar point of the

surface, the offset in emission is taken as evidence of rotation of the nucleus with a period some tens of times the elapsed interval between maximum heating and maximum emission. Some asteroids are highly irregular or elongated. Examination of light curves for Icarus and others might yield an approximation to Encke's period. It would be of great interest to determine whether the emitting area is a particular section which is exposed each time it comes around to the sunlit hemisphere or merely the warmest section of a uniformly coated surface. In either case, three implications are straight-forward: First, the apparent dependence of emission on local heating makes certain regions around the nucleus, e.g., behind it or along the axis of rotation, auspicious for observation with the least hazard to a hovering spacecraft; second, if the emission streamers proceed from particular locations on the surface, the surface should show visible structural detail, and observation from a position above a pole should afford an opportunity to measure the spin rate, even at considerable distance (where nuclear features are still unresolvable); third, removal of most of the available volatiles by the time of perihelion, at the latest, should reveal an irregular surface with resolvable features, making post-perihelion measurement of spin rate feasible with reduced hazard in any position around the nucleus.

Encke does not become entirely inactive after perihelion. Figure 2-25 is a scatter diagram of magnitudes against heliocentric distance, where the magnitudes are those compiled by Vsekhsvyatskii (Reference 2-3; see Appendix J) for post-perihelion observation since 1885. The dashed lines define the general trend in the magnitude-distance correlation. While the scatter is too great to define any dependable curve through the points, it is immediately apparent that the slope of H with r is much too high for the $1/r^2$ asteroidal law of brightness to apply. The solid line representing an arbitrary asteroidal dependence through the center of the magnitude range, shows this. It may be concluded therefore that Encke's asymmetric behavior with respect to perihelion has the advantage that many measurements, including those of the momentum properties of emitted gases, may be made at close range during the outbound pass with little risk.

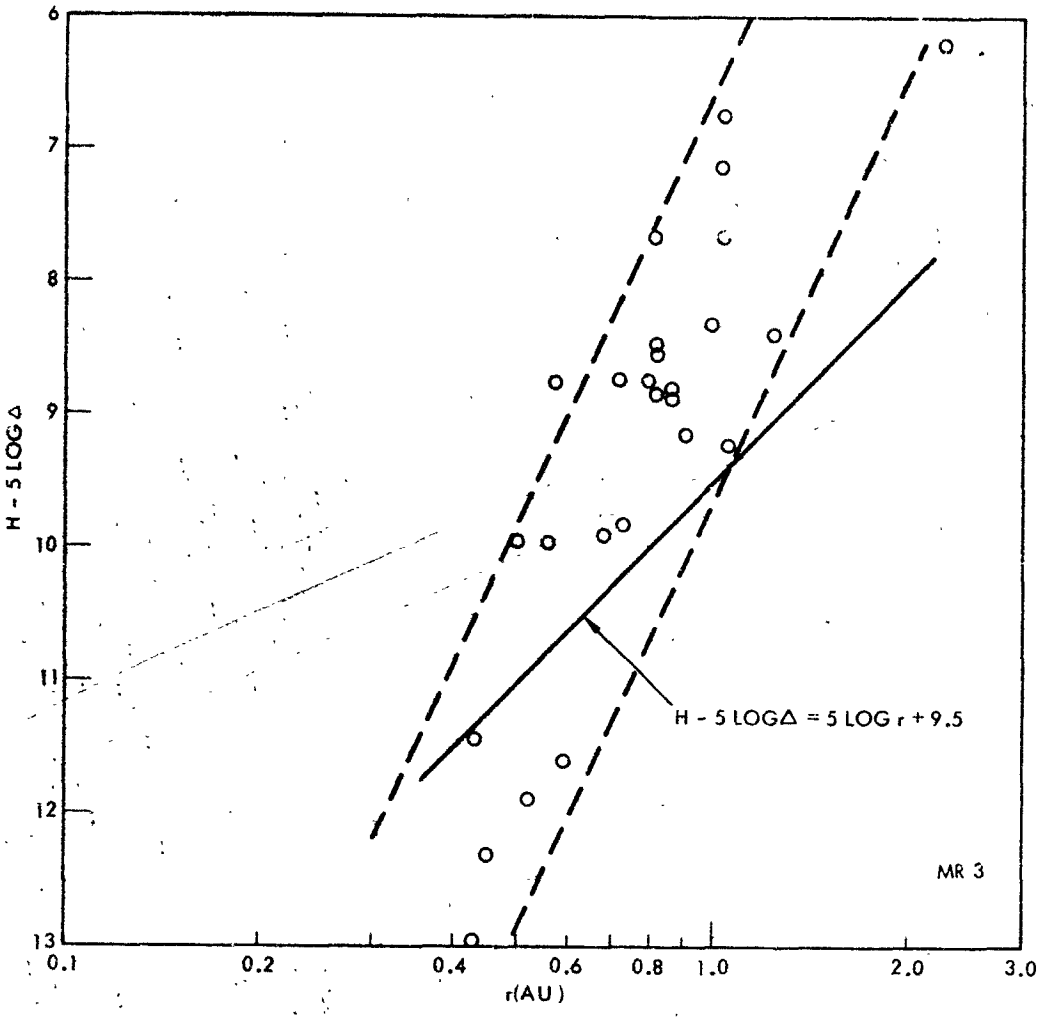

Figure 2-25. Scatter Diagram of Post-Perihelion Magnitudes vs Heliocentric Distance, Showing Failure of Brightness to Follow Asteroidal Law r^{-2}

2.7.3 Variation of Temperature of Nucleus with Heliocentric Distance

The thermal properties of the coma, both un-ionized and ionized the size of the coma, and the distribution of various gas species within it depend on the temperature of the surface of the nucleus from which the gases are emitted. This temperature should properly rise with the solar radiation received by the nucleus as the sun is approached. A nominal functional form for the temperature of an asteroid is (Reference 2-2)

$$T = \frac{350}{r^{1/2}}$$

The evaporation of the ice of a cometary nucleus requires modification of this simple relationship, which is not applicable to a uniformly

ice-encrusted comet when it gets close enough to the sun to emit an appreciable amount of material. Delsemme (Reference 2-12) studied the effect of the heat of vaporization on the surface temperatures of comets and concluded that the correct temperature between r = 0.3 and 4 all should vary with an exponent of r equal to 0.06 and 0.12, i.e., the power of r itself varies with r, but the net effect is to maintain a temperature with relatively little heliocentric dependence once a minimum of about 200°K is achieved at r ≈ 4 AU.

In the case of Encke, with its probably depleted, nonuniform nucleus, a nonuniform surface temperature should be anticipated. Large areas of exposed, nonvolatile surface may follow Levin's asteroidal law, at least approximately. Figure 2-26 displayed this possible heliocentric dependence of temperature for the exposed material between perihelion and 3 AU. The temperature of sections of the surface of Encke's nucleus that emit the ice grains and gases forming the halo and coma may be expected to deviate significantly from the curve of Figure 2-26, and remain relatively constant at about 200°K.

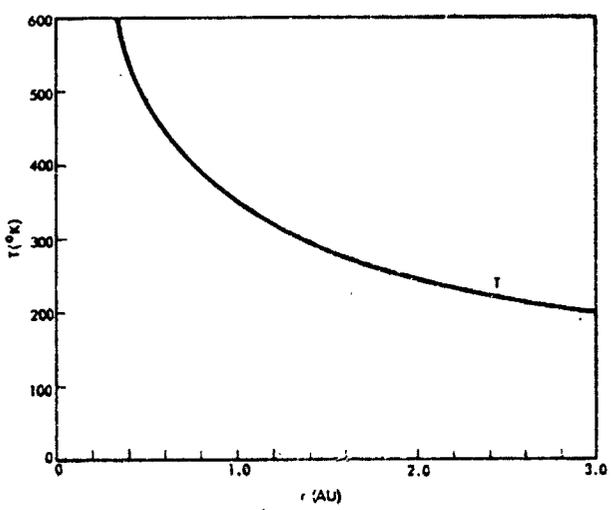

Figure 2-26. Temperature and Velocity of Emission

The actual distribution of temperature of the nucleus is dependent on all those unknown properties that only a closely approaching spacecraft can determine.

2.7.4 Photometric Properties and Projected Images of Encke

2.7.4.1 Magnitude Laws

An assessment of the photometric aspects of an Encke rendezvous mission begins with two basic functional forms of the comet's brightness, or light flux density L. The flux density L_N from the nucleus is assumed to follow the asteroidal law

$$L_N \propto A\phi R_N^2 / r^2 \Delta_S^2,$$

where A, ϕ, R_N, r are as defined in Section 2.2 and Δ_S is the distance from the spacecraft to the comet. Light from any material emitted by the nucleus is assumed to follow a higher power law expressing the increasing [illegible] of luminous material with decreasing r (Reference 2-2), approximated without phase typically by

$$L_C \propto AR_N^2/r^4\Delta_S^2.$$

Subscript C in this case stands for coma. The r^{-4} dependence is a fair approximation to some theory (Reference 2-47),* and has been found by experience to apply roughly to the comas of many comets, including Encke's (Reference 2-47, 2-3). Delsemme (Reference 2-42) has recently presented an argument for an r^{-6} dependence of certain three-stage spectral emissions, notably from H and OH. The principal component of Encke's observable coma is C_2. Expressions for flux L are converted to magnitude H by

$$H = -2.5 \log L = H_0 - 2.5 \log \frac{A\phi R_N^2}{r^n\Delta^2}$$

where H_0 is a standard magnitude accounting for the required proportionality constant, and n is chosen to correspond to the appropriate source object.

2.7.4.2 Magnitude of the Nucleus

One basis for estimating nuclear magnitudes is the same equation used by Roemer (Reference 2-7), already cited:

$$H_N = -26.72 - 2.5 \log \frac{A\phi R_N^2}{r^2\Delta^2}.$$

Roemer found that the product $AR_N^2 \cong 0.24$ (which gave $R_N = 3.5$ km for an assumed albedo A = 0.02).* Substituting this value (with R_N in AU) in the above equation yields:

$$H_N = 13.2 - 2.5 \log \frac{\phi}{r^2\Delta_S^2}.$$

*See also Section 2.2

Here, $H_{No} \equiv 13.2$ represents the magnitude of Encke's nucleus as it would have been seen circa 1960 at 1 AU from both earth and sun, with phase angle $\theta = 0^{\circ}$ ($\phi = 1$), i.e., looking at it from the sun when it crossed the earth's orbit inbound. As will be pointed out, this expression is not entirely consistent with other estimates and may give a result a bit high.

2.7.4.3 Magnitude of the Coma

Evaluation of coma magnitude does not have the foundation provided by Roemer for the nucleus. Values of 10.4 and 10.8 were given for the constant H_{Co} in 1961 (Reference 2-48), which would make H_{Co} a little less than three magnitudes brighter than H_N during that pass. The coma was also said to have been four magnitudes brighter than the nucleus in the same epoch, but it is not obvious how the various "nuclei" and estimates are to be harmonized among independent references. For example, the 10.4 and 10.8 figures for H_{Co} were linked with an $r^{-3.3}$ brightness dependence, different from the r^{-4} usually quoted.

The equation used here for the 1984 apparition is

$$H_C = 12.5 + 2.5 \log r^4 \Delta_S^2,$$

which serves as a compromise among heuristically-determined formulae. The value of $H_{Co} = 12.5$ was obtained by taking $H_{Co} = 10.5$ in 1961 and assuming a two-magnitude loss in brightness of the coma by 1984, a reasonable extrapolation of the mean trend in Figure 2-12. The r^{-4} dependence is used in here for simplicity and in deference to tradition. The comparative results which will be presented would not be severely altered by other choices, given the uncertainty of many of these quantities.

2.7.4.4 Magnitude of the Halo, or Halo-Nucleus Combination

In the icy halo model of coma formation, the nucleus is surrounded by a region of sublimating ice particles of possibly very high albedo. The entire halo is graded, being some 10^4 km in radius (at 1 AU) for the largest, most slowly sublimating, cm-sized grains and progressively smaller for progressively smaller grains down to micron size. All grain

sizes are presumably present near the nucleus, giving the halo a comparatively dense, highly reflective center (Figure 2-18). The brightness of the halo therefore deserves attention because, if present, part of it would appear in an image of the comet's center, even at close range, conceivably competing with the nucleus in intensity. Competition between halo and nucleus may very well affect the estimates of nuclear magnitude above. The approach adopted here is a combination of empiricism and theory that results in reasonable, although speculative, values of the range of halo brightness.

According to Delsemme (Reference 2-42), the production rate of expelled snow particles should vary with heliocentric distance as $r^{-2.1}$, while the production of gases, depending directly on solar radiation, should follow the usual inverse square law. The secondary production of neutral and radical gases trapped in the snowy grains, an essential feature of Delsemme's model, would then vary as the product $r^{-2.1}r^{-2} = r^{-4.1}$. Tertiary production of H^+ or OH^- from the grain-released gases could add a third r^{-2} factor, and Delsemme's paper was in fact written to record the close agreement of some H^+ and OH^- observations with an r^{-6} dependence for one comet (1969g).

If the halo's production varies as $r^{-2.1}$, and if nuclear brightness follows the asteroidal r^{-2} law, light from nucleus and the center of the halo should be virtually indistinguishable in high-resolution images of the comet. This might partially explain the reported failure of Encke's "nuclear" magnitude to follow exactly an inverse square law with heliocentric distance (Section 2.2). Unknown phase, spin axis, and asymmetry effects would also contribute to the comet's true magnitude vs distance dependence. Obviously, the reverse also holds: the contribution of the halo cannot be separated easily from that of the nucleus. The following calculations allow for the difficulty.

If light from the nucleus and part of the halo are indistinguishable, then some of the light attributed to the nucleus may come from the innermost halo. The light from the entire halo should not exceed this by much, since the center is its brightest part. The nucleus magnitude H_N therefore represents something of an upper limit to the halo's magnitude, if all the

light attributed to the nucleus is assigned to the halo. By the same reasoning, the nucleus is not as bright as the expression for H_N suggests.

The nucleus should not be exptected to exhibit the same secular decline in magnitude as the emitted material from Encke, now that it is largely depleted and not likely to be uniformly coated with an icy crust. The halo, however, should continue to diminish from pass to pass. If two magnitudes are added (meaning brightness is diminished) to account for secular decline in grain production by 1984, an upper limit is obtained for the central halo's brightness. The resulting expression can serve as a crude version of the expected maximal brightness of the central halo during the subject mission:

$$H_H = 15.2 - 2.5 \log \frac{\phi}{r^{2.1} \Delta_S^{\,2}}$$

The phase ϕ is not necessarily the same function as in the earlier expression.

2.7.4.5 Magnitude of the Tail

No simple means of estimating the brightness of the tail of Encke is at hand. Its dependence on solar activity via some threshold effect is not amenable to computation. When the tail has appeared, it has obviously been bright enough to be recorded along with the coma and, especially, the nucleus, while its density probably approximates an r^{-4} or r^{-6} law. Since the tail has tended to appear more often at $r < 1$ AU (say, $r = 0.75$) than at $r > 1$ AU, it seems reasonable to attribute to it an absolute brightness some two or three magnitude fainter than that of the coma. It should always be remembered that the light whose brightness is discussed does not have the same spectral content for the nucleus, coma, and tail.

2.7.4.6 Image Brightness

In addition to the brightness of entire cometary features, it is desirable to know the relative "viewing" or "surface," brightnesses of these features as they appear in an image of the comet. The relative brightness of two features can be treated directly in terms of brightness

per unit area or per picture element. If, at a given distance from the comet, a feature of magnitude H_1 occupies a relative area A_1, and a second feature of magnitude H_2 occupies Area A_2, the ratio of relative brightness per unit area is given by $B_1/B_2 = (A_2/A_1)\ 10^{(H_1 - H_2)/2.5}$.

Typical area ratios for cometary features discussed above are, if R_N = 1.8 km, R_H (central halo radius) = 10^2 km:

$$A_N/A_C = 3.24 \times 10^{-10}$$
$$A_N/A_H = 3.24 \times 10^{-4}$$
$$A_H/A_C = 10^{-6}$$

Comparative brightness ratios are useful for estimating dynamic ranges needed by an image system, but it is also important to place expected brightnesses on a common, absolute, scale for all features. The magnitude equations of the preceding paragraphs apply to stellar objects without resolved images, or to the total, integrated light from resolved images. Once a feature has been resolved, its surface brightness follows a different rule from its total brightness. If we consider only the simplest representation of a resolved feature, where the feature and its image are assumed circular, then the area of the resolved image will vary with the square of the image's radius, hence with its subtended angle, and finally therefore with Δ_S^2. Meanwhile the whole feature's brightness will continue to increase with Δ_S^{-2} as a result, the Δ_S^2 terms will cancel, and the surface brightness or brightness per unit area of a resolved feature will remain independent of Δ_S after it has formed a measurable image. Dependence on r will, of course, remain unaltered.

2.7.4.7 Comparative Brightness During Approach

The plots of Figure 2-27 display the behavior of the brightness (magnitudes) of coma and nucleus, or nucleus-halo, vs Δ_S ($\Delta_S \leq 1$ AU)

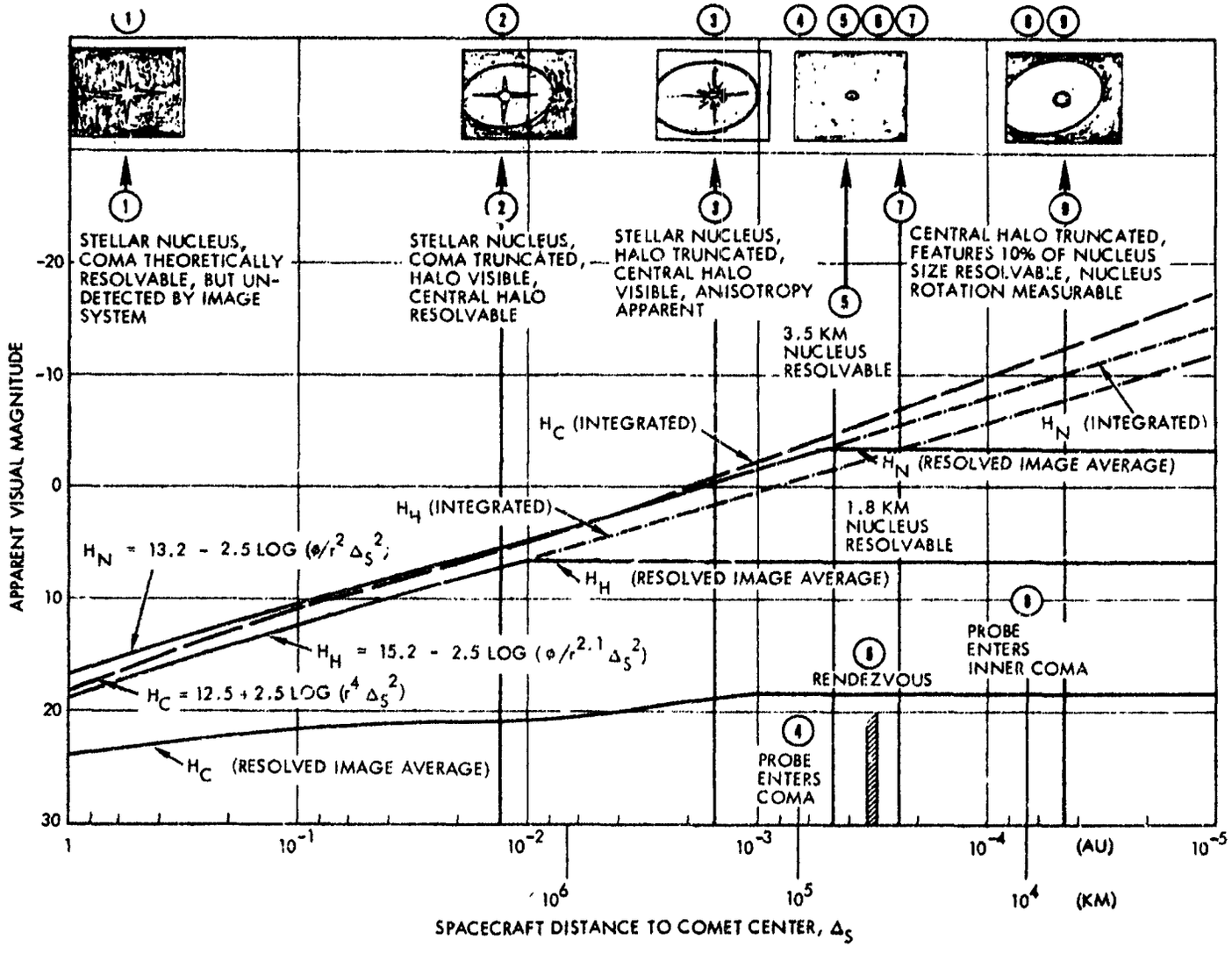

Figure 2-27. Magnitudes of Encke's Features vs Cometocentric Distance along the Proposed Cruise Path, with Conceptual Views, above, of Various Cometary Features at Noted Distances

during the approach of the rendezvous spacecraft to Encke along the preferred trajectory for the mission. The lunar phase function of Figure 2-28 was applied in obtaining the estimates, for both nucleus and halo, but its contribution was negligible. None of the functions H_C, H_H and H_N in Figure 2-27 (upper three curves) are likely to be accurate to better than ±1 to ±2 magnitudes, but their relative position should be quite reliable.

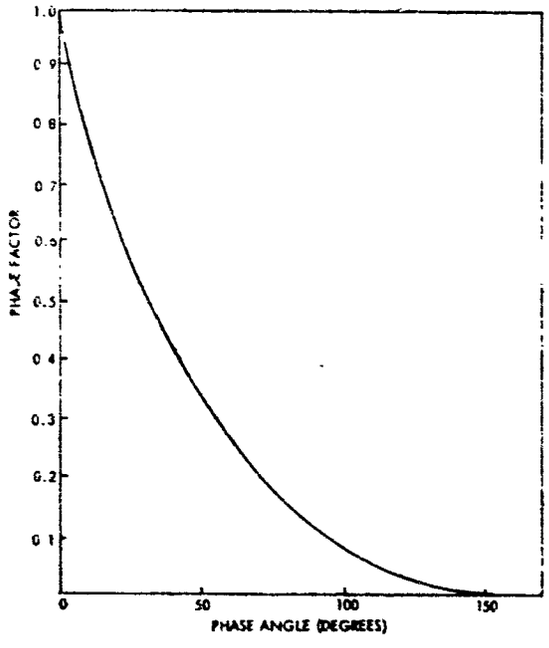

Figure 2-28. The Lunar Phase Function

Dashed and solid line representations of brightness characteristics are used to distinguish between the integrated brightness of a resolved feature (dashed line) and the average brightness per unit area of its resolved image. Therefore below the distance Δ_S at which the image system begins to resolve the feature two line representations are shown. At the left of the graph (Δ_S = 1 AU) the magnitude H_N of the nucleus is 16.6. Until the period where image resolution begins ($\Delta_S \simeq 0.7 \cdot 10^4$ AU) the magnitude varies in accordance with r^{-2}. From there the integrated brightness continues to increase, but the surface, or average, brightness of the resolved image remains constant. The magnitude of the central halo follows a similar pattern, but with the surface brightness becoming constant earlier ($\Delta_S = 10^{-2}$ AU). The coma, having been already resolvable at distances greater than 1 AU, has its integrated and averaged magnitudes entirely separate throughout the figure. The remainder of Figure 2-27 will be described below.

2.7.4.8 Image System

For the following description, an imaging system is assumed of viewing angle 4 x 5 degrees and resolution 100 microradians.* It is on the basis of this resolution that the points at which surface brightness

*See Appendix F

becomes important in Figure 2-27 were determined. In the description below, coma and central halo are treated as though uniform in surface brightness, which is almost certainly not the case.

The sketches in the upper part of Figure 2-27 are conceptualizations of Encke's appearance at the times of significant events during the approach of the spacecraft to the comet. They are described as follows, numbered as in the figure:

1) The coma is resolvable but is probably an undiscernible object of surface magnitude $H_C \approx 24$ when $\Delta_S = 1$ AU, at the left edge of the figure. The nucleus, or nucleus-halo, is a central condensation of stellar appearance. Nucleus, halo, and integrated coma are some 5-8 magnitudes brighter than each element of the coma's image, which has varied little in brightness per unit area from the point of its resolution, depending only on r and not on Δ_S.

2) At $\Delta_S = 2 \times 10^6$ km $\approx 10^{-2}$ AU, the coma if detected begins to be truncated by the image system, while its inner region, made up of parent gases and halo form a discernible central bright center. The central halo is barely resolvable as a 100μrad dot. Its resolved image remains constant in brightness per unit area after this point, with $H_{CH} \leq 6.5$.

3) At $\Delta_S = 1.6 \times 10^{-3}$ AU $\approx 2.6 \times 10^5$ km, the inner coma, or halo begins to be truncated. The central halo is a distinct feature, although probably appearing only as a bright central condensation around a brighter, but unresolved, nucleus. Its (uniform) surface brightness $\gtrsim 6.5$ should contrast with the still stellar nucleus of magnitude $H_N \approx 0$.

4) The probe enters the coma at $\Delta_S = 10^5$ km $\approx 6.6 \times 10^{-4}$ AU.

5) At $\Delta_S = 7 \times 10^4$ km $= 4.7 \times 10^{-4}$ AU, a large nucleus of $R_N = 3.5$ km should become just resolvable as an element of $H_N = -3.5$ much brighter (≈ 10 magnitudes) than its surroundings. The central halo ought to appear as a distinctly asymmetric condensation.

6) Nominal rendezvous occurs at $\Delta_S \approx 5 \times 10^4$ km (see Section 5.5.4).

7) A nucleus of $R_N = 1.8$ km. becomes resolvable at $\Delta S = 2.4 \times 10^{-4}$ AU, 3.6×10^4 km, with $H_N \approx -7$.

8) The probe enters the inner coma or outermost halo at $\Delta_S = 10^4$ km.

9) At $\Delta_S = 7 \times 10^3$ km, the central halo should become truncated while a 3.5 km nucleus should be a distinct,

brilliant object with image elements much brighter (10 magnitudes) than those of the halo surrounding it. Inhomogeneities 1/10th the diameter of the nucleus should be barely resolvable, and rotation of the nucleus should be apparent.

The foregoing synopsis of milestones is indicative, rather than accurate. The contact surface, for example, has not been included, although it may turn out to be the most obvious feature in the images of the comet, while the halo may be negligible. Visibility estimates, based on present technology, may be conservative for 1984. All objects except the nucleus should be understood as little more than regions whose outlines are defined by steep photometric gradients, rather than discrete boundaries. Temporal effects caused by possible solar activity, cometary bursts, or distinct streamers may be visible on approach to the comet. Finally, the formulas on which photometric magnitudes of halo and coma are based might become poor approximations as the comet is approached because the complicated viewing geometry for a large, close object is not incorporated in the photometric laws applied here.

To complete an assessment of the mission-related photometric properties of Encke, the variation of surface brightness of the nucleus with r is shown in Figure 2-29 for various positions from which the spacecraft might view it as the comet approaches perihelion. The plotted estimates are for two nucleus radii, 1.8 and 3.5 km, and five phase angles, indicated in the figure.

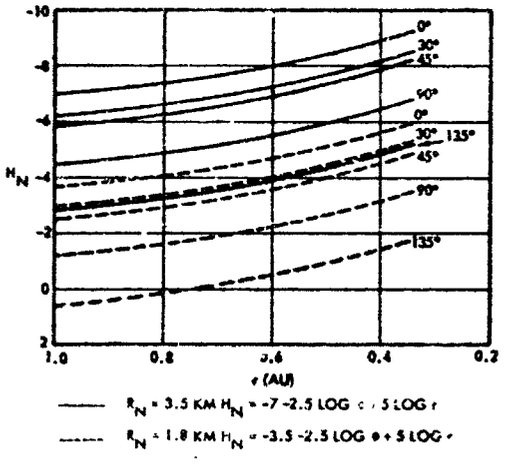

Figure 2-29. Surface Brightness of Nucleus from Rendezvous to Perihelion for Two Sizes of Nucleus and Five Viewing Angles

2.7.4.9 Implications for Encke Rendezvous Mission

No aspect of this evaluation of Encke's properties argues more strongly the value of a rendezvous-type mission than the above attempt to assess the brightness of Encke's component parts. The heliocentric brightness laws of any comet are intimately connected with the physical processes that produce them. Surely one of the most valuable results of a rendezvous with Encke will be the establishment of the correct dependencies of light on r for every contributing feature, especially those such as nucleus and halo, whose theoretical functional forms have kept them essentially inseperable to the present time.

2.7.5 Interference by the Icy Halo

The snowy conglomerate model of Delsemme, with its postulated halo of ice crystals surrounding the nucleus, poses a potential hazard to the integrity of the equipment, the clarity of optical images, and the performance of mass-sampling devices on a rendezvous spacecraft. The discussion which follows suggests that proper instrumentation and exploration strategy should reduce any hazard considerably. (Cf. Section 6.3.)

As Figure 2-17 shows, the nearly 90 percent of ice crystals that lie between 100μ and 1 mm in radius would be expected to reach no further than 1000 to 3200 km from the nucleus over the heliocentric distance between rendezvous and perihelion. Many would not go beyond 400 km at perihelion. If the number of grains released at 1 AU is 1 $cm^{-2}sec^{-1}$ at the surface of a spherically symmetric nucleus, then the flux of 100μ to 1 mm particles is no more than about 10^{-7} $cm^{-2}sec^{-1}$ at 3200 km, equivalent to one particle per cm^2 in 125 days. Smaller particles would not reach 3200 km, and only about five percent of the total, or 5×10^{-9} $cm^{-2}sec^{-1}$ of larger grains would pass the 3200 km cometocentric distance. If the average particle (3 mm radius) weighs 5×10^{-5} gm, the momentum with which it would strike the spacecraft at 1 km/sec would be 5 gm-cm/sec, and its energy would be 0.025 joule. These values represent extreme upper limits: The initial ice grain sizes and masses used in the estimate are reduced to zero by sublimation by the time they reach their estimated maximal distance, and few, if any, ever

acquire a terminal velocity of 1 km/sec. If the production rate of grains varies with heliocentric distance as $r^{-2.1}$, the estimated fluxes would increase to only $(1/0.34)^{2.1}$, or 10 times the values above, at perihelion. But, of course, at perihelion the bulk of the grains would no longer reach beyond about 1000 km from the nucleus.

The rough calculations suggest that the comet's gas emissions can be comfortably examined from outside the halo by a mass spectrometer located between 10^3 and 10^4 km cometocentric distance, while most of the inner halo is observed and nuclear features just barely resolved optically (Section 2.7.4.8), without a serious hazard to the optical sensors. The spacecraft can approach the nucleus for better image resolution as Encke approaches perihelion, with no increased hazard. After perihelion, there should be no difficulty at all. Unfortunately, the rate at which an optical particle detector, such as Sisyphus can expect to count grains is low at 10^3 km, but it could be improved by moving the spacecraft closer to the nucleus. It might be desirable to add heating elements or heated glass windows to exposed sensors to evaporate the tiny ice grains occasionally encountered. Indeed, it might be worthwhile to develop a frost or snow detector that would measure the size and flux distributions of icy grains by observing their effect on a polished surface or through a glass plate and their response to heating.

The foregoing calculations probably overstate the grain densities for Encke. The total emission of grains, if the same proportionality is assumed between grain and gas production, is some 3×10^5 gm/sec, which for a nucleus of R_N = 2 km, gives only 0.03 grains/cm^2/sec, or three percent of the production of "average" grains in the estimate above. Thus, the grain flux at various distances from Encke's nucleus is substantially less than that above and if the nonuniformity of production is translated into an asymmetric flux distribution in the halo, observation from a spacecraft at the proper angles should be safe at virtually any distance, even near perihelion.

Comparable arguments apply to the presence of nonvolatile dust in Encke's coma. The production rate of such dust is believed to be even lower than that assumed for ice grains.

REFERENCES, SECTION 2

2-1 Roemer, E., Cometary Notes, Proc. Astron. Soc. Pax., April, 1961.

2-2 Levin, B. J., Are Gases Evaporated or Desorbed from Cometary Nuclei?, Mem. Soc. Roy. des Sci. de Liège, 12, 65, 1966.

2-3 Vsekhsvyatskii, S. K., Physical Characteristics of Comets, NASA TT F-80, Office of Technical Services OTS 62-11031, 1964.

2-4 Biermann, L. and Lüst, R., The Interaction of the Solar Wind with Comets (Natural and Artificial), The Solar Wind, ed. by R. J. Mackin and M. Neugebauer, p. 355, JPL Report 32-630, 1966.

2-5 Whipple, F. L., and Douglas-Hamilton, D. H., Brightness Changes in Periodic Comets, Mem. Soc. Roy. des Sci. de Liège, 12, 469, 1965.

2-6 Mianes, P., Grudzinska, S., and Stanikowski, A., Observations Physiques de la Comete Periodique Giacobini-Zinner (1959b), Annales Astrophys., 23, 788, 1960.

2-7 Roemer, E., The Dimensions of Cometary Nuclei, Me. Soc. Roy. des Sci. de Liège, 12, 23, 1966.

2-8 Marsden, B. G., Comets and Nongravitational Forces, Astron. J., 73, 367, 1968.

2-9 Matsen, In press, Physical Properties of the Minor Planets, Proceedings of the 12th I.A.U. Colloquium, T. Gehrels, ed., 1971.

2-10 Delsemme, A. H., and Wenger, A., Physico-Chemical Phenomena in Comets-I Experimental Study of Snows in a Cometary Environment, Planet. Space Sci., 18, 709, 1970.

2-11 Delsemme, A. H., and Miller, D. C., Physico-Chemical Phenomena in Comets-III, The Continuum of Comet Burnham (1960 II), Planet. Space Sci., 19, 1229, 1971.

2-12 Delsemme, A. H., Vers un Modelle Physico-Chemique du Noyon Cometaire, Mem. Roy. des Sci. de Liège, 12, 77, 1966.

2-13 Brandt, J. C., The Physics of Comet Tails, Amer. Rev. of Astr. and Astrophys. 6, 267-286, 1968.

2-14 Jacchia, L. G., Meteors, Meteorites and Comets: Interrelations, in The Moon, Meteorites, and Comets, vol. IV of The Solar System, ed. by B. M. Middlehurst and G. P. Kuiper, p. 774-798, U. of Chicago Press, 1963.

REFERENCES, SECTION 2 (CONTINUED)

2-15 Van Schmus, W. R., and Wood, J., A chemical-petrologic classification for the chondrite meteorites, Geochim. et Cosmochim. Acta, 31, 747-766, 1967.

2-16 Wetherill, G. W., Cometary versus asteroidal origin of Chondrite meteorites, in press, Physical Properties of the Minor Planets, Proceedings of the 12th I.A.U. Colloquium, T. Gehrels, ed., 1971.

2-17 Sekanina, Z., Dynamical and Evolutionary Aspects of Gradual Deactivation and Disintegration of Short-Period Comets, Astron. J., 74, 1223, 1969.

2-18 Marsden, B. G., Comets and Nongravitational Forces, II, Astron. J., 74, 720, 1969.

2-19 Sekanina, Z., Total Gas Concentration in Atmosphere of the Short-Period Comets and Impulsive Forces upon Their Nuclei, Astron. J., 74, 944, 1969.

2-20 Vsekhsvyatskii, S. K., and Ilichishina, N. I., Absolute Magnitudes of Comets, 1965-1969, Sov. Astron., 15, 310, 1971.

2-21 Encke, J. F., Berliner Astron. Jahrbuch für 1826, p. 13 , 1823.

2-22 Bessel, F. W., Astron. Nachr, 13, 3, 1836.

2-23 Whipple, F. L., A comet model I, The acceleration of comet Encke, Astrophys. J., 3, 375-394, 1950.

2-24 Marsden, B. G., Comets and Nongravitational Forces, III, Astron. J., 75, 75, 1970.

2-25 Marsden, B. G., and Sekanina, Z., Comets and Nongravitational Forces, IV, Astron. J., 76, 1135, 1971.

2-26 Liller, W., Photoelectric photometry of Comets, Astron. J., 66, 372-380, 1961.

2-27 McCrosky, R., Fragmentation of faint meteors, Astron. J., 60, 170, 1965.

2-28 Whipple, F. L., Problems of the Cometary Nucleus, Astron. J., 66, 375-380, 1961.

2-29 Sekanina, Z., (in press), I.A.U. Colloquium No. 12.

2-30 Sekanina, Z., (in press), I.A.U. Symposium No. 45.

2-31 Swings, P., Le Spectre de la Comete d'Encke, Ann. Astrophys., 11, 124-136, 1948.

2-32 Dufay, J., and Bloch, M., Recherches sur les spectres des cometes, Ann. Astrophys., 11, 107-123, 1948.

2-33 McCrosky, R., Orbits of photographic meteors, Smithsonian Astrophysical Observatory Special Report 257 (20 pp.), 1967.

2-34 Hamid, S., and Whipple, F. L., Helwan Obs. Bull., 41, 1, 1951.

2-35 Hamid, S., and Whipple, F. L., On the Origin of the Taurid Meteors, Astron. J., 55, 185-186, 1950.

2-36 Wetherill, G. W., and Williams J. G., Evaluation of the Apollo asteroids as sources of stone meteorites, J. Geophy. Res., 73, 635-648, 1967.

2-37 Mendis, D. A., Holzer, T. E., and Axford, W. I., Neutral Hydrogen in Cometary Comas, Astrophys. and Space Sci., 15, 313, 1972.

2-38 Biermann, L., and Trefftz, E., Z. Astrophys., 59, 1, 1964.

2-39 Biermann, L., JILA Report No. 93, Univ. of Colorado, 1968.

2-40 Biermann, L., Comets and Their Interaction with the Solar Wind, Quart. J. Roy. Astron. Soc., 12, 417, 1971.

2-41 Biermann, L., Paper presented at Conf. on Cosmic Plasma Phys., ESRIN, Rome, 1971.

2-42 Delsemme, A. H., Comets: Production Mechanisms of Hydroxyl and Hydrogen Halos, Science, 172, 1126, 1971.

2-43 Bertaux, J. L., and Blamont, J., Observation de l'Emission d'Hydrogene Atomique de Comete Bennett, Comt. Rend. Ac. Sci., Ser. B, 270, 1581, 1970.

2-44 Finson, M. L., and Probstein, R. F., A Theory of Dust Comets. I-Model and Equations, Ap. J., 154, 327, 1968.

2-45 Delsemme, A. H., and Miller, D. C., Physico-Chemical Phenomena in Comets-II, Gas Adsorption in the Snows of the Nucleus, Plant. Space Sci., 18, 717, 1970.

2-46 Biermann, L., Brosowski, B., and Schmidt, H. U., The Interaction of the Solar Wind with a Comet, Solar Phys., 1, 254, 1967.

2-47 Bobrovnikoff, N. T., Comets, Astrophysics, ed. J. A. Hynek, p. 302, McGraw-Hill, New York, 1951.

2-48 Vsekhsvyatskii, S. K., Physical Characteristics of Comets Observed during 1967-1965, Soviet Astronomy - AJ, 10, 1034, 1967.

3. SCIENTIFIC OBJECTIVES

3.1 SCIENTIFIC PRIORITIES

Most cometary specialists would no doubt agree that acquiring information about the nucleus should be the primary goal of a mission to rendezvous with a comet. The nucleus, after all, is the comet most of its lifetime along most of its trajectory and is the source of the more familiar, secondary features it displays on approaching the sun. Moreover, it is the nucleus whose substance and structure may offer clues to the material and dynamics of solar system formation and to the ultimate formation of an extinct comet. Not all cometary nuclei are likely to be equally approachable or observable, however, because of potentially hazardous dust, dense snow, or high momentum of expelled gas. At the same time, the resources available for cometary missions are limited, so that even a comet ideally suited to nucleus observations cannot justify a mission solely for that purpose. A mission to Encke in 1984 should therefore seek a balanced set of measurements tailored to this particular comet in that particular year.

3.1.1 Specialized Characteristics of Encke/1984

The three most significant peculiarities of Encke/1984 and their implications are summarized in Table 3-1. In 1984 Encke will offer a target whose properties invite a mission with the very priorities a comet investigation should have. The nucleus will be as nearly depleted of emissible material as a moribund but still active nucleus can be and will be exposed to observation by an imaging optical system. Nonetheless, the activity of the nucleus should produce enough material similar to that emitted by other comets to allow reliable sampling of the gases responsible for the coma. Also, the processes of interaction between the coma and the solar wind should be detectable locally even though the tail is unlikely to be observable from earth. Finally, it should be possible to approach the nucleus closely, say within 10 to 100 km, after perihelion if not sooner, to inspect it in detail and measure its mass and surface properties. The assignment of priorities to measurable features of Encke is guided here by these special considerations.

Table 3-1. Special Considerations of Encke Mission

CHARACTERISTICS OF ENCKE	PHYSICAL IMPLICATIONS	MISSION IMPLICATIONS
1. STEADILY DIMINISHING EMISSION AND OUTBOUND INACTIVITY	ABSENCE OF RETAINED ICY CRUST; MIGRATION OF VOLATILES; POROSITY OF SURFACE OF NUCLEUS; APPROACHING EXTINCTION	NUCLEUS SHOULD BE DEFINABLE, OBSERVABLE OBJECT WITH DISTINCT FEATURES; LOW OUTBOUND EMISSION FAVORABLE TO CLOSE OBSERVATION OF RELATIVELY INACTIVE NUCLEUS AFTER PERIHELION; SUFFICIENT EMISSION BEFORE PERIHELION TO PROVIDE DATA ON GENERAL COMETARY GASES.
2. VARIABLE OBSERVABILITY	SMALL OBJECT; APPEARANCE POSSIBLY DEPENDENT ON SOLAR ACTIVITY	CLOSE APPROACH NECESSARY; 1984 FAVORABLE FOR TELESCOPIC CORRELATION, BUT PROJECTED SOLAR ACTIVITY POSSIBLY UNFAVORABLE FOR VISIBILITY OF TAIL FROM EARTH; EMPHASIS ON NUCLEUS JUSTIFIED
3. LOW CONTINUUM REFLECTION	RELATIVELY LITTLE SOLID PARTICLE EMISSION	RELATIVELY FAVORABLE ENVIRONMENT FOR CLOSE NUCLEUS OBSERVATION BEFORE PERIHELION, ESPECIALLY OUT OF ORBIT PLANE

3.1.2 Classes of Observable Features and Their Priorities

The features of the comet nucleus may be divided into relatively superficial, astrometric qualities and physical or chemical qualities associated with the detailed composition and structure of the nuclear material. These may in turn be divided according to whether they refer to the lithic, nonvolatile or the icy, volatile components of the nucleus. The coma is more finely comprised of the neutral inner coma, including the possible icy halo, the ionized coma, and the vast hydrogen cloud, or extended coma, that reaches out to a million kilometers from the nucleus. All these features are grouped into six classes in Table 3-2 from a combined phenomenological and mission-oriented standpoint that lists their measurable properties and emphasizes the priority with which they ought to be observed. In this view, the inner coma is regarded as a source of derivative information about the nucleus rather than primary information about the origin of the visible coma.

The classes in Table 3-2 do not represent a progressive and gradual decrease in priority from top to bottom. Rather, the first three classes together represent priorities differing little among each other

Table 3-2. Classes of Observable Features in Decreasing Order of Priority for 1984 Encke Rendezvous

CLASS	MEASURABLE FEATURES	
1. EXTERNAL PHYSICAL CHARACTERISTICS OF NUCLEUS	• SIZE	• MASS
	• ROTATION	• SHAPE
	• APPEARANCE OF DETAILS	• ALBEDO
	• PHASE FUNCTION	• FINE SCALE TEXTURE
	• TEMPERATURE	
2. STRUCTURE AND COMPOSITION OF NUCLEUS: NONVOLATILES	• SURFACE MATERIAL ABUNDANCE	• SUBSURFACE TEMPERATURE
	• SUBSURFACE THERMAL AND ELECTRICAL CONDUCTIVITY	• INTERNAL THERMAL AND ELECTRICAL CONDUCTIVITY
	• MAGNETIC PROPERTIES	
	• INTERNAL STRUCTURE	• SURFACE CHEMICAL COMPOSITION
	• EXPELLED PARTICLE COMPOSITION	• EXPELLED PARTICLE SIZE, VELOCITY AND SPATIAL DISTRIBUTION
3. COMPOSITION OF NUCLEUS AND INNER COMA: VOLATILES	• FLUX, VELOCITY, COMPOSITION AND DENSITY OF NEUTRAL GASES	
		• ICY GRAINS
4. COMA FORMATION	• FLUX AND SPATIAL DISTRIBUTION OF RADICALS	• FLUX AND SPATIAL DISTRIBUTION OF IONS
5. SOLAR WIND INTERACTION AND TAIL FORMATION	• RADICAL AND ION SPATIAL DISTRIBUTIONS	• SPATIAL DEPENDENCE OF FLUX, VELOCITY, DENSITY AND COMPOSITION OF MODIFIED SOLAR WIND
	• SPATIAL MODIFICATION OF SOLAR WIND MAGNETIC FIELD	• OCCURRENCE AND DISTRIBUTION OF PLASMA AND ELECTROMAGNETIC WAVE MODES
6. EXTENDED COMA	• SIZE AND SHAPE OF HYDROGEN CLOUD	

but all considerably higher that that of Class 4. The highest priority is assigned those characteristics least known and least likely to be measured without a rendezvous mission. The listing in Table 3-2 is an expression of priorities appropriate to a 1984 rendezvous mission to Encke strictly from a scientific point of view. An actual mission and an actual payload must take other considerations into account. The list, however, is important as a guide to the selection of scientific objectives. The selection in this report requires additional discussion of these cometary features together with the techniques that might be employed in their observation.

3.2 SELECTION OF OBJECTIVES

3.2.1 Candidate Measurements

Table 3-3 lists the types of instrumentation and their special requirements from which a comet rendezvous mission is expected to draw for its payload.

Table 3-3. Candidate Measurements

MEASURABLE FEATURES	MEASUREMENT TECHNIQUES OR COMBINATIONS OF TECHNIQUES	SPECIAL REQUIREMENTS
	1. EXTERNAL PHYSICAL CHARACTERISTICS OF THE NUCLEUS	
SIZE	TV, BISTATIC RADAR RANGING	
	TV, RADAR ALTIMETER RANGING	
MASS	HOVERING FORCE, EMISSION PRESSURE, BISTATIC RADAR, OR RADAR ALTIMETER RANGING	
	GRAVITY GRADIOMETER, BISTATIC RADAR OR RADAR ALTIMETER RANGING	VERY CLOSE APPROACH
	DOPPLER, BISTATIC RADAR OR RADAR ALTIMETER RANGING	
ROTATION	TV	
SHAPE	TV	
APPEARANCE OF DETAILS	TV	
ALBEDO	PHOTOMETRY	
PHASE FUNCTION	PHOTOMETRY	
FINE SCALE TEXTURE	PHOTOPOLARIMETRY	
TEMPERATURE	IR RADIOMETER	
	2. STRUCTURE AND COMPOSITION OF THE NUCLEUS: NONVOLATILES	
SURFACE MATERIAL ABUNDANCE	X-RAY SPECTROMETRY	MATERIALS RESTRICTIONS, LANDER OR EXTREMELY CLOSE APPROACH, LONG DWELL
	γ-RAY SPECTROMETRY	SAME AS ABOVE
	NEUTRON ACTIVATION, γ-RAY SPECTROMETRY, X-RAY ACTIVATION ANALYSIS	LANDER
	α BACK-SCATTERING	LANDER, HIGH VOLTAGE
SUBSURFACE TEMPERATURE	THERMAL PROBE	LANDER
SUBSURFACE THERMAL AND ELECTRICAL CONDUCTIVITY	THERMAL AND ELECTRICAL PROBES, HEATERS AND COILS	LANDER
MAGNETIC PROPERTIES	MAGNETOMETER, INDUCTION COIL	LANDER
INTERNAL THERMAL AND ELECTRICAL PROPERTIES	MAGNETOMETER, THERMAL PROBE	LANDER, SOLAR WIND MONITOR
INTERNAL STRUCTURE AND DYNAMICS	SEISMOMETER	LANDER
	SEISMOMETER, 1 KG CHARGE	LANDER, CHARGE DELIVERY APPARATUS
SURFACE CHEMICAL COMPOSITION	GAS CHROMATOGRAPHY	LANDER
EXPELLED PARTICLE COMPOSITION	IMPACT IONIZATIONAL ANALYSIS	
EXPELLED PARTICLE SIZE, VELOCITY, MASS SPATIAL DISTRIBUTION	PHOTOPOLARIMETER	
	TIME-OF-FLIGHT SENSOR	
	MOMENTUM AND TIME-OF-FLIGHT SENSOR	
THERMOMAGNETIC COMPOSITION	MAGNETOMETER	CLOSE APPROACH

Table 3-3. Candidate Measurements (Continued)

MEASURABLE FEATURES	MEASUREMENT TECHNIQUES OR COMBINATIONS OF TECHNIQUES	SPECIAL REQUIREMENTS
	3. COMPOSITION OF NUCLEUS: VOLATILES	
FLUX, VELOCITY, DENSITY, COMPOSITION SPATIAL DISTRIBUTION OF NATURAL GASES	MASS SPECTROMETRY	SCANNING ABILITY
FLUX, VELOCITY, DENSITY, COMPOSITION SPATIAL DISTRIBUTION OF ICY GRAINS	TV PHOTOPOLARIMETRY	SCANNING ABILITY
	4. COMA FORMATION	
FLUX AND SPATIAL DISTRIBUTION OF RADICALS	SPECTROPHOTOMETRY SPECTROMETRY	SCANNING CAPABILITY SCANNING CAPABILITY
FLUX AND SPATIAL DISTRIBUTION OF IONS	TV MASS SPECTROMETRY SPECTROPHOTOMETRY SPECTROMETRY	SCANNING CAPABILITY SCANNING CAPABILITY SCANNING CAPABILITY
ELECTRON DENSITY	ELECTRON PROBE PLASMA WAVE DETECTION	SCANNING CAPABILITY, SOLAR INPUT MONITOR LOW WAVE BACKGROUND NOISE
	5. SOLAR WIND INTERACTION AND TAIL FORMATION	
RADICAL AND ION SPATIAL DISTRIBUTION	SPECTROPHOTOMETRY	SCANNING CAPABILITY
SPATIAL DEPENDENCE OF FLUX, VELOCITY, DENSITY, AND COMPOSITION OF MODIFIED SOLAR WIND	PLASMA ANALYSIS ION MASS SPECTROMETRY	SCANNING CAPABILITY, SOLAR WIND MONITOR
ELECTRON DENSITY	ELECTRON PROBE PLASMA WAVE DETECTION	LOW WAVE BACKGROUND NOISE
SPATIAL MODIFICATION OF SOLAR WIND MAGNETIC FIELD	MAGNETOMETER	LOW MAGNETIC INTERFERENCE, SOLAR WIND MONITOR
OCCURRENCE AND DISTRIBUTION OF PLASMA, ELECTRIC AND ELECTROMAGNETIC WAVEMODES	PLASMA WAVE DETECTION ELECTROMAGNETIC WAVE DETECTION	LOW WAVE BACKGROUND NOISE, SOLAR WIND MONITOR SAME AS ABOVE
	6. EXTENDED COMA	
SIZE AND SHAPE OF HYDROGEN CLOUD	SPECTROPHOTOMETRY, LYMAN-α	SCANNING CAPABILITY

Clearly, the entire list is too extensive to be assigned to any single mission. Moreover, certain instruments impose special requirements, e.g., a lander package, that are rather demanding for any mission. It is also clear that certain instruments can fulfill several functions. Thus selectivity is essential in defining mission objectives and payload instruments.

3.2.2 Mission Constraints

The scientific objectives of the rendezvous mission developed in this report have been subjected to three major constraints:

1) The suggested instrument complement is to represent a "fundamental rendezvous payload" which is justifiable in the sense that elimination of any instrument would make the mission substantially less appealing, scientifically, while addition of any instrument would burden it unacceptably from an economic standpoint.

2) In the interest of economy, the simplicity of a single spacecraft is preferred over the complexity inherent in the use of separable instrument packages for landing on the nucleus or monitoring the solar wind outside the extended coma.

3) The mission will be unique, or at least likely to remain so for a long time. That is, it may not be assumed that the proposed payload will be one of several, each of which can be specialized to observe certain features, leaving other features to be examined by different payloads.

In addition, a fourth, weaker constraint has been considered: that a separate flyby or flythrough mission to Encke or to a similar comet will take place in the foreseeable future, e.g., as a precursor.

The first constraint obviously calls for judgments not likely to be made identically by all cometary researchers. All the constraints together have been interpreted in the following way in preparing this assessment: a preferred set of objectives and a payload are to be selected which depends on a single spacecraft, provides substantial information within the first three classes of measurable features, and provides some information on all classes that would be difficult or impossible to obtain without a rendezvous-type mission.

3.2.3 Considerations in Selecting Measurements

The following paragraphs discuss the considerations involved in selecting an instrument complement satisfying the constraints of this mission.

3.2.3.1 Remote Observation of the Nucleus

Characterization of the nucleus remains the principal objective of the mission, regardless of constraints. Unfortunately, almost the whole of the Category 2 properties of the nucleus require an extremely close approach or an actual landing on the nucleus. These properties must therefore simply be skipped over in developing a "fundamental" set of objectives and instruments. Since the nucleus is a completely unknown and uncharted object, a lander package can hardly be justified as part of a "minimal" payload when even the most elementary properties to be found by the lander are undetermined at the outset. The fate of the recent Soviet Mars lander underscores this.

In contrast, the elementary, or astrometric, properties of the nucleus are measurable from a distance and their observation should be the primary objective of the mission. The items of Class 1 (Table 3-2) are vital features, none of which has been directly measured to any accuracy. This objective is made more feasible by the numerous properties of the nucleus that can be recorded by a relatively few instruments, especially by a TV imaging system. A system capable of resolving features of dimension one-tenth the diameter of the nucleus would be adequate for the scientific imaging requirements.

Although the material of the nucleus will be essentially inaccessible while at rest on the surface, some of it will be expelled and thereby amenable to measurement at a distance. The most promising avenue is analysis of neutral gases by means of mass spectrometry in the inner coma. Such analysis, since it bears on the question of composition of nuclear constituents is next in importance to remote measurements of the nucleus itself.

Along with the gases emitted by the nucleus there should be solid particles, both lithic nonvolatiles, and icy grains. Provided the spacecraft is not moving too quickly, the impacts from the emissions should

be of relatively slow speed, and thus not cause much physical damage. However, this characteristic makes it also difficult to make any direct measurements of the nature of the solid material since it is necessary to make one pass through the coma at a relatively high speed (of the order of 1 km sec^{-1}) if the traditional methods for detecting solid particles are employed. Whatever compositional data can be obtained on solid particles will have been acquired by detectors carried by a fast flyby or flythrough mission and need not be contemplated here. In any case, careful use of the TV, a photometer, an optical particle detector, and a polarimeter, allowing the instruments to look in a direction other than the nucleus, may be of great help in recording the physical characteristics of the solid debris. An effort might be made to fly the spacecraft through the plane of the orbit of the comet several times in order to determine whether there are any traces of a Type II dust tail.

3.2.3.2 The Neutral Coma

The neutral gases emitted by the nucleus are of interest not only because they represent nuclear matter, as already discussed, but also for their own sake as hitherto unobserved parent material of the visible coma. It is desirable to measure their density distribution, wind speed and direction, and composition. Some attention should be given to the possibility of measuring time variations in these quantities, both from the point of view of sudden brightenings (if any), and the more gradual changes associated with the motion of the comet towards and away from perihelion. As far as the atoms and free radicals are concerned, it will be necessary to make observations of the emission and absorption of light (IR, visible, UV) by one means or another. The molecules which are the parents of the atoms and radicals can be examined in more detail, since a mass spectrometer can be used without any fear that wall effects will distort the results. A mass spectrometer must effectively measure the flux of a given constituent from a given direction. In most applications this does not create a difficulty as far as measuring densities are concerned, since it is usually possible to estimate the relative velocity by some independent means. In the case of a cometary coma, however, we are dealing with a neutral atmosphere which is expanding radially away from a nucleus at an unknown highly supersonic

speed. In order to measure this speed, and hence convert flux measurements into density measurements, it seems necessary that some use should be made of the motion of the spacecraft, since this will produce an aberration of the neutral molecules. If the mass spectrometer scans in a plane defined by the velocity vector of the spacecraft relative to the nucleus, and the direction to the nucleus and the aberration angle can be measured, then from the known speed of the spacecraft it should be possible to determine the speed of the expanding coma gas. It is assumed, of course, that the gas is moving radially away from the nucleus. It may be more convenient to use a series of separate entrance ports rather than physically moving the instrument. The angular resolution required will be determined by the radial speed of the gas, and the speed of which the spacecraft moves around the nucleus. The spacecraft must not move too slowly, since then the aberration will be too small to measure.

3.2.3.3 The Ionized Coma, Contact Surface, and Tail

Reasons have been given for believing that there should be a relatively dense "ionosphere" surrounding the cometary nucleus, bounded by a contact surface on the upstream side and flowing away as a Type I tail on the downstream side. The ions are likely to be mostly photoions produced from parent molecules (e.g., CO^+, CO_2^+), but there may also be appreciable quantities of ions of daughter products especially H^+ and O^+. The electron temperature may be high, since they are photoelectrons and may not have sufficient time to come into equilibrium with the rest of the gas. The ion temperature may be only 1000° K or so, but the electron temperature could easily be several times larger. The plasma may also be flowing into the tail of the comet at rather high speeds (several km sec^{-1}). Experiments include multichannel photometers, retarding potential analyzers, or Langmuir probes to measure the electron density and temperature, ion mass spectrometers to measure the composition of the plasma, and an orientable Faraday cup or similar device to measure the flow speed of the plasma. The electron content of cometary plasma along the line of sight does not seem to be large enough to make propagation experiments worthwhile, but radio frequency plasma resonance experiments may be a useful means

of determining the density and composition. In both the neutral and ionized components of the coma it should be possible to make use of techniques which have proved successful in the earth's upper atmosphere and ionosphere. Figure 3-1 shows the spectral range covered by a combination of one UV and one visible-light spectrophotometer.

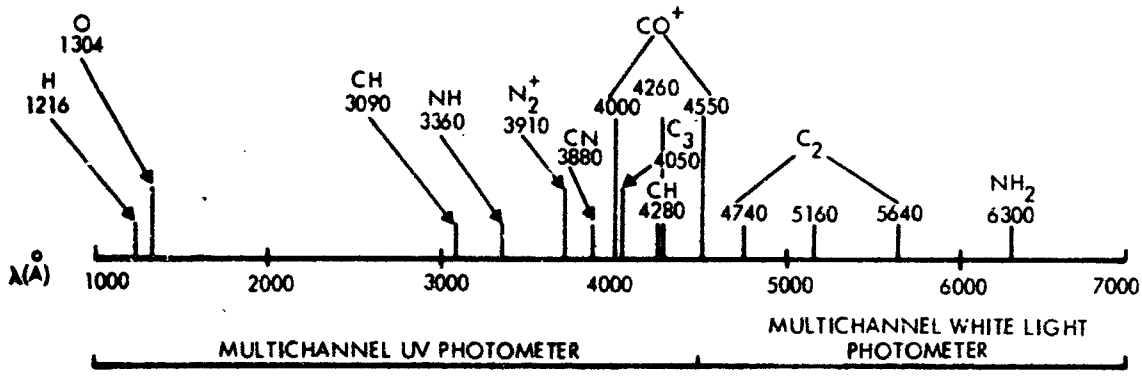

Figure 3-1. Spectral Range of Principal Constituents

Magnetic fields play a vital role in the interaction of the ionized coma with the solar wind. The most important measurement to be made with a magnetometer, apart from supporting the solar wind measurements, is to determine the manner in which the interplanetary magnetic field penetrates the ionosphere of the comet. It is necessary to determine whether in fact a contact surface exists, and the extent to which it is stable. Type I tails appear to have their roots in the cometary ionosphere, and it appears that the magnetic field can be held for a considerable length of time. It is not out of the question that a neutral sheet should form in the wake of the comet, and that transient reconnections of the field in the tail should occur similar to those which appear to occur in the tail of the earth's magnetosphere.

3.2.3.4 Solar Wind Measurements

It is important to determine characteristics of the solar wind flow around the comet, and in particular to determine (1) the strength and configuration of the bow shock, and (2) the shape and presence of the contact surface. The characteristics of the flow will be somewhat similar to those of the earth's magnetosheath (i.e., low Mach number),

but it is complicated by the probable presence of substantial quantities of singly-ionized ions of cometary origin. A Faraday cup, or electrostatic analyzer of the usual type should be adequate to measure the gross features of the plasma flow. Determination of the composition of the interaction-influenced solar wind (which is probably the most interesting) will necessitate the use of more sophisticated instrumentation, perhaps a crossed-field spectrometer of the type flown on several recent IMP spacecraft.

3.2.3.5 Energetic Particle Measurements

There seems to be no case for measuring energetic particles of galactic and solar origin as part of a comet rendezvous mission. However, it would be useful to include in the payload a thin-walled Geiger tube capable of detecting electrons within energies >20 keV, and soft X-rays. The X-ray albedo of the nucleus may in itself be of some interest, and there is a reasonable case to be made for expecting that energetic electrons may be produced in some of the more violent and unstable regions of the whole solar wind cometary environment (notably at the bow shock, the contact surface, and in the tail).

3.3 SUMMARY OF SELECTED OBJECTIVES

Table 3-4 is a compilation of selected scientific objectives chosen to be consistent with the priorities and constraints discussed above for a single spacecraft on a 1984 rendezvous mission to Encke.

Table 3-4. Selected Minimal Objectives of 1984 Encke Rendezvous

1) Measure external physical characteristics of nucleus (all of Class 1 in Table 3-2).

2) Measure size, velocity, and spatial distribution of expelled nonvolatile particles (last item of Class 2 in Table 3-2).

3) Measure flux, velocity, density, and composition of expelled neutral gases and icy grains (all of Class 3 in Table 3-2).

4) Measure flux and spatial distribution of ionized coma gases (second item of Class 4 and first item of Class 5 in Table 3-2).

Table 3-4. Selected Minimal Objectives of 1984 Encke Rendezvous (Continued)

5)	Measure the magnetic and electrical properties in solar wind interaction phenomena (second and last items of Class 5 in Table 3-2).
6)	Measure modified solar wind in the coma (item 2 in Class 5 of Table 3-2).

4. SCIENTIFIC PAYLOADS

4.1 SELECTION OF INSTRUMENTS

In order to translate the scientific objectives and reasoning of preceding sections into a payload list to which mission-planning factors can be related, a set of specific instruments has been selected as representative payload hardware. It is recognized that actual flight payload assignments are often difficult, controversial, and occasionally even arbitrary. The constraint that the selection ma[illegible]re define an essential, minimal, or fundamental payload makes the probability very high that the choice will suffer all three characteristics. A given measurement may be regarded as essential by one scientist, superfluous by a second, and cause for mission cancellation by a budget planner.

4.1.1 Criteria of Instrument Selection

1) Instruments having multiple application to several unknown properties of the comet should take priority over those with comparatively limited use.

2) Instruments of secondary priority should place correspondingly less demand on the payload, e.g., less mass allocation.

3) Relatively undemanding instruments aimed at secondary objectives and very likely to make successful measurements are to be preferred over instruments aimed at primary objectives but which are partially redundant, demanding, or of doubtful prospect.

4) The choice of instruments and the judgment of whether they satisfy the other stated criteria should be based on an examination of the available parameters of "typical" existing devices.

5) An instrument aimed at relatively superficial measurement of a secondary property is to be considered fundamental and preferable to one aimed at detailed measurement of a primary property if inclusion of the former seems likely to encourage "broadened" support of the mission in the scientific community.

6) In addition to being selected for, or rejected from, a "fundamental" payload, all instruments considered should be categorized according to the roles they might play in a rendezvous mission and displayed so the selected ones may be examined in the context of all those reviewed.

7) Tentative provision should at least be made for instruments that promise to fulfill priority functions in a unique way, even at the risk that subsequent calculations show that successful measurements are uncertain.

4.1.2 Categories of Candidate Instruments

Instruments have been grouped in four categories:

Category I. The fundamental payload. Instruments in this category measure properties inaccessible from the earth and those unpromising for measurement with a flythrough payload; they would be relatively simple and tested by experience.

Category II. Instruments individually omitted from the fundamental payload because of at least one significant drawback, but from among which the payload complement might be augmented if weight and financial considerations were to permit it, or from which substitutions might be made if justified by further study.

Category III. Relatively simple instruments making up, and requiring, a separable lander package. This is a category of instruments aimed at high-priority objectives, but eliminated by the constraint that only a unitary spacecraft be regarded as fundamental.

Category IV. Instrumentation which would be valuable to a comprehensive mission in which constraints on spacecraft size, complexity, and separability were lifted entirely.

4.2 THE FUNDAMENTAL PAYLOAD

Table 4-1 lists the instrument complement selected for the fundamental payload. At the end of the table the estimated mass of this complement is shown, broken two different ways into subtotals. The subtotals display the emphasis on measurements of nuclear properties and on optical means of measurement. The first breakdown reflects the preference demanded by the situation anticipated for Encke in 1984. The second reflects a bias toward measurements compatible with the remote earth-based data whose limitations the rendezvous is intended to overcome, but on which most future cometary observations will continue to depend. As

Table 4-1. Category I Instruments. Fundamental Scientific Payload Complement for 1984 Encke Rendezvous

Instrument	Property to Which Applied
TV Image (100 ma resolution)	Size of nucleus
	Rotation of nucleus
	Shape of nucleus
	Appearance of details of nucleus
	Size of halo
	Shape of halo
	Size of coma
	Shape of coma
	Size of tail (uncertain)
	Shape of tail (uncertain)
Multichannel White Light Photometer	Albedo of nucleus
	Phase function of nucleus
	Albedo of halo
	Phase function of halo
	Brightness profile of halo
IR Radiometer	Temperature of nucleus
Photopolarimeter	Fine scale texture of nucleus
	Fine scale size distribution of ice grains of halo
	Fine scale size distribution of nonvolatile particles of coma
Microwave Altimeter	Mass of nucleus
	Size of nucleus
	Surface composition of nucleus
Radiometer UV 1000–4500Å	Distribution of ionized gases in coma, contact surface, and tail
Optical Particle Detector (Sisyphus)	Distribution, velocity of icy grains of coma
	Distribution, velocity of nonvolatile particles of coma
Mass Spectrometer	Flux, velocity, density, spatial distribution of neutral and ionized gases of coma
Magnetometer	Magnetization of nucleus
	Magnetic field configurations of contact surface, tail, and interaction region
Plasma Wave Detector	Electric waves in contact surface, tail, and interaction region
	Local electron densities in ionized coma
Langmuir Probe	Local electron densities in ionized coma
Plasma Probe	Flux, density, energy spectrum of solar wind and reduced solar wind in interaction region
Estimated mass of instruments measuring direct properties of the nucleus	43.0 Kg
Mass of remaining instruments	9.0 Kg
Total mass	52.0 Kg
Estimated mass of optical detectors	33.0 Kg
Estimated mass of altimeter	6.0 Kg
Estimated mass of gas and plasma property analyzers	13.0 Kg
Total mass	52.0 Kg

the table shows, most of the demanding instruments have application to several properties, some to properties of both nucleus and coma.

The list of instruments splits into two groups, those mounted in a fixed position and orientation, and those requiring a scanning capability. The fixed group consists of the optical particle detector, magnetometer, plasma wave detector, and Langmuir probe. The scanning group is divided into detectors that will predominantly follow the nucleus: the TV camera, photometer, IR radiometer, mass spectrometer, and microwave altimeter and detectors that will scan the coma or interaction region as well, i.e., the UV radiometer, photopolarimeter, mass spectrometer, and plasma probe. These subgroups should be mounted to have scanning capabilities independent of each other. As will be seen in Section 7, our spacecraft implementation does not reflect the latter requirement, but for simplicity provides only a single scan platform. This platform is time-shared in the sense of serving nucleus pointing and coma pointing needs on a part-time basis.

Obviously there are many details of instrumentation such as measurement ranges, power levels, individual masses, sensitivities, look angles, and data rates that are omitted from the table and, indeed, from the report. Eventually, an effort to define these quantities will have to be attempted, and the capacities of real instruments will have to be matched to these quantities. Since most of the principal objectives of a rendezvous mission involve features of which no direct measurements whatever exist, it is difficult to assign a desired accuracy to a given measurement. Virtually any figures would advance our knowledge. Indeed, it may be that accuracies or sensitivities with which individual measurements should be made can best be described in relation to each other. A poll of cometary specialists might reveal just how precisely the mass or reflectivity of the nucleus needs to be determined to derive information about Encke that would differentiate among theories of cometary, or solar system, origin, if this is a serious goal of cometary research.

One area in which scientific work needs to be done is in the theoretical characterization of the nonacqueous and ionized coma. No theoretical computation like that of Mendis et al. (Reference 2-37; see Figure 2-15) for the H_2O gases has been done for CH_4 or for the ions. The question, therefore, of how much mass flux of, say, CO^+ a mass spectrometer should expect to encounter at given cometocentric distance, or how much light flux from, say, NH_2 a spectrophotometer should anticipate over a given solid view angle at a given distance in a given direction, is unanswered, even to a reasonable approximation. A decision whether particular existing instruments would be suitable to determine such unestimated fluxes is clearly not now supportable. It would be misleading to include data that would suggest that such questions had been answered in the context of selecting a "fundamental" payload as defined here. A considerable amount of work is still to be done.

4.3 EXPANDED-PAYLOAD COMPLEMENTS

4.3.1 Category II Instruments

Table 4-2 is a list of devices considered for the fundamental payload but omitted because of various drawbacks affecting each individually. If a payload of capacity larger than that needed for the fundamental complement were available, instruments on this list might be chosen for further study and possible addition to the experiment package. The gravity gradiometer or multichannel radiometer seems an appropriate first choice for inclusion in an enlarged fundamental complement. In addition, instruments are currently under development that will be capable of determining the composition of nonvolatile particles without requiring high-velocity impacts (Wetherill private communication). These are not included in the chart, but should they be available by 1980, would certainly belong in Category II, and probably in Category I as defined here.

The argument by which the gravity gradiometer was assigned to Category II instead of Category I is worth recounting, since it illustrates the way in which the criteria of Paragraph 4.1.1 were applied. Measuring the mass of the nucleus is an objective of the highest priority, one for which redundancy could be justified. No gravity gradiometer has yet been flown on a spacecraft, however, and two other means of determining the mass are available without the addition of a separate device.

Table 4-2. Category II Instruments. Instruments Individually Omitted from Fundamental Payload

Instrument	Approx Mass (Kg)	Property to Which Applied	Reason Excluded from Fundamental Payload
Scanning Multichannel Spectroradiometer	8.0 Kg	Albedo, phase function, brightness profiles of nucleus and halo in selected spectral bands	Massive and partially redundant to white-light photometer
Gravity Gradiometer	2.5 Kg	Gravity gradient of nucleus	Redundant to doppler tracking measurements available without special equipment
X-Ray Spectrometer and Y-Ray Spectrometer	18.0 Kg	Composition of surface material of nucleus	Subject to interference (background) problems; require very close approach to nucleus for utility
Visual Range Spectrometer, IR Fourier Spectrometer, and UV Spectrometer	45.0 Kg	Composition of emitting gases of coma	Massive instruments partially redundant to earth-based measurements of secondary properties, possibly requiring unacceptably long integration times
Impact Ionization Sensor	6.5 Kg	Composition of asteroid belt solid particles	Expected relative velocities of vehicle and particles too low in coma; expected density of particles too low during cruise
Total mass	80.0 Kg		

First, there is the prospect of hovering at a measurable thrust just balancing gravitational attraction. Secondly, minute gravity perturbations of the spacecraft passing the nucleus at close range can be determined by doppler tracking from earth, provided the relative velocity is only a few meters per second. (These methods will be discussed in Section 6.6.3.) The emission of gas from the nucleus would obviously affect the application of either method, perhaps drastically. But a device to measure the outward mass flux is part of the fundamental payload (mass spectrometer). Thus the proper correction for the wind should be available a posteriori. Further, nonuniform emission from the nucleus and the reduced cometary activity after perihelion passage may yield data at times when a significant correction need not even be applied.

4.3.2 Category III Instruments

Table 4-3 encompasses a set of what might be termed "fundamental experiments" of a lander package. The set would provide some detailed

Table 4-3. Category III Instruments. Fundamental Lander Payload Complement

Landing Instruments	
Neutron Activation-Spectrometry	
X-Ray Activation Analysis	
αBack-Scattering	
Thermal Probe	
Electrical Conductive Probe	
Magnetometer	
Seismometer	
Magnetic Induction Meter	
Estimated Mass	20 Kg
Lander Vehicle	30 Kg
Total	50 Kg

data on composition and structure of the nucleus, which might have implications regarding formation of the comet and possibly of the solar system as well. This set is of priority interest but has not been examined carefully for this mission because of the unacceptable complexity entailed in provision for a separable package.

4.3.3 Category IV Instruments

Table 4-4 presents two sets of experiments that represent what might be termed "luxury" packages for a 1984 Encke rendezvous. The first set, which would be stationed in the solar wind in front of the comet and free of its influence, is of vital importance to real understanding of the interaction of the solar wind and the coma. This is especially true for measurements made in the interaction region near perihelion where the properties of the solar wind are currently unknown. The properties of the interaction region, however, constitute a secondary objective of the mission under study.

Table 4-4. Category IV Instruments. Comprehensive Payload Complements

Solar Wind Monitoring Instruments	
Solar Wind Plasma Analyzer	
Magnetometer	
UV Photometer	
Plasma Wave Detector	
Estimated Mass	7 Kg
Detachable Vehicle	40 Kg
Total	47 Kg
Landing Instruments	
Active Seismometer	
Gas Chromatograph	
Sampling Device	
Estimated Mass	56 Kg

The second set of Table 4-4 would allow sophisticated analysis of the properties of the surface and interior of the nucleus and could be part of a fully comprehensive lander package. Such devices on a first rendezvous seem improbable, even under relaxed constraints, but would provide important data.

5. MISSION ANALYSIS

5.1 OBJECTIVES AND CONSTRAINTS

Mission characteristics for the 1984 Encke rendezvous were investigated to determine payload performance as a function of flight time, arrival time, and thrust parameters. A representative set of trajectory data was initially furnished by Mr. Carl Sauer of JPL. Additional trajectory simulations were performed by TRW in the course of the study.

Principal criteria and constraints in the selection of a nominal trajectory and of spacecraft size and power are: (1) sufficient payload capacity to carry the basic science instrument complement defined in Section 4; (2) reasonably fast transfer to the comet; (3) favorable timing of the rendezvous from the standpoint of most effective comet exploration; and (4) achievement of these objectives at a reasonably low-power level. The trade-offs involved in selecting the mission profile and system characteristics are discussed in this section.

In addition to the characteristics of the transfer phase, operational modes in the comet's vicinity are of principal interest and are discussed in this section. Relative excursions, maneuver and stationkeeping requirements, and other dynamic and kinematic characteristics associated with exploration close to the nucleus were investigated. Navigational requirements of the comet rendezvous were derived on the basis of earlier work by JPL (Reference 5-1), IITRI (Reference 5-2), and TRW, with emphasis on the combined use of onboard and ground-based navigation.

5.2 ASSUMED ELECTRIC PROPULSION AND LAUNCH VEHICLE PERFORMANCE DATA

The following engineering characteristics and constraints, consistent with the state of technology of solar electric propulsion, were assumed:

1) Solar array

- The boom-deployed rollup array of the type developed by General Electric under JPL contract has a specific mass of 15 kg/kw. An increase of panel size to power levels greater than the 2.5 kw prototype, as required for the Encke rendezvous mission, is consistent with G. E.'s design approach.

2) Power processors

- Specific mass 5 kg/kw
- Efficiency 91 percent

3) Ion thrusters

- Mercury electron bombardment thrusters are assumed here. The maximum burn time on any single thruster is not to exceed 10^4 hours (416 days). (Actually, on the basis of earlier studies by JPL and TRW, a maximum of only 350 days per thruster is anticipated for this mission.)
- In our performance calculations we assume a fixed I_{sp} of 3000 seconds consistent with currently available thruster designs, with a thruster efficiency of 0.70.

4) Total specific mass

- Values of the total specific mass of the solar array plus electric propulsion hardware was assumed as 30 kg/kw in trajectory calculations. This value was subsequently confirmed to be realistic by taking into account the required number of spare thrusters and power processors.

5) Propellant tankage

- For preliminary mission analysis, the tankage mass is assumed to be three percent of the maximum propellant load.

6) Solar array power output

- The solar array output power as function of solar distance (for distances above 0.68 AU) is assumed as shown in Figure 5-1, based on JPL data.
- For solar distances below 0.68 AU a constant power output (1.40 times reference power at 1 AU) can be achieved if the maximum array temperature is limited to 140°C through array rotation away from the sun. Otherwise the power output would drop sharply as temperature increases (see Figure 5-1).

Boosters of the Titan family, Titan IIID/Centaur D-1T with five or seven segment solid rocket strapons were specified as launch vehicle candidates. Trajectory calculations immediately established that the

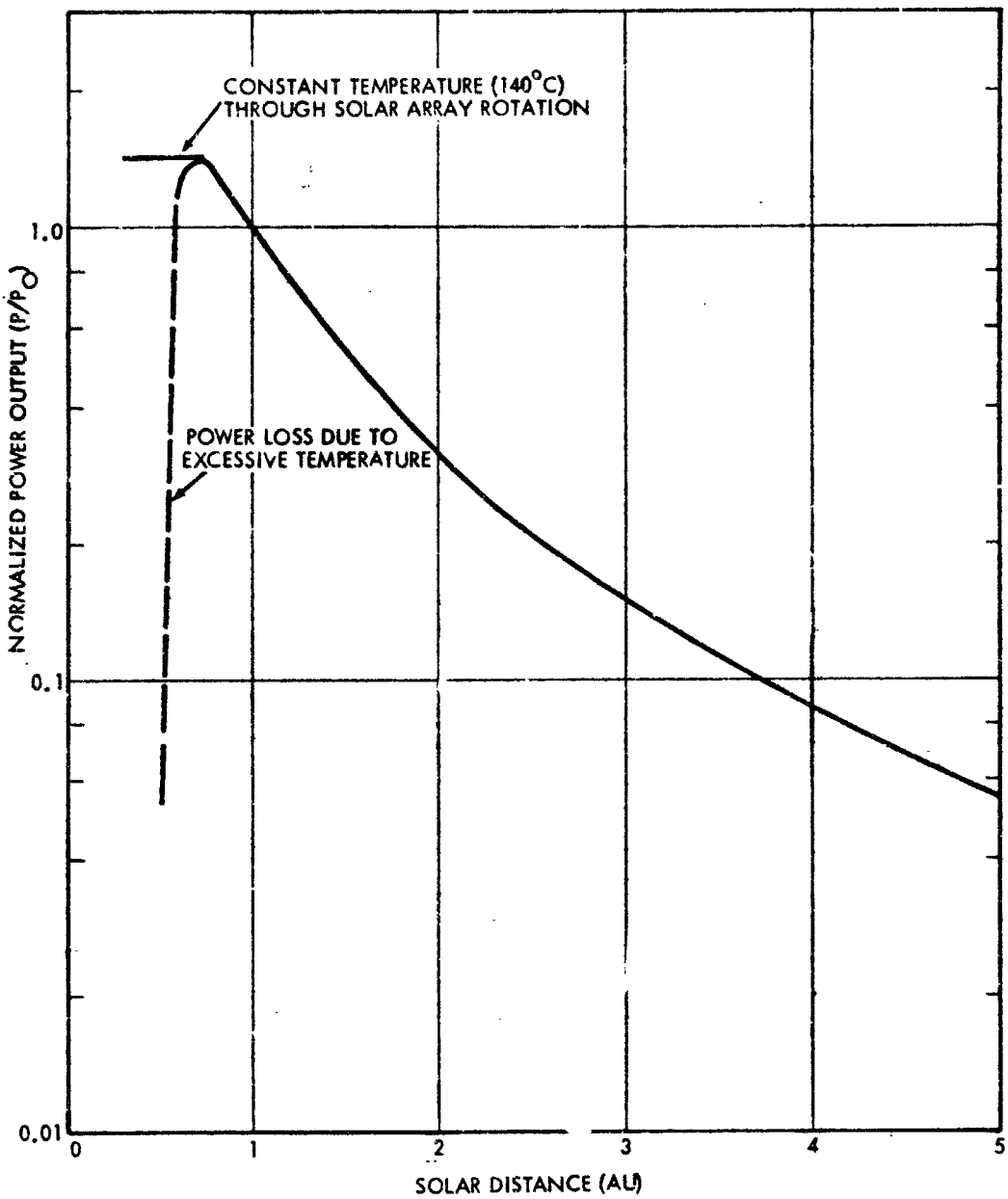

Figure 5-1. Normalized Solar Array Output Power (Reference: JPL SEMMS Study)

higher performance seven-segment Titan, is not required since even the five-segment Titan has more than sufficient injection capability for this mission. Its nominal performance specified by JPL is shown in Figure 5-2 assuming a standard 14-foot Viking shroud. For the optional 10-foot Intelsat shroud considered in this study the injected mass capability would be about 100 kg greater.

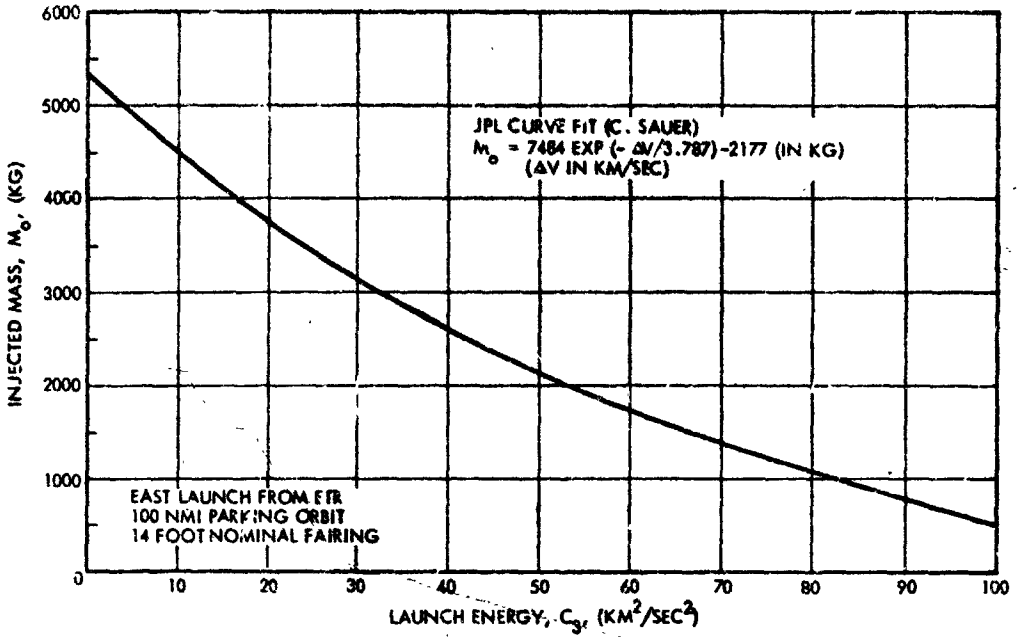

Figure 5-2. Injection Performance of Titan IIID(5)/Centaur (JPL Model)

5.3 TRANSFER TRAJECTORY CHARACTERISTICS

5.3.1 General Discussion

Various types of transfer trajectories are available for a 1984 Encke rendezvous as illustrated schematically in Figure 5-3. The same arrival time, 50 days before perihelion passage, is assumed in the examples shown.* We distinguish between direct (Mode A) trajectories with transfer angles significantly less than 360 degrees and indirect (Mode B) trajectories with transfer angles approaching or exceeding 360 degrees.

Launch dates for the direct trajectories occur about one year apart when earth is near the longitude of the comet's perihelion. Typical trip times are 700 and 1050 days, respectively. The smaller or larger aphelion distances reflect the different trip times.

*Subsequent tradeoff studies showed that a later arrival, 40 days before perihelion, is preferable as will be discussed later.

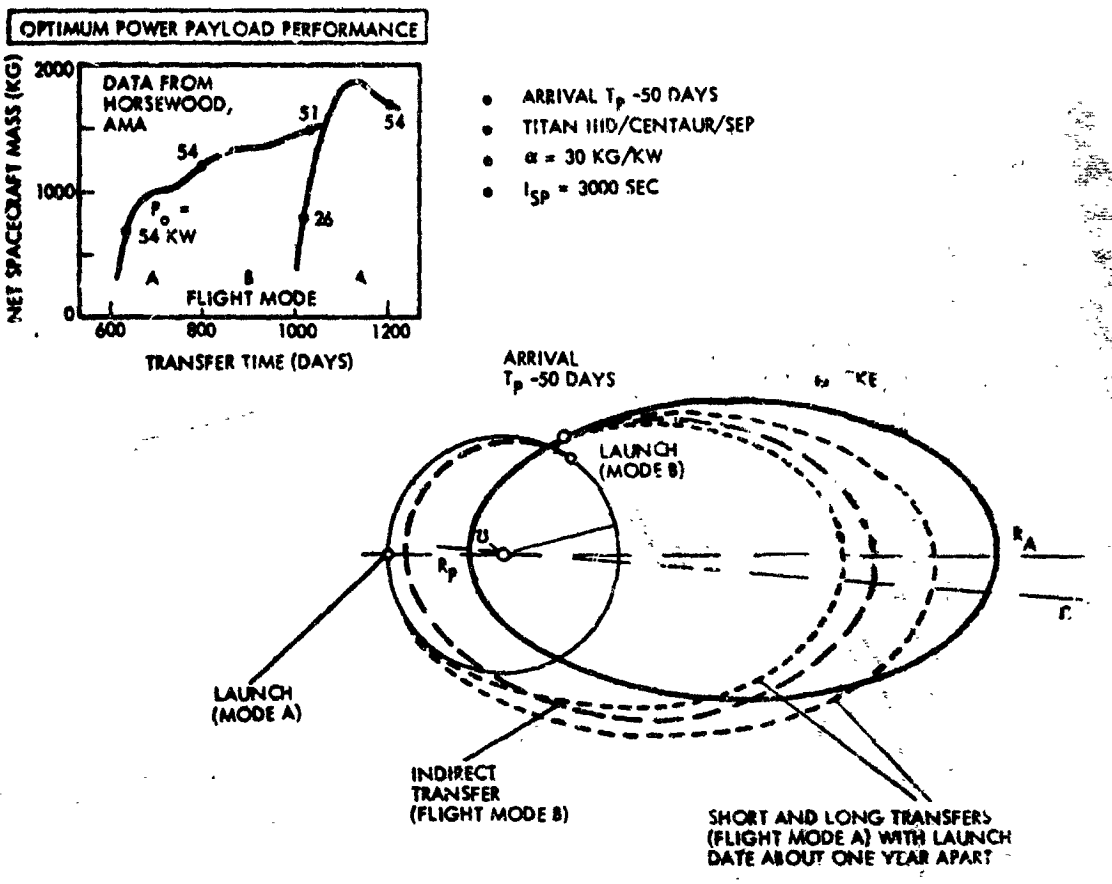

Figure 5-3. Basic Characteristics of Transfer Trajectory and Payload Performance

Launch dates for indirect trajectories are spread over a wide range of longitudes, complementing the launch dates for direct flights. Trip times range from 800 to 1000 days. A typical feature of indirect trajectories is the initial passage inside the earth orbit. This is necessary to adapt the flight time to given departure or arrival dates incompatible with direct transfer.

The graph inserted at the upper left of Figure 5-3 shows the trend of net spacecraft mass* variation with flight time based on optimal propulsion power. Actually, only a fraction of the "optimal" power level

*The term net spacecraft mass is used to designate the mass remaining after the mass of the solar array, electric propulsion hardware, and propellant mass is subtracted from the initial gross mass.

indicated in this graph is required to deliver an adequate payload. Earlier studies by JPL, TRW and IITRI have established that power levels of 20 kw and below are sufficient. If the resulting net spacecraft mass is at least 500 kg, about 100 kg of this mass is available for net scientific (instrument) payload, allowing about 300 kg for spacecraft structure and engineering subsystems, and 100 kg for various weight penalties and contingencies. Scaling laws that relate net spacecraft mass to power level have been derived and are well documented in the above referenced studies. These are directly applicable here.

Referring again to the transfer trajectories shown in Figure 5-3, an explanation of the time-varying thrust profiles that are used in the direct and indirect flight modes is needed. The principal thrust component applied in the orbital plane must initially point in a forward direction to increase the aphelion radius. Subsequently, as the spacecraft approaches aphelion the thrust vector must be pointed in a retrograde direction to decrease the perihelion radius. To match Encke's small perihelion radius (0.34 AU) a large total retroimpulse is required near aphelion although the solar electric power available here is only 10 to 20 percent of its initial level at earth departure. This explains the relatively large initial power that is characteristic of the Encke rendezvous mission. After aphelion and during the rendezvous approach the thrust vector points again in posigrade direction to further increase the aphelion of the spacecraft orbit until it matches that of the comet.

An appreciable amount of out-of-plane thrusting is required in addition to the principal in-plane thrust, to match the comet's orbit inclination (12.0 degrees) and line of nodes. In the direct transfer trajectories launched near the comet's descending node the out-of-plane thrust component is needed largely to increase orbit inclination. In the case of indirect transfers the out-of-plane component is needed for inclination changes as well as nodal shift.

5.3.2 Representative Performance Characteristics

Figure 5-4 shows performance characteristics of representative trajectories for a SEP reference power of 15 kw.* The upper portion presents net spacecraft mass as function of flight time for fast and slow transfers, with arrival time as a parameter. The lower portion of the chart shows the net spacecraft variation with SEP power ranging from 5 to 15 kw for trip times of 800 and 1050 days.

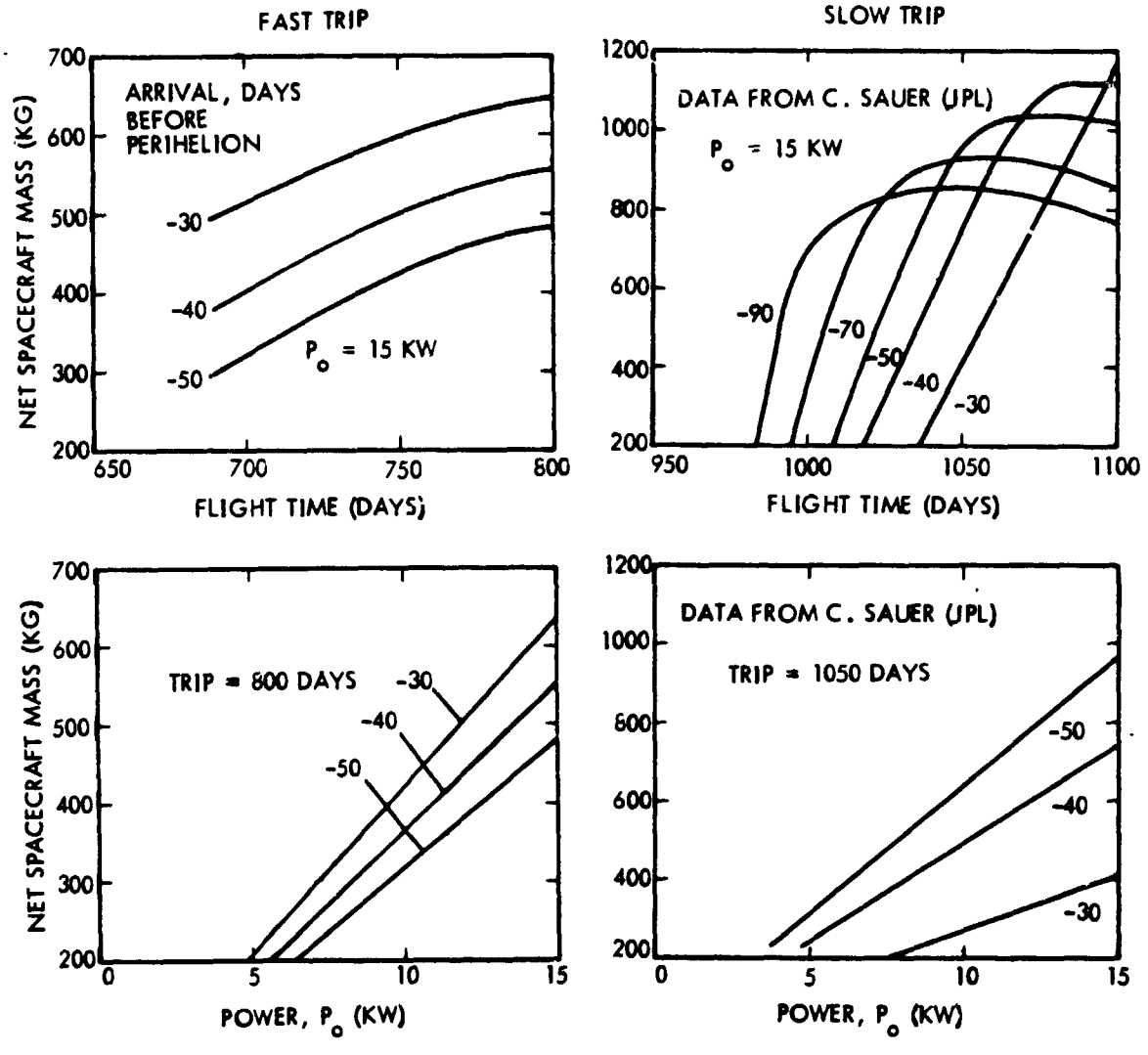

Figure 5-4. 1984 Encke Rendezvous Performance vs Flight Time and Power (I_{sp} = 3000 sec; α = 30 kg/kw; Titan IIID/Centaur/SEP)

*i. e., the input power into the electric propulsion power processor, referenced to 1 AU solar distance.

Time of arrival has a significant effect on net spacecraft mass, with an increment of up to 100 kg obtainable for a 10-day delay in arrival time in the case of fast missions. An even stronger influence of arrival time is noted in the case of slow trips (upper right of the chart). A change of the trend in payload mass variation with flight time and arrival date is also apparent in this graph, in contrast with the characteristics of fast missions. (See also Figure 5-6.)

The net spacecraft mass obtainable in fast trips is between 350 and 600 kg; this increases to about 1200 kg in slow trips. The fast trips use direct transfers for flight times between 700 and 750 days, and indirect transfers for longer flight times. The slow trips also include direct and indirect transfers depending on the launch date, the steep portion of the performance curves corresponding to direct flights, and the shallow portion to indirect flights.

Figure 5-5 shows the influence of hyperbolic departure velocity, V_{∞}, on payload performance for fast and slow trips, with arrival time as parameter. The upper portion of the chart shows required thrust time; the lower portion shows net spacecraft mass. Performance increases with diminishing departure velocity because more of the total energy is contributed by electric propulsion, as reflected by the increase of total required thrust time (shown in the upper portion of the chart). The lower limit of V_{∞} is reached when the thrust time equals the flight time.

Increasing the total thrust time as a way to gain payload capacity is desirable as long as this does not compromise system reliability. We have investigated this tradeoff and found that in the case of "short" 700 to 800-day trips an extension of thrust time is much more important in the interest of gaining payload capacity but also more acceptable from a reliability standpoint than in the case of long trip times. Nevertheless, it appears desirable to allow for at least some coast time even in a short flight mode to provide a margin against certain propulsion system contingencies. (As will be discussed below the selected nominal 800-day mission profile includes a coast period of about 50 days.)

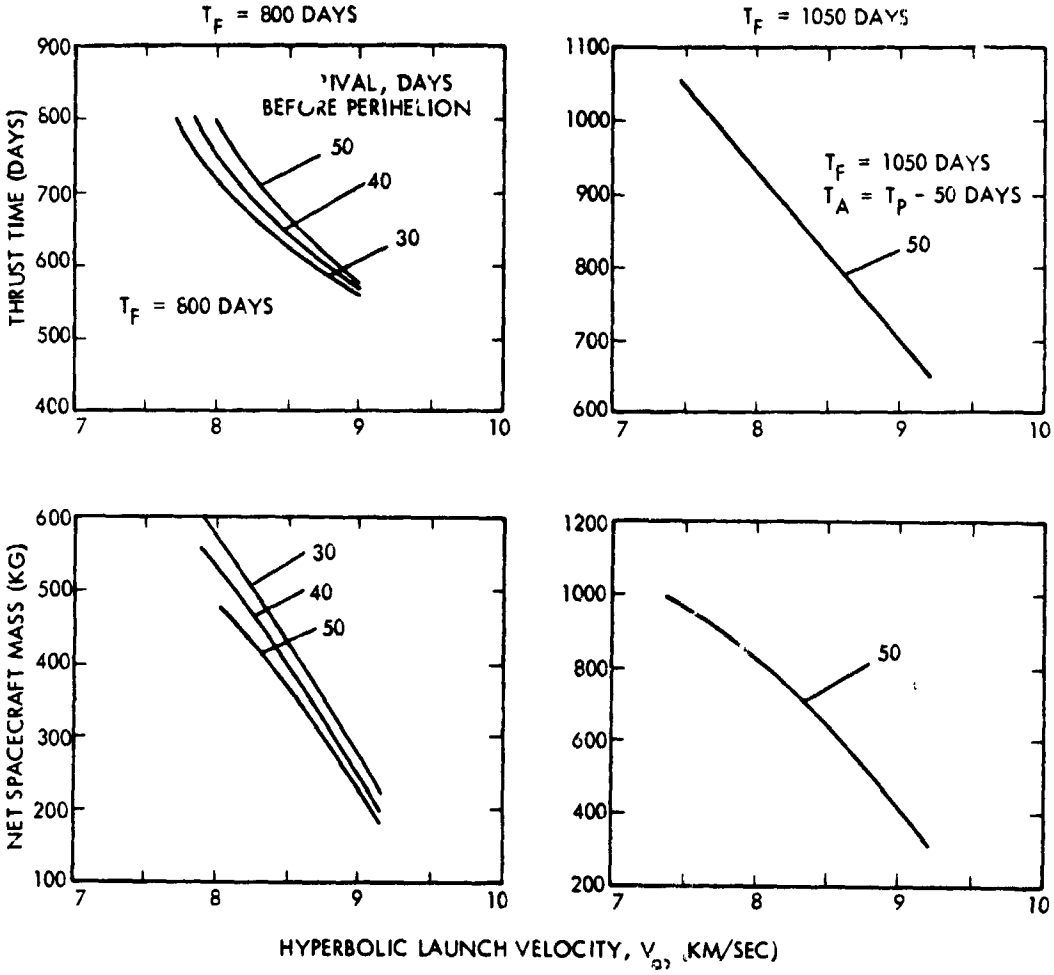

Figure 5-5. Payload Performance and Thrust-On Time (1984 Rendezvous; P_0 = 15 kw; I_{sp} = 3000 sec; α = 30 kg/kw; Titan IIID/Centaur/SEP)

Figure 5-6 shows an overall mission map which summarizes results of the trajectory and performance analysis for 15 kw of SEP reference power. Contours of net spacecraft mass are plotted against launch time and arrival time. Flight times are indicated by diagonal lines of slope +1. Payload contours are shown for short and long trip times. The choice of direct or indirect transfer trajectories is determined by the launch date.

5.3.3 Selection of Preferred Transfer Trajectory

Regions of favorable and unfavorable operating conditions, and criteria for selection of a preferred transfer trajectory can be conveniently delineated in the mission map as shown in Figure 5-7. The following factors exhibited in this map are relevant to the trajectory selection (not necessarily in the order of priority):

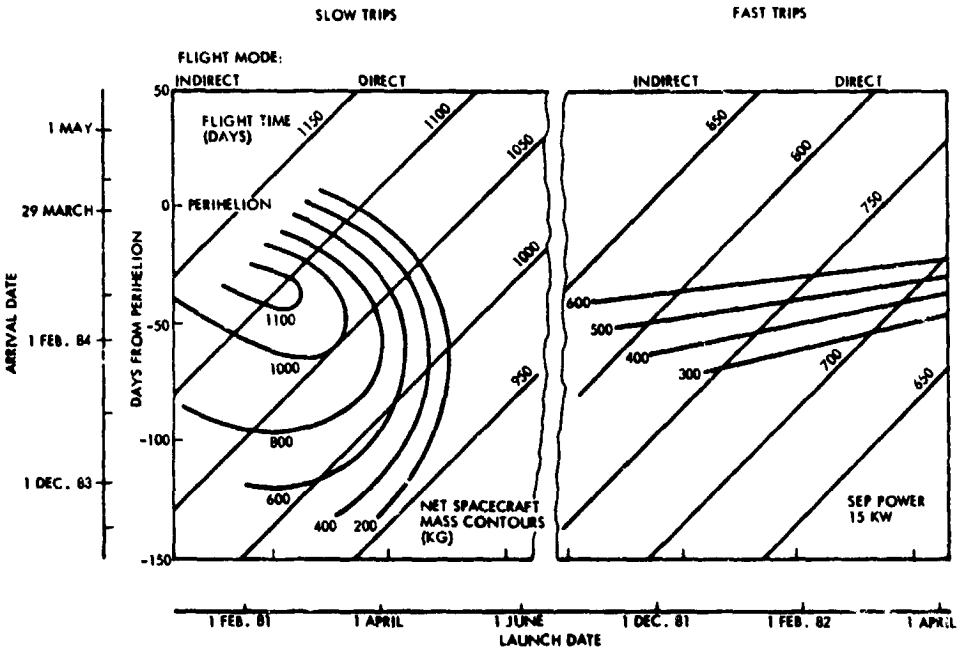

Figure 5-6. 1984 Encke Rendezvous Mission Map (SEP Power 15 kw, I_{sp} = 3000 sec, α = 30 kg/kw; Titan IIID/Centaur)

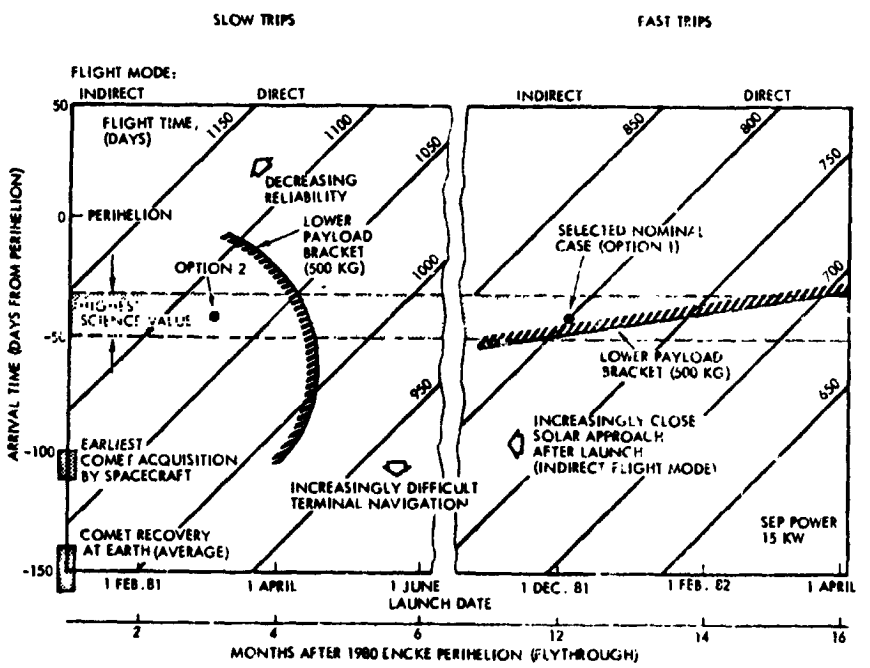

Figure 5-7. 1984 Encke Rendezvous Mission Map; Criteria for Trajectory Selection

a) Net spacecraft contours delineate regions of adequate payload performance, indicated by cross hatching.

b) The preferred time of arrival, dictated by scientific observation objectives, is indicated by a shaded horizontal strip (50 to 30 days before perihelion).

c) Diagonal lines are time of flight contours. Since reliability decreases with flight time, (and total thrust time) these lines can also be interpreted as reliability contours. Short flight times are preferred.

d) The launch date is relevant in dictating the required procurement schedule and in relating the 1984 rendezvous to the 1980 flythrough opportunity. Time elapsed between the postulated earlier Encke flythrough (November 1980) and launch of the rendezvous spacecraft is shown in a separate scale at the bottom of the map.

   A late launch (e.g., December 1981) is preferable for most effective utilization of data on Encke received from the flythrough mission. It also provides additional lead time for program development.

   The launch date also dictates the use of direct or indirect flight modes with April 1981 and 1982 being in the center of direct flight opportunities. Indirect transfers that initially approach very close to the sun (e.g., with launch dates in the fall of 1980 and 1981) should be avoided, as they may lead to potentially severe early solar array degradation.

e) Navigation is constrained by timing of the spacecraft arrival at the comet: for ground based navigation the time of comet recovery and for onboard navigation the time of earliest onboard acquisition (indicated at the left) is relevant. Terminal navigation is facilitated by arrival timing 50 days before perihelion or later consistent with scientific objectives.

f) Spacecraft design criteria and environmental conditions favor arrival timing no earlier than about 50 days before perihelion and no later than about 30 days before perihelion consistent with science constraints.

Some of these criteria require further discussion.

Payload performance (criterion a) must be reinterpreted if an SEP power different from 15 kw is selected. Direct scaling is appropriate; e. g., if the power is scaled down to 10 kw a net spacecraft mass of 500 kg would correspond to an equivalent value of 750 kg on the map. For 12 kw the equivalent net spacecraft mass is 625 kg.

Time of arrival (criterion b) is partly dictated by the comet exploration strategy (see Section 6). Our study shows that with arrival 40 days before perihelion adequate time is available for coma/tail exploration maneuvers when the comet is most active, while arrival at the nucleus is still possible before perihelion.

Other criteria for time of arrival selection are imposed by spacecraft design, spacecraft environmental protection and electric propulsion constraints. For example, late arrival with the terminal thrust phase occurring close to perihelion makes the mission more critically dependent on the solar array, increases the thermal load on the thrusters and demands addition of standby thrusters.

The preferred operating region is delineated by the brackets of favorable arrival times (30 to 50 days before perihelion), short flight times 750 to 850 days and the lower limit of net spacecraft mass, 500 kg. The dates of the selected nominal trajectory (Option 1) are:

- Flight time 800 days, arrival on 16 February 1984 40 days before perihelion
- Launch date 8 December 1981

The net spacecraft mass is 527 kg at 15 kw, or 422 kg at 12 kw of nominal SEP power. If a small increase in payload capacity is needed we may use one of the following options:

- Increase flight time to 830 days: $\Delta M_1 = 25$ kg
- Change arrival date to $T_P - 35$: $\Delta M_2 = 32$ kg
- Change SEP power to 13 kw: $\Delta M_3 = 35$ kg
- Combination of all three options: $\Sigma \Delta M_i = 92$ kg

We conclude that sufficient incremental payload capacity is available in the immediate vicinity of the nominal operating point.

An alternate operating point that is available if increased payload capacity is absolutely required is shown in the mission map as Option 2:

- Flight time 1075 days; arrival on 16 February 1984 40 days after perihelion
- Launch date 8 March 1981

The net spacecraft mass is 1100 kg at 15 kw or 880 kg at 12 kw. This trajectory option would permit a reduction in SEP power level to 5.8 kw to yield the same payload as Option 1.

Figure 5-8 shows the ecliptic plane projection of the selected nominal trajectory (Option 1). Note that this is an indirect trajectory which passes to within 0.74 AU of the sun 65 days after launch. Figures 5-9 (a) through 5-9 (c) show time histories of heliocentric longitude

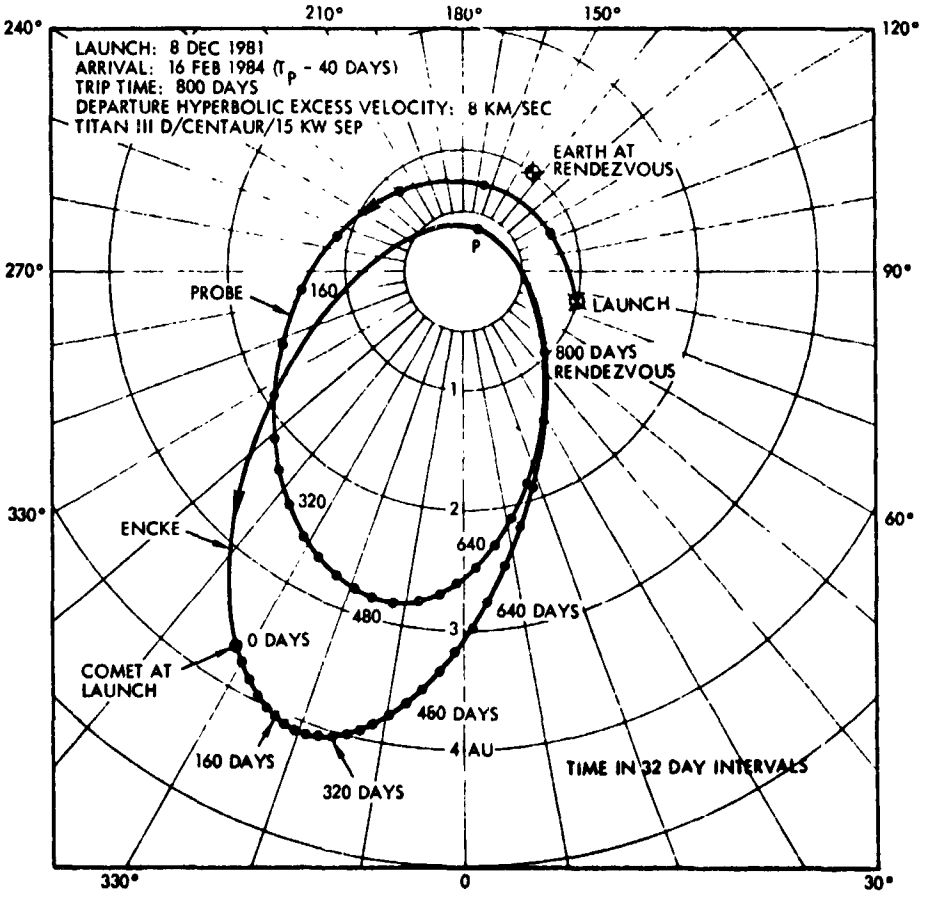

Figure 5-8. Nominal 1984 Encke Rendezvous Trajectory (Projected into Ecliptic)

FOLDOUT FRAME 1

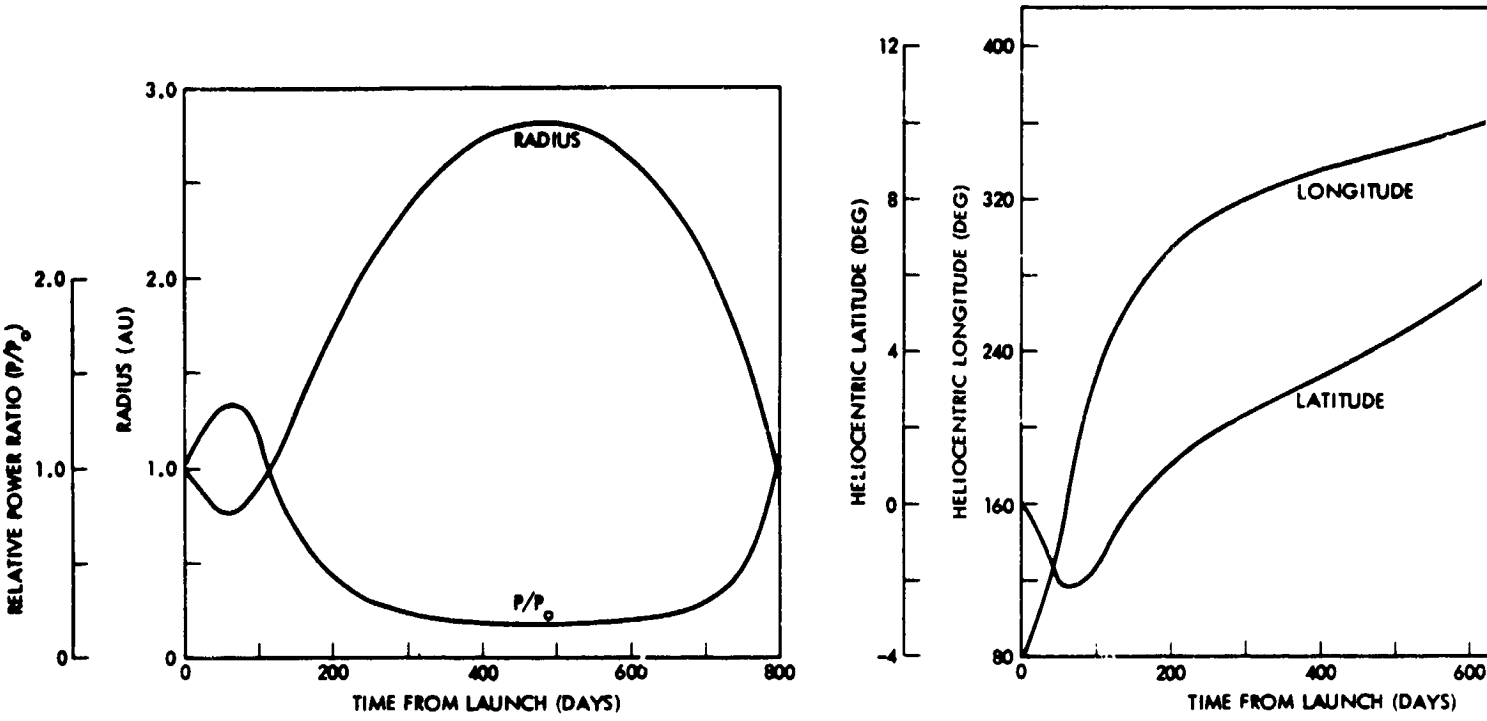

(A) RADIUS, POWER, LONGITUDE AND LATITUDE

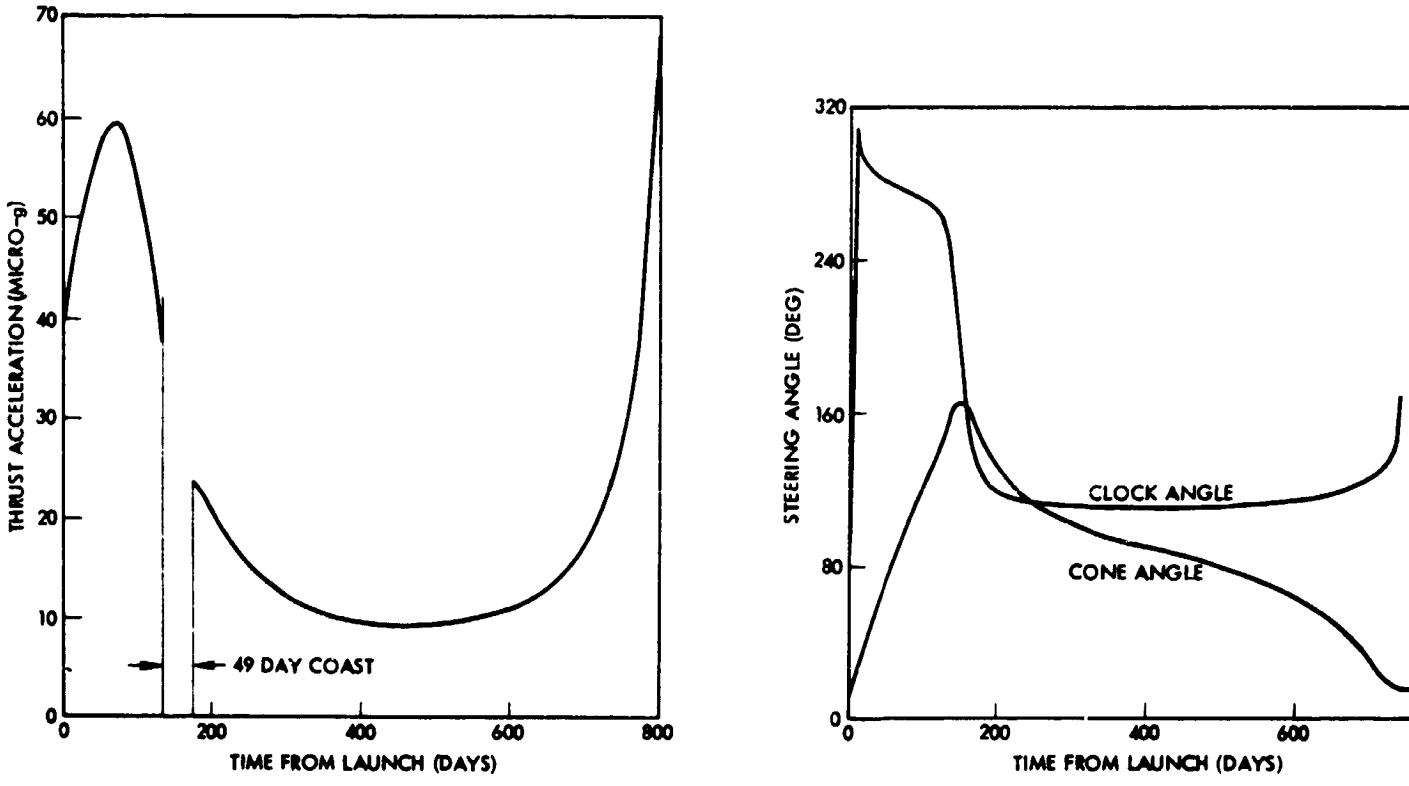

(B) THRUST ACCELERATION, CONE AND CLOCK ANGLE

FOLDOUT FRAME 2

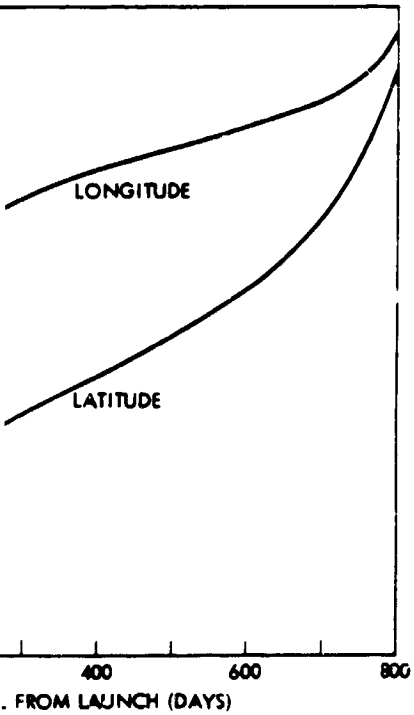

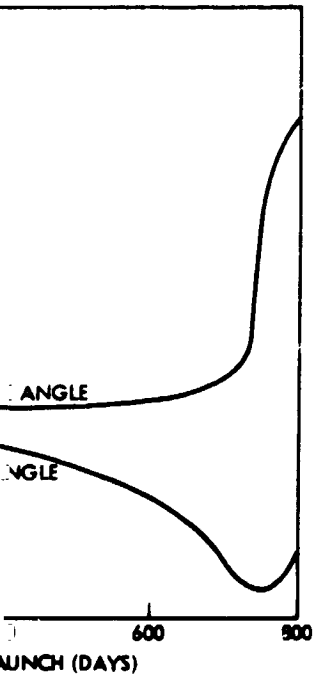

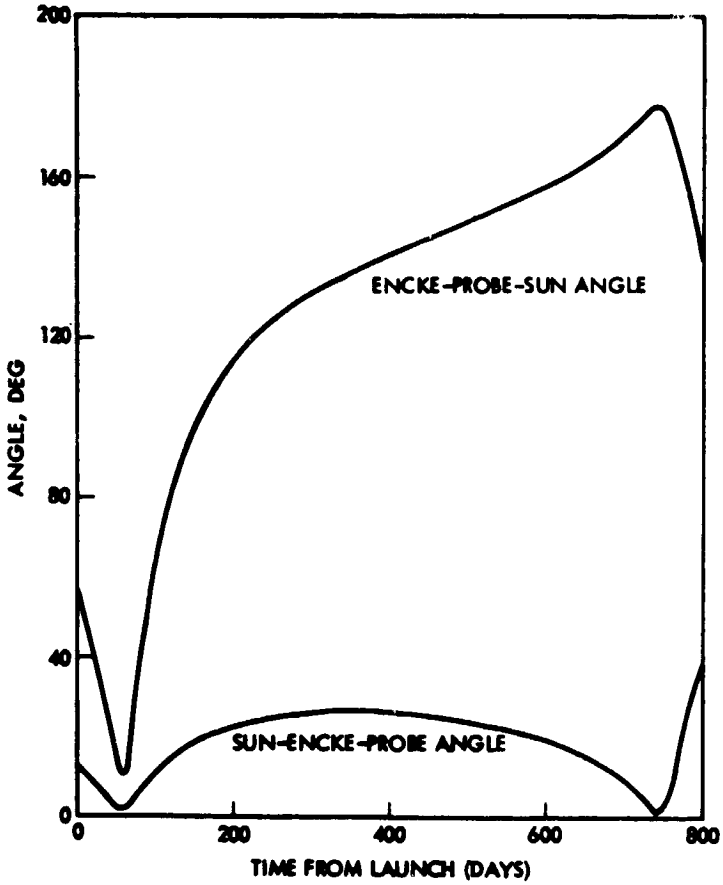

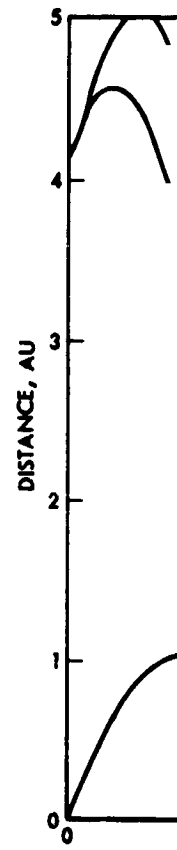

(C) RELATIVE GEOMETRY CHA

PRECEDING

FOLDOUT FRAME 3

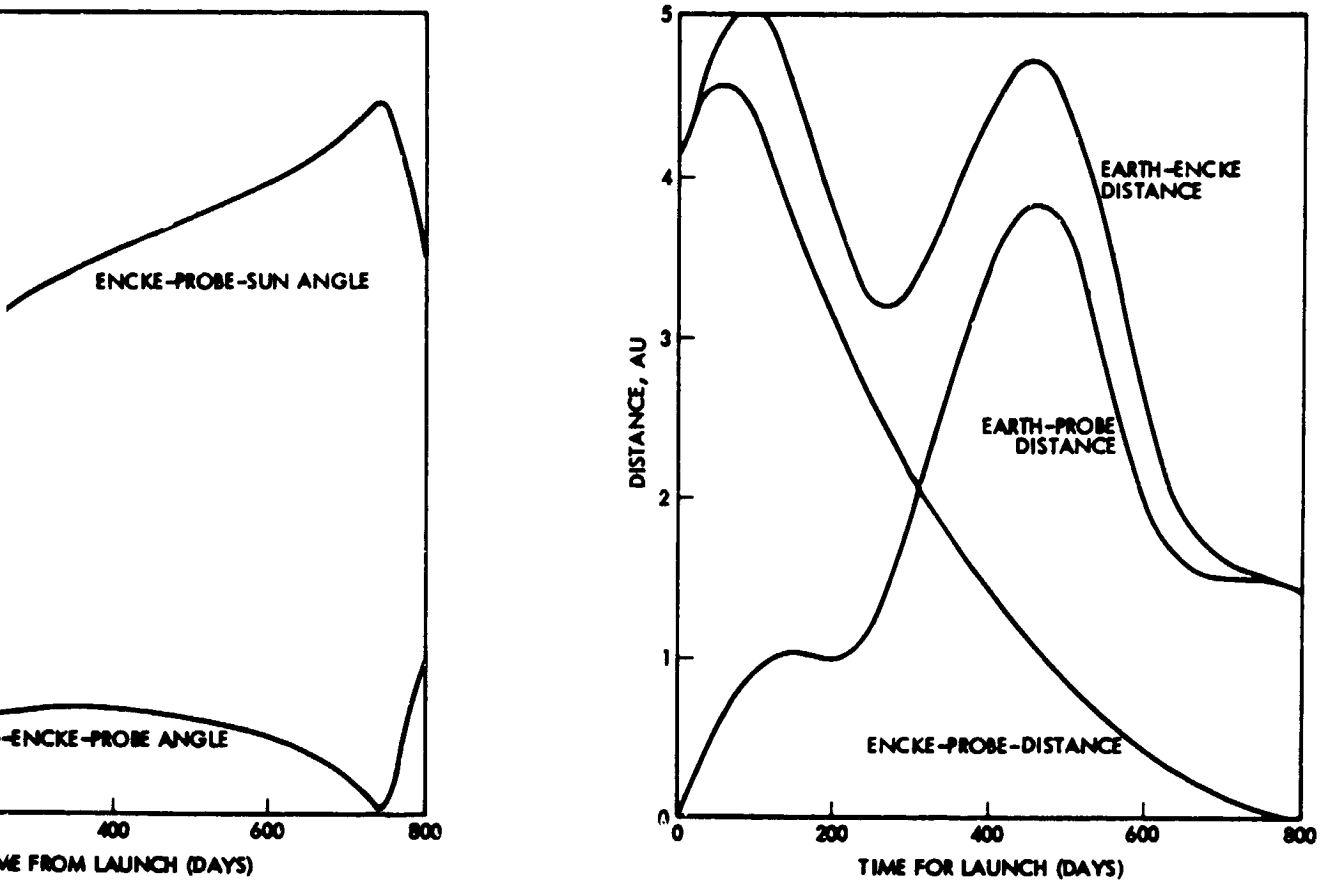

(C) RELATIVE GEOMETRY CHARACTERISTICS

PRECEDING PAGE BLANK NOT FILMED

Figure 5-9. Nominal Trajectory Time Histories

and latitude, radius, power profile, thrust acceleration, thrust cone and clock angle* and relative geometry characteristics with respect to earth, sun and comet. A coast period of 49 days is included starting 130 days after launch. (A payload increase of about 30 kg is achievable by excluding this coast period, i.e., increasing the total thrust time to 800 days, and using a departure hyperbolic velocity of 7.5 rather than 8 km/sec.)

Figure 5-10 shows the relative trajectory with respect to the comet for the last 100 days of the transfer, projected into the comet orbit plane. The graph at the bottom of Figure 5-10 shows thrust vector cone and clock angles as well as line-of-sight angles to the comet in spherical coordinates for the last 100 days before rendezvous. During the time interval critical for onboard terminal navigation the thrust vector orientations are almost diametrally opposite to the line-of-sight orientations. It follows that the optical navigation sensor must look in the general direction of the thrust beam, subject to field-of-view obstruction by the spacecraft body. This may require reorientation of the spacecraft long enough to permit an unobstructed view of the target by the TV sensor, possibly accompanied by thrust interruption.

5.3.4 Non-Optimal Thrust Pointing

A study of payload reduction that would result from non-optimal thrust pointing was performed to determine whether a rotatable solar array is essential to the mission. As shown by the time history of optimal thrust vector cone angles for the nominal 800-day mission (Figure 5-9(b)), the largest departure from the average, (about 90 degrees from the sun-line) is ±80 degrees. Constraining the cone angle to a fixed value in the 70 to 90 degree range reduces the net spacecraft mass by about 20 percent (104 kg), i.e., more than the total projected net payload capacity for science instruments. A 3.1 kw increase in power would be required to offset this effect. In the case of a slow transfer (1050 days) the net spacecraft capacity is decreased by about the same amount (100 kg). In view of

*Cone and clock angles are defined in accordance with conventional JPL usage, (see also Section 6.7.2).

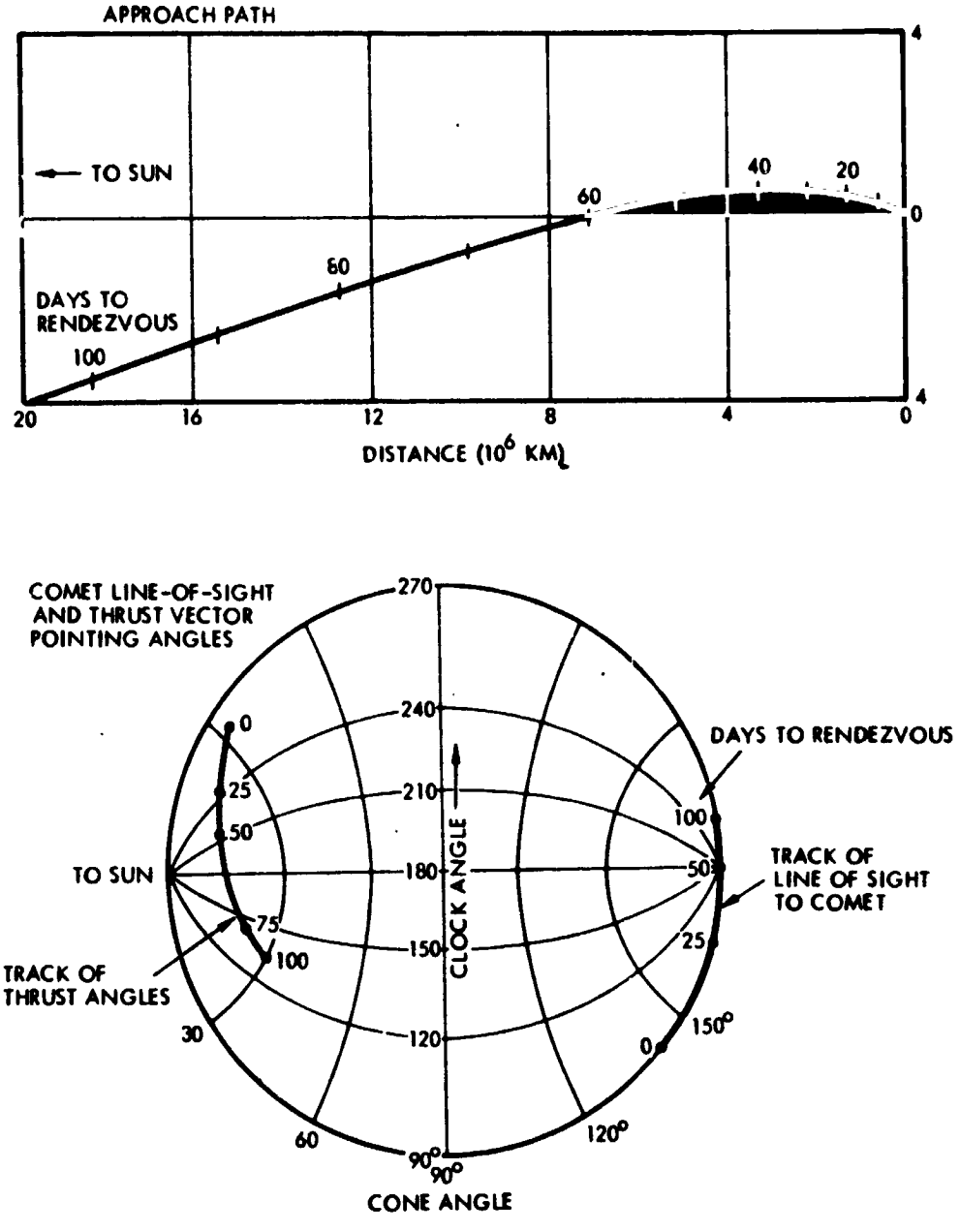

Figure 5-10. Final Approach to Rendezvous and Pointing Geometry

the much larger payload capacity provided by this mission mode this loss is only 10 percent and therefore more acceptable.

The possibility of rotating the entire spacecraft by a limited angle (±20 degrees) from the average fixed orientation, was also considered as an alternative to using solar array rotation. This resulted in a payload loss of about 50 kg, or 10 percent, in the fast mission mode. It would still have to be compensated by an equivalent power increase of 1.6 kw.

The weight increment required for adding a solar array rotation drive and electronics is estimated to be 16 kg based on an earlier design study. The decisive factors which make a rotational solar array drive preferable are not only the improved payload performance, but also the important functional advantages of unconstrained thrust pointing for guidance and comet exploration maneuvers, and greater convenience in rotating the solar array away from full sun orientation for thermal protection at solar distances below 0.68 AU, as will be discussed in Section 7.

5.4 RELATIVE MOTION

5.4.1 Relative Trajectories Through Coma and Tail

Coast trajectories of the spacecraft relative to the comet center were calculated to permit:

- Investigation of alternate coma and tail exploration modes
- Selection of a preferred excursion pattern
- Evaluation of time and maneuver requirements during this mission phase.

Figure 5-11 shows typical coast arcs in cometocentric coordinates with the sunline pointing to the left and the comet's velocity pointing upward as indicated by arrows. The trajectories originate at the comet center, running toward or away from the sun. To illustrate the influence of the comet's orbital position we assumed two starting times, $T_o = T_p - 50$ days (Figure 5-11(a)) and $T_o = T_p$ (Figure 5-11(b)). The curves are for different departure angles θ defined as the orientation of the initial velocity $\Delta\bar{V}_1$ relative to the vertical coordinate axis, positive in clockwise direction. The elapsed time is indicated parametrically by dashed curves.

To simplify the computation the effect of the infinitesimal nucleus gravity was neglected and the initial velocity was assumed to be the result of an impulse maneuver, although electric propulsion is preferred over chemical propulsion to conserve propellant mass. The impulsive thrust approximation is quite adequate because the low-thrust system

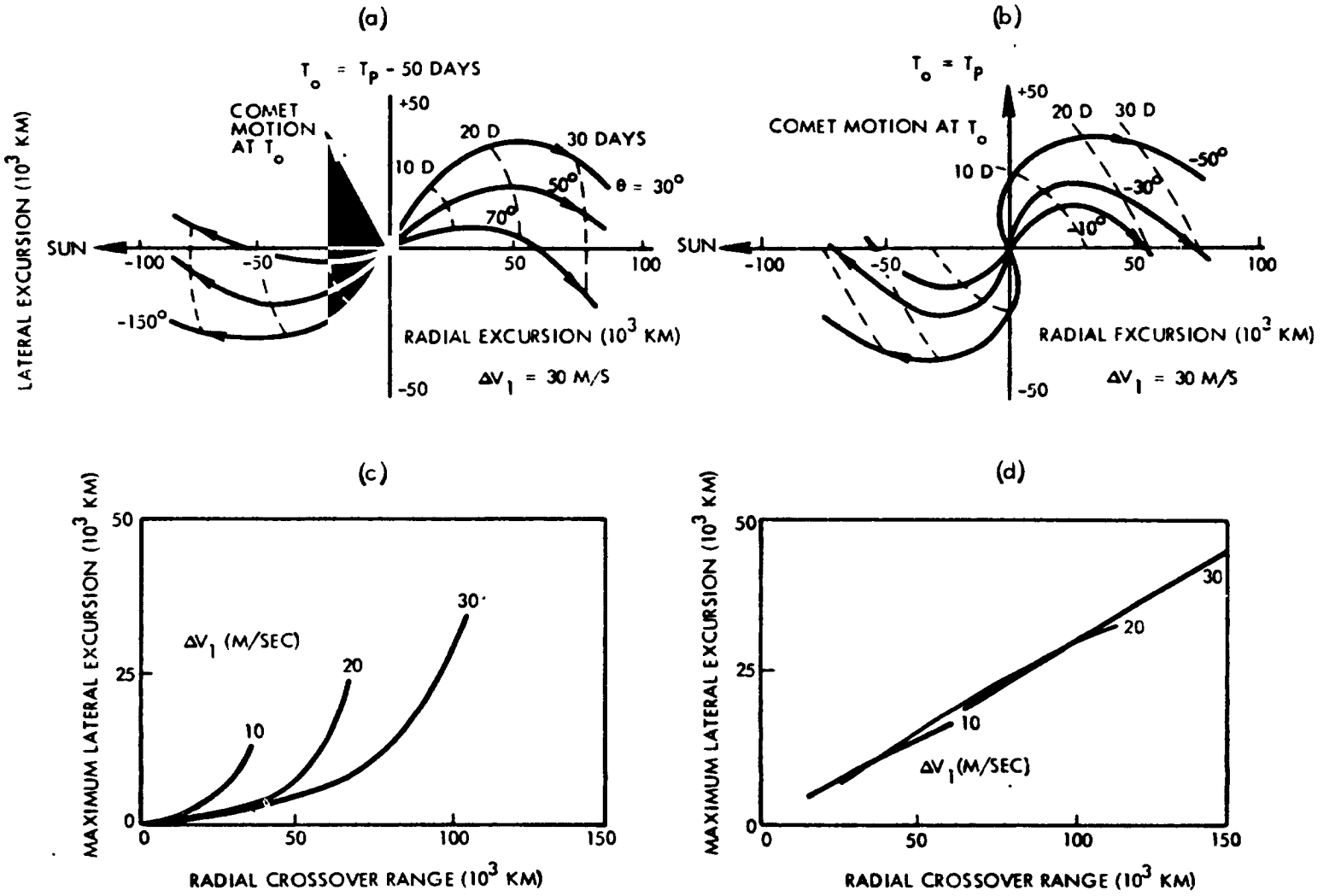

Figure 5-11. Relative Motion with Respect to Comet Center (No Initial Offset)

having a ΔV capability of 40 to 50 m/sec per day would be used only during a very short initial segment of each arc. The curved characteristics reflect the effect of solar differential gravity and Coriolis acceleration in the rotating frame of reference. Figures 5-11(c) and 5-11(d) show the maximum lateral excursion and the crossover range achievable with initial velocity increment ΔV_1 as parameter. For example, with ΔV_1 = 30 m/sec applied at $T_o = T_p$ a distance of about 50,000 km can be reached in 20 days.

Figure 5-12 shows corresponding trajectories for ΔV = 20 and 30 m/sec obtained with an initial offset of 50,000 km on the sunward side starting at $T_o = T_p$ - 50 days and running toward the comet center. Identical coast arcs would be obtained for a symmetrical offset point on the other side of the comet center simply by rotating the graph 180 degrees around the origin, as can also be seen in Figure 5-11. This is explained by the symmetry of the dynamic effects governing the relative motions.

In addition to coast arcs that are the result of an initial velocity, Figure 5-12 also shows the drift, or control-free path, that would occur if no ΔV were applied, as the result of the solar differential gravity that exists at the offset point. The rate of drift increases linearly with the radial offset distance. Continuous or intermittent thrust is necessary to cancel the drift rate if stationkeeping is desired.

Since the relative motions considered here are very small orbit perturbations relative to the comet, maximum excursions being at least three orders of magnitude smaller than the solar distance, the velocities and resulting excursions can be scaled proportionally. With this technique composite pattern of excursions and their velocity requirements can be readily synthesized from the data provided above.

Figure 5-13 shows two types of comet exploration maneuvers thus obtained. The first type has been analyzed by IITRI (Reference 5-2). It provides excursions of $\pm$20,000 km from the nucleus for about 60 days including a stationkeeping period of ten days. The ΔV requirement is about 160 m/sec.

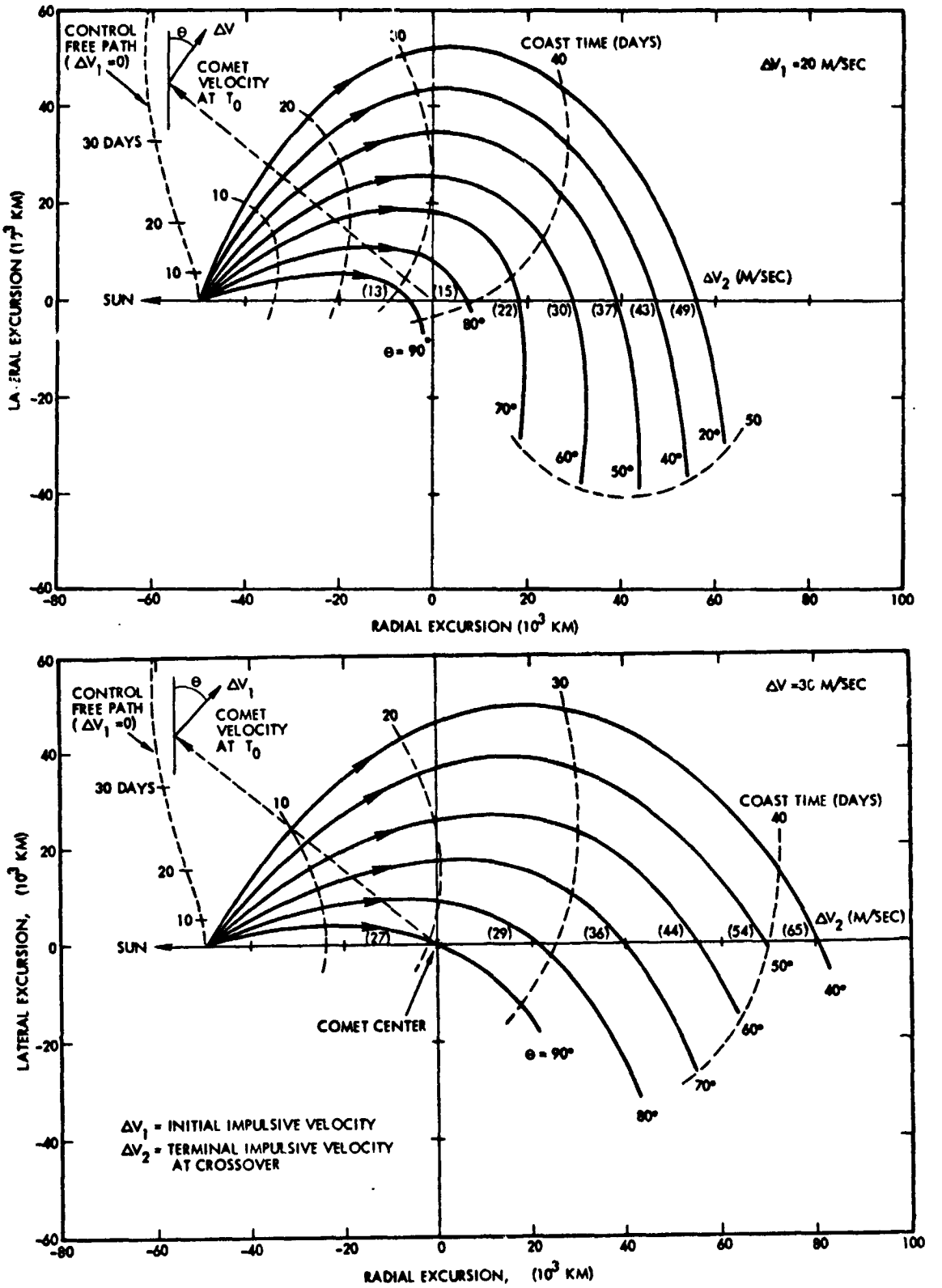

Figure 5-12. Relative Trajectories with Initial Offset ΔR_o = -50 x 10^3 km; T_o = T_p - 50 Days

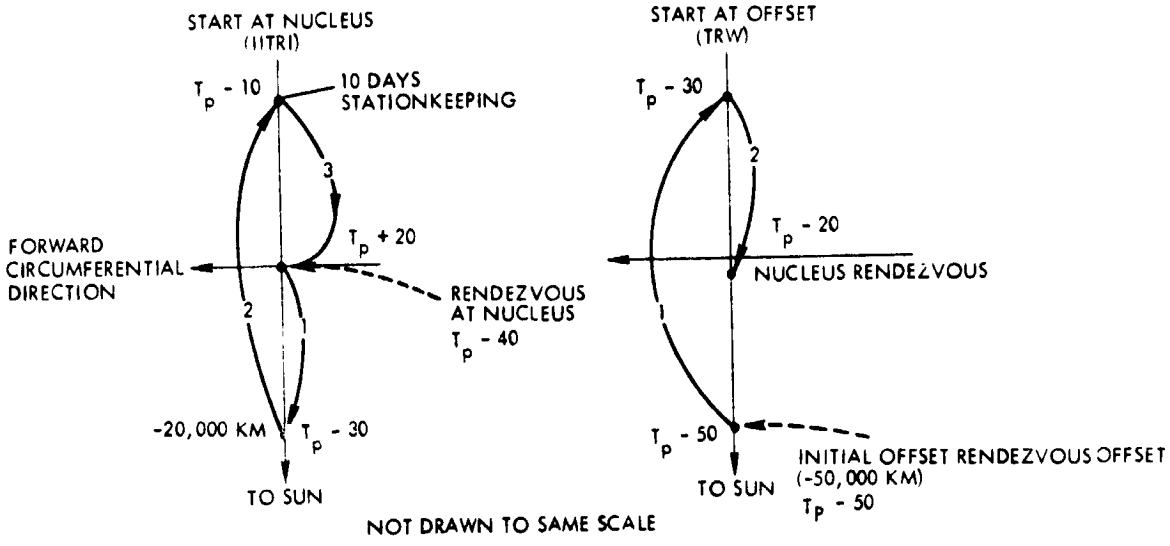

LEG	TIME	ΔV (M/S)	ΔR (KM)
1	T_p - 40	22	0
	T_p - 30	24	-20×10^3
2	T_p - 30	22	-20×10^3
	T_p - 10	26	$+20 \times 10^3$
	T_p - 10 TO T_p	39*	$+20 \times 10^3$
3	T_p	23	$+20 \times 10^3$
	T_p + 20	11	0

*10-DAY STATIONKEEPING

LEG	TIME	ΔV (M/S)	ΔR (KM)
1	T_p - 50	60	-50×10^3
	T_p - 30	61	$+50 \times 10^3$
2	T_p - 30	60	-50×10^3
	T_p - 20	55	-1×10^3

(NO STATIONKEEPING)

Figure 5-13. Comet Exploration Maneuvers

The second type starts at a 50,000 km offset on the sunward side rather than at the nucleus and includes an excursion toward or into the tail to 50,000 km. The time requirement is 30 days, and the total ΔV is about 240 m/sec. The depth of tail exploration can be adapted in accordance with observations from earth, as determined by the presence or absence of a prominent tail during the 1984 encounter. This exploration mode appears preferable, since it permits systematic mapping of the coma and tail during the most active phase of the comet while avoiding the more hazardous nucleus environment during that time. This will be further discussed under exploration strategy (Section 6).

An important consideration in defining preferable exploration patterns is that of effective protection against the severe thermal environment during closest solar approach, i.e., the 60-day period centered at perihelion. We note that in the second comet exploration pattern shown above the final nucleus rendezvous phase occurs almost at perihelion and thrust modes that require pointing the ion engines directly at the sun must be avoided to prevent excessive heating.

It should be noted that the excursion pattern discussed in this section is confined essentially to the orbital plane of the comet. Excursions out-of-plane should be minimized because, in contrast with relative motions in the plane, the velocity that would be required to return to the nucleus increases rapidly with distance. Out-of-plane relative trajectories are shown in Figure 5-14, where x and z are coordinates of the comet's meridian plane with x pointing radially away from the sun, and the z axis pointing south.

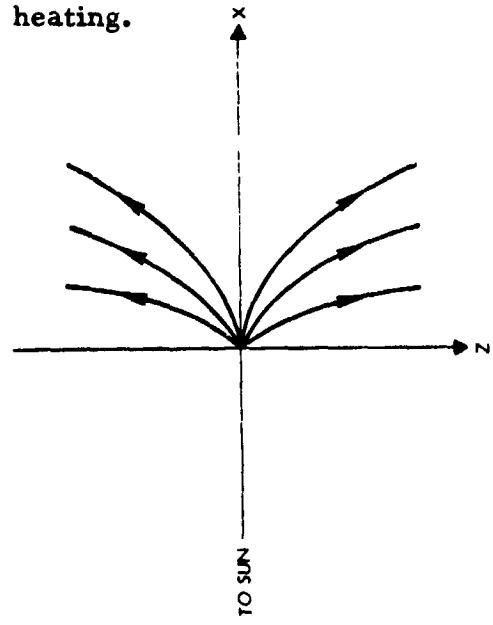

Figure 5-14. Relative Trajectories with Out-of-Plane Components

5.4.2 Perturbing Forces and Stationkeeping Requirements

The principal perturbing influences acting on the spacecraft that are of interest from a standpoint of stationkeeping requirements are these:

1) Solar differential gravity
2) Solar pressure
3) Gas flow pressure
4) Nucleus gravity

Solar differential gravity is only an apparent perturbation effect which is introduced by our adopting the rotating cometocentric coordinate system as a reference frame. However, it is by far the dominant effect that must be compensated if stationkeeping at a fixed relative position, more

than a few hundred km from the nucleus, is desired. It may be expressed in first order approximation by the following linearized equations:

$$\Delta a_r = -\frac{\mu\rho}{r_o^3}(3 + \sin^2 \gamma_o)$$

$$\Delta a_p = -\frac{\mu\rho}{2r_o^3} \sin 2\gamma_o$$

where

Δa_r = relative acceleration along the solar radius, positive inward

Δa_p = relative acceleration perpendicular to the solar radius, positive in the direction of the comet's motion

ρ = radial component of relative distance of the spacecraft from the comet center, positive in antisolar direction

r_o = solar radius

μ = gravitational constant

γ_o = orientation of comet velocity vector with respect to circumferential direction in heliocentric coordinates, positive when pointing inward.

The component Δa_p is much smaller than Δa_r, and vanishes at perihelion ($\gamma_o = 0$). Because of the factor $1/r_o^3$ the differential gravity effect is about 25 times larger at perihelion than at 1 AU, i.e., at the time of arrival. For an offset of 20,000 km at perihelion the acceleration is about 6 micro-g. Thus for a 1000-kg spacecraft a compensating thrust force of about 0.06 Newtons (13 millipounds) would be required for stationkeeping, i.e., more than ten percent of the typical SEP thrust capability (100 millipounds) available. A duty cycle of 1:8 would be required if full thrust were used intermittently for stationkeeping at this distance. This corresponds to a ΔV of 5.1 m/sec, and a propellant expenditure of 0.166 kg per day of stationkeeping.

Figure 5-15 shows the different perturbing forces acting on a 1000 kg spacecraft having a 100 m^2 solar array, as function of distance ρ from the nucleus. The solar distance is 0.34 AU (perihelion). Forces due to gravity and gas flow pressure, decreasing with the inverse square of the distance ρ tend to cancel if the solar array is fully deployed. A model of maximum gas flow pressure was derived from the estimated mass flow rate from the nucleus of 6×10^5 grams/second, or 10^{13} g/year (see Section 6). Note that this mass flow model has an uncertainty range of an order of magnitude. The resulting maximum gas flow pressure is about 60 millipounds at the surface of the nucleus, but only one millipound at a distance of 10 km. Partial retraction of the solar array would reduce the gas flow pressure effect, but at the same time makes the net difference between gravity and flow pressure forces larger.

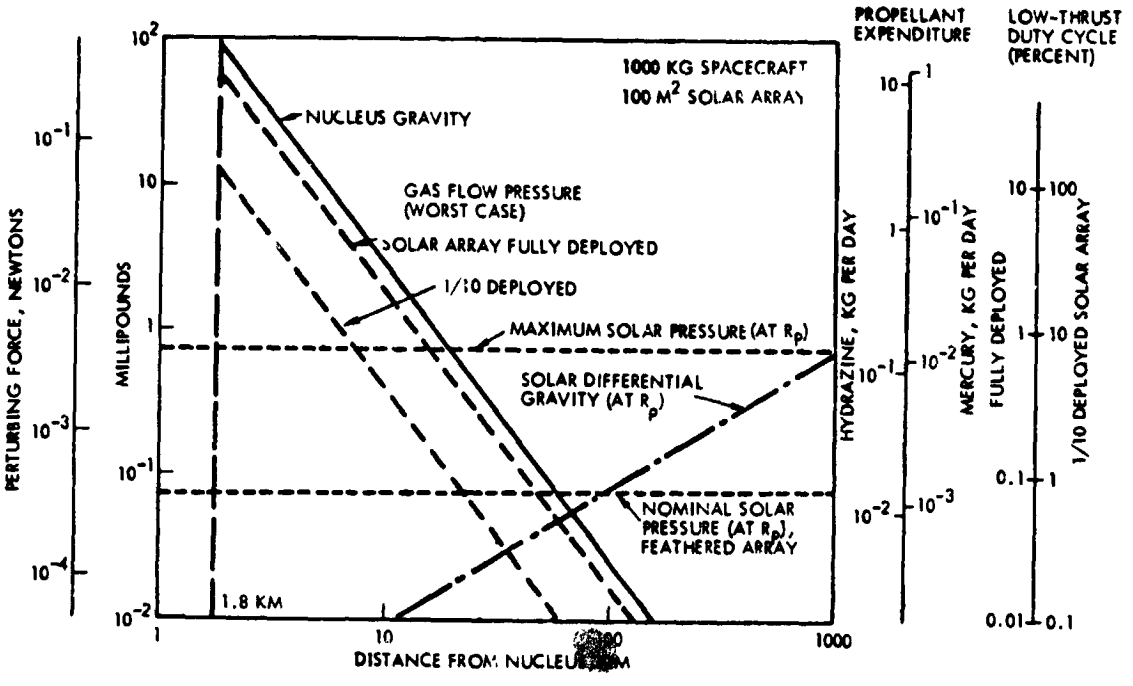

Figure 5-15. Perturbation Forces and Thrust Requirements in Center of Comet

Gravity acceleration at the surface of the nucleus (radius = 1.8 km), based on an assumed mass of 2×10^6 g is 0.41×10^{-3} m/sec^2. Thus the gravity force that would be acting on a spacecraft hovering near the surface is 90 millipounds. The nucleus gravity and solar differential

gravity effects are equal at a distance of 30 to 40 km as shown in the graph.

Solar pressure at perihelion was determined for a fully deployed solar array and a feathered array, i. e., an array turned away from the sun for thermal protection. It ranges from 0. 1 to about 1 millipounds.

We observe that the combined effects of the various perturbing forces are smallest at distances ranging from 20 km to several hundred km. This local dip in the perturbing forces is of interest, if the spacecraft should be required to maintain station for an extended period (20 to 30 days) in the penumbra of the nucleus for purposes of thermal protection, as discussed in the following paragraph.

5. 4. 3 Thermal Protection of Spacecraft Behind Nucleus

The possibility of placing the spacecraft behind the nucleus for some period of time to provide thermal protection during close solar approach has been suggested in the literature. Preliminary analysis of this concept leads to the results shown in Figure 5-16 (a) through (d). If, for example, the spacecraft hovers in the penumbra at about 196 km distance from the nucleus in partial solar eclipse of 50 percent, the maximum attainable at this distance, if the sun subtends an angle of 1. 58 degrees (0. 34 AU), a corresponding reduction of the thermal factor Q (Q = ratio of local solar flux to flux at 1 AU) by 50 percent can be achieved. The maximum thermal factor reached at perihelion, Q_{max} = 8. 65, is thus reduced to 4. 33 which corresponds to an equivalent solar distance of 0. 48 AU. Figures 16(c) and (d) show the shielding effectiveness of staying in partial eclipse as a function of time. For example, the thermal factor is reduced to 5 if the probe remains in partial eclipse for 23 days centered at perihelion. The required dwell time for 60 percent shielding is 33 days. These cases correspond to an equivalent closest solar approach of 0. 45 and 0. 54 AU, respectively.

The radial distance from the nucleus must be varied with time as shown in Figure 5-16(d) to maintain a specified effective thermal factor Q^* which is Q times the eclipse fraction. The dependence of the eclipse fraction upon radial distance and lateral offset is shown in Figure 5-16(b).

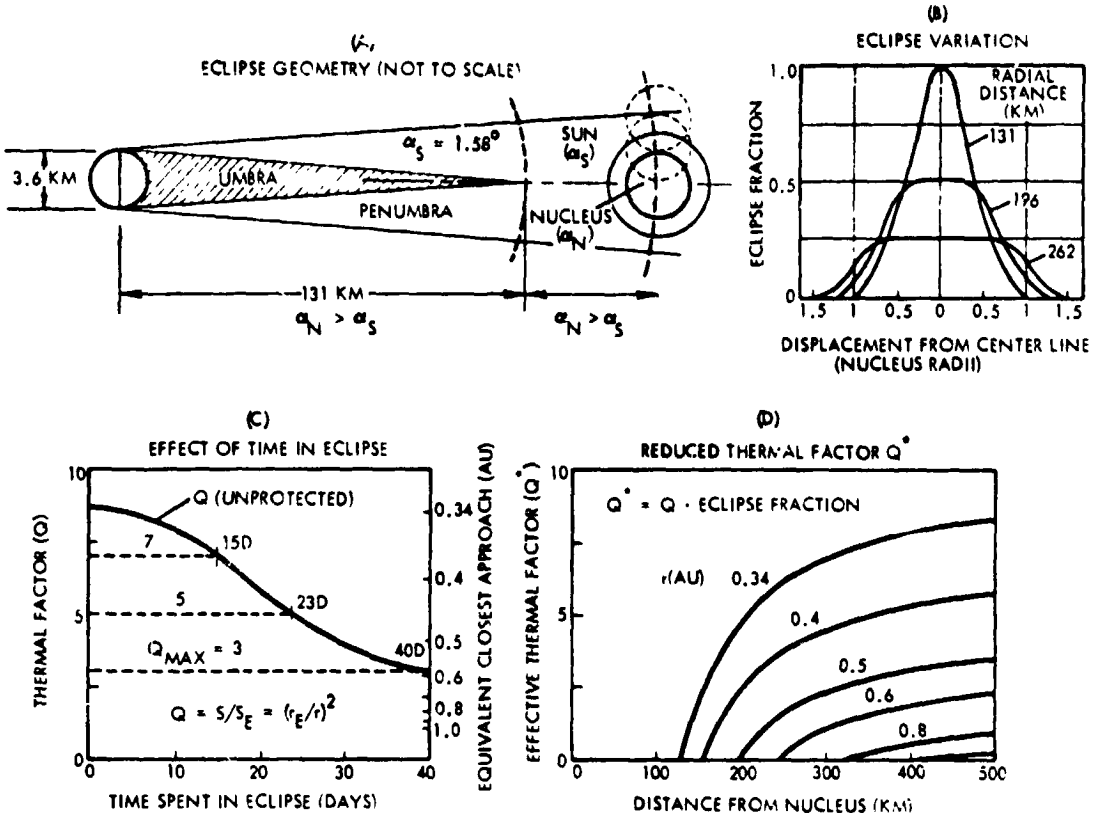

Figure 5-16. Thermal Protection of Spacecraft Behind Nucleus

As previously mentioned, the stationkeeping requirements to compensate for solar differential gravity are modest at distances of 100 to about 1000 km. Intermittent thrust at duty cycles of the order of one percent, even with a partially retracted solar array, would be adequate to maintain the desired position in the penumbra. The spacecraft will tend to drift in a retrograde direction and must be pushed back toward the penumbra's leading edge by intermittent thrust action. In addition, low thrust will be required to change the relative position with respect to the nucleus from 200 to about 500 or 1000 km in accordance with changing solar distance as shown in Figure 5-16(d).

The advantage of thermal protection must be weighed against the constraint on spacecraft position during an important part of the mission, hence a possible reduction of scientific data yield, and against the stationkeeping maneuver requirements. We recommend this thermal protection approach only as an emergency measure to cover unforeseen

contingencies and to save a mission that would otherwise fail due to excessive heating.

5.4.4 Chemical Propulsion Requirements

In addition to performing the primary propulsion tasks of the earth-to-comet transfer, including the necessary guidance maneuvers, the SEP system can also serve to perform most of the auxiliary thrust functions required during the comet exploration phase. Thus, a full-fledged, auxiliary chemical propulsion system is avoided and the propellant mass expended during this phase of the mission is drastically reduced. Maneuver requirements that cannot be met by low-thrust propulsion can be handled by the hydrazine attitude control thrusters. Use of these thrusters in a dual mode for velocity control and attitude control is flight proven, simple and economical. The low impulsive thrust of 0.005 g's also minimizes dynamic loading of the solar array and other flexible appendages (e.g., experiment booms).

The question of how much hydrazine propellant must be provided for auxiliary thrust pruposes is important because of the stringent limitations on payload capacity imposed by the selected transfer trajectory and power level. A generalized parametric approach is used here to delineate propulsion tasks that should be performed by the auxiliary chemical thrusters. This approach takes the time constraints of SEP maneuvers and the mass penalties of chemical propulsion maneuvers into account.

Figure 5-17 shows regimes of typical low-thrust and high-thrust operations in a force versus velocity diagram with thrust time as parameter. Propellant mass for chemical versus electric propulsion is also shown on the abscissa axis, assuming a gross spacecraft mass of 1000 kg.

The propulsion requirements for guidance corrections, stationkeeping, coma, tail and nucleus exploration maneuvers can be handled adequately by low thrust with times of operation ranging from several hours to several days. This is delineated by the shaded area at the lower right. A large saving of propellant mass compared to chemical propulsion can thus be

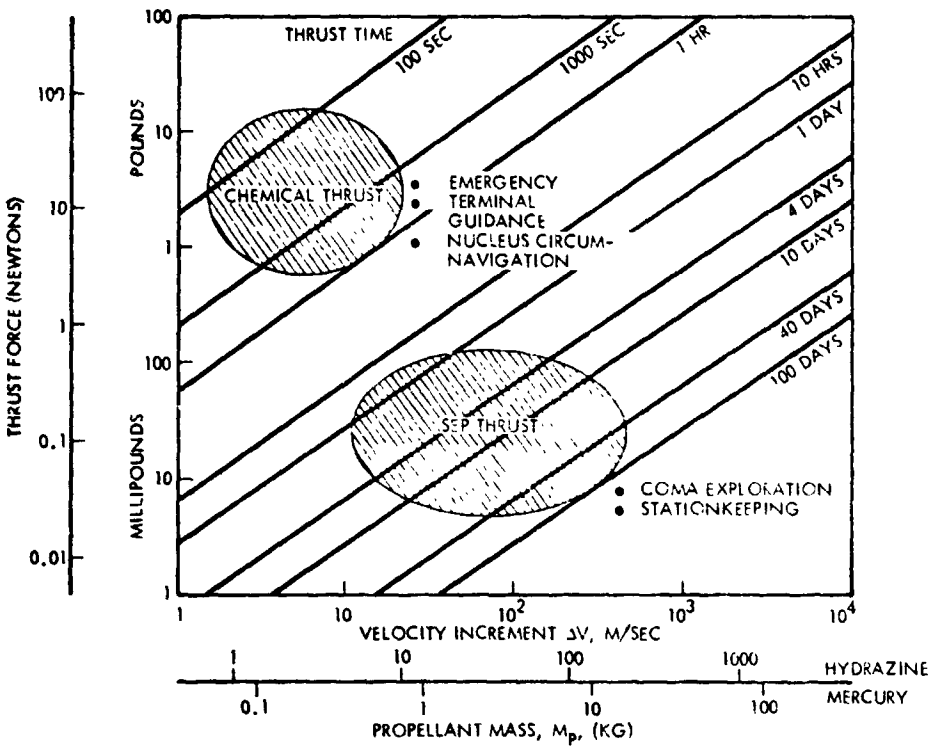

Figure 5-17. Regimes of SEP and Chemical Propulsion Use (1000 kg Spacecraft)

achieved. However, small rapid maneuvers in the vicinity of the nucleus such as terminal approach maneuvers, collision avoidance maneuvers, and circumnavigation, delineated by the shaded region in the upper left, require chemical propulsion because of time constraints.

This is further explained by Figure 5-18 in terms of the range of maximum excursions achievable by the low-thrust system as a function of time, compared to what is needed in various comet exploration phases. The solid line designated S_P shows the maximum transverse maneuver achieved by full thrust application (see diagram inserted at the upper left). The dashed lines S show the forward motion of the spacecraft during the same time interval at typical velocities for coma/tail exploration, terminal nucleus approach and near-nucleus maneuvers, 50, 5 and 0.5 m/sec, respectively. Intersections of the dashed lines and the solid line relate worst-case maneuver durations with required excursions. It is apparent that the long-duration maneuvers in coma and tail and during the

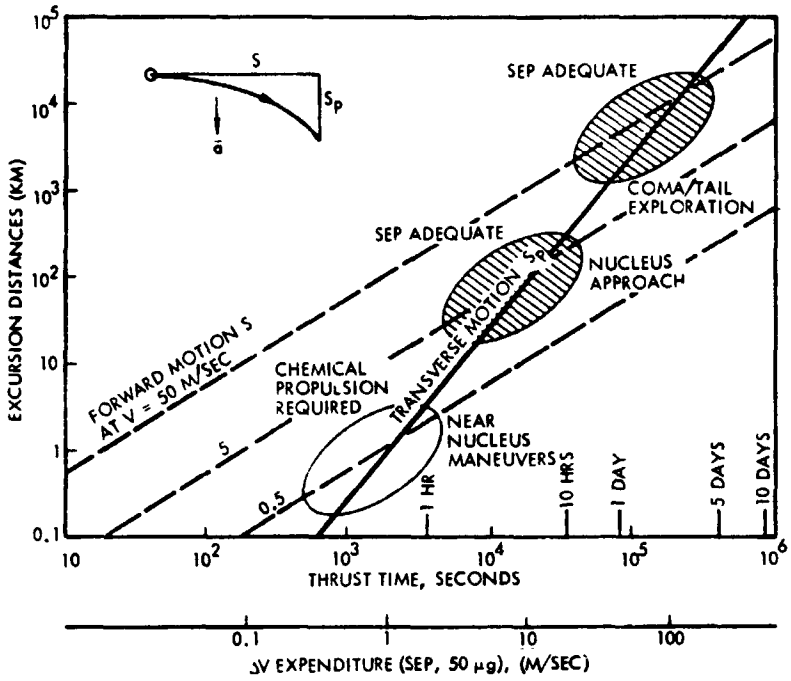

5-18. Maneuver Capabilities of SEP Thrust in Representative Tasks (1000 kg Spacecraft, Maximum Acceleration: 50 micro-g)

nucleus approach with excursions of the order of 10,000 and 100 km can be met adequately by electric propulsion whereas the close-range maneuvers of 1 to 10 km would require too much time, and therefore demand addition of the chemical propulsion capability. The time delay of 10 to 30 minutes that elapse between transmission of a ground command signal and the return of a TV image from the spacecraft must be taken into account in setting time limits for maneuver execution. An estimate of the total maneuver requirements for which the use of the hydrazine propulsion is essential (i.e. 10 to 20 maneuvers*) is 40 to 50 m/sec which corresponds to about 20 kg of hydrazine propellant. This figure takes into account the 2:1 savings in ΔV expenditure that is achieved by impulsive thrusting compared to SEP operation with 100 percent thrust time.

*See also Section 6.6.2 for ΔV requirements.

5.5 NAVIGATION

5.5.1 Navigation Concept

Previous studies (References 5-1 through 5-4) have established the feasibility of accurate low-thrust navigation using ground-based precision doppler tracking and orbit determination. For a comet rendezvous mission an onboard terminal navigation sensor is required in addition to determine the vehicle's relative position with respect to the comet. This is necessary since the uncertainty of the comet's trajectory characteristics dominates all other error sources.

As shown in Figure 5-19, taken from a recent comet rendezvous study by IITRI (Reference 5-2), the ground station receives the results of the optical fixes made by the spacecraft sensor, performs orbit determination based on these data as well as on doppler tracking data and telescopic observations of the comet, and transmits terminal guidance commands to the spacecraft. Thus, in spite of the complexity of the overall navigation task the spacecraft onboard system can be kept reasonably simple.

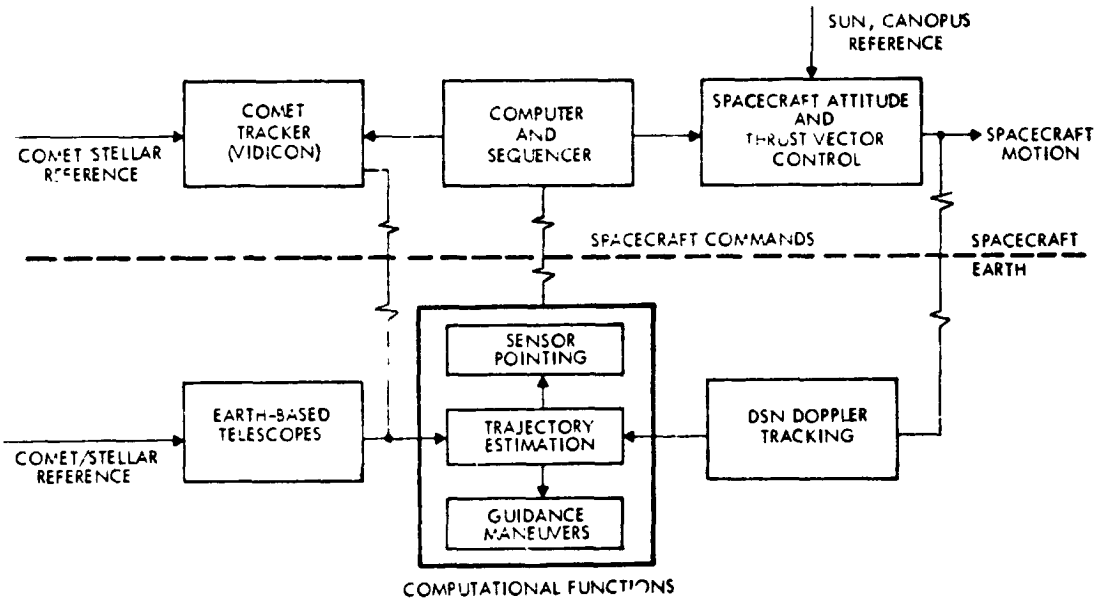

Figure 5-19. Rendezvous Navigation Functional Diagram (From IITRI Study)

Several factors inherent in the trajectory characteristics of a low-thrust mission to Encke are helpful in simplifying the navigation problem:

1) Low-thrust operation permits substantial guidance corrections at negligible extra propellant cost. This includes major terminal guidance maneuvers after ground-based recovery and onboard acquisition of the comet.

2) The low closing rate permits successive terminal navigation measurements and trajectory corrections without critical time constraints.

3) Encke's ephemeris can be predicted with higher accuracy for a given mission year than that of other comets because of its short orbital period, frequent observations in the past and the highly developed theory of its non-gravitational perturbations.

Results obtained by IITRI (Reference 5-2) for a 1980 Encke rendezvous mission are directly applicable to the 1984 mission because at least the second half of the transfer trajectory is comparable with similar arrival dates relative to Encke's perihelion passage.

In this study we have adopted IITRI's midcourse navigation data but modified the terminal phase by introducing a simpler mechanization. Instead of requiring a high accuracy for arrival at the nominal target point, i.e., the comet's nucleus in the case of IITRI's mission concept, we are proposing rendezvous in two stages.

1) The nominal first target point is at a large offset distance, typically 50,000 km from the nucleus on the sunward side. Accuracy at this stage is not critical for accomplishing the mission.

2) The final rendezvous target is the nucleus which is reached after initially performing a sweep through the coma/tail region and removing residual navigation errors at the same time.

3) Thus, an accurate final rendezvous can be achieved without demanding early target acquisition or high-resolution accuracy by the spacecraft optical navigation sensor.

This modified terminal navigation concept will be discussed below in greater detail.

5. 5. 2 Representative Navigation Characteristics of a Single-Stage Rendezvous Mission

Navigational characteristics of the transfer phase obtained in the IITRI study are summarized in Table 5-1. The results reflect the uncertainty in measuring position and velocity by doppler tracking due to the "process noise" of random thrust magnitude and pointing angle errors. Coast periods which occur initially and toward the end of the transfer phase improve tracking accuracy and thus keep position and velocity uncertainties at a low level.

Table 5-1. Midcourse Navigation Characteristics of 1980 Encke Rendezvous (From IITRI Study, Reference 5-2).

General	
Trip time to rendezvous	950 days
Rendezvous date	T_p - 50 days
Unguided terminal position deviation	1.7×10^6 km*
Unguided terminal velocity deviation	205 m/sec
Orbit Determination	
Maximum position uncertainty in midcourse	~4000 km
Maximum velocity uncertainty in midcourse	0. 25 m/sec
Terminal position uncertainty**	750 km
Terminal velocity uncertainty**	0. 4 m/sec
Guidance	
Maximum position deviation in midcourse	245×10^3 km
Maximum velocity deviation in midcourse	11 m/sec
Terminal position deviation**	1000 km
Terminal velocity deviation**	0. 5 m/sec

*All accuracy figures represent 1σ

**Assumes earth-based reference; does not reflect errors relative to comet.

Current studies performed by JPL show that DSIF tracking accuracy can be improved even without such coast periods by using the new quasi-long-baseline interferometry technique and by refined filtering. In any case, the comet position uncertainty assumed to be 3,000 km (1σ) at the rendezvous point is generally several times larger than the resid· al error of ground-based orbit determination of the spacecraft toward the end of the transfer phase. Hence, the requirement for terminal navigation by means of an onboard optical sensor.

Table 5-2 summarizes the characteristics of terminal navigation in the single-stage rendezvous investigated by IITRI. The optical sensor is assumed to have a 0.1 milliradian (20 arc sec) angle tracking error, in accordance with the specified angular observation accuracy of the high-resolution TV image system of Mariner 1969 and 1971 which was confirmed experimentally during Mars encounter (References 5-5 and 5-6). IITRI's study assumes that the comet can be acquired by the optical

Table 5-2. Terminal Navigation Characteristics of 1980 Encke Rendezvous (From IITRI Study, Reference 5-2)

General		
Observation interval		One day
Observation error		20 arc sec
Vidicon detection threshold		9th magnitude
Onboard recovery		60 days before rendezvous
Nominal aim point offset		1000 km
Approach Orbit Determination		
Initial range** uncertainty	before earth-based recovery	29,000 km*
	after earth-based recovery	24,000 km
	after onboard recovery	10,000 km
Terminal range uncertainty		10 km
Initial miss** uncertainty	before earth-based recovery	18,000 km
	after earth-based recovery	~3,500 km
	after onboard recovery	400 km
Terminal miss uncertainty		10 km

*All accuracy figures represent 1σ.

**Range measured along approach velocity
Miss orthogonal to approach velocity.

navigation sensor as an object of 9th magnitude at a range of about 4×10^6 km, 60 days before rendezvous. At this time the miss uncertainty decreases sharply by about an order of magnitude to 400 km; after 50 days of continuous tracking it will be reduced to 10 km. Range uncertainty decreases only much later, but reaches values below 100 km four days

before rendezvous. These values were obtained with initial miss and range uncertainties of 20,000 to 30,000 km that reflect comet ephemeris uncertainty before recovery of the comet at earth, as listed in Table 5-2.

5.5.3 Comet Ephemeris Uncertainty

The positional uncertainty of Encke prior to recovery at earth, in a given mission year, in estimated as 30,000 km (1σ) and the uncertainty of the time of perihelion passage as 0.005 to 0.01 days. After earth recovery, which typically occurs at 150 days before perihelion, the comet ephemeris can be rapidly updated, and position uncertainties reduced by about an order of magnitude. These uncertainty levels are reflected in the IITRI study. Additional information received from B. G. Marsden, of the Smithsonian Astrophysical Observatory* indicates that the time uncertainty of perihelion passage can be reduced to 10^{-4} days under favorable circumstances. Residuals of angular position for Encke are about 2 arc sec. A time uncertainty of 10^{-4} days at perihelion projects to 10^{-3} days at the time of rendezvous which is consistent with a positional uncertainty of 3,000 km at that time. Residual velocity uncertainties at perihelion are estimated to be of the order of 20 to 30 m/sec. This projects into an uncertainty about six times smaller at 1 AU, typically 3 to 5 m/sec. These estimates play an important role in the proposed simplified terminal navigation approach.

5.5.4 Simplified Terminal Navigation in a Two-Stage Rendezvous

The two-stage rendezvous concept simplifies terminal navigation and reduces the accuracy requirement of optical navigation fixes. Two options are of interest:

a) Incomplete terminal navigation prior to the nominal rendezvous as a result of late comet acquisition.

b) Deferment of terminal navigation until after the nominal rendezvous.

In the first case the navigation error at the nominal aim point is about 1,000 km. In the second case the error is about 3,000 km (1σ), since the

*Personal communication. (See also Appendix D.)

spacecraft trajectory has not been updated with respect to the comet. This error therefore reflects all of the comet's position uncertainty.

The large position error that remains at the start of the coma exploration phase is of no serious concern since enough time is left for precise terminal navigation while passing through the coma. The small terminal guidance corrections of 5 to 10 m/sec can be readily performed by the electric propulsion system during turnaround maneuvers. Spacecraft orientations required for these maneuvers are compatible with thermal control capabilities (see Section 7).

This approach has the following advantages.

1) The TV system resolution that is required for navigation purposes can be reduced so as not to exceed that required for scientific observation purposes (i.e., 0.5 milliradians).

2) Onboard target acquisition may be delayed at least until ten days before the nominal first rendezvous when the range is less than 10^6 km and target brightness has increased to 4th magnitude. This permits a reduction of the TV optical system size and sensitivity and eliminates ambiguity in target identification.

3) A wider field of view (5 by 5 degrees) is provided. This increases the number of bright reference stars available for navigational fixes by a factor of 20 on the average.

In summary, compared to terminal navigation in the single-stage rendezvous concept, navigational fixes carried out during the 30-day transverse of the coma are simpler, faster and more accurate because of larger line-of-sight rotation rate, smaller target range, smaller relative velocity, and greater target brightness. The system becomes less costly, not only because of simpler optics but also because of reduced calibration and pointing accuracy requirements.

Terminal guidance accuracy can be determined in first approximation based on the geometry of target observation illustrated in Figure 5-20. The sketch at the left shows the influence of angle errors on the triangulation scheme where T_1 and T_2 are two consecutive relative positions of the target as viewed from the spacecraft. The subtended angle ϵ is found by

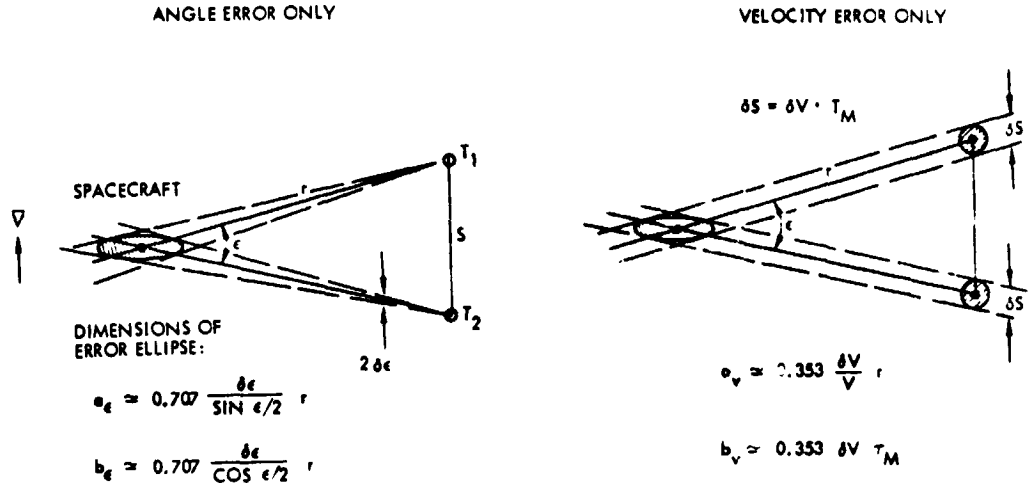

Figure 5-20. Effect of $\delta\epsilon$ and δV on Terminal Navigation Accuracy (Simplified Geometrical Model)

repeated observation of the target with respect to nearby reference stars. The angle error $\delta\epsilon$ of the navigational sensor determines the dimensions a_ϵ, b_ϵ of the error ellipse for a given baseline S and subtended angle ϵ. This navigation error is plotted in Figure 5-21 as a function of range with subtended angle ϵ as a parameter.

Referring again to Figure 5-20, the influence of a velocity error δV on the triangulation accuracy is shown on the right. In the presence of a velocity error the baseline becomes $S + \delta S = (V + \delta V)T_M$ where T_M is the time interval between observations. The error distance δS determines the dimensions of the error ellipse for a given nominal baseline and subtended angle. The resulting navigation error is plotted in Figure 5-22 as a function of range with $\delta V/V$ and $\delta V\, T_M$ as a parameter.

An improvement of the relative velocity error $\delta V/V$ is to be expected as a result of continued orbit determination. Thus, the navigation error a_ϵ can be assumed to be reduced in the manner shown by dashed arrows.

The geometry diagram shows that an increase in the line-of-sight rate reduces the error due to $\delta\epsilon$ but also, indirectly the error due to δV since the observation time interval T_M can be shortened, and δS is

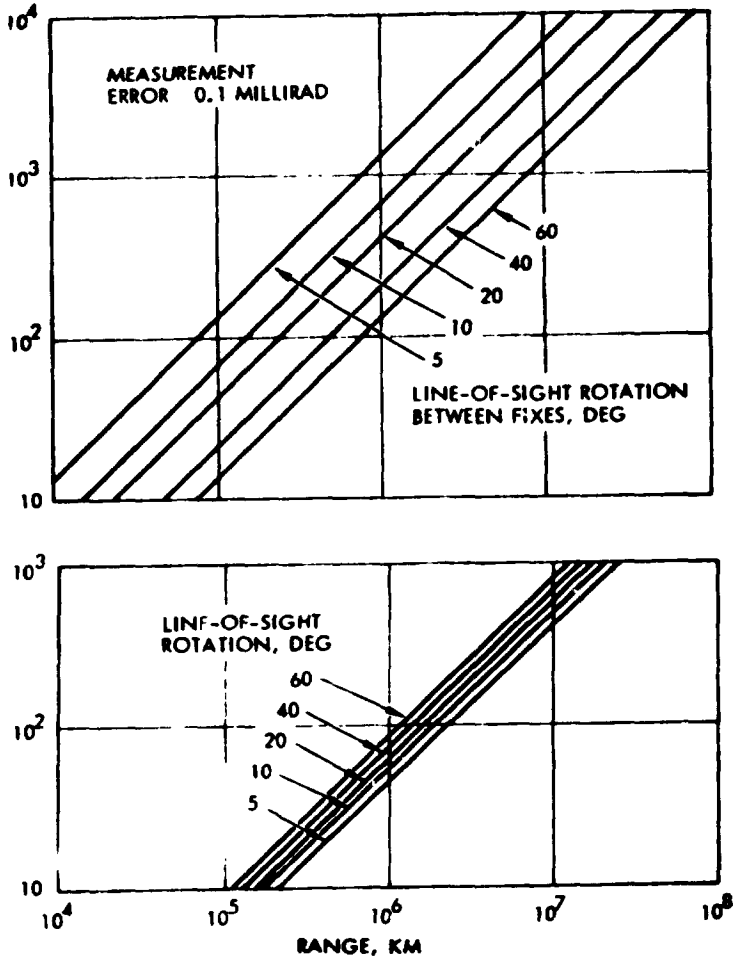

Figure 5-21. Terminal Navigation Error Due to $\delta\epsilon$

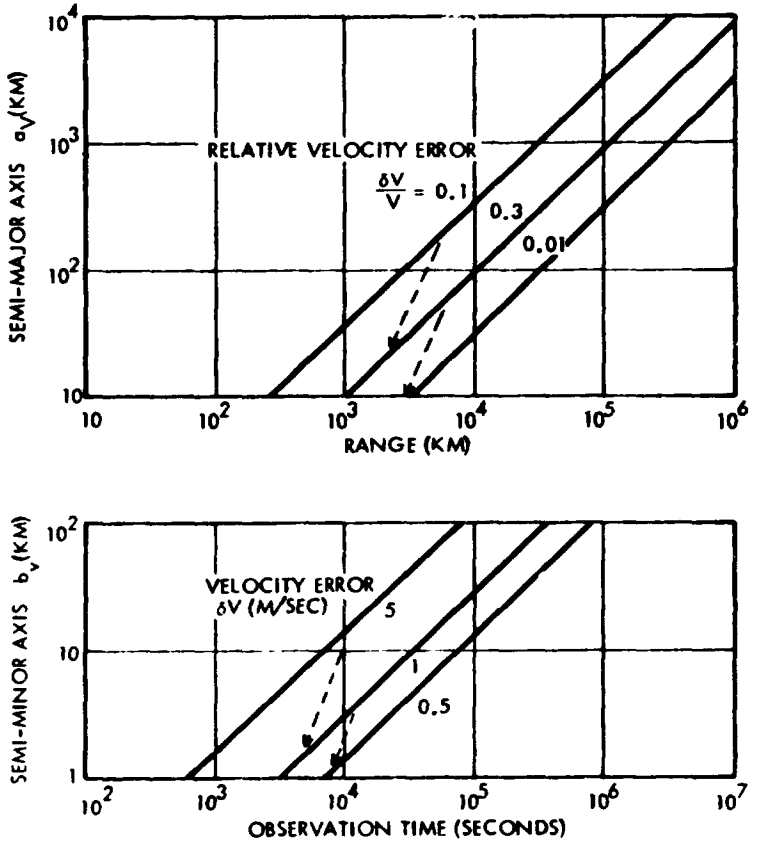

Figure 5-22. Terminal Navigation Error Due to δV

proportional to T_M. Although the illustration does not show the out-of-plane error components, it is easily seen that they are of the same size as the semi-minor axis of the respective error ellipses shown in Figure 5-20.

Table 5-3 summarizes representative navigation accuracies obtainable at two phases of the final rendezvous approach. The errors due to $\delta\epsilon$ and δV are assumed as statistically independent and combined in an RSS sense in the last columns of the semi-major and semi-minor axes.

A large reduction of navigation error due to the decreased range at the second nucleus passage as shown in the table is typical for this navigation technique. We note that with a reduction of velocity uncertainty δV during the time between the two passes (not reflected in the results shown) the a_V and b_V components should be further decreased. These results are based on a sensor accuracy $\delta\epsilon$ of 0.5 milliradians. The proposed sensor design (see next section and Appendix F) with an accuracy of 0.25 milliradians would further reduce the navigation errors in terms of the direct $\delta\epsilon$ contribution and reduced observation time T_M.

Table 5-3. Terminal Navigation Errors in Two-Stage Rendezvous

Sensor Accuracy 0.5 millirad
Velocity Error 1 m/sec
Relative Velocity 60 m/sec

Location and Time of Measurement	Observation Interval	Navigation Errors (km)					
		Semi-Major Axis			Semi-Minor Axis		
		a_ϵ	a_v	a_{RSS}	b_ϵ	b_v	b_{rss}
1. First nucleus passage							
r = 25,000 km	One day	43	147	153	4.5	30.4	30.8
T_1 + 10 days	Two days	21	147	148	4.5	60.8	60.8
2. Second nucleus passage							
r = 1000 km	One hour	1.6	3.5	3.8	0.2	1.3	1.3
T_1 + 30 days	Two hours	0.8	3.5	3.6	0.2	2.5	2.5

Figure 5-23 shows the stepwise reduction of gross navigation error levels during the final approach phase based on the foregoing discussion. Additional analysis of the orbit determination procedure and guidance maneuver characteristics is required to define the navigation accuracy achievable by this approach in greater detail, and to optimize the sequence of operations.

5.5.5 Navigation Sensor

Characteristics of the TV image system required for terminal navigation and scientific observation of the nucleus are presented in Appendix F. A summary of the characteristics that are needed to implement the navigation concept discussed above are summarized here.

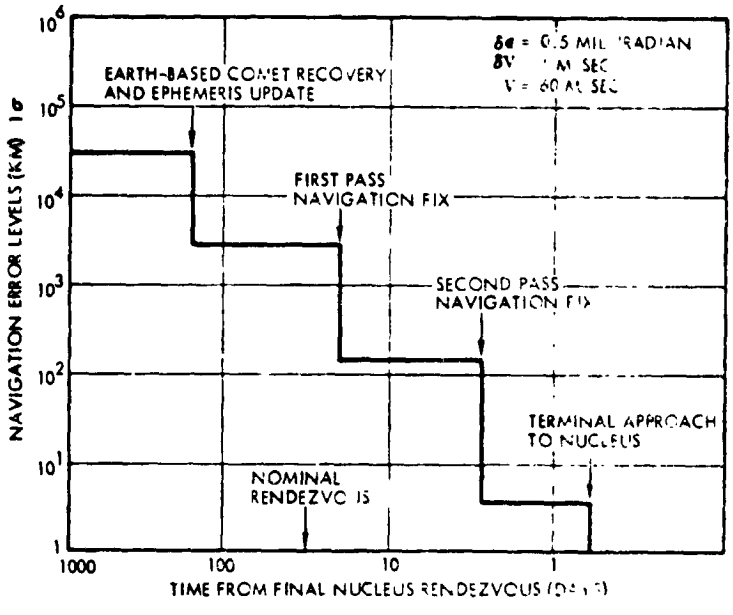

Figure 5-23. Gross Terminal Navigation Error Levels

We have selected an optical system with 125-mm focal length and f/2 aperture ratio. The total field coverage is 4.4 x 5.6 degrees. The instrument sensor is the same slow-scan vidicon employed in the Mariner 1969 and 1971 cameras. Each pixel represents an angular resolution element of 0.12 mrad.

Pre-encounter calibration of the instrument should allow measurement of the nucleus line-of-sight direction relative to surrounding reference stars to an accuracy of 0.25 mrad (3σ). To detect reference stars of magnitude 6.5 the image system requires an exposure time of 33 seconds. Thus, a very low drift rate of about 2×10^{-4} degree/second (4 μrad/sec) must be maintained to hold image smear below one pixel per frame. This is near the limit of present spacecraft attitude control capabilities. Drift

rates about an order of magnitude larger would be allowable if a higher sensitivity silicon vidicon, e.g., the Viking type, were used in the TV image system, requiring an exposure time of about 3 seconds for a sensitivity threshold of magnitude 6.5 (Reference 5-7).

The signal processing design uses a peak detection scheme to narrow the coma/nucleus image size for improved angular definition of the comet center with respect to available reference stars. In the 24.6 degree^2 field of view the average number of available stars of magnitude 6.5 or brighter is between 10 and 11 at the galactic equator and 2 to 3 at the galactic pole. The viewing geometry during the final phase of the transfer trajectory is such that the comet appears at about 50°S 30 days from rendezvous, and at 32°S at rendezvous. Thus, a sufficient number of reference stars (three to four on the average) should be available for navigation fixes, with conditions improving gradually toward rendezvous.

5.6 LAUNCH PHASE CHARACTERISTICS

5.6.1 Launch Period

Launch period constraints can be deduced from the net spacecraft mass contours that were shown in Figure 5-6 with respect to launch and arrival dates. The fast and slow trip options differ greatly in their sensitivity of net mass to variation of the launch date in the operating regimes of interest: the fast trip option shows a small payload loss of about 2 kg per day of launch delay if the arrival date is held fixed. The payload loss in the slow trip region of interest (Option 2) is much larger ranging from 5 to 20 kg per day. However, a larger payload margin is available in this case, so that the mass penalty for a typical 15-day launch period could be more readily accepted than in the case of fast trips. In the preferred operating mode (Option 1) we propose to avoid launch delay penalties by allowing the arrival date to vary slightly with launch date. The constant payload contours show that one day of arrival delay would be required for every four days of launch delay. The launch period could thus be extended to 30 days without apparent detriment to the mission.

5.6.2 Launch Phase Geometry

Only a rudimentary analysis of the launch phase geometry was carried out to determine whether significant constraints on launch azimuth and parking orbit coast period are imposed by the mission. For the nominal trajectory, with launch on or about 8 December 1981, the declination of the departure asymptote is about 20°S. This permits a direct ascent trajectory, or indirect injection with less than 25 minutes coast arc which is consistent with current Centaur stage operational constraints, both options permitting due east launch from Cape Kennedy. Under these very favorable launch geometry conditions we have a daily launch window of several hours within the available azimuth angle range at Cape Kennedy and where azimuth weight penalties are minor.

The departure angles will change greatly when a launch nearer the longitude of Encke's descending node is selected, e.g., slow trips with launch in February/March 1981. In these cases a large southern declination (50 to 60 degrees) of the departure asymptote would be required for optimal out-of-plane departure, and a more detailed analysis of launch geometry constraints must be performed.

REFERENCES, SECTION 5

5-1 F. E. Goddard, R. J. Parks, A. Briglio, Jr., and J. C. Porter, Jr., "Solar Electric Multimission Spacecraft (SEMMS)," 617-4, Jet Propulsion Laboratory, Pasadena, California, March 17, 1972.

5-2 "Comet Rendezvous Mission Study," Preliminary Report, IIT Research Institute (Final report in preparation), June 1971.

5-3 J. F. Jordan, K. H. Rourke, "Guidance and Navigation for Solar Electric Interplanetary Missions," AIAA Paper No. 70-1152, presented at the 8th Electric Propulsion Conference, Stanford, California, August 31, 1970.

5-4 "Study of a Common Solar-Electric-Propulsion Upper Stage for High-Energy Unmanned Missions," 16552-6007-R0-00, prepared for NASA/OART by TRW Systems, July 14, 1971.

5-5 T. C. Duxbury, "A Spacecraft-Based Navigation Instrument for Outer Planet Missions," Journal of Spacecraft and Rockets, Volume 7, No. 8, August 1970, pp. 928-933.

5-6 C. H. Acton, Jr., "Processing On-Board Optical Data for Planetary Approach Navigation," AIAA Paper No. 72-53, presented at the 10th Aerospace Sciences Meeting, San Diego, California, January 17-19, 1972.

5-7 J. A. Gardner, "1976 D'Arrest Comet Mission Study," Jet Propulsion Laboratory, No. 760-66, May 10, 1971.

6. EXPLORATION STRATEGY AND MISSION PROFILE

6.1 SELECTION CRITERIA

To formulate a preferred strategy of comet exploration and define the mission profile we adopted the following criteria and guidelines:

1) Define a mission sequence which achieves the scientific objectives effectively in terms of timing, exposure duration, areas covered, viewing options provided, etc.

2) Make best use of available spacecraft resources such as payload capacity, mounting space, power and maneuverability

3) Adapt the exploration strategy to environmental conditions so as to minimize hazards to spacecraft survival

4) Select operating modes that are consistent with the goals of simplicity and cost economy

5) Provide mission profile flexibility, permitting changes as conditions warrant

6) Select an exploration strategy that effectively complements the capability of an earlier flythrough mission.

These guidelines emphasize the capabilities inherent in a rendezvous mission as distinct from a flythrough mission with the goal of making most effective use of the long residence time and flexible maneuver modes available in rendezvous. The exploration strategy also should be designed to exploit the unique advantages offered by electric propulsion in performing this mission thus enhancing the scientific yield. These include the extended maneuvering capacity, operational flexibility and abundant power available during coast phases to operate scientific payload instruments and to support high data rate telemetry.

6.2 EFFECT OF ENVIRONMENT ON STRATEGY

To meet environmental constraints and to survive the hazards inherent in a comet mission the spacecraft and its payload must be designed with the proper protective features. This includes thermal protection, meteoroid damage protection of critical components by shielding against particles streaming from the nucleus, etc.

Spacecraft design features as well as the mission profile must be compatible with the environmental constraints. Operating modes that demand excessive spacecraft protection against the environment and, conversely, constraints on operational freedom dictated by lack of protective spacecraft design are to be avoided. Consider, for example, the extreme thermal environment encountered by the spacecraft at or near the perihelion passage. Clearly, an inactive spacecraft that is allowed to remain at a fixed attitude relative to the sun can be thermally protected more readily than one that must reorient frequently for propulsion maneuvers. However, such a spacecraft would have only very restricted exploration capabilities. Our approach permits spacecraft reorientation over a relatively wide angular range providing flexibility in maneuvering and payload pointing without imposing extreme thermal control problems. However, to achieve certain required thrust orientations the spacecraft must rotate 180 degrees around the sun line in order to maintain effective thermal control. Thus, an exposure of the thermally sensitive rear area to direct sun illumination can be avoided as will be discussed later in this section.

The best exploration strategy is one that minimizes the exposure and accepts risks only to the extent that they are inevitable in achieving the fundamental scientific objectives. Thus, we cannot avoid the potentially hazardous exposure to the efflux of the nucleus, but we can design the mission to minimize the risk. For example, we propose a late approach to the nucleus after initially exploring the coma/tail region, because the nucleus will be less active by the time the comet approaches perihelion, and hence less hazardous for a close approach. A close approach to about 10 km or less is necessary to be able to measure gravity with reasonable accuracy (see below). We can also adopt a flexible approach by continuing the coma exploration phase until in situ measurements reveal that the nucleus activity is beginning to subside, and a close approach to the nucleus is likely to be less hazardous.

Figure 6-1 illustrates, in a general way, the relation between scientific value gained and the attendant risk to survival of the spacecraft. The merit of late arrival at the nucleus is expressed by a function

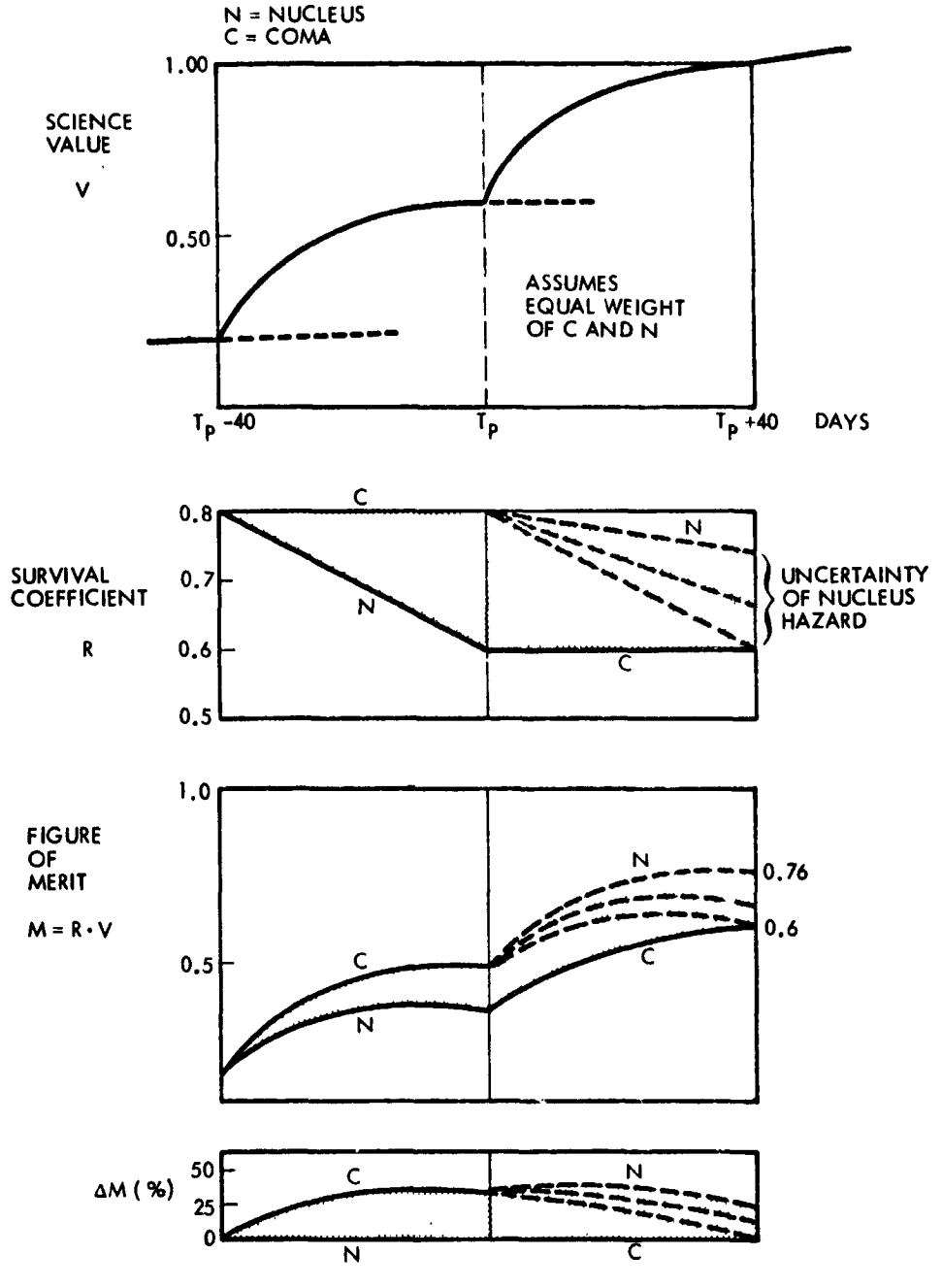

Figure 6-1. Figure of Merit of Two Comet Exploration Strategies

which is the product of "scientific data yield" times probability of survival. Scientific data yield V is expressed in normalized form where 1.0 represents the ideal data return of the completed mission. Probability of survival R declines less rapidly in the coma than near the nucleus, particularly when taking into account the initial most active phase of the nucleus. Thus the product M = R·V shows a distinct advantage (0.76 versus 0.6) of early coma exploration as compared to early nucleus exploration.

Table 6-1 gives further examples of the effect of environmental factors on the choice of mission strategy. Some aspects of thermal protection and meteoroid/particle flux protection have already been discussed above. In addition, the table lists such influences as solar pressure, solar differential gravity, solar flare activity, the observability of a prominent cometary tail, and the effect of the earth-comet geometry on the choice of mission modes.

Table 6-1. Environmental Effects on Mission Strategy

Environmental and Physical Factors	Affected Mission Objective	Available Mission Strategy Options and/or Preferences
Dust particle flux from nucleus	Close approach to nucleus (visual observation, gravity measurement) Extended hovering at nucleus Gravity measurement	Defer nucleus approach until flux decreases
Thermal environment at and near perihelion	Survival through perihelion Feasibility of some propulsion maneuvers and payload pointing maneuvers Operations near nucleus (hover and circumnavigation)	Limit orientation angles when closest to sun (accept constrained maneuver modes) Restrict coma exploration maneuvers Restrict hover position, i.e., to nucleus terminator Seek shelter in penumbra in emergency
Observability of tail from earth	Depth of tail exploration	Change coma/tail exploration path as warranted
Occurrence of major solar flare during comet exploration	Observation modes of solar wind interactions	Change excursion path as warranted Exit and reenter comet envelope
Solar pressure and differential gravity	Hover stability near nucleus and distant from nucleus	Thrust intermittently Partially retract solar array
Small nucleus gravity	Gravity measurement Gravity orbit feasibility	Approach close to nucleus Defer gravity orbit until large solar distance is reached
Large earth distance (long communications delay)	TV command control feasibility High data rate TV	Defer close approach to nucleus until communication distance is near minimum
Earth-sun-comet position	Communication blackout near perihelion	Avoid critical mission sequences during this period (~2 days)

6.3 MODEL OF PARTICLE FLUX AND IMPACT RATE NEAR NUCLEUS

A model of the flux of non-volatile material from the nucleus was derived as a quantitative basis for estimating the environmental hazard in close nucleus vicinity.

Based on the estimated maximum flux rate of particulate matter (see Section 2) i.e., 6×10^4 grams/sec, about 10 percent of the total flux consisting of volatiles and particles, and using a flux density model of cometary matter defined in NASA SP-8038 (October 1970),

$$\log_{10} S = -18.73 - 1.213 \log_{10} m$$

$$(S \triangleq \text{particles/meter}^3)$$

a particle flux is obtained as a function of particle size m and distance r from the nucleus as follows (R_o = nucleus radius):

$$\log_{10} F = -5.237 - 1.213 \log_{10} m - \log_{10} r/R_o$$

$$(F \triangleq \text{particles per } m^2\text{-sec})$$

The assumed relative velocity is 10 m/sec. This flux rate model is uncertain by at least ± 1 order of magnitude. Figure 6-2 shows the resulting flux density and impact rates of particles of one gram and one milligram size on a spacecraft and solar array of typical dimensions, assuming the array to be fully deployed and oriented at right angles to the flow vector.

The large impact rates, i.e., 10^4 to 10^5 milligram size particles per day in the immediate vicinity of the nucleus present a potential hazard in spite of the low impact velocity because they may impair delicate instruments and degrade the effectiveness of thermal protection blankets. There is little experimental or theoretical knowledge to date on qualitative degradation effects of a large flux of small particles at low velocities. However, we believe that the main concern is fouling of delicate instruments and equipment (sensors, ion engines, moving parts) and degradation of the solar array and of thermal properties of

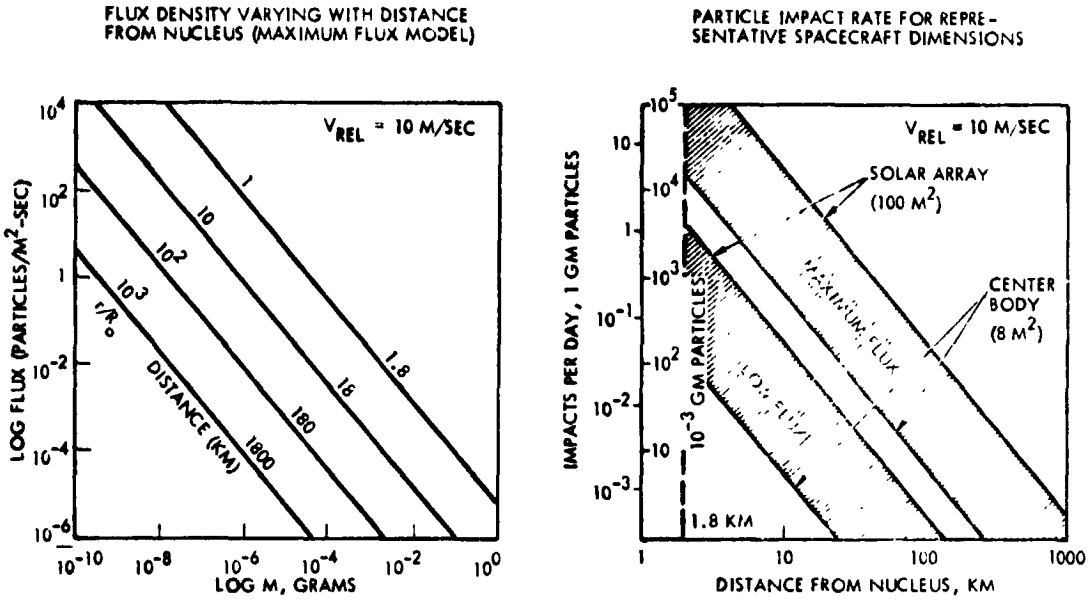

Figure 6-2. Particle Flux and Impact Rate Near Nucleus

insulation blankets, if a significant percentage of the exposed area is covered by particles that stick to the surface. The probability of particles adhering to spacecraft surfaces increases inversely with impact velocity. Small particle deposition may be of concern if they cover a significant area during long exposure. For a quantitative evaluation of potential hazard presented to the spacecraft we are making the following assumptions:

- Low emission velocity (~3 m/sec average) assumed
- Velocity up to 100 m/sec in sporadic outbursts and due to solar pressure
- Spacecraft relative velocities not exceeding 10-30 m/sec
- Low-density particles (0.1 - 1.0 g/cm^3) of fluffy structure unlikely to cause impact damage at these velocities
- Only larger particles (10^{-1} to 10^{-2} cm) may cause some denting or chipping of glass surfaces.

As a worst case example, we have assumed a flux of 10^{-6} gram particles at the nucleus surface estimated as 10^6 particles/m^2 sec. For an assumed density of 0.5 g/cm^3 the particle diameter is about 6×10^{-4} cm. With the further assumption of a sticking fraction of one

percent of the incoming particles we obtain an arrival rate that would cause an area of about 0.03 m^2 per square meter or three percent of the exposed surface to be covered per day. Clearly, this condition would jeopardize survival of the vehicle, or at least unimpaired functioning of critical elements, for any reasonable time required for nucleus observation. It is therefore advisable to postpone a close approach until such time when the flux has subsided.

6.4 FUNCTIONAL CONSTRAINTS ON EXPLORATION SEQUENCE

In addition to the environmental factors discussed before there are functional constraints dictated by the spacecraft design, propulsion capabilities, sensor characteristics, etc., that influence the choice of mission modes. Although spacecraft design features were not covered in detail in this study these constraints and their influence on the mission strategy can be discussed in general terms.

Principal constraints of this type are summarized in Table 6-2. The problem of thermal protection of the spacecraft under the extreme environment that exists during the perihelion passage has been previously noted. The design approach addressed to this problem will be discussed in Section 7. The spacecraft will be protected against direct solar heating by a multilayer aluminized Kapton thermal blanket on all exterior surfaces except the louvered radiating surfaces needed for waste heat rejection on the rear side of the equipment and propulsion modules. Exposed design elements and appendages will be protected by low-absorptivity high-emissivity coating. Thus thermal control can be achieved even under the extreme solar flux at perihelion provided the spacecraft attitude is maintained so as to protect the sensitive rear area from direct illumination. Limited angular excursions from the nominal orientation (with the center body normal to the sun) are therefore allowed for propulsion and payload pointing purposes.

Other spacecraft functional constraints listed in Table 6-2 include the primary (electric) propulsion pointing mode, the navigation sensor location and field of view limitation, scan platform mounting provisions and field of view, and solar array orientation requirements, all covered in Section 7.

Table 6-2. Functional Constraints on Mission Sequence

Functional Constraint	Affected Mission Phase or Operating Mode	Available Mission Profile Options and/or Preferences
Thermal control constraint	See entry in Table 6-1	
Thrust vector pointing requirement	Restricted sensor pointing angles during thrust phases	Point as required for optimal thrust, or Point off-optimally and accept weight penalty Accept pointing constraints during short thrust periods
Solar array orientation and retraction requirements	Constraint on spacecraft roll orientation restricts sensor pointing Field-of-view restriction of payload instruments if solar array is "feathered" Thrust power limitation if solar array is partly retracted near nucleus	Accept constraint in sensor operation and field of view Avoid major maneuvers at times when solar array is retracted
Navigation sensor field of view constraint (target obscuration by spacecraft body)	Approach navigation phase hampered by target obscuration	Reorient spacecraft as required for navigational fixes Revise navigational techniques (two-phase rendezvous)
Payload sensor field of view constraints	Limitation on scan capability	Reorient spacecraft during coast to circumvent field of view restriction Place sensor platform on extended deployment arm
High-gain antenna pointing requirements	Earth lock required during all mission phases and pointing modes	Use two-axis gimballed antenna mount and three-position deployment arm to meet earth pointing requirements Accept occasional restriction of payload sensor field of view
Radar altimeter pointing restriction	Relative positions of earth, sun and nucleus during nucleus observation require front area coverage by antenna	Plan nucleus gravity measurement in accordance with spacecraft and antenna pointing capabilities

The intermittent use of electric propulsion during the comet exploration phase does not basically interfere with scientific measurements of electric and magnetic fields if proper attention is paid to compensation of stray magnetic fields and to electrostatic cleanliness (see Appendix G). However, the presence of ion beam exhaust products in the vicinity of the spacecraft may affect mass spectrometer readings and optical/photometric observations. Thus the mission strategy should

be designed around the minimum number of thrust periods necessary to achieve the desired exploration paths.

As mentioned before, an exploration sequence starting with coma/tail exploration and approaching the nucleus subsequently appears preferable, under the functional constraints imposed by rendezvous propulsion and navigation tasks. These factors are summarized as follows:

1) Terminal navigation is simplified since large miss uncertainties are permitted at the first (nominal) rendezvous target point.

2) Terminal navigation fixes with respect to the nucleus can be performed effectively and rapidly during the coma exploration phase.

3) Exploration of the coma before the nucleus saves propulsive effort because the residual approach velocity can be utilized for coma exploration. This not only conserves propellant but eliminates potential propulsion/payload interactions at a time when measurements of particles and fields phenomena are important, e.g., in the bow shock and transition zone being traversed during the last 5 to 10 days before nominal rendezvous.

4) During final approach to, and operation near the nucleus we desire high telemetry data rates and short communication time delays to facilitate close control of the vehicle by ground command and TV feedback. Arrival at the nucleus around perihelion time decreases the communication range to 0.6 AU from the initial 1.4 AU at rendezvous. This means that the data rate can be increased by a factor of six, while the radio signal round-trip delay is decreased from 22 minutes to about 10 minutes.

5) Accuracy of nucleus gravity measurements is enhanced by the above sequence. If the passive, doppler measurement technique is to be used which hinges on the detection of very small velocity increments (of the order of 1 mm/sec), the signal-to-noise ratio of the measurements is of critical importance. A range reduction in the ratio of 2.5:1 available at closest approach to earth, i.e., near perihelion, would provide a significant advantage.

   Secondly, if the gas flow from the nucleus has subsided, there will be less of a distorting influence on gravity measurement whether by passive doppler technique or by an active thrust-while-hover detection of radial forces (see below).

6.5 MISSION TIMING AND DURATION

Among the alternate mission profiles those with short trip times are preferable because (1) reliability problems, especially those of the SEP system, are lessened and (2) more effective use can be made of results that would be obtained from a 1980 Encke flythrough which under the ground rules of our study is being assumed as a possibility (see Section 1). In addition, the fast mission with its later launch date provides greater procurement flexibility.

The selected nominal mission with a trip time of 800 days (Option 1 as defined in Section 5) would be launched eight to nine months later than a typical long trip time mission (Option 2). The time difference may be a significant advantage if the spacecraft under development for the 1984 mission must be modified as a result of data returned from Encke during the postulated 1980 flythrough, considering the extremely short "turn-around time" available. Practical questions regarding the feasibility of such modifications and their impact on the spacecraft development and test program are discussed in Appendix H.

Figure 6-3 summarizes several options in rendezvous timing and mission duration and indicates the preferred options (in heavy outline). The criteria for this selection are listed on the right. The preferred timing of arrival at the comet 30 to 50 days before perihelion passage has already been discussed. This choice is dictated by the scientific objective of observing the comet during its most active phase, as much as possible, before perihelion without the weight penalty that would be prohibitive for an earlier arrival. The severe thermal environment at 0.34 AU should be planned for since a mission without extended stay time at the comet would not gain the full advantage inherent in the rendezvous mode.

The payload advantage of late arrival, amounting to 5 to 10 kg per day for a 15-kw system as discussed before, cannot be matched in the case of early arrival unless a longer trip time is used, or the power level is increased. However, even with this penalty we selected 40 days before perihelion as a nominal arrival date because of the broader scientific coverage achieved by this option.

Figure 6-3. Rendezvous Timing and Exploration Sequence

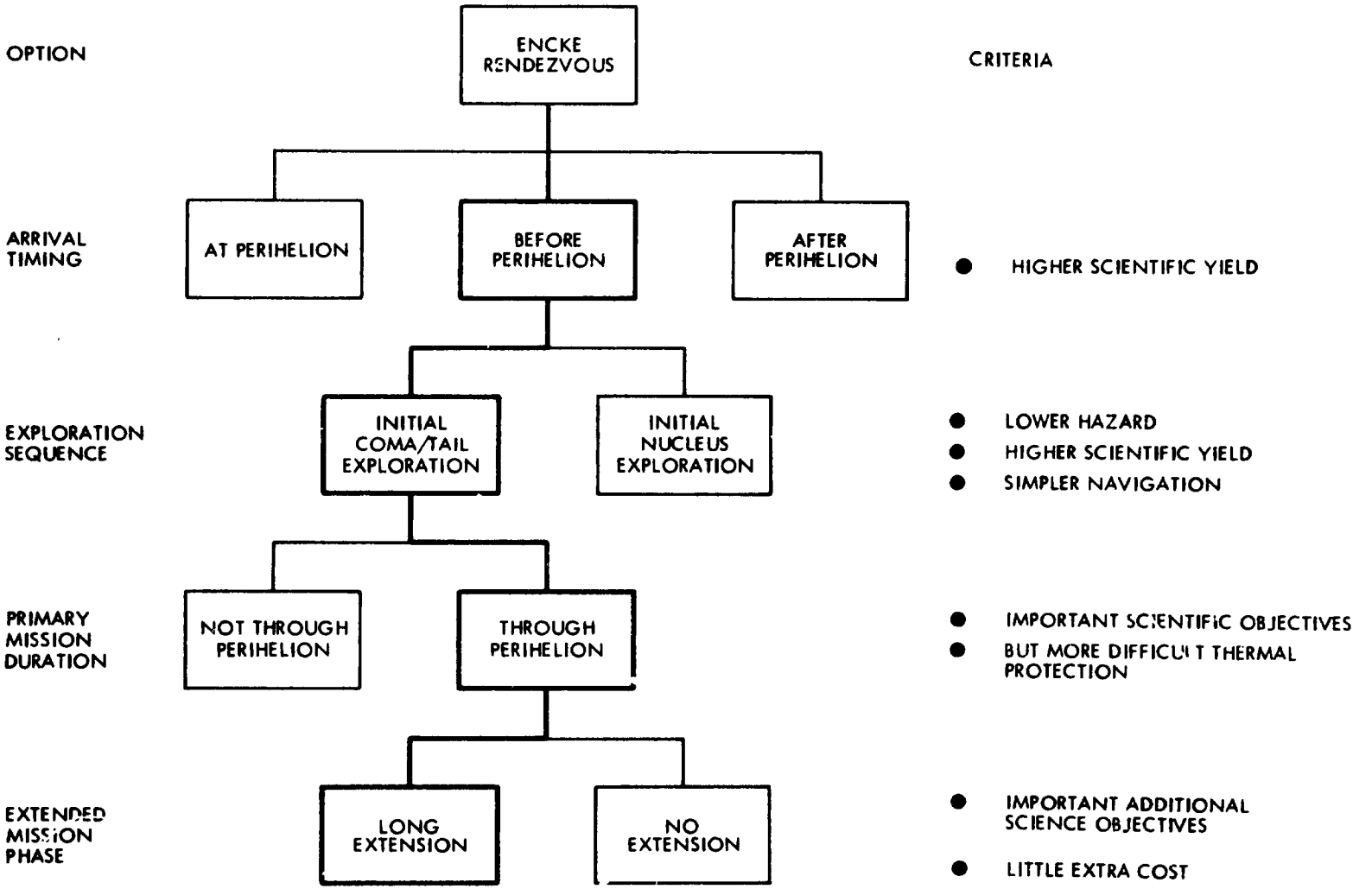

Regarding the total length of the comet exploration phase we are selecting as a primary goal a duration of 80 days, starting 40 days before and ending 40 days after perihelion. This has the advantage of permitting a comparison of cometary phenomena that occur at symmetrical points of the incoming and outgoing comet trajectory, especially detection of the causes of Encke's pronounced asymmetrical behavior before and after perihelion.

As a secondary goal we extend the duration of the encounter phase as far as possible toward aphelion. If it is assumed that the spacecraft must be designed to survive the perihelion passage and continue operation for 40 days there is every reason to expect it to survive for an extended time during the outbound phase. Observation during dormancy (which is the state of the comet during 90 percent of the orbital period) has interesting scientific objectives as stated before.

Tracking a spacecraft traveling with the comet during the extended outbound mission phase could also serve the important scientific objective of accurate determination of long-term comet trajectory perturbations. This is intended to confirm current theories of Encke's non-gravitational accelerations (Section 2). Asymmetry of these perturbations with respect to perihelion and the directionality of the gas flow can thus be reconstructed with higher accuracy than during the relatively brief comet visibility phase.

A possible simplification of continued stationkeeping requirements during this extended mission phase may be achieved by placing the spacecraft in a tight thrust-free orbit around the nucleus after the sphere of influence has increased to 75-100 km, at solar distance greater than 3 AU. However, this scheme is only conceptual and requires further analysis.

6.6 COMET OBSERVATION AND MAPPING STRATEGY

6.6.1 Gross Coverage of Cometary Features and Coma Exploration

Figure 6-4 illustrates regions of special interest in and around the comet that should be visited with some priority. These include the area of the postulated shock front, transition zone, outer and inner coma

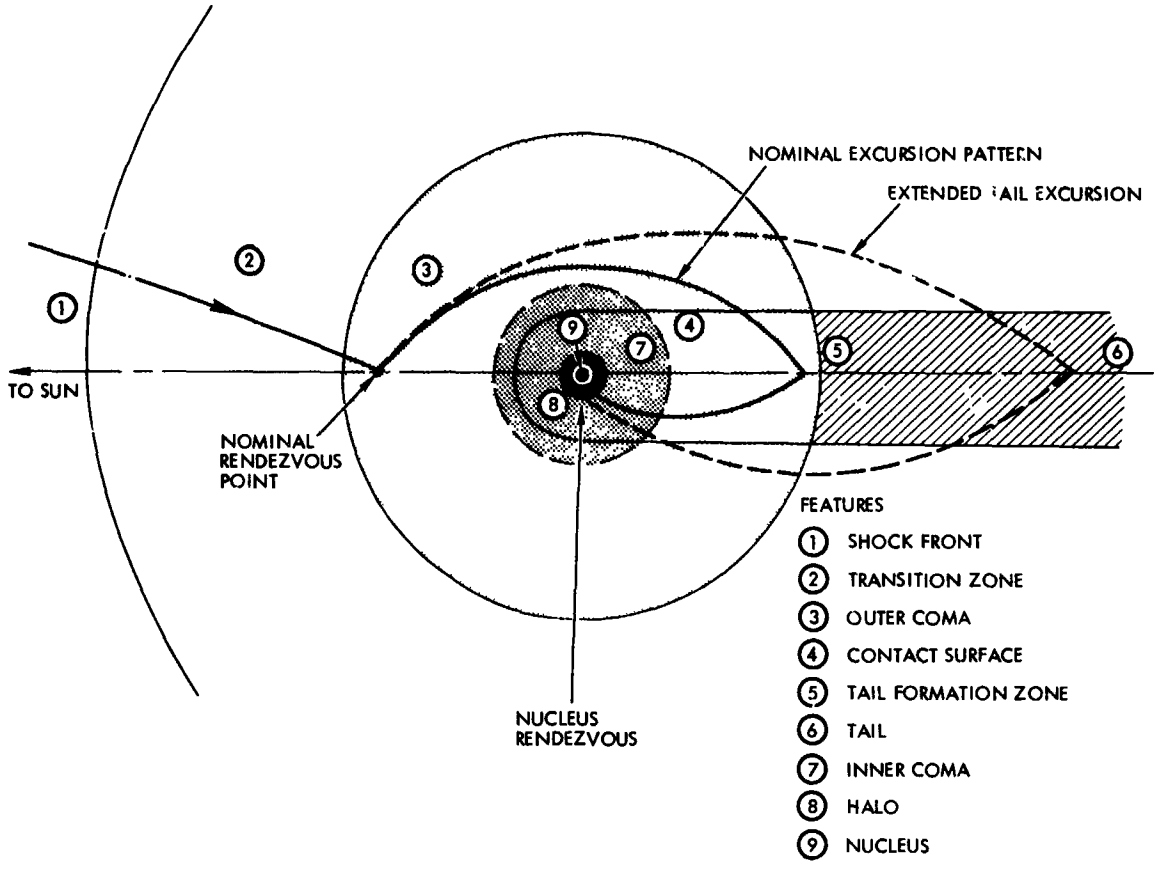

Figure 6-4. Excursions through Principal Comet Features (Not to Scale)

and contact discontinuity, the region where tail phenomena begin to form, and the nucleus and its halo. A mapping path of the type previously discussed (Section 5) is shown which passes all of the points of interest. After mapping the coma/tail regions (30 days) and performing close-up observations of the nucleus (20 days) the 80-day primary exploration time still permits 30 days of further exploration. Most of this time may be spent in exploring the coma/tail region, possibly leaving and reentering the comet envelope to explore the contact surface. Three-dimensional coma exploration may also be performed during this time. Thus, we can take advantage of the two principal characteristics offered by a low-thrust rendezvous: ample time and ample maneuvering capability.

By comparison a ballistic flythrough mission can cover only a few of the points of interest and in too little time for systematic mapping. The relative trajectory is nearly a straight line parallel to the $\overline{V}_\infty$ vector

and is dictated by mission dates and launch energy. (For selected encounter dates this path can at least be chosen to run roughly parallel to the comet's axis, moving in a radially outward direction.)

An interesting option available to the low-thrust vehicle is variation of the depth of penetration of the coma and tail region. E.g., if ground observation should find that Encke is developing a pronounced tail as the spacecraft approaches rendezvous, a simple change of the exploration path further into the tail region can be made at an acceptable extra propellant and time expenditure as shown by the dashed path in Figure 6-4.

The 1984 mission year offers a nearly optimal relative geometry for viewing the tail, if visible in that year, as shown in Figure 6-5.

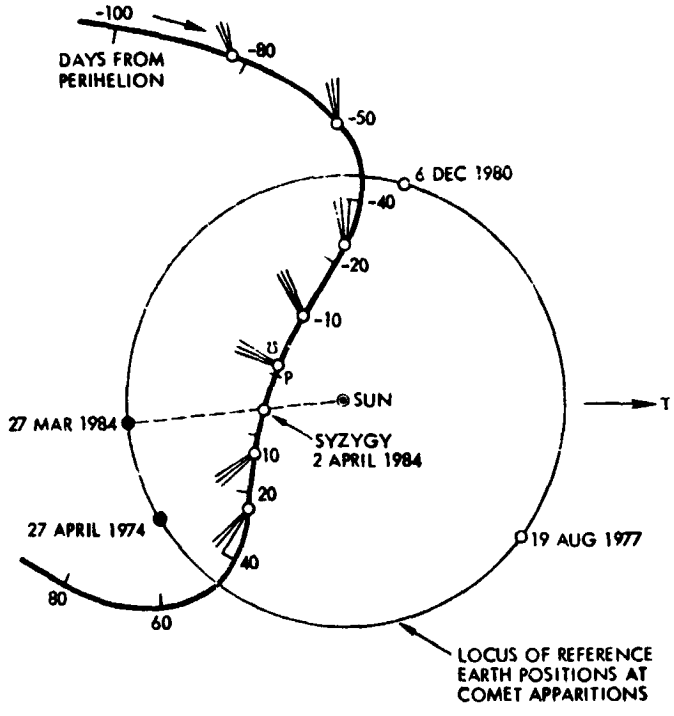

Figure 6-5. Viewing Conditions of Encke's Tail from Earth (Encke's Relative Trajectory in Bipolar Coordinates Projected into Ecliptic Plane)

(This "bipolar" plot has many useful applications in the analysis of mission characteristics as will be discussed in Appendix A.) Since the tail extends radially away from the sun, it can be seen broadside during almost the entire encounter except during 10-15 days of the comet's closest solar proximity when the tail is pointing in the direction of earth.

Since the comet has a nearly rotationally symmetric structure it would appear that mapping in the orbital plane is adequate to infer from it the corresponding characteristics out of plane. This would conserve propellant expenditure and time. However, any asymmetry in the third dimension that can be observed by the spacecraft would provide important additional scientific data on the nature of the comet. Such out-of-plane excursions might be performed after the basic in-plane coma/tail mapping and the nucleus exploration is completed.

There is no clear-cut requirement for stopping the coma traverse in any particular area to keep the spacecraft in a stationary hover mode. As discussed in Section 5 hovering at large distances from the comet center requires an appreciable amount of intermittent thrusting which complicates the mission sequence and potentially interferes with delicate particles and fields measurements. Since the coast velocity relative to the comet is only about 30-60 m/sec observations are actually made under quasi-stationary conditions. This facilitates the differentiation of spatial variations and temporal variations of cometary phenomena with fair accuracy.

6.6.2 Nucleus Exploration

Exploration of the nucleus can be performed in the hover or circumnavigation mode. The hover mode permits continuous observation of surface features from a favorable vantage point such as the vicinity of the terminator. E.g., from this position it is convenient to measure thermal transients on the surface associated with sunrise or sunset. Hovering over the pole has advantages of observing the rotating body from a more revealing perspective and measuring the surface temperatures under extended uniform heating conditions assuming that the pole does not happen to be precisely on the terminator. The position of the

pole can be readily deduced from a sequence of TV images that show successive positions of moving features with respect to the terminator. Hovering over a nonpolar region permits mapping the elevation of the rotating terrain by means of an altimeter radar. At very close distance a gravity gradiometer could be used to deduct mass concentrations in addition to measuring the total mass of the nucleus. However, the gradiometer is not included in the fundamental payload because other techniques are available to perform gravity measurements without extra instrumentation, and because it would require a very close approach distance (see below).

These operations are carried out more conventially and systematically in the hover mode than during circumnavigation, and at a fixed spacecraft attitude. Continuous or intermittent stationkeeping maneuvers are required. However, with a surface gravity of only 40 μg, hovering at a reasonably small stand-off distance requires only a fraction of the available SEP thrust capability (50 μg). Thus, at a distance of two nucleus radii a duty cycle of 1:5, with thrust periods of 24 minutes every two hours, is sufficient to maintain altitude within ±250 meters. A simple onboard radio altimeter can be used for automatic control of this slow altitude limit cycle. As mentioned before, the pressure of outflowing gas actually will tend to counteract the small gravity force and reduce the propulsion requirements even more. Since the solar array will be in a "feathered" orientation, nearly 90 degrees from the sunline, it is apparent that the outflowing gas will produe a greater lifting effect at positions near the terminators where flow velocity is normal to the solar paddles, than elsewhere.

The mission sequence also must include circumnavigation maneuvers for unconstrained observation from all sides. Because of the almost negligible gravity field of the nucleus a conventional orbit governed by gravitational forces is impractical. This can be seen readily when considering the sphere of influence of the nucleus relative to solar gravity. Assuming a mass of 2×10^{16} grams, which is 17 orders of magnitude less than the sun's, the sphere of influence is only 8.5 km at the comet's perihelion, and 23.8 km at 1 AU. Uncertainty of the actual mass of the nucleus, and the presence of perturbations other than solar gravity make

a gravity orbit around the nucleus even more problematic. Adequate velocity control would be extremely difficult from a practical standpoint: a tight orbit at a radial distance of three nucleus radii would have a circular velocity of only about 0.5 m/sec. If this velocity were inadvertently increased by 40 percent (0.20 m/sec) the spacecraft would escape the nucleus gravity field, whereas a loss of 30 percent (0.15 m/sec) would cause it to hit the surface.

A more feasible alternative is circumnavigation with the aid of periodic maneuvers as illustrated in Figure 6-6. The "orbit" is a triangular, quadrangular or other pattern, not necessarily symmetrical, with turn maneuvers about every two hours. For the dimensions shown the relative velocity is 2 m/sec and each turn maneuver requires a ΔV of about 3 to 4 m/sec adding up to about 12 m/sec for a complete orbit. The maneuver requirements are compatible with the available SEP thrust capability of 2 m/sec per hour. Low-thrust maneuvers would of course mean rounded corners, not shown in the figure. The schematic diagram also ignores the effect of gravity which would make the sides of the polygon pattern bulge out (less than 100 meters for the assumed path velocity and dimensions).

Disadvantages of using SEP thrust for these maneuvers are the frequent reorientations of the spacecraft and the undesirably long thrust duration per orbit. This suggests a reduction in path velocity or an increase in orbit size. The preferred alternative is to use chemical (hydrazine) propulsion since no reorientation is required to perform the hydrazine thrust maneuvers if multiple thrusters are used as illustrated in Figure 6-6 for the quadrilateral orbit. Although a greater amount of propellant would be expended per orbital pass, this will be acceptable because the vehicle, rather than circumnavigating continuously, will probably spend most of the time in the hover mode using SEP thrust.

A preferred mode of operation for purposes of low-thrust propulsion would be to rotate the spacecraft continuously at the small constant rate of one revolution per orbit. This provides the desired thrust angle variation without discrete attitude reorientation maneuvers. The spin

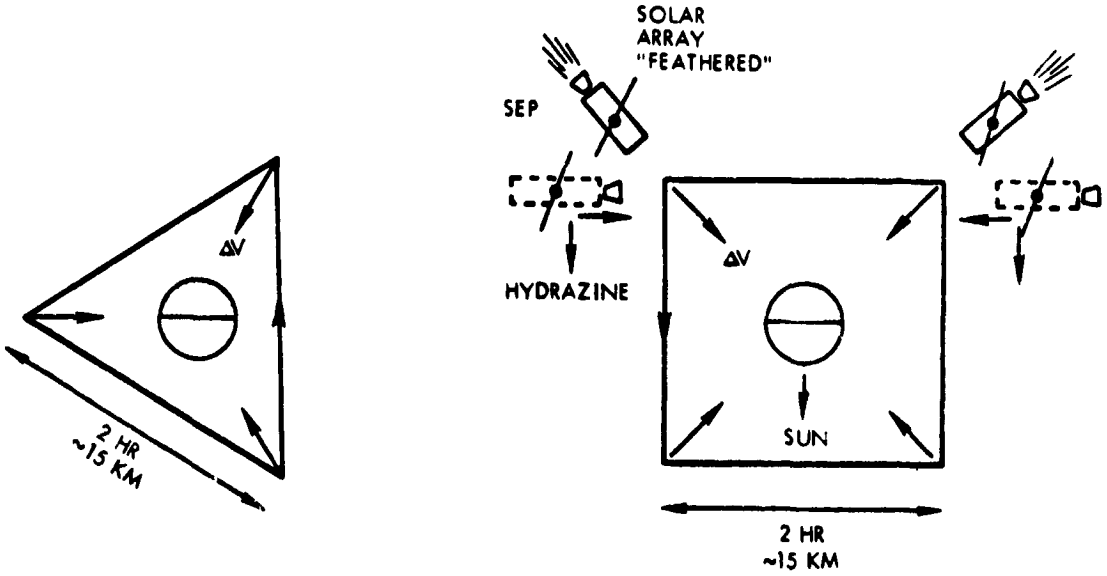

Figure 6-6. Nucleus Circumnavigation Maneuvers at Close Distance

vector does not have to point exactly at the sun since solar array re-orientation away from the sun is required for thermal protection anyway. Alignment with the sun implies an orbital plane that coincides with the terminator.

This operating mode has the additional advantages of pointing the payload end of the spacecraft continuously at the nucleus, and of maintaining a constant, or nearly constant, solar aspect angle alleviating thermal control problems. Incidental to the choice of orbital plane at or near the terminator is the avoidance of solar eclipses.

6.6.3 Nucleus Gravity Measurement

For a small body such as the nucleus of Encke, assumed to have a radius of only a few kilometers (our model uses R = 1.8 km) and a mass of 2×10^{16} g, any gravity measurements short of landing on the surface require a very close approach distance. Three types of measurements have been considered:

1) Doppler velocity measurements from the ground with a sensitivity of 0.5 mm/sec

2) Gravity gradiometry

3) Measurement of thrust expended for hovering at low altitude.

The various techniques of gravity measurement are illustrated in Figure 6-7. The various measurements actually are not identical in scientific data yield, but can be used if necessary for backup purposes.

The doppler technique requires not only a close approach but a low flyby velocity to produce a perceptible velocity change. We assume closest approaches of a few km and velocities in the range of 2 to 10 m/sec. To maximize the doppler frequency the flyby trajectory should be traversing the nucleus at right angles to the earth line-of-sight. Figure 6-8 shows the altitude required to measure the gravity of a 3.3 g/cm^3 body within one percent as a function of its radius with flyby velocity as parameter, based on a recent paper by J. D. Anderson (Reference 6-1). Also shown is a curve for gradiometer measurement, based on a 30-second integration time and a noise threshold of 0.3 Eötvös Units, based on a paper by R. L. Forward of Hughes Research Laboratories (Reference 6-2). With less conservative assumptions on noise threshold and a longer integration time the altitude can probably be increased by an order of magnitude. A closest approach of less than 10 km will still be required to perform an accurate gravity measurement.

The gradiometer technique has the advantage of being insensitive to nongravitational forces acting on the spacecraft. Both the doppler technique and the thrust-while-hover gravity measurement would be affected by any appreciable gas flow pressure on the vehicle which in the worst case is of the same order of magnitude as the local gravity. In the hover mode this effect can be easily isolated by a series of measurements with the solar array fully or partially exposed ("feathered") with respect to the radial flow direction. As a by-product this would also yield the dynamic flow pressure, from which the flow rate and density of the emitted gas can be inferred.

In all cases, an accurate range measurement is required for which a simple low-powered radio altimeter is proposed with a range of the order of 50 km (see Appendix E). The altimeter also permits an indirect determination of relative velocity based on line-of-sight rotation. Furthermore, the dimensions of the nucleus can be derived from the distance measurement and the subtended angle. Mass and dimensions yield the nucleus density.

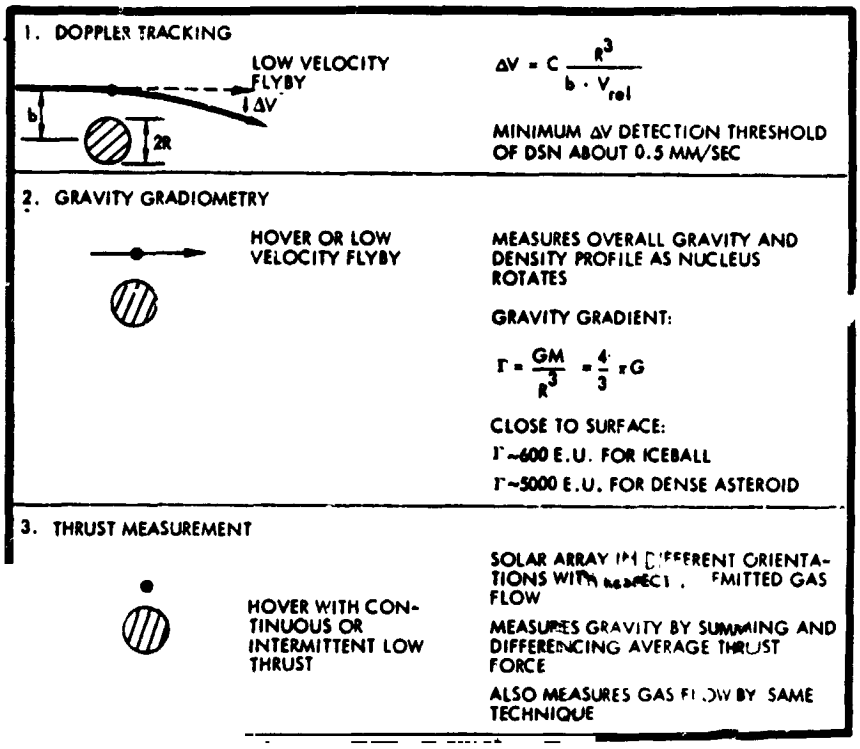

Figure 6-7. Gravity Measurement Techniques

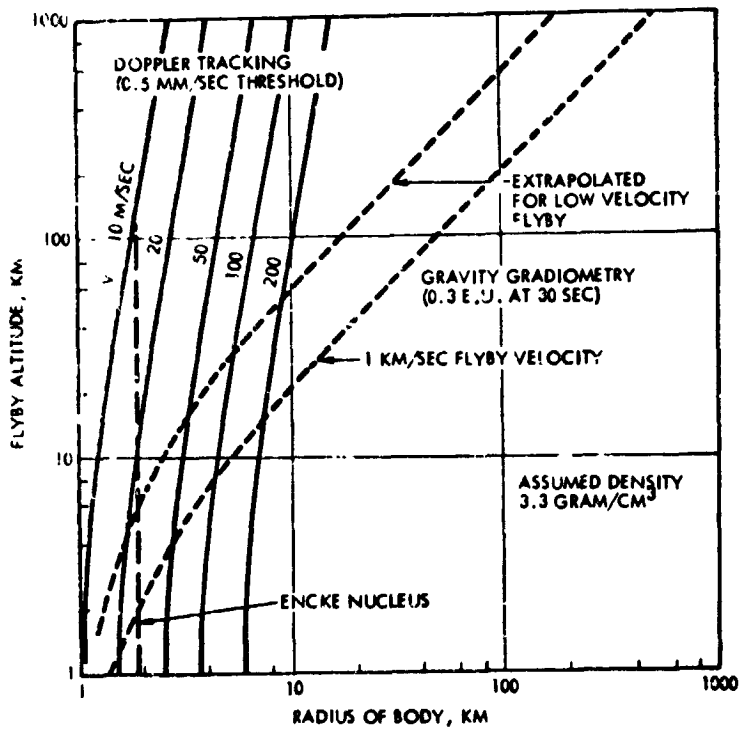

Figure 6-8. Flyby Altitudes Required for Doppler and Gradiometer Techniques of Gravity Measurement

6.7 SPACECRAFT AND INSTRUMENT POINTING MODES

6.7.1 Constraints and Requirements

To show the feasibility of the various mission phases discussed thus far a more detailed examination of typical spacecraft orientation and instrument pointing modes is required. The objective is to show that the spacecraft with its body-mounted and articulated appendages, including the two-gimballed scan platform, the two-axis steerable high-gain antenna, and the one-axis rotatable solar array, can meet the basic pointing requirements of the mission. The major pointing constraints and requirements are as follows:

1) The thrust vector must be pointed over a wide range of cone and clock angles* relative to a sun oriented reference system to maximize the payload. This requires rotation of the center body relative to the solar array and/or rotation of the entire spacecraft around the sunline.

2) The solar array must be oriented away from the sun, up to 80 degrees from the nominal orientation, for thermal protection.

3) The center body orientation relative to the sun is constrained by thermal control requirements.

4) The high-gain antenna must be capable of pointing at earth under all attitudes of the vehicle with earth view angles (cone angles) up to 180 degrees from the sunline.

5) In any spacecraft attitude the one-axis rotatable attitude reference star sensor must be able to lock on a bright reference star that is not obscured by the solar arrays, without stray sunlight interference.

6) The gimballed payload scan platform must be capable of pointing the instruments at all comet phenomena of interest prior to and during the entire exploration phase. In particular, the TV image system used as terminal navigation sensor, must be able to view the central coma and/or nucleus before and after encounter through a wide range of body orientations.

7) Finally, the one-axis altimeter radar must be able to point at the nucleus during close approach and hover maneuvers.

*These angles to be defined in the next subsection.

These requirements and constraints were analyzed in sufficient depth to permit definition of preliminary spacecraft design concepts and operating modes. Typical results are presented below. We have attempted to reduce the complexity of the articulation system and pointing sequences as much as possible, but feel that further simplification is desirable. To define a mission profile with a minimum number of spacecraft reorientations more detailed analysis beyond the scope of this study is required to cover alternative pointing options and perform functional tradeoffs. A survey of available reference stars should also be performed to select preferred acquisition and tracking modes for attitude control.

6.7.2 Coordinate Systems Used

Two spacecraft-centered coordinate systems were adopted to facilitate analysis of time-varying pointing requirements.

Sun-Oriented System. The first is a sun-oriented system x_s, y_s, and z_s as shown in Figure 6-9(a), with z_s pointing to the sun; y_s orthogonal to z_s in a plane normal to the ecliptic and containing the spacecraft;

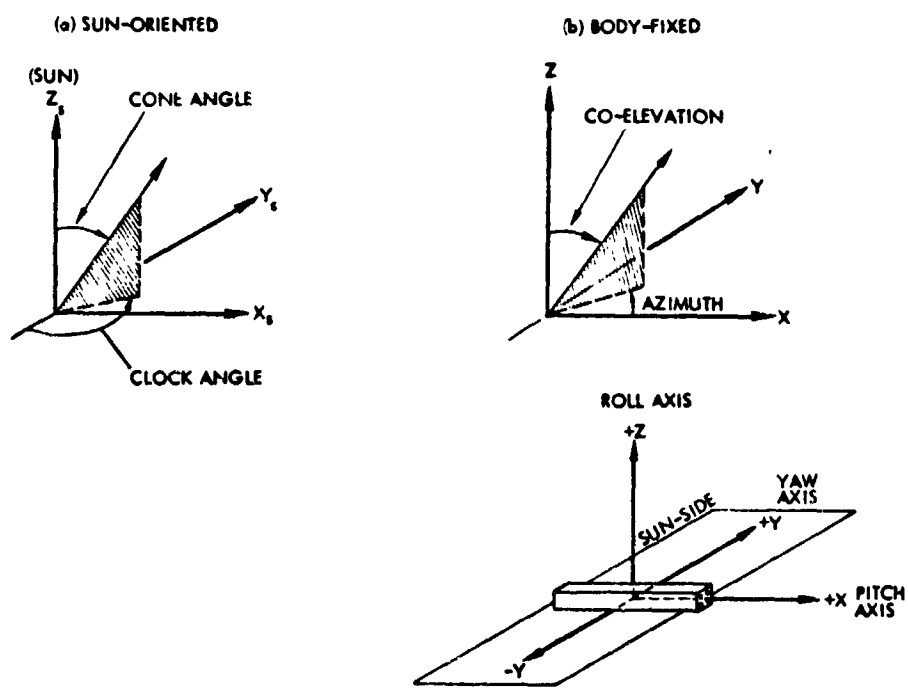

Figure 6-9. Sun-Oriented and Body-Fixed Coordinates

and x_s normal to y_s and z_s. In the nominal attitude the vehicle is aligned with these coordinates such that the solar array is normal to z_s, and the thrust exhaust beam is in the direction of x_s. Pointing angles in this system are denoted as cone and clock angles (see Figure 6-9(a)), in agreement with conventional usage at JPL.

Body-Fixed System. The alternate coordinate system x, y, and z, shown in Figure 6-9(b), adopted from JPL's SEMMS study, is body-fixed, with the x-axis in the direction of the exhaust beam; the z-axis normal to this and to the undeflected solar array; the y-axis being orthogonal to x and y extends along the solar array length axis. Pointing angles in this system are denoted as co-elevation and azimuth in correspondence with the cone and clock angles of the x_s, y_s, z_s system. Azimuth is measured in the x-y plane from the exhaust beam axis, x. The positive sense is clockwise when looking along the z-axis. Figure 6-10 shows the angular transformation between the two systems, as projected onto a unit sphere.

In this section we shall describe orientation and pointing requirements in one or the other coordinate systems as appropriate: generally, the relative motion of a target object is first defined in the sun-oriented reference system in terms of cone and clock angles, then interpreted in body-fixed coordinates, in terms of azimuth and co-elevation as will be illustrated by several examples in the following paragraphs.

6.7.3 Pointing Requirements during the Transfer Phase

The optimal thrust pointing profile during the transfer phase was presented in Section 5 in terms of thrust vector cone and clock angle time histories (see Figure 5-9b). From these characteristics and the relative positions of spacecraft, sun and earth we can derive orientation requirements of the spacecraft center body in sun-oriented coordinates, and solar array and antenna pointing requirements in body-fixed coordinates. These steps are necessary to establish compatibility of the optimal thrust pointing profile with thermal control constraints and with pointing limitations of the solar array, the high-gain antenna and the star seeker.

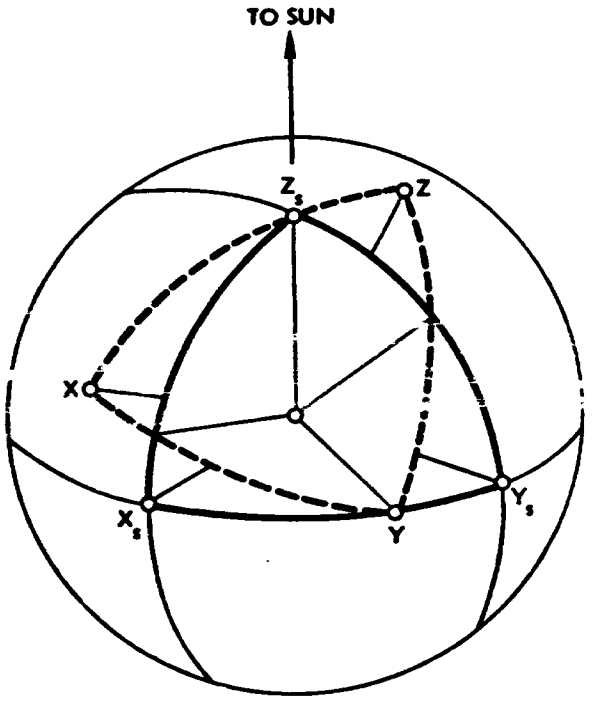

1. SUN (Z_s) ALWAYS IN X, Z, PLANE
2. SOLAR ARRAY BOOM (Y) ALWAYS IN X_s, Y_s PLANE

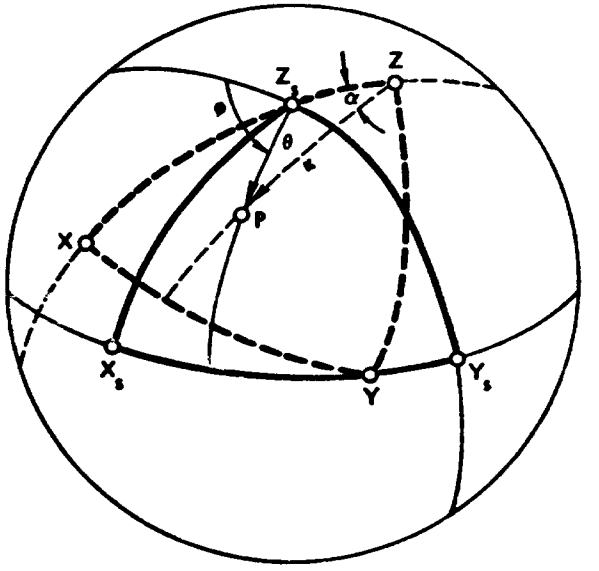

COORDINATES OF AIM POINT P

X_s, Y_s, Z_s SYSTEM: θ - CONE ANGLE
ϕ - CLOCK ANGLE

X, Y, Z, SYSTEM: κ - CO-ELEVATION
α - AZIMUTH

Figure 6-10. Angular Transformation between Sun-Oriented and Body-Fixed Coordinates

Figures 6-11a and b show three-dimensional loci of the spacecraft -x axis (thrust vector) and +z axis in sun-oriented coordinates, x_s, y_s, z_s, plotted on a unit sphere. The coordinate grid inscribed on the sphere consists of circles of constant cone and clock angles. Time from launch is marked along the vector loci. The apparent motion of the earth line-of-sight in this coordinate system is confined (approximately) to the x_s-z_s plane and is indicated by time marks around the periphery (Figure 6-11a). We note that the thrust vector describes a loop that follows roughly a circular arc, starting on the reverse side of the sphere as indicated by the dashed portion of the curve. However, during the major part of the transfer phase the thrust vector points toward the visible northern half of the sphere, as indicated by the solid part of the curve. Since the x_s-y_s plane approximately coincides with the ecliptic plane this thrust profile produces the change in orbit inclination and line-of-nodes that is required to match those of Encke.

The z axis locus shown in Figure 6-11b follows a "figure-eight" pattern around the sun line. To exhibit this pattern more clearly the aspect of the spherical projection has been changed from that used in Figure 6-11a. The y axis orientation can be readily derived from the x axis and z axis loci as function of time.

As a result of the prescribed thrust axis motion and the restriction that the solar array centerline (y axis) be always located in the x_s, y_s plane, we obtain a nearly monotonic and uniform slow rotation of the spacecraft around the sun line, completing roughly one revolution during the transfer phase. This rotation requires that the star reference sensor be rotatable over a wide range of azimuth angles.

By inspection of the z axis locus in Figure 6-11b we can establish whether the rear surface of the spacecraft is exposed to solar illumination at any time during the transfer phase. In our example the positive z axis always stays within the hemisphere centered on the sun line. Thus the spacecraft rear surface is never exposed. (The cone angle margin always exceeds 10 degrees). If the locus had crossed the x_s-y_s plane at any time, a 180-degree spacecraft pitch maneuver around the x axis would be required to return the positive z axis to the sun centered hemisphere while leaving the thrust orientation unchanged.

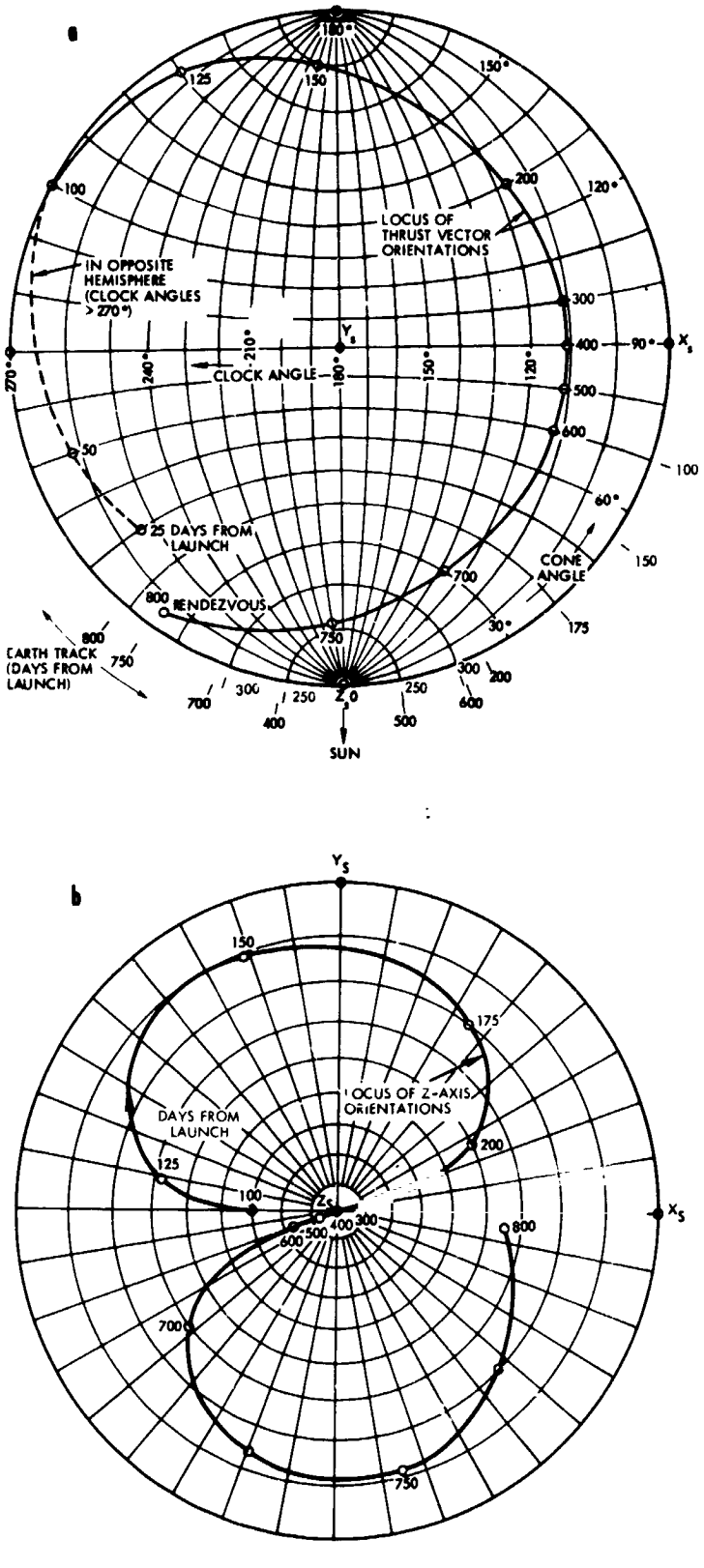

Figure 6-11. Locus of Thrust Vector and z Axis Orientations during Transfer Phase (x_s, y_s, z_s Coordinates)

Figure 6-12 shows the locus of the earth line-of-sight in body-fixed coordinates (x, y, z) derived by transformation from the sun-oriented coordinates used in Figure 6-11.* The dashed portion of this locus corresponds again to points on the reverse side of the unit sphere. Time marks show the time elapsed since launch. The apparent motion of the sun line in this coordinate system is indicated by time marks around the periphery. We note that during two 20-day intervals, first about 160 days, and again about 750 days after launch, the earth and sun lines fall within a zone of 80 ± 10 degrees of co-elevation and within the same quadrants of azimuth. Thus the solar paddles, deflected nearly 90 degrees from the x-y-plane at those times as dictated by the sun's position, could potentially obstruct the high-gain antenna's view of earth. Such a contingency can occur only in one or the other, not both, of these instances depending on antenna placement, configuration and size of its deployment arm, and solar array dimensions (see Section 7.1).

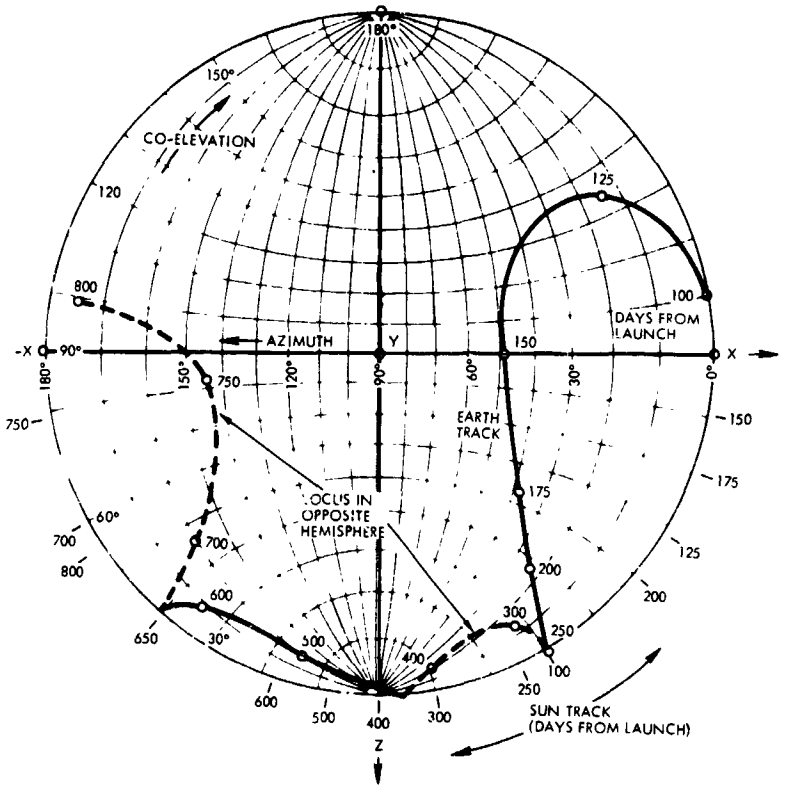

Figure 6-12. Sun and Earth Track in Body-Fixed Coordinates

If the antenna is placed at the spacecraft end designated by the -x-axis, opposite the ion thruster package, the earth view obstruction by the solar array is avoided during the critical rendezvous approach (i.e.,

*This plot was obtained by graphical analysis and is accurate only within about ±3 degrees, which is sufficient for purposes of this discussion.

740-760 days after launch). Furthermore, by using the nominal mission profile with a coast period from 135 to 185 days after launch, the earlier instance of earth view obstruction can also be avoided since the spacecraft orientation program reflected in Figure 6-12 can be temporarily changed to circumvent this condition.

The figure also indicates the times at which the earth and sun lines coincide, or nearly coincide, viz. about 240, 450 and 650 days after launch. Among these three syzygies, the superior conjunction occurring 450 days after launch may cause a temporary communications blackout.

6.7.4 Sensor Pointing Requirements During Coma/Tail Exploration

Figure 6-13 shows a preferred mode of pointing the spacecraft and payload sensors during a typical coma mapping path, and delineates phases during which the various sensors are turned on. The gimballed instrument platform can be scanned over a range of three-dimensional viewing angles that nearly cover 3π steradians. To have an unobstructed view of the nucleus during the first and second legs of the traverse both for scientific observations and navigational fixes, the spacecraft is reoriented so that the payload module points toward the nucleus. Thermal control requirements constrain the center body orientation but within rather wide limits. Reorientation is required during the brief thrust phases that control the coma exploration trajectory and terminal guidance.

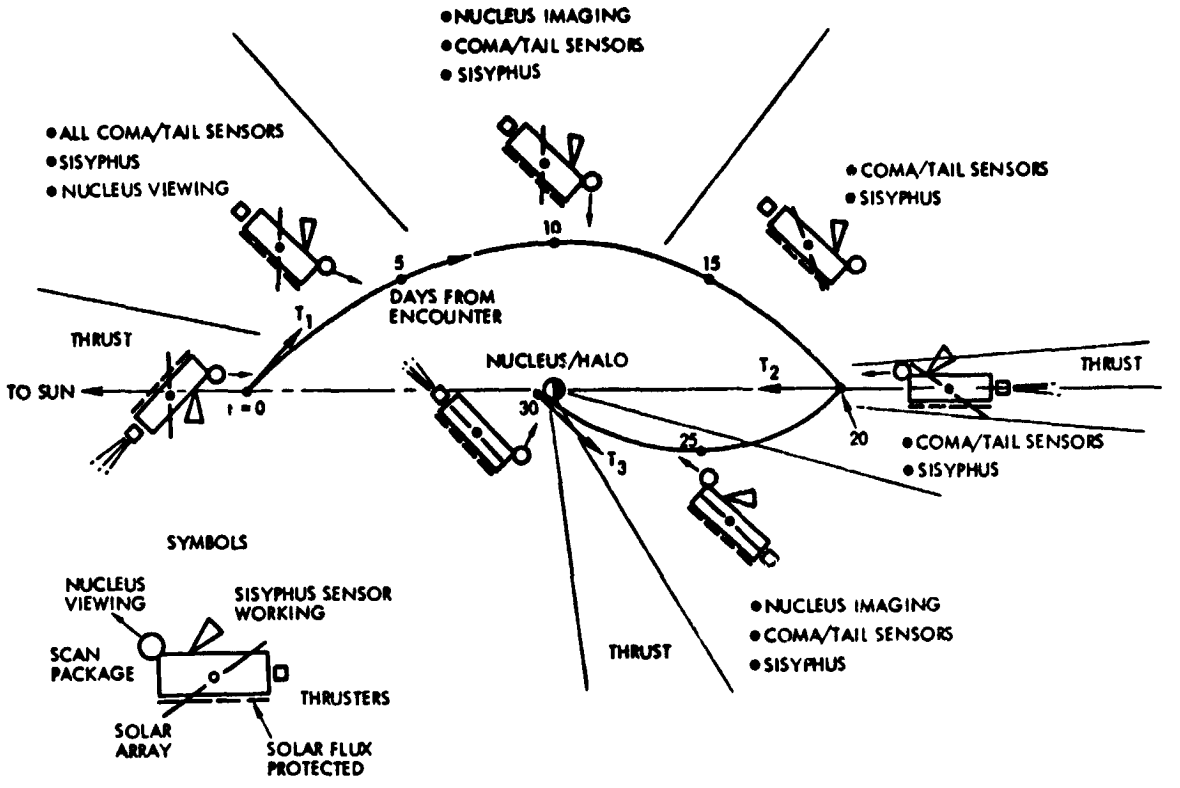

Figure 6-13. Coma Exploration Phases and Orientation Requirements

Figure 6-14 shows the orientation sequences of the scan platform and the high-gain antenna in terms of sun-oriented and body-fixed coordinates; the plots differ by a 45-degree offset during the first and by 135 degrees during the second leg of the exploration path. The motion of the spacecraft, the comet and earth can be assumed as being coplanar for purposes of this analysis, hence only two-dimensional tracks are shown in this diagram. A 180-degree roll maneuver is required between the two cruise phases to avoid sun illumination of the rear surface of the spacecraft.

The short one to two-day thrust phases at the beginning and the end of each leg of the exploration path require additional reorientations (not shown in the diagram) that can be deduced from the indicated thrust vector orientations T_1, T_2 and T_3.

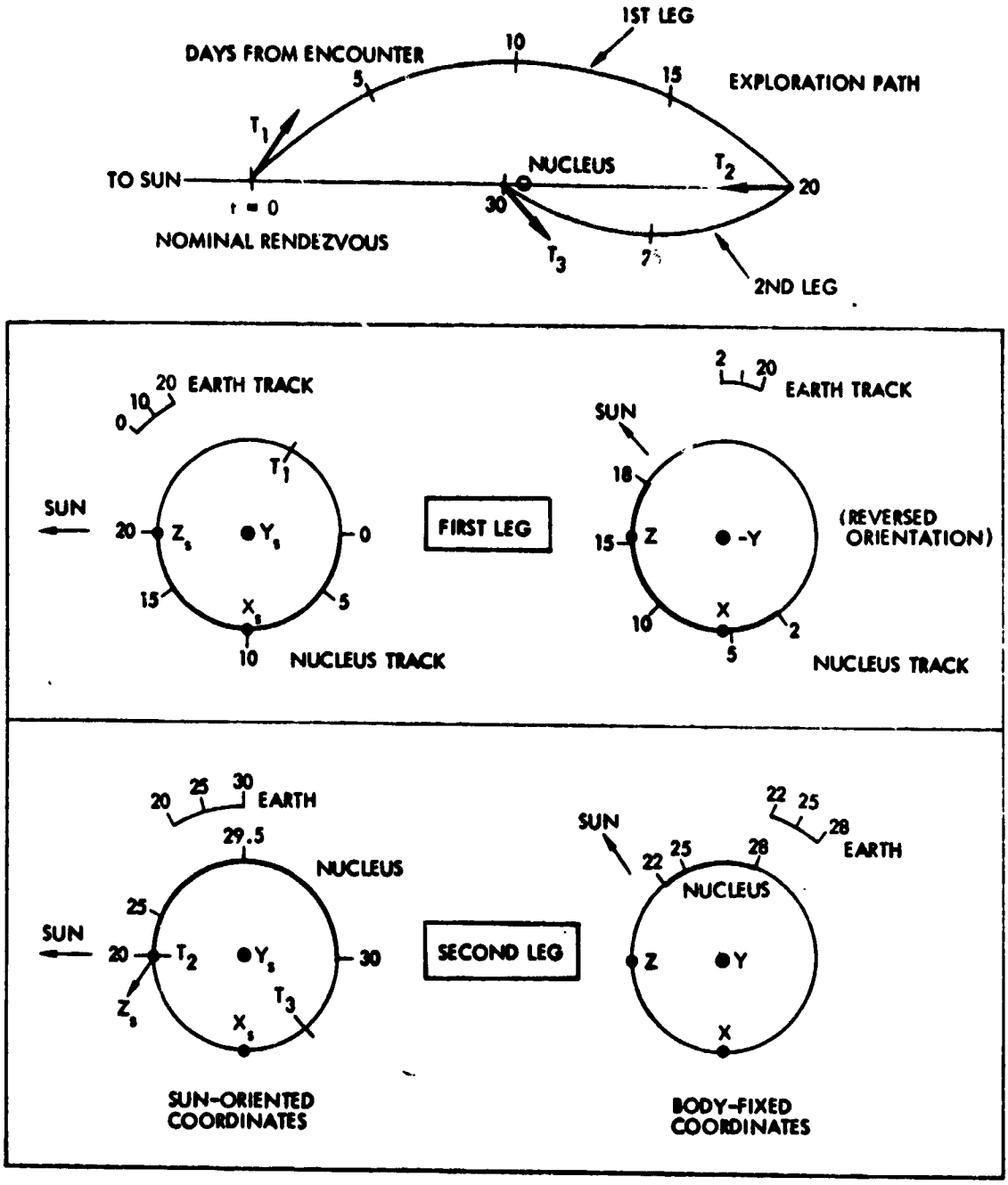

Figure 6-14. Pointing Requirements During Coma Exploration

6.7.5 Pointing Requirements During Nucleus Circumnavigation

As a first option we considered circumnavigation in fixed-body orientation (Figure 6-15) to minimize thermal control problems and frequent attitude maneuvers. The circumnavigation orbit is shown here

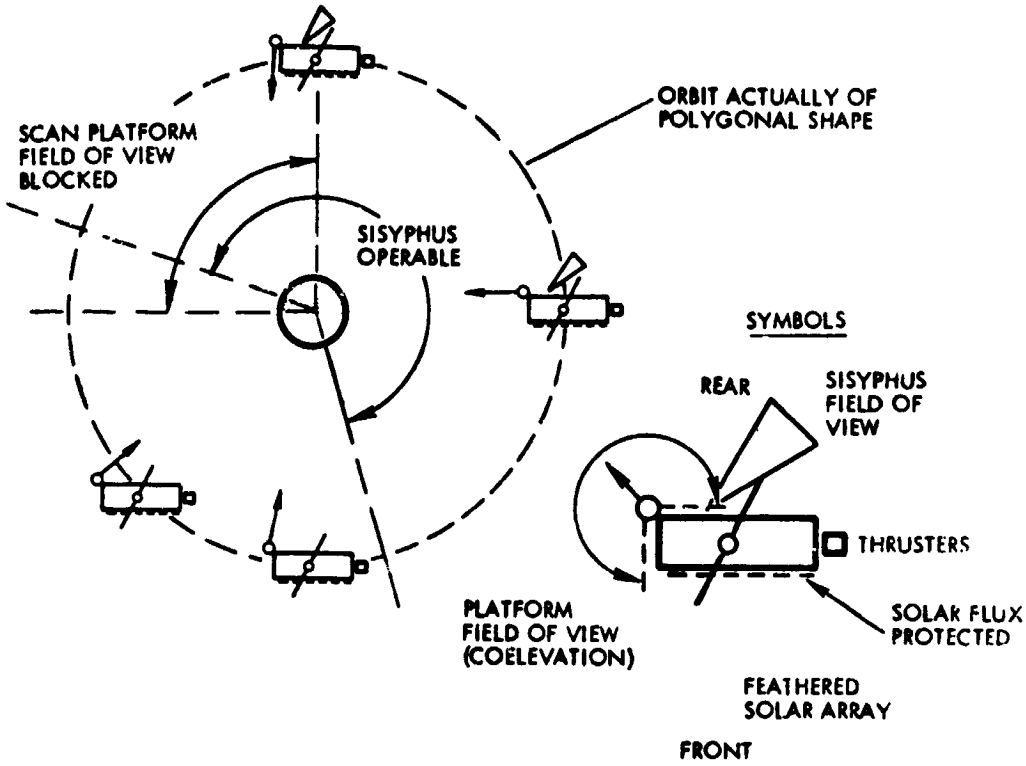

Figure 6-15. Nucleus Observation with Fixed-Body Attitude (Schematic)

schematically as a circle; actually it would be in the shape of a polygon, as previously discussed (Figure 6-6). Orbiting in a fixed-body attitude is compatible with the use of hydrazine thrust at the "corner points." The use of SEP thrust would require radial pointing of the vehicle at each turn in the orbital pattern.

This operating mode limits observation by scan platform-mounted sensors as shown in the diagram. A cone angle range of about 270 degrees is desired for acceptable nucleus viewing during 3/4 of the "orbit." The body-mounted Sisyphus particle detector is oriented at a 135-degree co-elevation and 0-degree azimuth and can operate over about 2/3 of each orbit without interference of stray light from the nucleus.

As an alternate option we also considered a continuous slow revolution of the spacecraft about the z axis which would allow intermittent radial thrusting at the corner points of the orbit without discrete reorientation maneuvers (see Section 6.6.2). In this mode the scan platform can point at the nucleus either continuously or intermittently in a time-shared mode as desired. Since the earth line-of-sight describes a cone relative

to the body coordinates, i.e., around the axis of revolution z, this nucleus viewing mode requires continuous reorientation of the antenna if the z axis is oriented to the sun. Earth cone angles of 50 and 150 degrees correspond to nucleus circumnavigation dates 30 days before and 10 days after perihelion, respectively. As an alternative, the spin axis can be pointed at earth to avoid continuous antenna reorientation. This means that the sun line would move in a conical pattern which is acceptable as long as the cone angle does not exceed 60 or 70 degrees, i.e., until about 15 days before perihelion passage.

6.8 OTHER SCIENTIFIC EXPLORATION OBJECTIVES AND OPTIONS

6.8.1 Cruise Phase Science

During the transfer phase the spacecraft penetrates the asteroid belt entering at a heliocentric latitude of 1.5 degrees and emerging 477 days later at a latitude of 7.9 degrees. The spacecraft traverses the asteroid belt at distances between 0.05 AU and 0.28 AU from the ecliptic plane. Some observers have placed the asteroid dust belt within a distance of 0.1 AU on both sides of the ecliptic. This would correspond to ±2 degrees of heliocentric latitude at the radius of greatest asteroid density, 2.8 AU from the sun. The Encke spacecraft, being the first vehicle to traverse the asteroid belt substantially off the ecliptic plane, can be used advantageously to map meteoroid distribution as a function of radial as well as out-of-ecliptic distance. The long exposure (447 days between entry and exit at 2 AU) provides enough time for statistically significant sampling in the different zones.

Figure 6-16 schematically illustrates the three-dimensional transfer trajectory and its penetration of the asteroid belt. During the initial passage the spacecraft crosses the asteroid belt "above" the ecliptic plane, i.e., at northern latitudes. During the extended mission phase the spacecraft follows Encke toward aphelion and crosses the asteroid belt for a second time, this time below the ecliptic plane.

An interesting objective of meteoroid detection and classification would be a sampling of different Taurid meteoroid streams. Since the Taurids are presumed to have originated from comet Encke this would

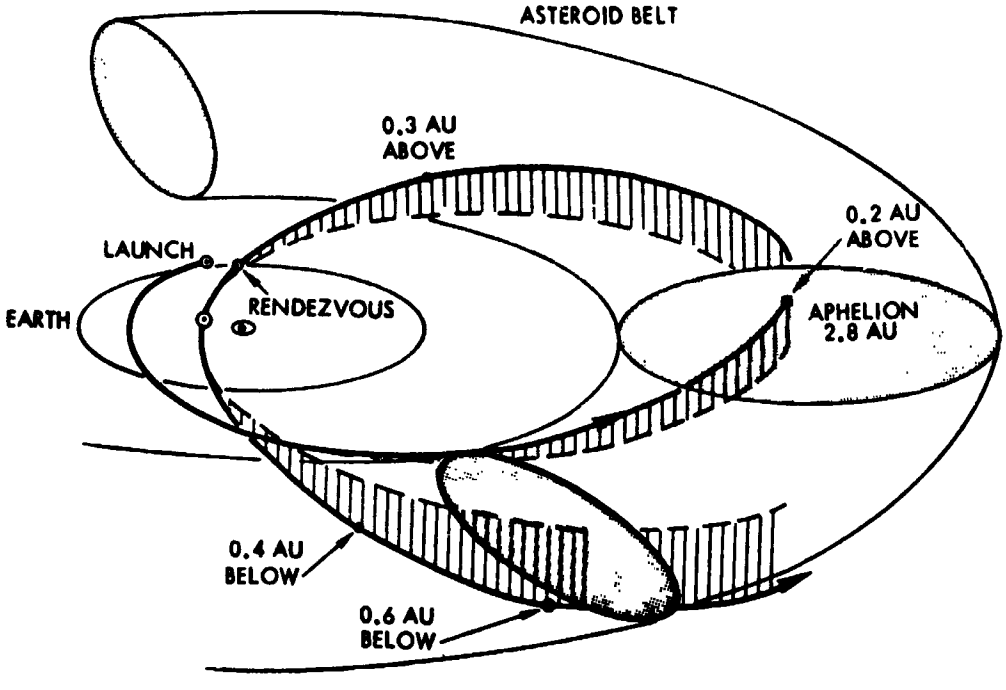

Figure 6-16. Asteroid Belt Penetration During Mission

give the possibility of gathering data on the flux density and orbit parameters of this material as well as its chemical composition. At the high expected encounter velocities (15-30 km/sec) an impact mass spectrometer could operate effectively while it would be useless at the low velocities prevailing during the comet rendezvous.

Appendix C discusses meteoroid detection during the cruise phase and concludes that, considering the small size of practical impact sensors, the frequency of encounter is quite low (low enough to eliminate serious concern about survival). From these data it appears not sufficiently justified to include impact sensors such as TRW's cosmic dust analyzer (impact ionization mass spectrometer) or NASA-GSFC's momentum and velocity sensor in the fundamental payload.

The optical meteoroid sensor (Sisyphus) with its large effective cross-sectional area (250,000 m^2 at a range of 1 km) has dual applicability during transit and encounter and is therefore included in the basic payload complement. Pointing requirements for this body-fixed instrument were obtained based on predicted encounter angles of asteroidal and cometary particles. A compromise orientation of zero degree

azimuth and 135 degrees co-elevation was adopted that would be effective during a large fraction of the total mission time.

Figure 6-17 shows an orbital plot of seven regularly observed Taurid streams and of comet Encke, projected into the ecliptic plane.

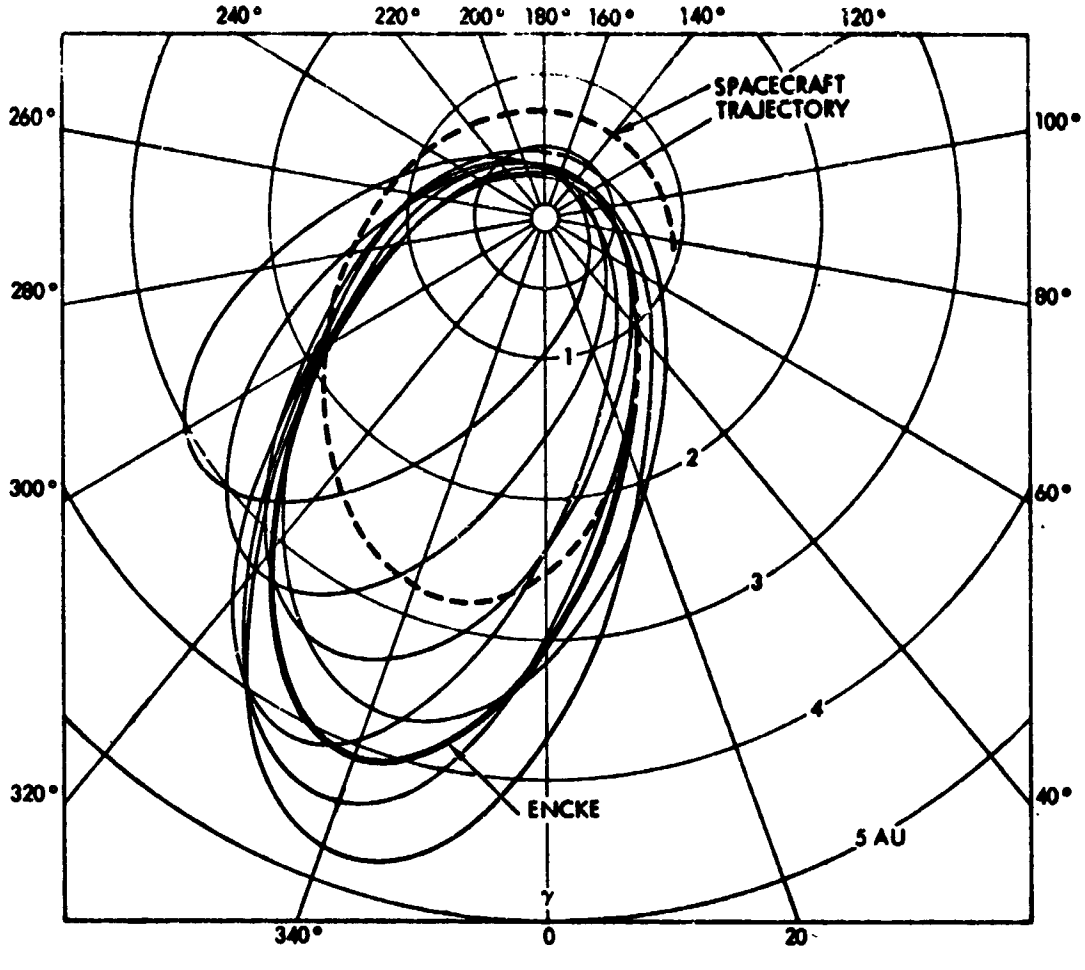

Figure 6-17. Taurid Streams Encountered by Spacecraft on Way to Encke Rendezvous (Projected into Ecliptic)

The Taurids have orbit inclinations between two and eight degrees, aphelion distances from 3.1 to 4.8 AU and their orbital axes vary in orientation by about 40 degrees, with the longitudes of perihelion generally smaller than Encke's. It may be argued that the Taurid streams exhibit orbit characteristics of earlier phases of Encke's

evolution, since major perturbations of the comet do not affect an entire stream of small particles in the same manner. Thus a detection of Taurid orbital characteristics during transit encounters (especially of streams that cannot be observed from earth) will be of potentially great scientific interest. The Sisyphus detector is designed to differentiate orbit parameters sufficiently well to serve this objective.

Figure 6-17 shows that the Encke spacecraft is likely to cross outbound trajectories of Taurids early in the mission and inbound trajectories after passing aphelion and on approaching the rendezvous point. Since the out-of-plane aspects of the trajectories shown were ignored, this prediction is only qualitative. More detailed analysis would be required to substantiate this point.

6.8.2 Asteroid Flyby Options

The long tour through the asteroid belt offers the interesting possibility of visiting one or several known asteroids as a secondary mission objective. The payload designed for comet nucleus observation is suitable for asteroid observations, particularly if the flyby is at close range. Such options are being considered with growing interest by the scientific community and have been recently investigated by R. Bourke and D. Bender of JPL (Reference 6-3) and by D. Brooks of NASA/Langley.* The extended dwell time in the asteroid belt, the flexible choice of transfer trajectories, and the modest propulsion effort required for large excursions from a given nominal trajectory make the multiple target mission concept feasible without appreciable propellant penalty, e.g., only five percent extra propellant in a typical case investigated by Bourke and Bender.

A computer search for conveniently located flyby targets was performed. Table 6-3 lists several asteroids that are within less than 30×10^6 km of the nominal 800-day 1984 Encke rendezvous trajectory. Massalia is among the 20 largest asteroids with an absolute magnitude of 7.38.

*Unpublished notes

Table 6-3. Closest Approach of Nominal 800-Day Trajectory to Some Known Asteroids

Asteroid		Time (Days)	Miss (10^6 km)
No.	Name		
20	Massalia	460	26
111	Ate	690	18
123	Brunhild	520	14
352	Gisela	320	16

6.8.3 Deployable Lander and Solar Wind Monitor Probes

The concept of carrying a deployable nucleus lander probe or a solar wind monitor has considerable appeal from a standpoint of enhancing the scientific yield of a comet rendezvous mission. However, as mentioned before the overriding goals of simplicity and cost economy rule out any plan for carrying such a probe at present. We therefore limit the discussion to pointing out some implementation and delivery concepts.

The lander probe can be deposited from low altitude and would impact the nucleus at small velocity (1.2 m/sec ≃ velocity of escape) if allowed to descent by free fall. This reduces the tendency to bounce off and makes "hard landing" a practical possibility. A key to feasibility is the provision of an anchoring mechanism that can operate reliably in a wide variety of soils.

The probe would undoubtedly use the parent spacecraft as a communications relay. Hovering at an altitude of 5 to 10 km would serve this objective better than circumnavigation because contact periods are more frequently repeated in the former case depending on the expected length of survival of the probe after touchdown.

The second deployable probe concept is keyed to the objective of determining the correlation between solar wind "input" phenomena and events in the coma and tail that respond to these inputs. A reasonably simple spin-stabilized particles and fields probe such as the small P and F lunar orbiter (35 kg) carried by Apollo, or a Pioneer 6-9 type

vehicle of larger size would meet the scientific objectives of solar wind sensing. Ejected from the parent vehicle either on approach to rendezvous or after entering the coma, the monitor probe would travel radially inward, gaining a forward circumferential component in time due the Coriolis effect and solar differential gravity. At a separation velocity of only 10 m/sec the probe will cover a distance of the order of 10^6 km in about 100 days, sufficiently large to sample the solar wind phenomena unaffected by interaction with the coma, but not so large as to miss the correlation effect in a given sector of the solar wind.

Communication to earth via relay link can be readily achieved by a rotational fan beam like Pioneer's. This beam would be aligned with the common orbital plane of the probe and the parent spacecraft to avoid probe reorientation requirements.

Our SEP spacecraft design does not include a provision for carrying a daughter probe. However, it has sufficient mounting space and enough payload capacity if flown at a long trip time to accommodate a 50 kg or even 100 kg deployable probe. This option is available in case mission plans should be broadened to include such a probe.

6.9 MISSION PROFILE SUMMARY

The preferred nominal mission sequence is summarized in Table 6-4. Figure 6-18 illustrates this mission profile and shows the positions and times of key events. These results are to be interpreted as tentative based on the tradeoffs performed in this and the preceding section and on the scientific rationale developed in Sections 2 and 3. Formulation of a more detailed mission profile will be governed by the definition of the system and subsystem design and detailed operational modes of attitude control, navigation, electric propulsion, command and telemetry, ground system operations and by the design and operational constraints of the payload instruments.

The nominal sequence includes the preferred short transfer (800 days), arrival at the comet 40 days before perihelion, a nominal exploration phase of 80 days, plus an extended exploration phase of several hundred days with maneuvers in and out of the comet envelope.

Table 6-4. Summary of Flight Sequence

Event	Time (Days except as noted)
1. Launch	L
2. Deploy solar array and appendages	L + 2 hours
3. Acquire sun and star references	L + 3 hours
4. Initiate SEP thrust phase	L + 12 hours
5. Intermittent coast periods to refine navigation accuracy	-
6. Reduce housekeeping power drain near aphelion	L + 450
7. Resume normal housekeeping and telemetry operations	L + 550
8. Comet recovery at earth	L + 700 ± 30
9. Update targeting based on new comet tracking data	L + 710 ± 30
10. Acquire comet by onboard optical system	L + 790
11. Correct terminal approach trajectory as required	L + 795
12. Arrive at comet with 50,000 km offset, on sun side	R = L + 800 = P - 40
13. Hold position and observe comet at offset point	R to R + 1
14. Start coma/tail excursion on earth command	R + 1 to R + 30
15. Arrive near nucleus	About P + 30 = P - 10
16. Circumnavigate nucleus or hover	R + 30 to 50
17. Extended survey	R + 50 to 80
18. End nominal mission, start extended mission	R + 80
19. Stationkeeping and excursions on earth command	R + 80 to 200-300

L = Launch; R = Rendezvous; P = Perihelion

FOLDOUT FRAME 1

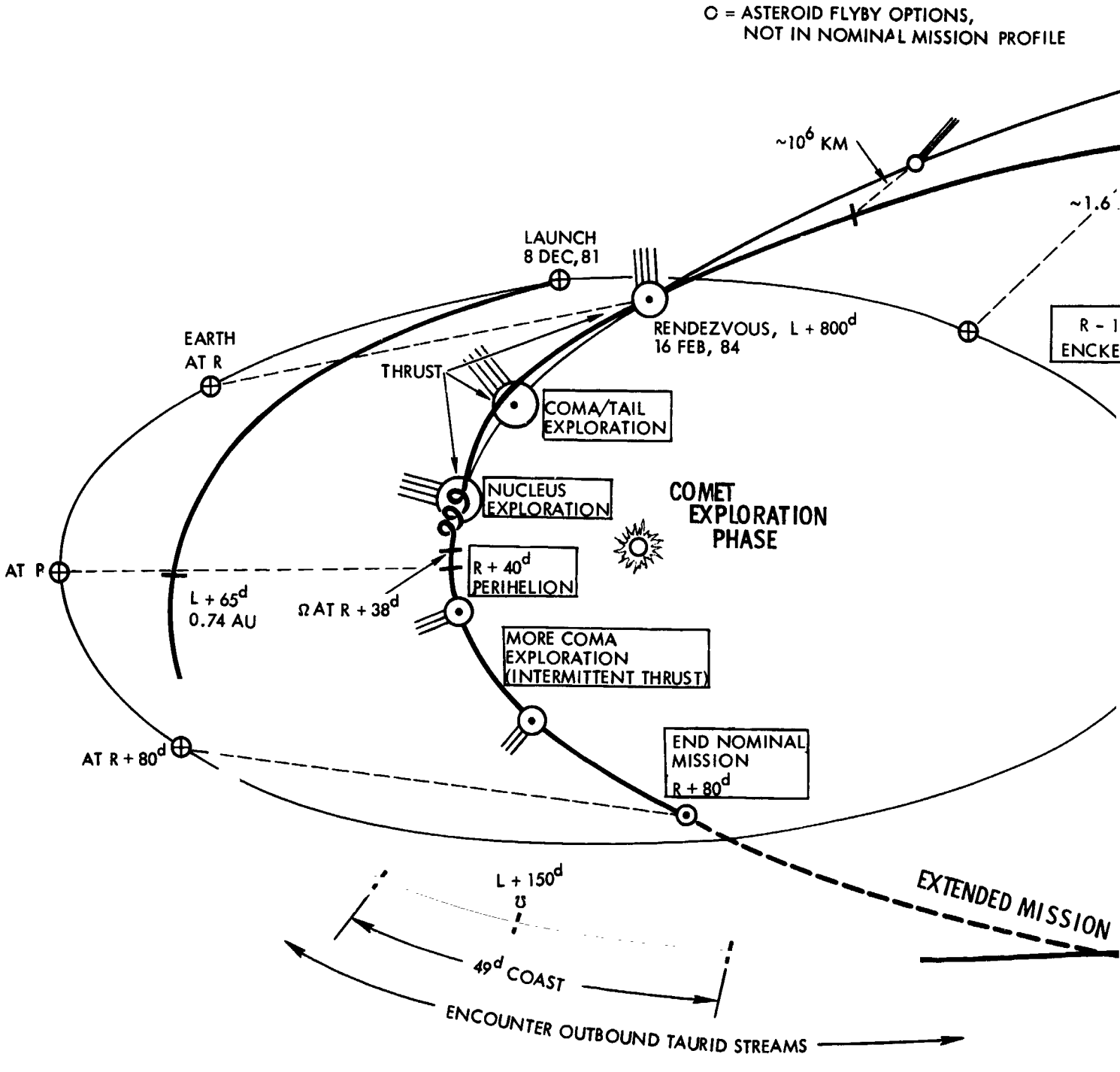

FOLDOUT FRAME 2

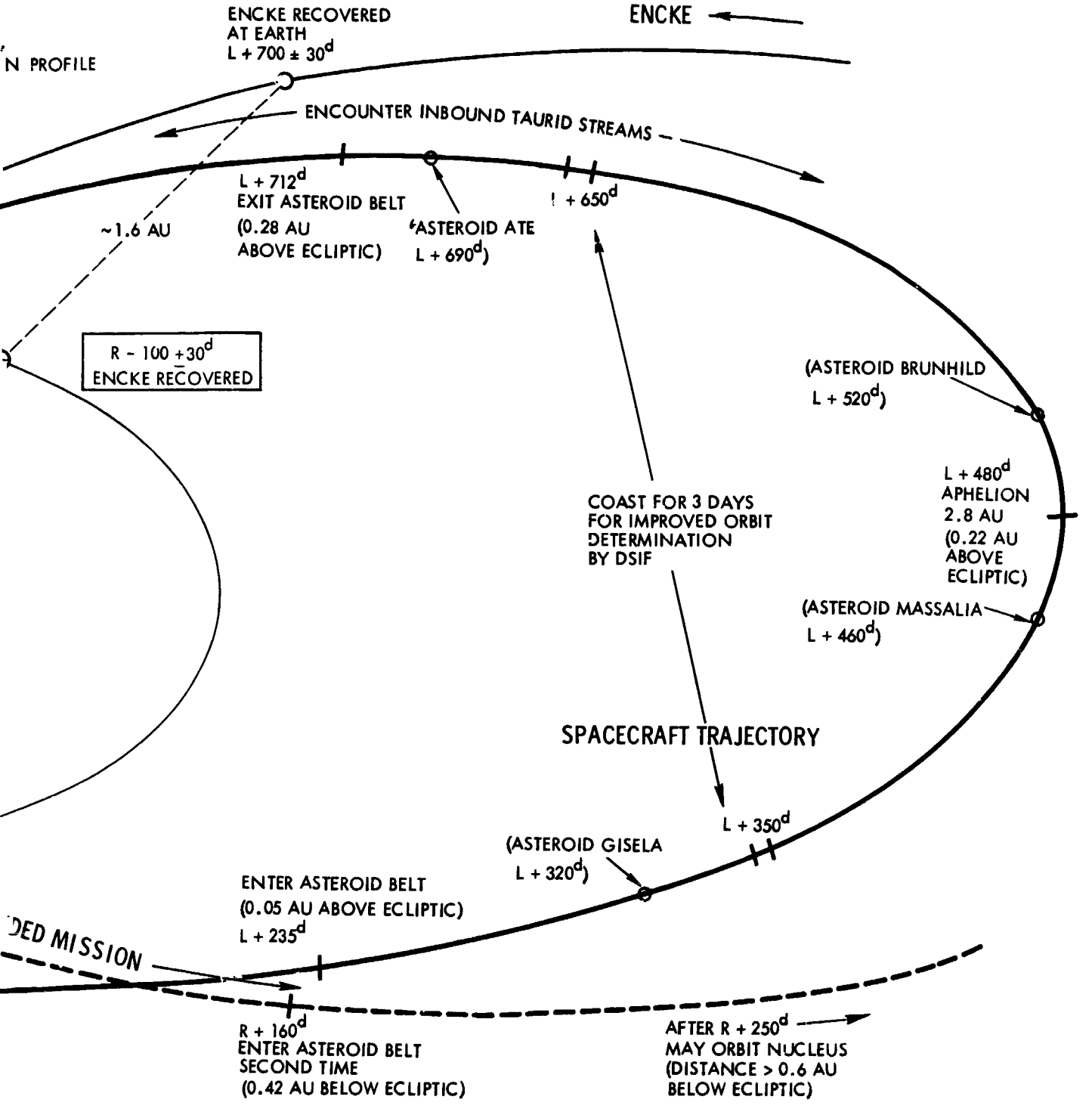

Figure 6-18. Mission Profile Schematic

Since the spacecraft must be designed to survive perihelion passage as well as solar distances above 2 AU in any case the extended mission life of several hundred days places no major design constraint on the spacecraft. This provides a significant additional yield of scientific data yet requires only modest extra propellant expenditures, typically 5 to 10 kg.

Table 6-5 lists various mission profile alternatives and/or departures from the nominal mission concept that have been studied in the

Table 6-5. Summary of Mission Profile Alternatives

Legend: P – positive (desirable); N – negative (undesirable) implication of change

CHANGE FROM NOMINAL MISSION PROFILE	EFFECT ON SCIENTIFIC OBJECTIVES OR YIELD		EFFECT ON COST, COMPLEXITY AND PLANNING		COMMENTS AND RECOMMENDATIONS
LATE ARRIVAL AT COMET (20 TO 30 DAYS)	P	MORE PAYLOAD CAPACITY			UNDESIRABLE BECAUSE OF LOWER SCIENTIFIC YIELD
	N	OBSERVATION TIME LOSS			
LONGER FLIGHT TIME (200 TO 300 DAYS)	P	MORE PAYLOAD CAPACITY	P	SAVES SEP POWER	UNDESIRABLE IN SPITE OF PERFORMANCE ADVANTAGES
			N	REDUCED RELIABILITY	
	N	DIFFICULT TO ADAPT PAYLOAD AS RESULT OF 1980 MISSION	N	DIFFICULT TO USE 1980 MISSION DATA	
INITIAL RENDEZVOUS AT NUCLEUS	P	INCREASED OPPORTUNITY FOR NUCLEUS/HALO OBSERVATIONS	N	GREATER HAZARD	NOT RECOMMENDED BECAUSE OF POTENTIAL HAZARD
			N	POTENTIALLY MORE DIFFICULT NAVIGATION TASK	
	N	LOSS OF SOME COVERAGE IN ACTIVE PHASE			
MINIMUM MANEUVERING WHEN CLOSE TO PERIHELION (20 TO 40 DAYS)	N	REDUCED SCIENTIFIC COVERAGE	P	ALLEVIATES THERMAL CONTROL PROBLEM	UNCONSTRAINED EXPLORATION PREFERRED. CAN ACCEPT THIS MODE AS BACKUP.
USE THERMAL PROTECTION BY NUCLEUS PENUMBRA (20 TO 40 DAYS)	N	SHARPLY REDUCED SCIENTIFIC COVERAGE	P	GREATLY REDUCED THERMAL LOAD	USE AS EMERGENCY MODE ONLY
			N	REQUIRES COMPLEX STATIONKEEPING	
OUT-OF-PLANE MANEUVERS ADDED TO COMA/TAIL SURVEY	P	MAY DETECT ASYMMETRY OF PHENOMENA	N	COSTLIER MANEUVERS IF FULL BENEFIT IN SCIENTIFIC COVERAGE IS TO BE GAINED	MAY BE INCLUDED AS SECONDARY GOAL AFTER INITIAL COMA AND NUCLEUS COVERAGE
EXTENDED DEPTH OF TAIL PENETRATION (10^5 KM OR MORE)	P	POTENTIALLY MAJOR INCREASE IN SCIENTIFIC YIELD (IF TAIL IS ACTIVE)	N	MAJOR INCREASE IN PROPELLANT CONSUMPTION IF TIME MUST BE CONSERVED	KEEP MISSION PLANS FLEXIBLE; EXECUTE AS CONDITIONS WARRANT
	N	REDUCES TIME FOR NUCLEUS OBSERVATION			
REPEATED COMET EXIT AND REENTRY	P	COVERS PHENOMENA IN TRANSITION ZONE	N	ADDITIONAL PROPELLANT AND TIME EXPENDITURE	MAY BE INCLUDED AS SECONDARY MISSION GOAL; EXECUTE AS CONDITIONS WARRANT
	N	MAY REDUCE NUCLEUS OBSERVATION TIME			
ASTEROID FLYBY(S) DURING TRANSFER PHASE	P	GREATLY INCREASED SCIENTIFIC YIELD OF MISSION	N	ADDED LAUNCH CONSTRAINT	RECOMMENDED AS SECONDARY MISSION GOAL IF MAIN GOAL NOT JEOPARDIZED BY IT
			N	ADDED MANEUVER REQUIREMENTS	
			N	MORE COMPLEX MISSION SEQUENCE	

foregoing analysis. Desirable and undesirable aspects of these changes are summarized and comments and recommendations are given in the last column. The outstanding characteristic of this rendezvous mission is its adaptability to late program plan entries and to desired changes in the mission profile and exploration sequence as warranted by the unforeseeable conditions that the spacecraft will find at the comet. This is largely due to the maneuver flexibility of the electric propulsion system, and the noncritical encounter conditions inherent in the rendezvous mode.

REFERENCES, SECTION 6

6-1 J. D. Anderson, "Feasibility of Determining the Mass of an Asteroid from a Spacecraft Flyby," IAU Asteroid Colloquium, Tucson, Ariz., March 8-10, 1971.

6-2 R. L. Forward, "Asteroid Mass Distribution Measurement with Gravity Gradiometers, "IAU Asteroid Colloquium, Tucson, Ariz., March 8-10, 1971.

6-3 D. F. Bender and R. G. Bourke, "Multi-Asteroid Comet Missions Using Solar Electric Propulsion," presented at AIAA 9th Electric Propulsion Conference, Bethesda, Md., April 17-19, 1972.

7. SPACECRAFT DESIGN CONCEPT

7.1 TYPICAL SPACECRAFT CONFIGURATION

A representative spacecraft configuration with design features required for the Encke rendezvous mission was adapted from several earlier solar-electric spacecraft studies. These sources include JPL's SEMMS Study (Reference 7-1), TRW's multi-mission spacecraft studies (References 7-2 and 7-3), and similar studies by North American Rockwell (Reference 7-4). The selection was guided by criteria such as efficient thrust operation during all mission phases, convenient payload instrument pointing modes for comet exploration, simplicity and cost economy.

Figure 7-1 shows the spacecraft in the cruise configuration. Figure 7-2 shows additional design detail, with the spacecraft in stowed configuration mounted on the Centaur upper stage. The 3.05-m (10 feet) Intelsat nose fairing with an extended cylindrical section provides ample stowage volume.

The vehicle consists of a flat oblong center body and two boom-deployed solar arrays. The center body is separated into two modules: the electric propulsion module with an articulated array of six mercury ion thrusters, power processors, propellant storage and feed system; and the equipment/payload module mounted below the propulsion module on the spacecraft adapter. The two modules are separated by a field joint for ease of assembly, handling and testing. The entire structure consists of open trusswork which for the large overall dimensions of the center body (about 4 x2 x 1 meters) offers weight advantages compared to a semi-monocoque box structure. Four longerons carry the main structural load to mounting points on the adapter. A 1.82-meter (6-foot) diameter high-gain antenna is mounted on a deployment arm that is hinged to the bottom of the equipment module. This biaxially rotatable antenna is stowed against the vehicle body during launch. After deployment it can be pointed in all directions in front and rear of the center body for an unobstructed view of earth.

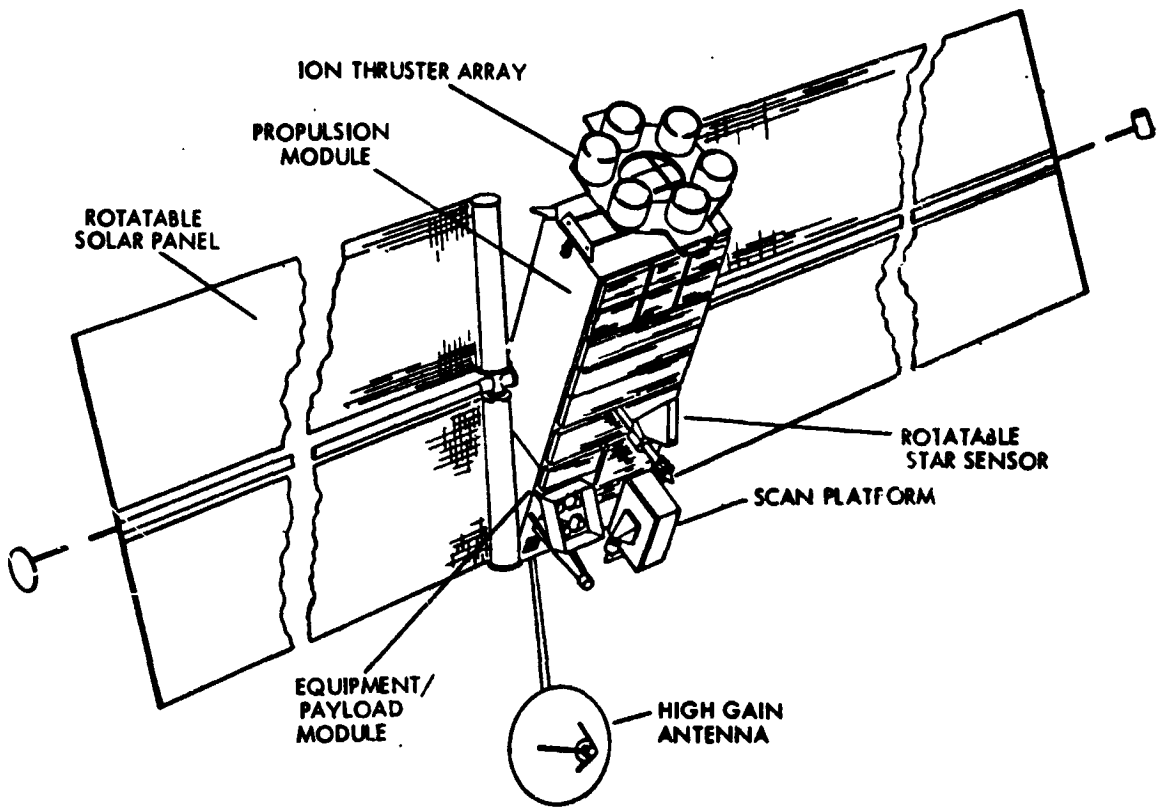

Figure 7-1. Spacecraft in Cruise Configuration

The vehicle is three-axis stabilized using the sun and a selected reference star as celestial references. Three-axis stabilization is the most effective means of providing thrust vector, solar array, high-gain antenna, and payload instrument pointing in all mission phases. Attitude control functions are performed during thrust periods by the articulated ion engines and during coast periods by hydrazine thrusters. The hydrazine thrusters are also used during the electric thrust phase (a) to control large attitude excursions and (b) to provide third-axis control capability when only one ion thruster is operating.

For small but rapid trajectory control maneuvers that are required when operating close to the comet nucleus (see Section 5.4.4), the vehicle's electric thrust capability is augmented by attitude control thrusters which at a nominal 2-pound (9-Newton) thrust level are adequate for this purpose. Use of the hydrazine system in the dual mode of attitude control and trajectory control saves the cost and weight of an additional chemical propulsion system.

OUT FRAME

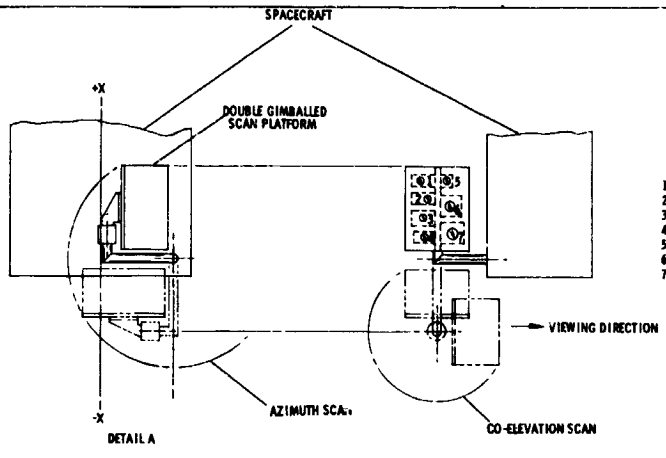

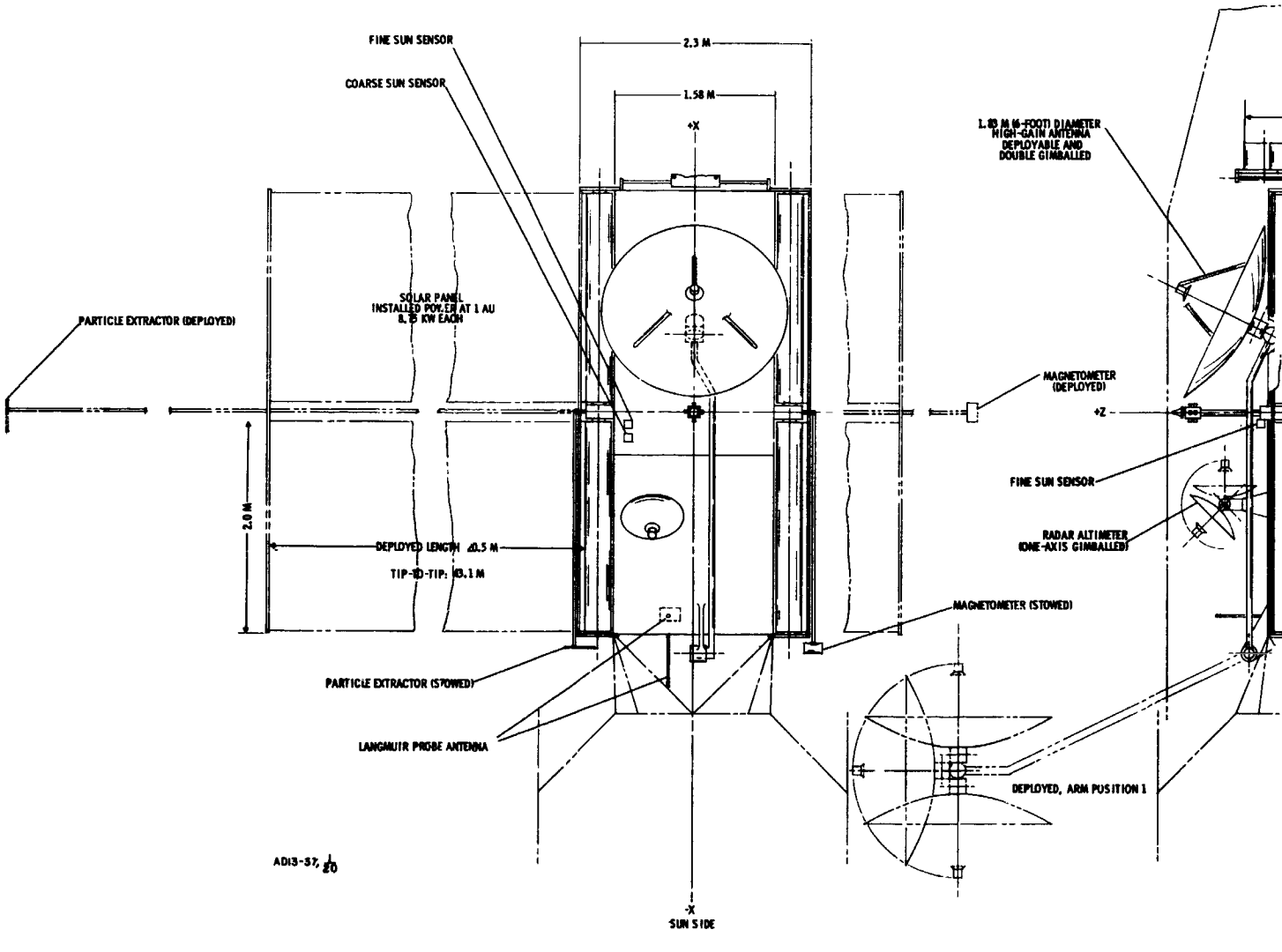

ADI3-37, 1/20

FOLDOUT FRAME 2

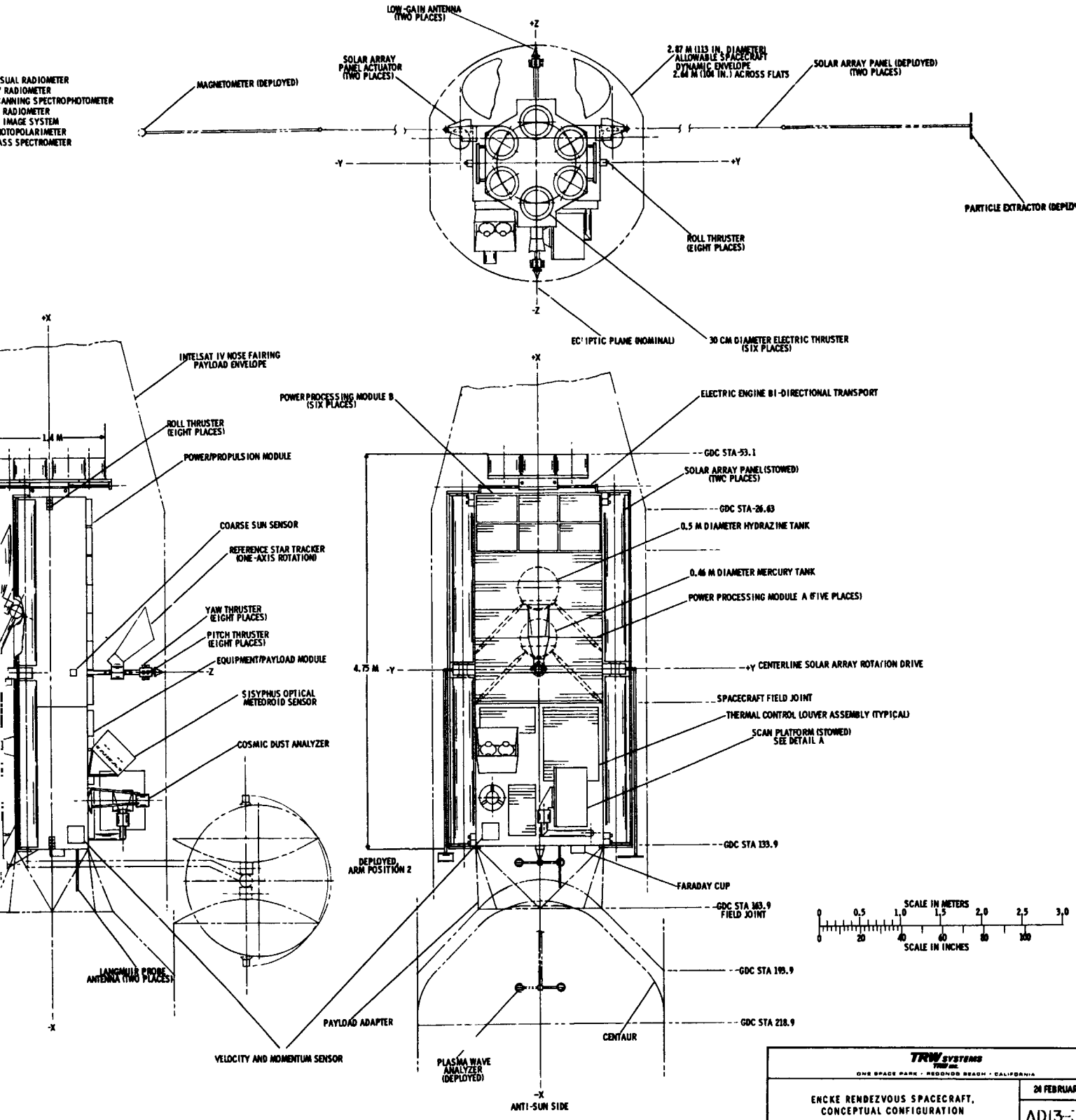

Figure 7-2. Spacecraft Configur
Stowed and Deployed

PRECEDING PAGE BLANK NOT FILMED

The two solar arrays use the rollout deployment principle developed by General Electric under JPL contract. A single boom serves as deployment actuator and support structure for each panel. Partial solar array retraction is desirable during the comet exploration phase. The General Electric solar array was designed for such a requirement. As an alternative to the rollout array configuration an accordion-folded array concept developed by TRW and Lockheed was also considered which would have the advantage of lower specific mass, simpler mechanization and greater panel stiffness. However, because of the more extensive development and test experience of the rollout array model accumulated to date, including a successful flight demonstration performed in 1971 with a similar model built by Hughes Aircraft, we have selected this design for our conceptual spacecraft configuration.

The solar arrays with a deployed length of 20.5 m by 4.2 m width for each panel have a total cell mounting area of 163 m^2 and generate 17.5-kw of gross power at earth departure. This includes an initial margin of 4.5-kw for solar array degradation and housekeeping power. The nominal net propulsion power at the power processor input terminals is 13 kw.

The solar array panels can be rotated up to ±90 degrees from an orientation parallel to the center body to permit optimal thrust vector pointing relative to the sun line; unconstrained terminal guidance and other maneuvers in the vicinity of the target, and controlled sun exposure at solar distances below 0.68 AU. Out-of-plane thrust vector pointing is achieved by rotating the entire vehicle around the sun line. Such roll maneuvers are facilitated by the one-axis rotatable star seeker mounted on the rear side of the vehicle. Rotation of the star seeker also permits selection and tracking of reference stars that are not obstructed by the solar panels.

The equipment and payload module houses the engineering subsystems, the scientific payload instruments and associated electronics. Several body-mounted, boom-deployed and articulated sensors are shown in the configuration drawing mainly to illustrate probable placement and field of view allocations. Not all of these, e.g., the impact

ionization cosmic dust analyzer and the impact velocity and momentum sensor, are included in the basic payload complement discussed in Section 4. The Sisyphus optical micrometeoroid sensor is mounted at an oblique angle, nominally pointing 45 degrees from the anti-solar line, as a best compromise for dust particle detection during the transit and comet exploration phases.

A double-gimballed scan platform attached to one corner of the payload module carries the TV image system and other optical sensors and spectrometers. This platform can be scanned over a wide range of azimuths and co-elevations without field-of-view obstruction, as illustrated schematically in Figure 7-3. Nearly all of the vehicle's rear hemisphere and half of its front hemisphere can thus be scanned readily by the platform sensors. This is facilitated by the choice of attachment point location and gimbal arrangement. Re-orientation of the center body by a 45-degree cone angle from its nominal attitude normal to the sun, has the advantage of allowing the scan platform to cover its full 3π steradian scan capability with minimum stray sunlight interference as was illustrated in Figure 6-13. The cone angles scanned by the sensors range from 45 to 180 degrees in this spacecraft pointing mode.

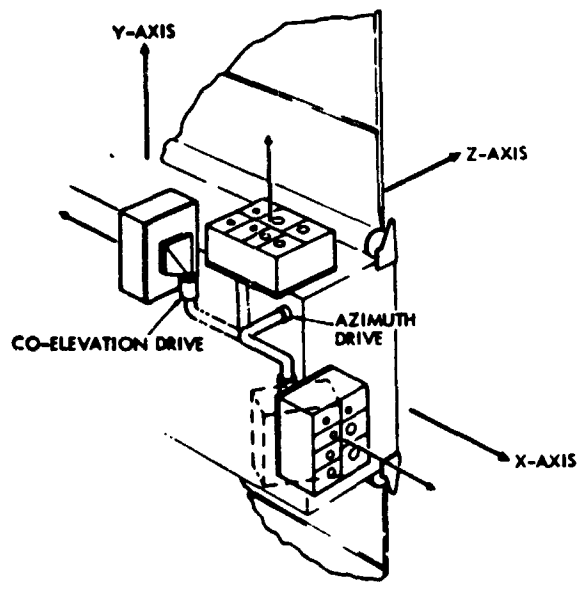

Figure 7-3. Scan Platform Articulation

A one-axis gimballed altimeter radar antenna of 2-ft diameter, required to support nucleus gravity measurements is shown on the front side of the spacecraft body. This location is selected because of the relative positions of earth, spacecraft and nucleus at the preferred time of close approach to the nucleus. This antenna can also serve as an auxiliary medium-gain backup antenna in the event of a main antenna gimbal malfunction.

7.2 PROPULSION AND POWER SUBSYSTEM

7.2.1 Power Subsystem

The required propulsion power of 13 kw at 1 AU (see Section 5) dictates the size of the solar array. In addition a sufficient power margin is needed initially to compensate for solar array degradation and harness losses, and for housekeeping power. Table 7-1 gives a summary of estimated power allocations which shows that under reasonably conservative assumptions a total installed solar array power of 17.5 kw at 1 AU is required for this mission.

Table 7-1. Summary of Estimated Power Allocations (kw)

Gross solar array power at 1 AU	17.5
Solar array degradation and losses, 19 percent	3.3
Housekeeping power reserve (provides minimum of 200 W at 2.8 AU aphelion distance)	1.2
SEP power processor input	13.0
SEP thruster input power at 1 AU (0.91 x 13.0)	11.8
Input power to each of four thrusters (11.8/4)	2.96
Thruster maximum power rating (reached at 0.92 AU during initial inbound passage)	3.3
Maximum power input to five thrusters at 0.74 AU (1.34 x 11.8 kw)	15.8
Maximum power rating of five thrusters (5 x 3.3)	16.5
(Percentage of maximum power of five thrusters reached at 0.74 AU, 100 x 15.8/16.5)	(96%)

The solar array must operate over a large range of temperatures varying typically from 50°C at earth departure to -100°C during the outbound phase of the mission to +140°C at solar distances of 0.68 AU and less during the inbound phase. This upper temperature limit is maintained when close to the sun by a programmed rotation away from full sun exposure starting at 0.68 AU solar distance. The required array offset angle increases to 75 degrees at perihelion (0.34 AU). With the solar array in "feathered" orientation the radiation pressure effect at close solar distance is greatly reduced. Partial solar array retraction is desirable during the comet exploration phase to further

reduce solar pressure and to minimize field-of-view obstruction of the platform-mounted sensors, as illustrated in Figure 7-4.

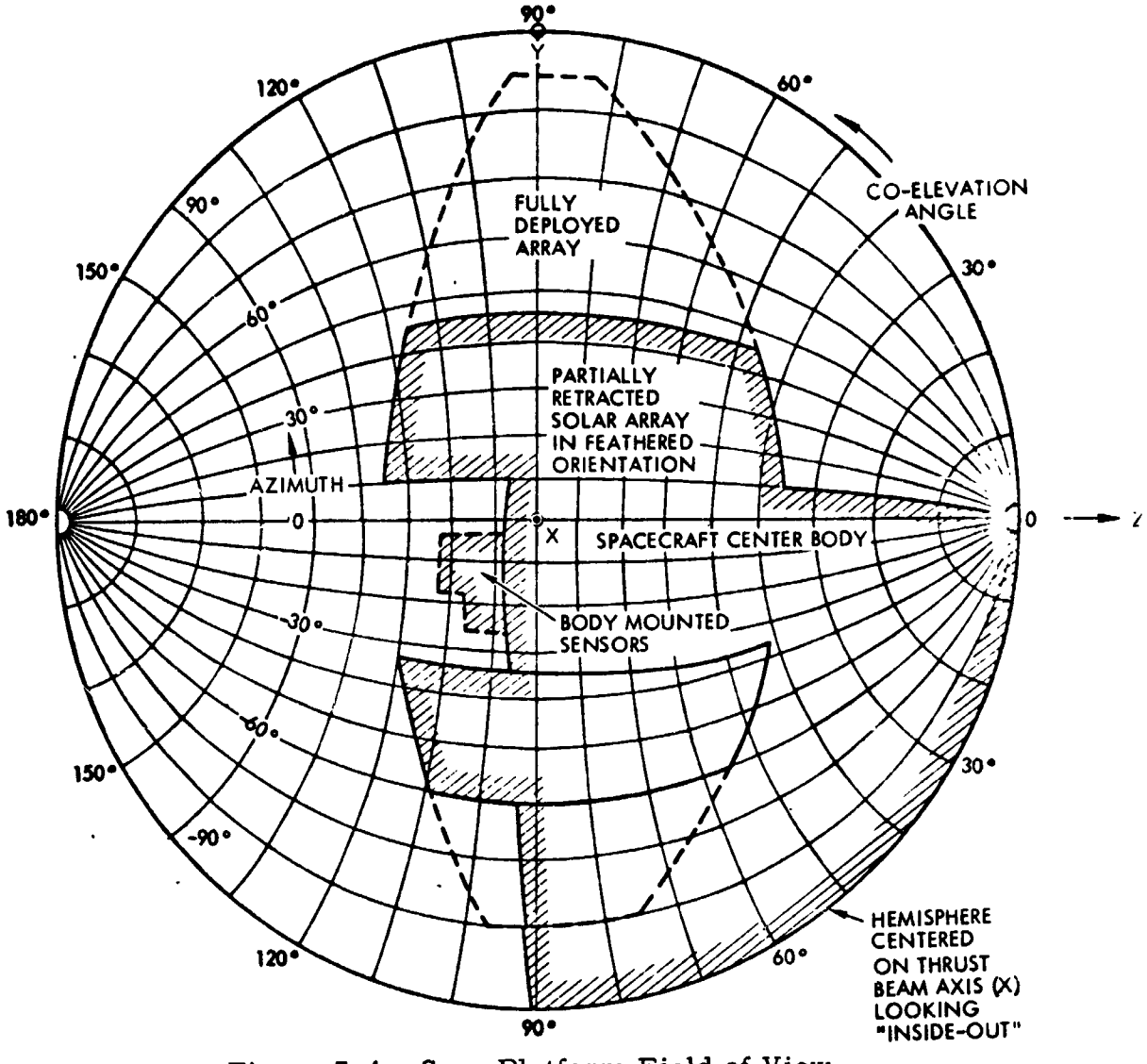

Figure 7-4. Scan Platform Field of View.

The large solar array temperature and voltage variations of this mission introduce problems in the electrical design of the propulsion power processor subsystems. With solar distances ranging from 0.34 AU to 2.8 AU the array voltage varies over a ratio of 3:1 which exceeds the present state of technology of high-efficiency power processors. Two alternative approaches were considered: (1) operation over the stated solar array voltage range; this requires additional

power processor development and causes weight and efficiency penalties totaling 10 to 20 percent; (2) reduction of output voltage variation by in-flight switching of solar array module interconnections. The first, more conservative approach was selected in our design concept.

The solar array is divided into 12 modules which are interconnected with a grounded center tap so that one output terminal is positive and the other negative with respect to vehicle ground. This arrangement doubles the input voltage to the power processor and permits an appreciable weight saving while reducing the risk of electron drainage currents flowing between the solar array and the ambient plasma.

7.2.2 Propulsion Subsystem

The power profile of the nominal 800-day transfer trajectory is shown in Figure 7-5. A tradeoff between the number of thrusters, reliability, and weight was performed based on results of an earlier study (Reference 7-3). By selecting a total of six thrusters, each rated at a nominal input power level of 3.3 kw, we obtain a thruster switching sequence that uses four thrusters initially as shown in the diagram. The number of thrusters operating during the 751-day total thrust period varies between five and one. The sixth thruster is available as a spare. This operating profile does not require any thruster to operate for more than 350 days and the resulting overall thrust system reliability is 0.95 based on a nominal thruster design life of 550 days.

The assumed thruster characteristics (3.3 kw at a 3000-second specific impulse and 70 percent efficiency, providing a maximal thrust of 35 millipounds) are consistent with the projected performance range of the 30-cm thrusters currently under development by JPL and NASA Lewis Research Center. Since the maximum thruster throttling ratio of 2:1 is not exceeded at any time during this mission, as shown in Figure 7-5, a high level of thruster efficiency can be maintained.

The thrusters are mounted in a hexagonal array on a two-axis translation platform based on the thrust vector control system design developed by JPL (Reference 7-5). This platform aligns the total thrust

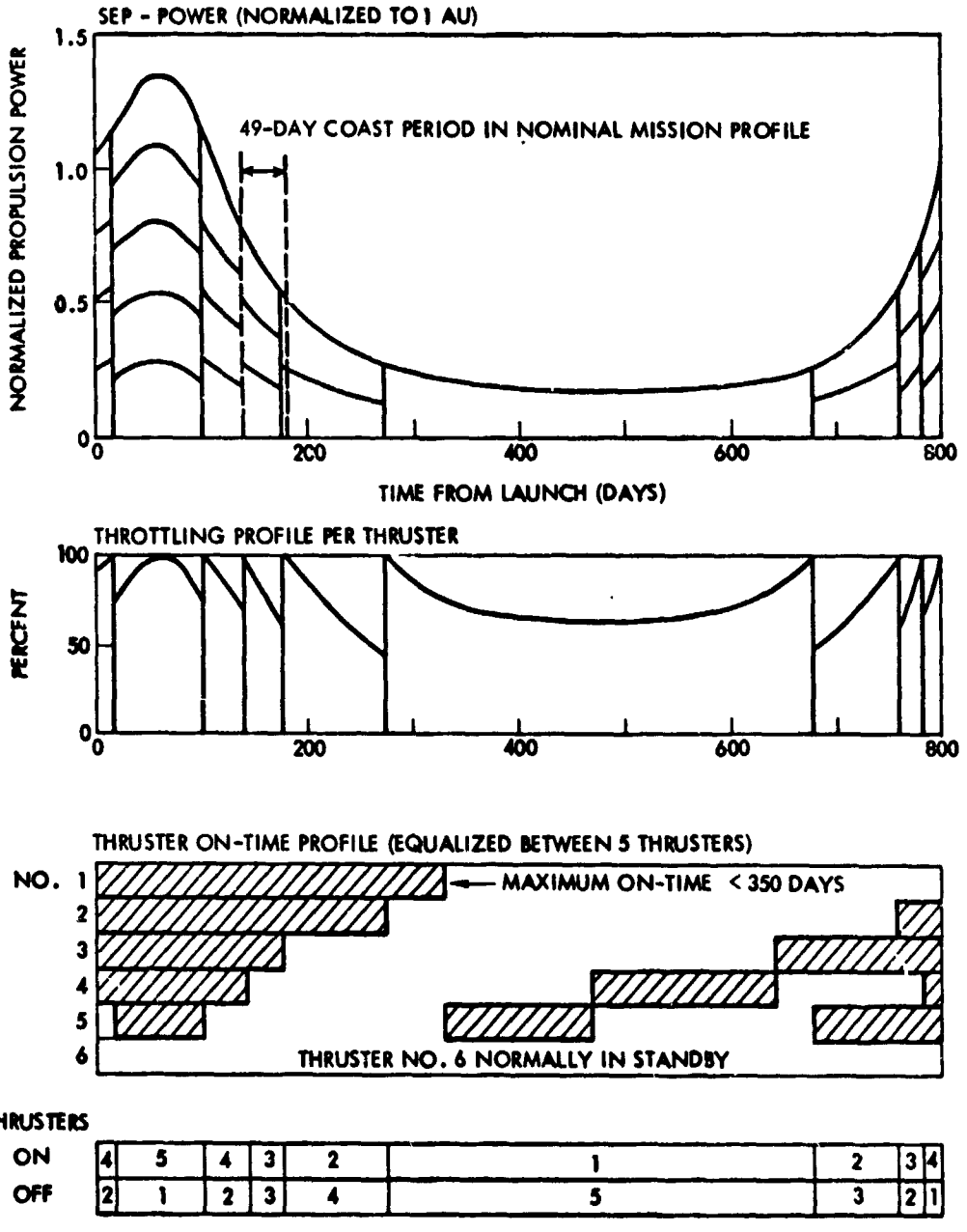

Figure 7-5. Propulsion Power and Thruster Switching Profile

vector with the spacecraft center of mass regardless of how many thrusters are in operation at any given time and automatically compensates for lateral shifts of the spacecraft center of mass which may be caused, e.g., by solar array deflections. In addition to the thrust vector alignment function, the TVC articulation system also performs continuous attitude control functions during the thrust phase. To add a third axis attitude control capability, each thruster is mounted on a

one-axis gimbal so that it can be deflected by a small angle around an axis extending to the center of the hexagonal array. Individual gimbal actuators are envisioned but one centrally located actuator could be used instead to drive all six gimbals.

The dimensions of the propulsion module (2.45 x 1.58 x 0.9 meters) are dictated primarily by the panel area of the power processor units that must radiate a maximum of 1.5 kw of dissipated heat based on a 91 percent power processor efficiency when the solar distance decreases to 0.75 AU during the initial inbound main thrust phase. For most effective waste heat rejection the power processors are mounted in the rear area of the propulsion module.

7.3 ENGINEERING SUBSYSTEMS

7.3.1 Attitude Control

The attitude control subsystem performs the following functions:

- Initial celestial reference acquisition after separation from the booster and reacquisition at any time during the operating life of the system
- Three-axis stabilization of the vehicle attitude within ±0.5 degree and thrust vector orientation by rotation of the spacecraft about the yaw and roll axes
- Antenna pointing at the earth with an accuracy of 0.5 degree
- Experiment pointing with ±0.5 degree accuracy
- Solar array rotation through ±90 degrees
- Computational support to the propulsion and power subsystems on a noncyclic basis.

The attitude control system includes coarse and fine sun sensors; a one-axis rotatable star reference sensor; two redundant rate integrating gyros; the reaction control system; and a control electronics assembly which provides interconnection and switching of subassemblies and establishes interfaces with other subsystems.

A control processor assembly consisting of two redundant digital computers provides logical control and computation functions within the

attitude control subsystem and supports other subsystems on a priority interrupt basis. The large number and diversity of attitude control operating modes and switching requirements can be significantly simplified by the use of this computer, with an increase in system reliability.

The spacecraft attitude is controlled within a relatively wide deadband (0.5 to 1 degree) such that limit cycle oscillations have a low frequency, about 0.01 cps. This is required to save attitude control propellant as well as to minimize dynamic interaction with the flexible solar array structure. Of principal interest in this connection is the frequency of the first asymmetrical bending mode of the spacecraft/solar array combination. This frequency is about one order of magnitude greater than the attitude control limit cycle frequency. Hence the two oscillation modes are effectively decoupled.

In addition to the nominal cruise control mode the attitude control system also provides a precision pointing mode with a drift rate small enough (2×10^{-4} deg/sec) to allow accurate navigation fixes by means of the TV image system with a maximum exposure time of about 30 seconds (see Section 5).

7.3.2 Communication and Data Handling

The design of these subsystems is keyed to the objective of limiting the required mission support by the Deep Space Network considering the prospect that the Encke rendezvous mission may be in progress concurrently with other interplanetary missions of long duration. Reasonably large telemetry data rates will be maintained by the spacecraft even at maximum communication range, with the uplink and downlink characteristics designed to rely primarily on the 85-foot rather than the 210-foot DSIF antennas.

Since electric power is abundant we selected a 25-watt transmitter for the baseline configuration operating at S-band. The size and payload capacity of the vehicle permits the use of a six-foot (1.82 m) high-gain antenna. Thus, even at a communication range of 3.8 AU, occurring at aphelion, a telemetry bit rate of 258 bps will be available using an 85-foot DSIF antenna. During rendezvous the data rate increases to

2048 bps at the initial encounter and to 16.3 kbps at the time of earth-comet opposition when nucleus exploration is in progress and a larger number of TV frames is to be transmitted. With the use of the 210-foot DSIF antenna these data rates would be increased to 16.3 kbps and 131 kbps, respectively.

7.3.3 Thermal Control

The thermal design must provide adequate temperature control to the vehicle, all its subsystems and appendages over the wide range of propulsion power and solar heat flux conditions that characterize the mission. The basic thermal control concept provides the spacecraft with an insulated body so as to minimize heat leaks into and out of the interior. Multilayer thermal insulation blankets consisting of aluminized Kapton sheets are used for effective passive control. Bimetallically actuated louvers are used to control the temperature of high-heat rejection components such as the power processors in the propulsion module, and TWT's and their power supplies in the equipment module. The two modules are also thermally decoupled since each is optimally operating at different temperature levels, and thermal transients occurring in the propulsion module would unnecessarily complicate thermal control of the more uniformly operating equipment module. Heaters are used to keep the propulsion module equipment above minimum temperatures of -55°C during coast phases.

External equipment is protected against excessive solar heating by low-absorptivity, high emissivity coating (Z-93 thermal white paint) and by multilayer Kapton insulation sheets where required to minimize heat leaks into and out of the equipment. The high-gain antenna dish uses stainless steel wire mesh coated with Teflon to withstand the extreme heating at close solar distances without serious deformation.

The ion engines are arranged in a hexagonal array, with up to five engines operating simultaneously. Under worst-case heating conditions local high temperatures may reach 295 to 320°C at 0.4 AU solar distance. Use of permanent magnets rather than electromagnets make this condition acceptable. These results are conservative since operation of adjacent engines is unnecessary during the comet exploration phase.

The solar array panels are protected against excessive solar-thermal radiation by rotation away from full exposure, as solar distance decreases below 0.68 AU, thus maintaining a maximum temperature of 140°C. Degradation due to overheating may become a problem if the solar array blankets do not remain ideally flat under extreme heat flux, but exhibit curling along the edges while held in the feathered orientation. The angle of solar incidence along the edges can thus become sufficiently large to cause permanent damage in this portion of the array. Actually, a large thermal degradation of the solar array can be accepted after rendezvous is achieved, nominally at 0.96 AU since much less than the full thrust power is needed to perform subsequent comet exploration maneuvers. However, for greater flexibility in mission planning, we must include the option of arriving at a later date, closer to perihelion. A promising design approach for controlling edge curl is shown in Figure 7-6. Solar array panels are stiffened by collapsible beryllium copper tubes installed along the edges and across the substrate, subdividing the array into rectangular modules. The stiffeners can be rolled up and deployed from the storage drums without difficulty. The estimated weight of this modification (8 to 12 kg for a 17.5-kw solar array) increases the total array weight by only four percent. Further study, engineering development, and test of this concept as a modification of the existing rollup array model is recommended.

A principal operating constraint of the spacecraft, particularly during closest solar approach, is to avoid exposure of the rear surface of the center body with its louvered radiating panels to direct sun illumination. As previously discussed in Section 6 all maneuver sequences can be adapted to this constraint. However, at times this requires a roll reorientation of the spacecraft by 180 degrees.

7.4 WEIGHT ESTIMATES

Although no detailed design of the selected spacecraft concept and its subsystems was performed during this study, preliminary weight breakdown estimates can be derived by extrapolation from the earlier designs on which our configuration is based (References 7-1 through 7-4). Table 7-2 shows the weight estimates for electric propulsion and power according to data derived in Section 5, and gives upper and lower weight

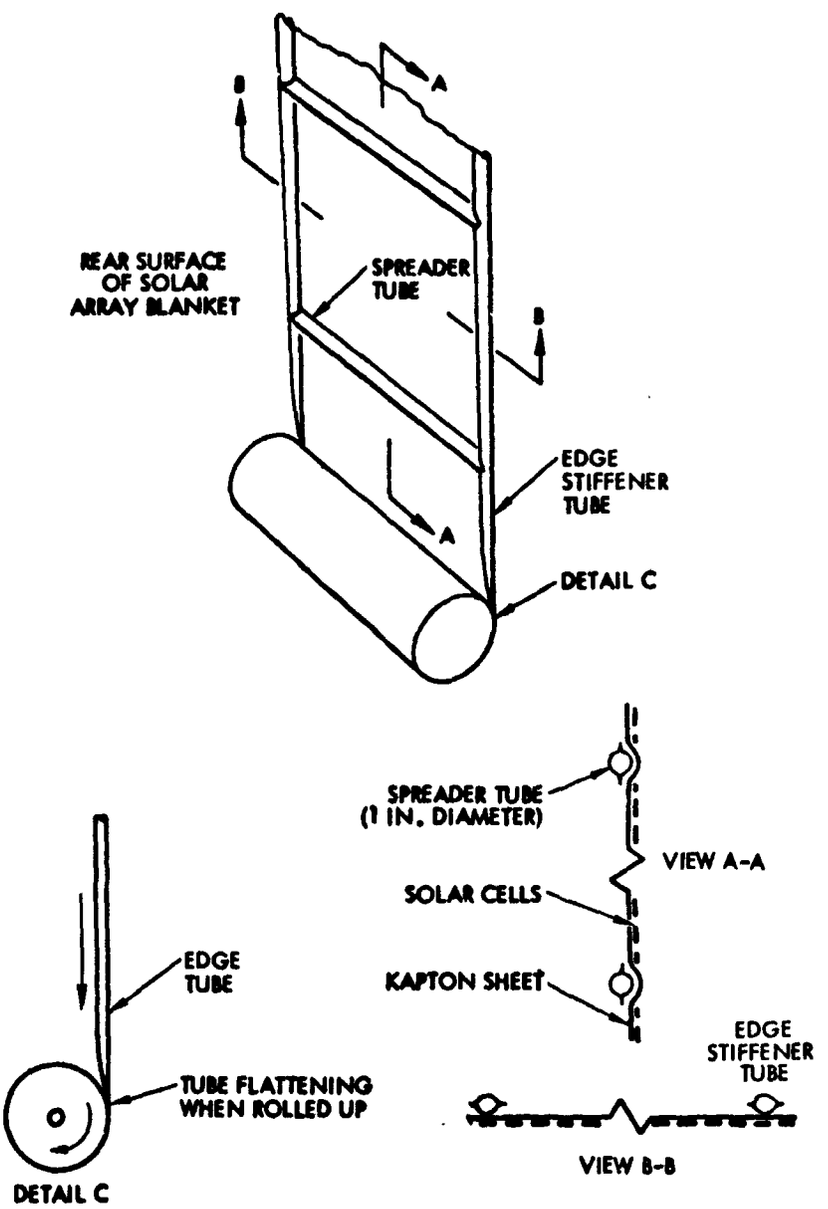

Figure 7-6. Solar Array Protection Against Edge Curl

Table 7-2. Estimated Weight Breakdown (kg)

Nominal 800-day mission; total thrust time: 751 days Gross solar array power 17.5 kw, SEP input power 13 kw (at 1 AU) Titan IIID/Centaur (five segments), offloaded 14 percent			
Gross injected mass at V_∞ = 8 km/sec		1380*	Launch penalties covered by 14 percent unused booster capacity
Solar electric propulsion dry mass		417	Based on α = 30 kg/kw plus 27 kg to accommodate initial power increase
Propellant mass (mercury)		536	
Net spacecraft mass		427	
Solar array degradation and housekeeping power		67	4.5 kw at 15 kg/kw
Structure and engineering subsystems		310 ± 20	
Structure	100-110		Weight elements adapted from previous SEP spacecraft studies by TRW and JPL (Reference 7-1 and 7-2)
Thermal control	30- 35		
Power	30- 35		
Attitude control	30- 35		
Electrical integration	25- 30		
Communications and data handling	50- 55		
Hydrazine and tankage	25- 30		
	290-330		
Net payload capacity (science)		50 ± 20*	

*Extension of thrust time by 49 days to 800 days would increase gross injected mass to 1460 kg and net payload capacity to 76 ± 20 kg (hyperbolic departure velocity decreased to 7.5 km/sec).

brackets for spacecraft structure and engineering subsystems. Comments that explain some of these estimates are added in the last column of the table. The resulting net weight capacity for payload instruments is 50 ± 20 kg. Since the lower estimate shows only a marginal payload capacity it is apparent that a more detailed design study is required to narrow the uncertainty range of subsystem weight assumptions. Areas that provide a significant weight reserve are: (1) reduction of mercury propellant mass through optimum use of the total launch vehicle injection capability and by reducing the 49-day coast period included in the nominal transfer trajectory; (2) savings in the amount of power margin allocated to solar array degradation and housekeeping; and (3) reduction of hydrazine propellant mass by better definition of emergency maneuvers that would require hydrazine rather than low-thrust propulsion capabilities. Preliminary analysis indicates that a net payload increase of up to 70 kg should be achievable if necessary by combining all of these steps. A

shift in arrival date by 10 days would yield an additional margin of 30 kg. Thus the desired scientific instrument complement of 50 kg can be readily accommodated with a substantial weight margin.

7.5 ADAPTATION TO LAUNCH BY THE EARTH ORBITAL SHUTTLE

The possibility of using the Earth Orbital Shuttle augmented by a chemical upper stage to launch interplanetary missions has important implications in connection with a 1984 Encke rendezvous mission. A preliminary investigation of the compatibility of our spacecraft with the Shuttle launch mode was conducted and the following potential advantages of this mode were identified:

- Substantial cost savings compared to the Titan IIID/ Centaur booster
- Ability to deploy the solar array and conduct a pre-flight orbital checkout, especially of the electric propulsion system
- Ability to detect and correct malfunctions, thus increasing the probability of mission success compared to the conventional automatic launch mode
- Salvaging the spacecraft if major repair is required that is not feasible onboard the Shuttle.

The possibility of adding this mission to the list of subscribers to the Shuttle program, along with other SEP missions now being contemplated for the 1980's should be a matter of interest to Shuttle program planners.

Figure 7-7 shows estimated performance characteristics* of the Shuttle with Centaur and Agena upper stages (solid lines) compared to the current Titan IIID/Centaur performance (dashed lines). The performance requirement for a nominal 800-day SEP Encke mission is seen to be well within the capability of the projected large-tank Agena upper stage. The Centaur upper stage would have sufficient performance to inject two vehicles of the Encke spacecraft class, although such a dual launch is not envisioned at this time.

Figure 7-8 illustrates the concept of orbital checkout of the electric spacecraft mounted on top of the Centaur stage. The stage is still attached

*Source: NASA/MSFC, 1971

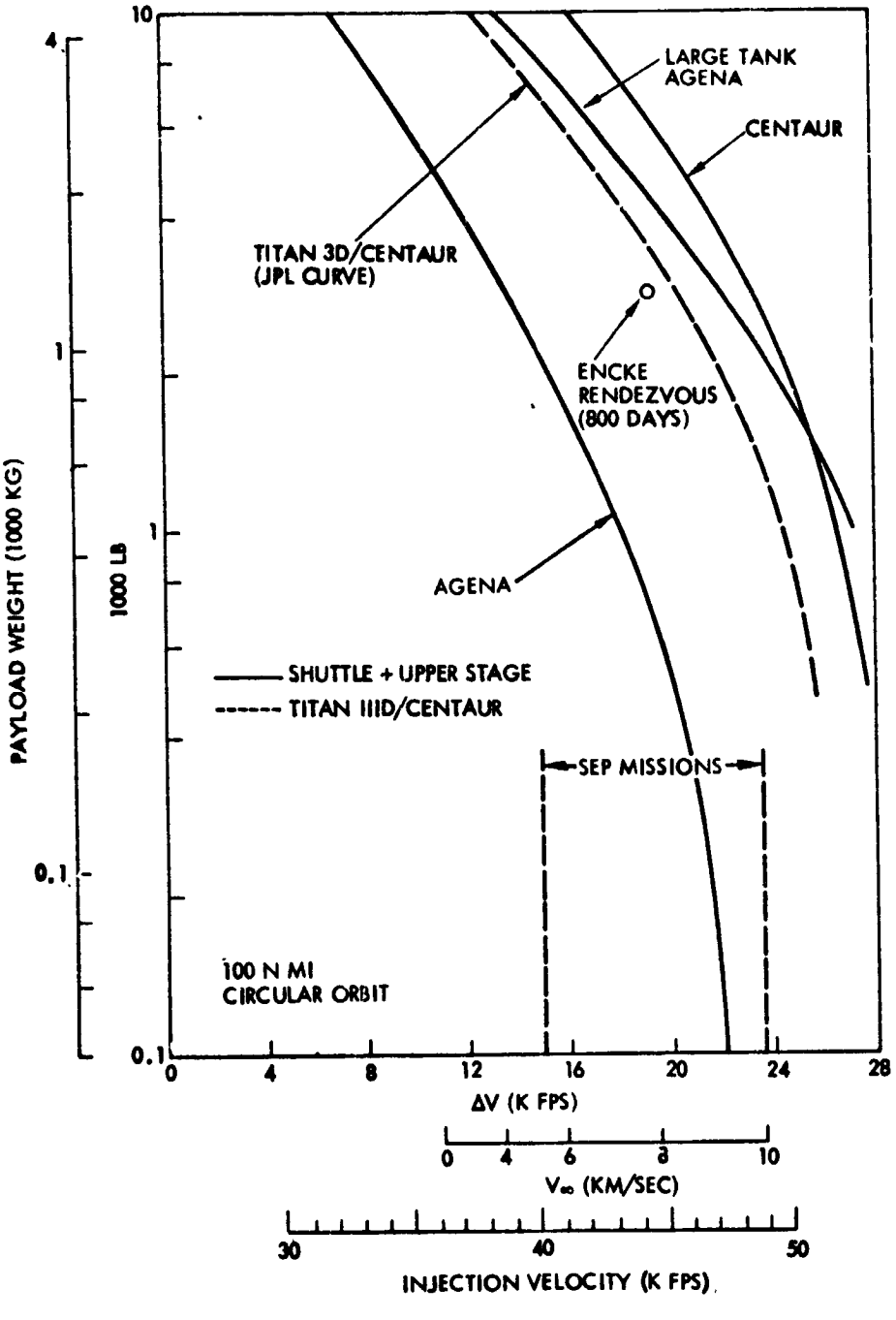

Figure 7-7. Assumed Injection Performance of Shuttle/Upper Stage Combinations and SEP-Launch Requirements

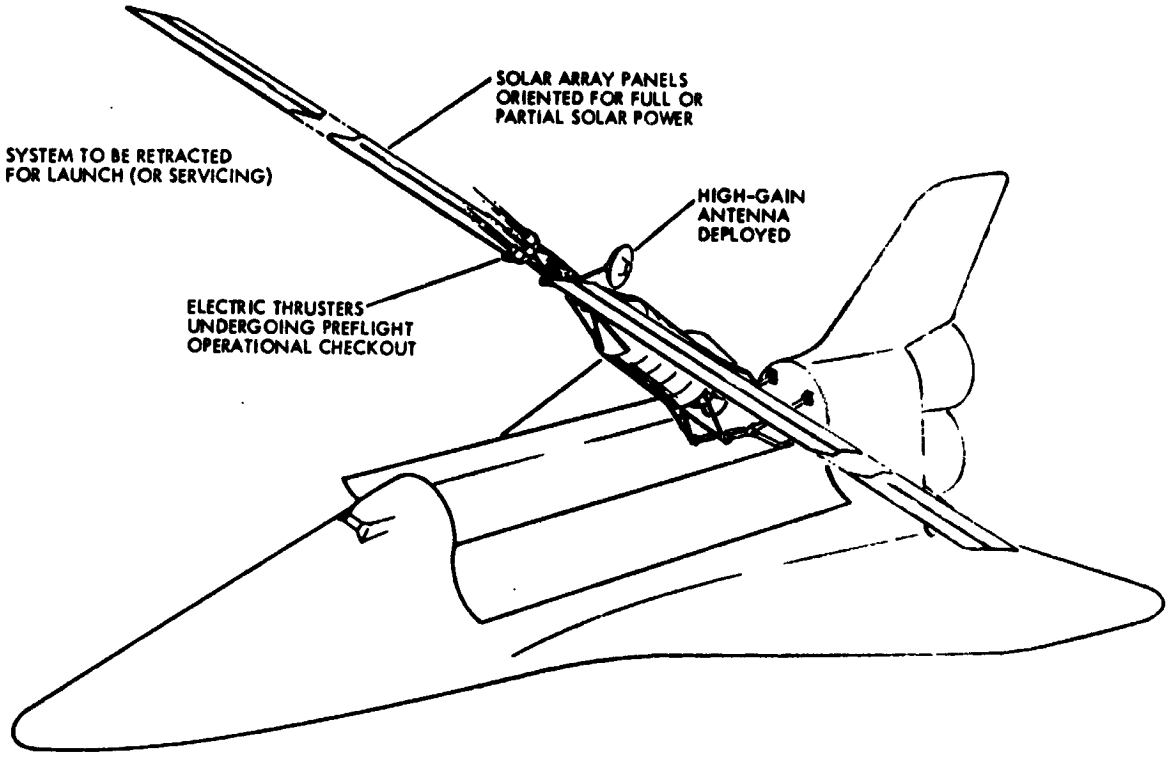

Figure 7-8. Spacecraft Deployed for Preflight Checkout in Shuttle Launch Concept

to the Shuttle by means of a deployed strongback, so that it could be retracted for servicing if necessary. The solar array is deployed and the electric thrusters on top of the vehicle are then turned on for a full thrust check run. A complete power and propulsion checkout is not feasible in ground test facilities of practical size. Some of the engineering systems and science payload checkout tasks are summarized below.

a) Engineering systems

- Deployment, retraction and rotation of solar array under zero g condition
- Thruster decaging, articulation and switching
- Full-power active thruster test
- Automatic thruster throttling and cutoff sequence under simulated solar intensity variation (array rotation); maximum power tracking by power processors
- Command sequences, data handling and telemetry
- Thermal control cycles in day and night phases.

b) Science payload

- Measurement of earth-orbit observables and sensor calibration (i.e., plasma probe, magnetometers, E-field meter, IR and UV sensors)
- SEP-interaction levels
- TV system checkout against known targets on surface
- Payload platform uncaging and articulation test
- Checkout of instrument command sequences, data handling, and telemetry.

We note that the launch configuration of the electric spacecraft designed for Titan IIID/Centaur launch, especially the placement of the propulsion module on top, is compatible with the Shuttle orbital checkout concept and no significant modification between the Titan launch and Shuttle launch appears to be required.* Further study of Shuttle launch implications to substantiate these preliminary conclusions is required and should be performed along with other feasibility and implementation studies projected for the Encke mission.

7.6 ALTERNATE SPACECRAFT CONCEPTS

A critical look at the large and relatively complex, three-axis controlled 17.5 kw spacecraft configuration that has resulted from this study inevitably leads to the question whether a simpler and less costly spacecraft concept could not be devised to provide a minimum Encke rendezvous mission capability. Is it possible to achieve a less sophisticated but adequate mission by giving up some design feattures that complicate the selected spacecraft concept following the same precepts that led to the definition of a minimum but essential science payload complement ? In our search for a simpler spacecraft implementation we have explored these avenues:

1) Reduction in propulsion power

2) Simplification of design features

*This aspect is relevant to possible multiple-mission uses of the SEP spacecraft.

3) Use of spin-stabilization rather than three-axis stabilization

4) Use of a ballistic three-impulse trajectory to achieve rendezvous without electric propulsion.

The first approach is feasible but would necessitate adoption of a longer flight time, typically 1050 days, as discussed in Section 5. In this case the propulsion power can be reduced to 7 kw and the gross (installed) power to about 10 kw. However the shorter flight time that necessitates 13 kw of propulsion power (17.5 kw of gross power) provides greater flexibility of mission planning, improves the probability of success, and provides a more adequate time interval to make use of data obtained from the 1980 Encke flyby. In addition, with 13 kw of propulsion power we gain mission growth potential, e.g., the capability of carrying a lander probe in a later mission that would use essentially the same spacecraft configuration. The adopted power level makes the spacecraft compatible with a number of other mission objectives as identified in JPL's SEMMS study, so that the development cost may be shared by different users. We conclude that the limited cost reduction achievable through a 7 kw (40 percent) power reduction imposes too many significant disadvantages in the framework of overall program considerations.

The second approach, simplification of design features, concerns such elements as the rotatable solar array, the antenna size, and the two-axis gimballed scan platform. The rotatable array is essential because of the high sensitivity of payload mass to optimal thrust pointing. As shown in Section 5, a 20 percent lower net spacecraft mass would result from thrusting along a nonoptimum fixed-cone angle. This would reduce the net (instrument) payload capacity to a marginal level, at best. Solar array rotation is essential for several other functional reasons as well, as previously discussed.

Antenna size is not critical to mission performance, but reduction from the selected 6-foot diameter would complicate data transmission during important events of the mission without offering a significant cost or weight saving. The gimballed scan platform is an essential feature of a three-axis stabilized spacecraft for effective comet exploration and cannot be eliminated.

The third approach, use of a simple spin-stabilized electric propulsion vehicle (Reference 7-6) was found to be incompatible with the propulsion requirements of an Encke rendezvous mission, owing to the thrust vector and solar array pointing constraints inherent in that design. For example, at 15 kw of propulsion power only 150 kg of net spacecraft mass would be delivered by the spinner, and even at 24 kw only 250 kg. (These data apply to a 950-day mission in 1980.) The possibility of performing a ballistic Encke rendezvous mission using major impulsive maneuvers at aphelion (3600 m/sec) and at the comet encounter (250 m/sec) has been investigated by IITRI, Reference 7-7. (These data are for a 1300-day mission in 1980.) For such a mission a simple spinner such as Pioneer, or a three-axis spacecraft such as Mariner, with an added chemical propulsion stage could be employed, the former within the launch performance envelope of a Titan IIID/Centaur/TE364-4. Further analysis, outside the scope of this study, is required to establish the feasibility of prolonged comet exploration by these ballistic vehicles and to compare their payload performance with that of the SEP spacecraft.

REFERENCES, SECTION 7

7-1 F. E. Goddard, R. J. Parks, A. Briglio, Jr., and J. C. Porter, Jr., "Solar Electric Multimission Spacecraft (SEMMS)," 617-4, Jet Propulsion Laboratory, Pasadena, California, March 17, 1972.

7-2 "Study of a Solar Electric Multi-Mission Spacecraft," 09451-6001-R0-03, prepared for Jet Propulsion Laboratory by TRW Systems, March 15, 1970.

7-3 "Study of a Common Solar-Electric-Propulsion Upper Stage for High-Energy Unmanned Missions," 16552-6007-R0-00, prepared for NASA/OART by TRW Systems, July 14, 1971.

7-4 S. P. Horio, "Solar Electric Propulsion Asteroid Belt Mission Study," SD 70-21-1, North American Rockwell Corporation, Downey, California, January 1970.

7-5 G. S. Perkins, K. G. Johnson, J. D. Ferrera and T. D. Masek, "A Mechanism for Three-Axis Control of an Ion Thruster Array," AIAA Paper 70-1156, AIAA 8th Electric Propulsion Conference, August 1970.

7-6 "Feasibility Study for a Multi-Mission Electric Propulsion Spacecraft, (Pioneer Concept)," Final Report 18305-6001-R000, prepared for NASA/Ames Research Center by TRW Systems, June 18, 1971.

7-7 A. L. Friedlander, J. C. Niehoff and J. L. Waters, "Trajectory and Propulsion Characteristics of Comet Rendezvous Opportunities," Report No. T-25, prepared for NASA by IIT Research Institute, August 1970.

8. COST CONSIDERATIONS

Determination of a cost estimate for the Encke rendezvous mission exceeds the scope of this study. To obtain reasonably valid cost figures at this time would require a spacecraft design study in a much greater depth. However, since cost economy was specified as a principal constraint in our selection of the mission concept and payload composition it is relevant to compare this mission with other types of comet exploration missions on a relative cost and complexity scale. In addition, we have evaluated the relationship of payload size to cost in a qualitative way and arrived at trends on cost-effectiveness that can be stated independent of detailed system characteristics.

Figure 8-1 summarizes principal features of four comet mission types, starting with flythrough as the simplest and lowest cost entry to

TYPE	PRINCIPAL ADVANTAGES	PRINCIPAL DISADVANTAGES	RELATIVE COST AND COMPLEXITY
FLYTHROUGH	• SIMPLE • SHORT TRIP TIME	• SHORT EXPOSURE TIME • INFLEXIBLE • NUCLEUS OBSERVATION UNCERTAIN • NAVIGATION DIFFICULT	LOWEST
RENDEZVOUS	• LONG RESIDENCE TIME • SYSTEMATIC MAPPING • CLOSE NUCLEUS APPROACH (HIGH SCIENTIFIC YIELD) • FLEXIBLE • SIMPLER NAVIGATION	• LONG FLIGHT TIME • MORE COMPLEX SYSTEM (SEP) AND FLIGHT SEQUENCES	INTERMEDIATE
RENDEZVOUS WITH NUCLEUS CONTACT	• HIGHER SCIENTIFIC YIELD (COMET ORIGIN AND EVOLUTION)	• HIGH RISK MISSION • NEEDS ADVANCED TECHNOLOGY (SURFACE ANCHORING, AUTOMATIC SURFACE OBSERVATIONS) • NEEDS SEPARABLE LANDER MODULE	HIGH
SAMPLE RETURN	• HIGHER SCIENTIFIC YIELD (COMET ORIGIN AND EVOLUTION)	• HIGH RISK MISSION • NEEDS STILL MORE ADVANCED TECHNOLOGY (TELE-OPERATORS, RETURN AND ENTRY GUIDANCE) • VERY LONG FLIGHT TIME (FIVE TO SIX YEARS)	VERY HIGH

Figure 8-1. Comet Mission Types

the extremely complex and costly class of a rendezvous and sample return. A rendezvous mission such as the mission studied here ranks second in terms of cost and complexity relative to the other mission types. However, the advantage of greater scientific data return through flexible and systematic comet exploration compared to a fast or even a slow flythrough that has been proposed, would warrant the additional complexity and cost.

Actually, the payload instruments required for a flythrough mission must be more sophisticated in response characteristics and resolution than those required in a rendezvous mission, and hence perhaps costlier to develop, in order to provide a reasonable scientific yield. At typical flythrough velocities of 15-20 km/sec the spacecraft would pass through the inner coma in less than 20 minutes and provide best viewing conditions for nucleus imaging at a range of less than 10,000 km for even a shorter period. The TV system resolution would have to be at least an order of magnitude higher than the 0.1 milliradian assumed for the rendezvous image system and exceeding that of the Mariner 1971 high-resolution camera.

Missions with nucleus contact or sample return to earth are much more complex and costly. The additional scientific value of data obtainable by these advanced missions relates particularly to the origin, evolution, and age of the comet.

Figure 8-2 shows brackets of total cost of some recent ballistic missions and of estimated cost of solar-electric missions that would use

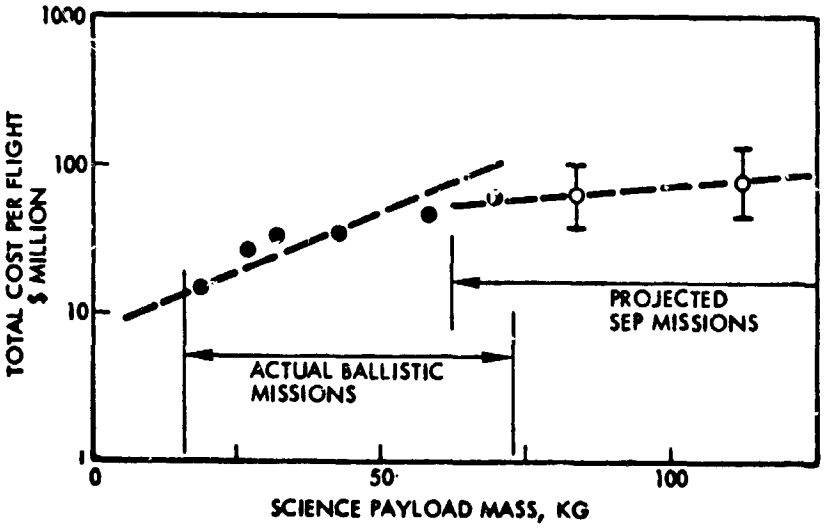

Figure 8-2. Cost Brackets of Representative Missions

spacecraft of a size and complexity comparable to the spacecraft concept described in Section 7 and capable of performing the Encke rendezvous (References 8-1 through 8-3). Figure 8-3 supports the above cost categories with an estimated cost breakdown from the recent TRW design

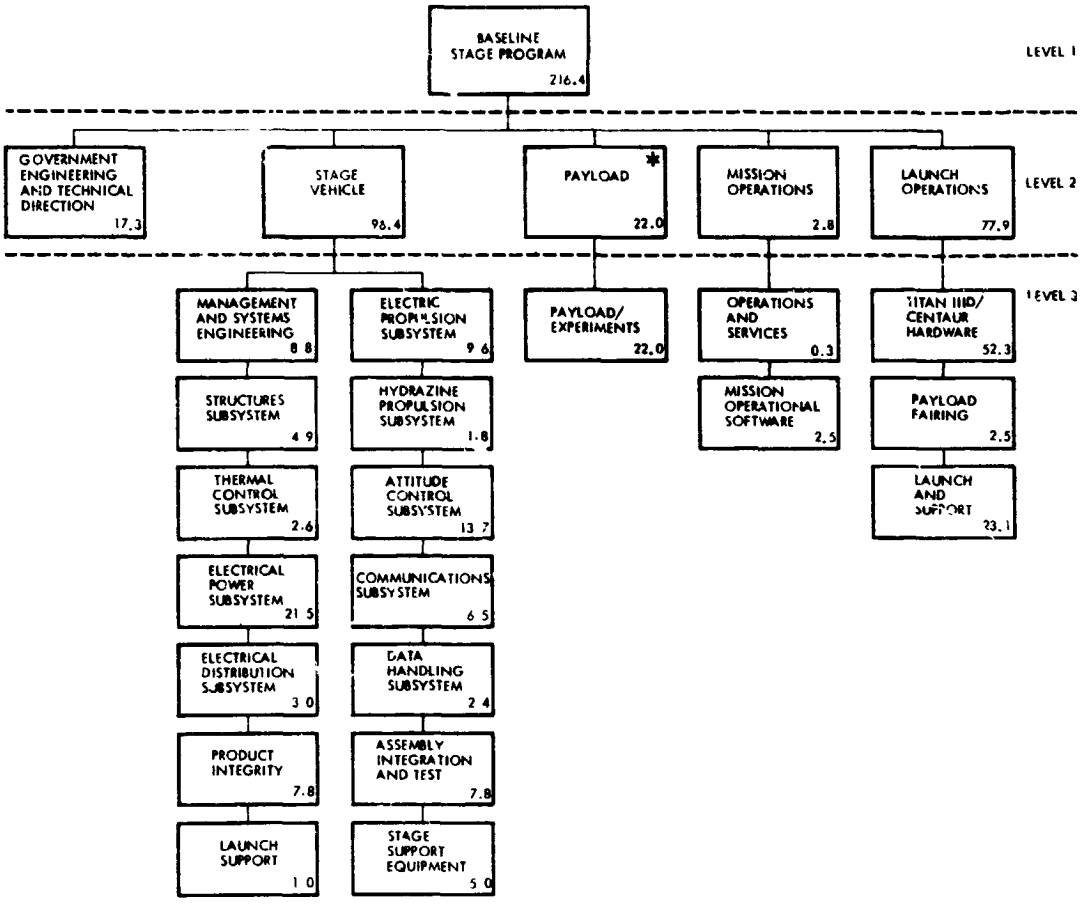

*Note: This payload estimate for three flights, i.e., $7.3 million per mission, is less than the minimum anticipated for the Encke rendezvous.

Figure 8-3. Program Elements and Cost Estimates from a Recent 17-kw SEP Vehicle Design Study (Reference 8-2)

study of a multi-mission SEP upper stage (Reference 8-2). More detailed cost figures cannot be presented in this context without additional study.

Rough estimates of payload cost categories in the above quoted examples anticipate a range of $15 to 25 million for instrument design, development, test, integration and scientific data support, i.e., typically 15 to 30 percent of the total project cost. With these cost brackets in mind it is apparent that payload cost alone is not a decisive factor in cost-effectiveness evaluation. It also follows that payload economy while important must not be overemphasized since the scientific value of the mission is strongly dependent on payload capabilities while the overall cost of the mission is a much weaker function of this variable.

These trends can be illustrated in a general way by the cost characteristics and scientific returns of a typical mission in the $50 to 100 million class, expressed in normalized form as shown in Figure 8-4.

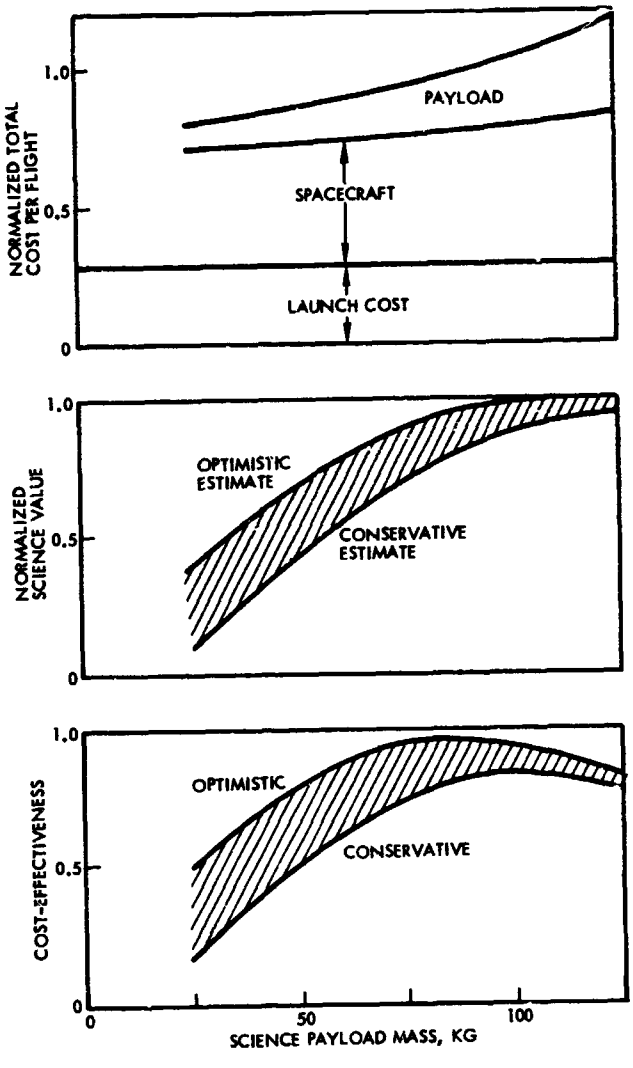

Figure 8-4. Cost Effectiveness Trends

The normalized cost and sciertific value are shown as functions of payload weight. From these curves a cost-effectiveness figure (scientific value per unit cost) is derived. Upper and lower brackets of the scientific value function reflect in a variation of the cost effectiveness by about 30 percent. The trend of these curves shows that the optimum occurs in the middle range of payload weights considered, i.e., at about 85 kg of payload weight. Characteristics of the Encke mission cost tradeoff are reflected by this trend.

REFERENCES, SECTION 8

8-1 "Study of a Solar Electric Multi-Mission Spacecraft," 09451-6001-R0-03, prepared for Jet Propulsion Laboratory by TRW Systems, March 15, 1970.

8-2 "Study of a Common Solar-Electric-Propulsion Upper Stage for High-Energy Unmanned Missions," 16552-6007-R0-00, prepared for NASA/OART by TRW Systems, July 14, 1971.

8-3 S. P. Horio, "Solar Electric Propulsion Asteroid Belt Mission Study," SD 70-21-1, North American Rockwell Corporation, Downey, California, January 1970.

9. RECOMMENDATIONS FOR FUTURE ACTIVITIES AND REQUIRED TECHNOLOGY DEVELOPMENT

In planning a rendezvous mission to Encke in 1984 (or any other year), many spacecraft design and mission analysis tasks are yet to be done, and even to be identified. However, there are also many scientific tasks still to be accomplished, and it should not be assumed that the scientific objectives of a mission to Encke rest entirely on the results of measurements by the rendezvous vehicle, and measurements to be confined to the actual time of rendezvous. The list below includes selected activities that should be regarded as integral parts of a mission to Encke, or to any other comet for that matter.

9.1 DESIRED FUTURE ACTIVITIES PREPARATORY TO THE SPACECRAFT MISSION

9.1.1 Development of Existing Data

There already exists on photographic plate and in data files a store of observations and measurements of, and inferences about, comets in general and Encke in particular that have not been fully exploited or pubicly exposed. It would be valuable to form a "Task Force Encke" to assemble and catalogue the best and most reliable data on this comet, especially from recent passes, and to compile and document the inferences that have or can be made from these data. For example, it would be helpful to have the heliocentric dependence of "nuclear" brightness, r^{-n}, documented graphically and the best value of n displayed explicitly. Similar documentation would be appropriate for brightness and diameter of any feature or layer of the comet that might be consistently identifiable, such as inner coma, coma, or tail.

9.1.2 Telescopic Observation

Substantial benefit will probably be derived from an improved program of cometary observation from earth in the next few years. In particular, there will be opportunities to examine Encke in 1974 (sunspot minimum, poor visibility), 1977 (low but rising sunspot numbers, poor visibility), and 1980 (high sunspot numbers, good visibility). Two of these opportunities, in 1974 and 1977, would produce recovery only after

perihelion, according to historical precedent. It would be appropriate therefore to plan on use of the best modern equipment, including, with emphasis, telescopes in southern hemisphere stations.

9.1.3 Theoretical Models

Computational approaches to cometary atmospheres, of the type developed by Mendis, et al (Reference 2-31), should be improved and extended. Allowance for Delsemme's icy grain sources of neutral gases and radicals should be made and the radial distribution of ionized products should be encompassed. Also, the calculations should be specialized to Encke, perhaps even including the probable nonuniformity of Encke's emissions.

9.1.4 Instrument Definition

Once an improved theoretical model has been established, the results should be applied to determine, or at least set limits on, the various parameters that spacecraft instruments will be expected to measure. Detailed definition of payload instrumentation and selection of specific detectors will then follow.

9.1.5 Solar Activity Correlation

A careful reevaluation and multifactor analysis of the historical presence and absence of Encke's tail and nucleus should be carried out and published at an early opportunity. The results can be tested during the 1974, 1977, and 1980 apparitions, which will span a wide range of sunspot numbers from minimum to maximum.

9.1.6 Solid-Particle Composition

Instrumentation for determining the composition of nonvolatile dust grains without requiring their ionization by impact should be developed and tested for inclusion in a rendezvous payload. An instrument of this type is under development at NASA, Ames Research Center, but no data on its characteristics have been published to date.

9.1.7 Laboratory Simulation

The experimental work of Delsemme and Wenger (Reference 2-11) has been an important recent contribution to the physics and chemistry

of comets. This type of simulation of cometary conditions should be continued and serious consideration should be given to repeating and extending such experimentation in an extraterrestrial laboratory such as might be available on the Shuttle.

9.1.8 Combination of Asteroid Flyby with Comet Mission

Opportunities of achieving one or several asteroid flyby's by small excursions from the nominal trajectory to Encke (Section 6) should be further evaluated, and if possible, included among the secondary objectives of the mission. NASA's Small Bodies Mission Panel has started deliberations on possible options of this type, their feasibility and relative priority in 1971 and is currently issuing its recommendations.* Further analysis and tradeoff between scientific value of multitarget flyby and possible increases in cost, complexity and the risk to the primary objective should be performed.

9.2 ADVANCED TECHNOLOGY REQUIREMENTS

Results of system analysis and design studies indicate that the implementation of the electric stage program depends strongly on technology development not only in the field of solar-electric propulsion but other critical areas as well, e.g., attitude control of large flexible structures; guidance and navigation with respect to targets having a poorly defined ephemeris and being hard to detect, such as asteroids and comets; thermal control under extreme conditions; communication and data handling with wide variations of mission characteristics and constraints.

9.2.1 Solar Electric Propulsion Technology

This technology has been greatly advanced in recent years, and its performance test by the SERT 2 mission in 1970 has been highly successful. Ion thrusters of the type and size envisioned for this mission (Section 7) are under advanced development and test by NASA and JPL. Advanced power processors are also being developed. However, a realistic all-up technology evaluation flight is being considered a necessity to provide sufficient confidence before undertaking a demanding and costly mission such as Encke rendezvous, with thrust times of the order of

*Private communication by R. Newburn of JPL, a participant.

700 days. However, the 1984 Encke mission with seven years of lead time remaining to date, and three years before system development would have to get started, could provide the ultimate incentive for undertaking the first-generation SEP flight program in the second half of this decade.

9.2.2 Thermal Protection

Advanced thermal control technology will be incorporated in the 1974 Mariner Venus-Mercury spacecraft and the Helios 0.25 to 0.3 AU solar probes, to be launched in 1974/1975. However, the Encke mission which includes outbound (2.8 AU) and inbound phases (0.34 AU) with a thermal flux variation of about 100:1 poses new and even more extreme thermal control problems. Among the problem areas to be addressed are flexible orientation modes and ion thruster operability under the maximum solar flux at 0.34 AU. The possible degradation of the solar array under these extreme conditions and the damage that may be caused by thermal warping of the solar cell blankets must be further investigated and techniques for its control should be developed and tested, including the panel stiffener concept proposed in Section 7.

9.2.3 Protection Against Cometary Dust, Ice Grains, etc.

The inevitable dust impact hazard in the inner coma and near the nucleus must be further investigated and techniques for protection of sensitive surfaces, optical apertures, etc., developed. The mission profile can be adapted so as to minimize the exposure but a quantitative evaluation of system degradation should be performed. One of the most sensitive parts of the spacecraft may be the ion thruster that would be contaminated and subject to short circuiting by even minute amounts of dust entering the discharge chamber and inter-electrode space. Since the thrusters are largely dormant during most of the comet exploration phase, the concept of providing a protective cover that can be folded back during intermittent short thrust periods appears promising.

9.2.1 Terminal Navigation

More analysis of the novel concept of two-stage rendezvous is required to evaluate its use and accuracy in apprcaching the nucleus. The

prospect of adding asteroid flyby to the mission objectives would increase the complexity and accuracy requirements of terminal navigation. However, the onboard optical sensor already provided for nucleus terminal navigation fixes provides asteroid detection capabilities to sixth magnitude consistent with requirements currently being established in parallel studies of asteroid rendezvous.

9.2.5 Remote Spacecraft Operation under Control by TV Command Link

During critical mission phases, particularly in close approach to the nucleus, the long round-trip communications time delay of 10 to 30 minutes is a severe impediment for effective use of the TV command link to control the spacecraft remotely. There will be a requirement of autonomous maneuvering and sensor pointing under onboard command sequencing and feedback control. This technology is needed for interplanetary missions of various types and has been under development for some time, e.g., by a study team at JPL.* It is recommended that conceptual and practical problems of autonomous and remote control be studied jointly by a team of spacecraft/mission designers and remote control specialists, with an initial review of available approaches, priorities, complexity levels, etc., to be followed by mission-oriented research.

*Private communication by L. Friedman of JPL.

Errata, Volume I, Study of a Comet Rendezvous Mission,
TRW Report 20513-6006-R0-00

Page

2-3 Figure 2-3, legend at lower right reads

C = Coma
N = Nucleus or Condensation
T = Tail

2-45 Figure 2-22, right hand column, third scale from top: 19^6 km should read 10^6 km

2-51 Figure 2-25, solid line should also be labeled "Asteroidal Brightness Law"

2-52 Figure 2-26, replace caption by:

Temperature of cometary material vs. heliocentric distance

6-6 Figure 6-2, in abscissa and ordinate legend of graph at left, delete the word LOG